Biomimetic reactor : compartmentalizing and coupling the regeneration of the NAD(P)H cofactor and the biocatalytic oxidation of hydrogen

Wassim El Housseini

Thèse

Présentée et soutenue publiquement pour l'obtention du titre de

DOCTEUR DE l'UNIVERSITE DE LORRAINE

Mention : Chimie

Par Wassim EL HOUSSEINI

Sous la direction de Mathieu ETIENNE et François LAPICQUE

Réacteur biomimétique : compartimenter et coupler la régénération du cofacteur NAD(P)H et l'oxydation biocatalytique de l'hydrogène

4 novembre 2022

Membres du jury:

Directeurs de thèse :	**Dr Mathieu ETIENNE**	**Directeur de recherche, LCPME-CNRS, Nancy**
	Dr François LAPICQUE	**Directeur de recherche, LRGP-CNRS, Nancy**
Président de jury:	**Prof. Jean Marc COMMENGE**	**Professeur, ENSIC, Nancy**
Rapporteurs:	**Prof. Edmond MAGNER**	**Professeur, Université de Limerick, Limerick**
	Dr Florence GENESTE	**Directeur de recherche, ISCR-CNRS, Rennes**
Examinateur:	**Prof. Shelley D. MINTEER**	**Professeur, Université d'Utah, Utah**
Membre invitée :	**Dr Elisabeth LOJOU**	**Directeur de recherche, BIP-CNRS, Marseille**

Thesis

Presented and publicly defended to obtain the title of

DOCTOR OF THE UNIVERSITY OF LORRAINE

Mention: Chemistry

By Wassim EL HOUSSEINI

Under the direction of Mathieu ETIENNE and François LAPICQUE

Biomimetic reactor: compartmentalizing and coupling the regeneration of NAD(P)H cofactor and the biocatalytic oxidation hydrogen

November 4, 2022

Jury members:

Thesis supervisors:	**Dr Mathieu ETIENNE**	**Research Director, LCPME-CNRS, Nancy**
	Dr François LAPICQUE	**Research Director, LRGP-CNRS, Nancy**
Jury President:	**Prof. Jean Marc COMMENGE**	**Professor, ENSIC, Nancy**
Reviewers:	**Prof. Edmond MAGNER**	**Professor, University of Limerick, Limerick**
	Dr Florence GENESTE	**Research Director, ISCR-CNRS, Rennes**
Examiner:	**Prof. Shelley D. MINTEER**	**Professor, University of Utah, Utah**
Guest Member:	**Dr Elisabeth LOJOU**	**Research Director, BIP-CNRS, Marseilles**

"Begin at the beginning," the King said, very gravely, "and go on till you come to the end: then stop".

-Lewis Carroll, Alice in Wonderland

Dedicated to my family

Abstract

The regeneration of cofactors NADH and NADPH is an important topic in biotechnology because many redox enzymes, such as alcohol dehydrogenases, imine reductases, and P450 monooxgenases, require cofactor to deliver their redox equivalent. However, because cofactors are particularly expensive, supplying stoichiometric cofactor when these enzymes are used in chemical synthesis is not economically feasible. To address this issue, a number of cofactor regeneration systems have been developed. Traditional regeneration systems for reduced cofactors have drawbacks because most of them require a carbon-based sacrificial co-substrate reductant and produce a by-product that is likely to be burned as waste, impeding downstream product purification and lowering the atom economy.

In this work, the implementation of redox biocatalysis in a flow reactor coupling separately hydrogen oxidation to NADH regeneration was developed. A hierarchization of the work was important in order to proceed with an efficient regeneration of NADH.

First, in a redox flow bioreactor hybridized by a gas diffusion electrode for hydrogen oxidation, the electrochemically mediated regeneration of NADH by a dissolved Rhodium complex ($[Cp^*Rh(bpy)Cl]^+$) was implemented. Initially, the reactor was optimized in terms of concentrations of rhodium complex and NAD^+ ($[NAD^+]/[Cp^*Rh(bpy)Cl]^+ = 40$), the non-humidification of hydrogen gas, the flow rates of H_2 gas and electrolytic solution (20 $mL.min^{-1}$), and the pH of the solution (7.2).

Secondly, in order to promote the best cycling of both the catalyst and the enzymatic cofactor and potentially easier purification of the synthesized molecules, the immobilization of the rhodium complex was proceeded on a carbon paper coated with MWCNT (Rh@CP-MWCNT). Rh@CP-MWCNT electrode was shown to be stable for periods of more than 5 days under flow conditions. Following that, the cofactor regeneration technique was applied to NADH-dependent biosynthesis using L-lactate dehydrogenase (LDH): the enzyme was immobilized on a separate layer placed approximately 50 µm from the Rh-CP-MWCNT matrix, and used in the flow cell. A cofactor concentration as low as 10 µM was found to be sufficient for the conversion of pyruvate with high faradaic efficiency (78 %) and total turnover number (TTN) levels of $1.8*10^4$, $2.5*10^3$, and $1.8*10^5$ for the Rh complex, the NADH cofactor, and the LDH enzyme, respectively.

On the other hand, to expand the study, chemical catalysts were exchanged by biological ones. FNR, Ferredoxin $NADP^+$ reductase, replaced the Rh complex at the cathodic compartment.

Despite the fact that the $NAD(P)^+$ cofactor is reduced at lower potentials (-0.7 V vs ref (H_2)) than the Rh complex (-0.3 V vs ref (H_2)), FNR has demonstrated the ability to regenerate both NADPH and NADH, and high levels of TTN for the NAD cofactor (10,000) were measured when coupled to the bioconversion of pyruvate catalyzed by LDH.

Furthermore, the exchange of platinum covering the gas diffusion electrode by hydrogenase, an electroenzymatic biocatalyst for hydrogen oxidation, was carried out on a gas diffusion layer that showed an efficiency towards hydrogen oxidation that was coupled to the reduction of NAD^+ catalyzed by the Rh complex in a batch reactor.

Third, after the optimization of the flow reactor and the successful immobilization of catalysts, the investigated study was focused on the simultaneous coupling between both the oxidation of hydrogen and the regeneration of the cofactor catalyzed by platinum (Pt) and the Rh complex, respectively. The motivation behind this study is that the standard potential of both Pt and Rh complex are close. Coupling both half reactions was successful after an optimization of the pH in the anodic and the cathodic compartments (pH = 7.2), the amount of both Pt and Rh complex, and the exchange of the Nafion^{TM} membrane by a polymeric separator in order to decrease the resistivity of the system.

Résumé

La régénération des cofacteurs NADH et NADPH est un sujet important en biotechnologie car de nombreuses enzymes redox, telles que les alcools déshydrogénases, les imines réductases et les monooxgénases P450, ont besoin de cofacteur pour fournir leur équivalent redox. Cependant, comme les cofacteurs sont particulièrement coûteux, l'apport d'un cofacteur stœchiométrique lorsque ces enzymes sont utilisées en synthèse chimique n'est pas économiquement réalisable. Pour résoudre ce problème, un certain nombre de systèmes de régénération des cofacteurs ont été mis au point. Les systèmes traditionnels de régénération des cofacteurs réduits présentent des inconvénients car la plupart d'entre eux nécessitent un co-substrat réducteur sacrificiel à base de carbone et produisent un sous-produit susceptible d'être brûlé comme déchet, ce qui entrave la purification du produit en aval et réduit l'économie atomique.

Dans ce travail, la mise en œuvre de la biocatalyse redox dans un réacteur à flux couplant séparément l'oxydation de l'hydrogène à la régénération du NADH a été développée. Une hiérarchisation des travaux était importante afin de procéder à une régénération efficace du NADH.

Tout d'abord, dans un bioréacteur à flux redox hybridé avec une électrode à diffusion gazeuse pour l'oxydation de l'hydrogène, la régénération électrochimique du NADH par un complexe de rhodium dissous ($[Cp^*Rh(bpy)Cl]^+$) a été mise en œuvre. Initialement, le réacteur a été optimisé en termes de concentrations de complexe de rhodium et de NAD^+ ($[NAD^+]$ /$[Cp^*Rh(bpy)Cl]^+ = 40$), de non-humidification de l'hydrogène gazeux, de débits de H_2 gazeux et de solution électrolytique (20 $mL.min^{-1}$), et de pH de la solution (7,2).

Deuxièmement, afin de promouvoir le meilleur cyclage du catalyseur et du cofacteur enzymatique et une purification potentiellement plus facile des molécules synthétisées, l'immobilisation du complexe de rhodium a été effectuée sur un papier carbone recouvert de nanotubes de carbone (Rh@CP-MWCNT). L'électrode Rh@CP-MWCNT s'est avérée stable pendant des périodes de plus de 5 jours dans des conditions de flux continu. Ensuite, la régénération de NADH a été couplée à la biosynthèse de pyruvate catalysée par la L-lactate déshydrogénase (LDH) : l'enzyme a été immobilisée sur une couche séparée et placée à environ 50 µm de la matrice Rh-CP-MWCNT. Une concentration de cofacteur de 10 µM s'est avérée suffisante pour la conversion du pyruvate avec une efficacité faradique élevée (78 %) et des

niveaux de recyclage (TTN) de $1,8*10^4$, $2,5*10^3$ et $1,8*10^5$ pour le complexe de Rh, le NADH et la LDH, respectivement.

D'autre part, pour élargir l'étude, les catalyseurs chimiques ont été remplacés par des catalyseurs biologiques. La FNR, Ferrédoxine $NADP^+$ réductase, a ainsi remplacée le complexe de Rh au compartiment cathodique.

Malgré le fait que le cofacteur $NAD(P)^+$ soit réduit à un potentiel plus négatif (-0,7 V vs ref (H_2)) que celui du complexe de Rh (-0,3 V vs ref (H_2)), la FNR a démontré sa capacité à régénérer le NADPH et le NADH, et des niveaux élevés de TTN pour le cofacteur (10 000) ont été mesurés une fois couplée à la bioconversion du pyruvate catalysée par la LDH.

De plus, l'échange du platine recouvrant l'électrode de diffusion gazeuse par l'hydrogénase, un biocatalyseur électroenzymatique, pour l'oxydation de l'hydrogène a été réalisé sur une couche de diffusion gazeuse qui a montré une efficacité envers l'oxydation de l'hydrogène qui a été couplée à la réduction de NAD^+ catalysée par le complexe Rh dans un réacteur batch.

Troisièmement, après l'optimisation du réacteur à écoulement et l'immobilisation réussie des catalyseurs, l'étude s'est concentrée sur le couplage simultané entre l'oxydation de l'hydrogène et la régénération du cofacteur catalysée par le platine (Pt) et le complexe Rh, respectivement. La motivation derrière cette étude est que le potentiel standard du Pt et du complexe de Rh sont proches. Le couplage des deux demi-réactions a été réussi après une optimisation du pH dans les compartiments anodique et cathodique (pH = 7,2), de la quantité de complexe de Pt et de Rh, et du remplacement de la membrane de Nafion^{TM} par un séparateur polymère afin de diminuer la résistivité du système.

Acknowledgements

First and foremost, I would like to express my sincere gratitude towards my thesis director, Dr. Mathieu Etienne; my co-director, Dr. François Lapicque; and supervisor, Dr. Elisabeth Lojou, for granting me this amazing opportunity to pursue my doctoral research.

Mathieu, thank you so much for accepting me to participate in this project, as well as for your guidance, knowledge, countless pieces of useful advice, and motivation. I would like to acknowledge his permanent positivity that allowed me to succeed in my work and to learn from my mistakes.

I would like to thank Dr. Alain Walcarius for accepting me into his group and for his suggestions and critical opinions over the years that helped me bring this work to completion. A special thanks to the ELAN team's permanent members.

François guided me with patience in my professional life, scientific research, and personal life. He was able to share his vast experience and hard-earned knowledge in the fields of electrochemistry and chemical engineering with me, which greatly aided my research. In addition, I could not thank him enough for the pleasant conversation over the coffee break, which was filled with joy and laughter. I would like to thank Dr Caroline Bonnet and Dr Stéphane Rael for their support and the grateful moments that we shared together during the past three years.

On the other hand, I could learn from Elisabeth to think critically and creatively, marking true steps towards being a researcher. I want to thank her for the support and the warm welcome during my visits to her lab. I am also very grateful to Dr. Ievgen Mazurenko, who gave me detailed guidance and support. I had the pleasure of working with him. I would like to thank

Dr. Anne de Poulpiquet and Hiu-Mun Man for the happy moments that we passed together in Marseilles.

I'd like to thank the jury members, Prof. Edmond Magner, Dr. Florence Geneste, Prof. Jean-Marc Commenge, and Dr. Shelley D. Minteer, for agreeing to serve as reviewers or examiners for my PhD dissertation. I'd like to acknowledge the reviewers, Prof. Edmond Magner and Dr. Florence Geneste, for the valuable time that they will take while evaluating the manuscript and the work.

I would also like to thank the admin and finance departments of the laboratory, especially Ms. Christelle Charbaut and Ms. Marie Tercier, for their constant help on admin matters.

I want to thank Mr. Charly Koenig and the workshop team for their crucial support during the design and setup of the experimental bench.

To Steve Pontvianne and Xavier Framboisier, I thank you for keeping up with all the analyses.

To my fellow friends in Lebanon, France, LCPME, LRGP, and BIP, you know who you are. I thank you all for the cherishing moments that we have had together...

I would like to thank my parents for their never-ending efforts and endless encouragement, which made this possible. I also thank them for working tirelessly to make this dream come true. I especially thank my brother Ali and his wife Shaza for always being next to me and believing in me. In addition, I want to thank my little brother Zein, who always inspires me with his courage and positivity. It would not have been possible without all of your support.

Last but not least, I would like to acknowledge the French National Centre for Scientific Research for funding the 80 Prime project and, therefore, my PhD.

Table of contents

List of figures

List of Schemes

List of tables

Abbreviations

Ag/AgCl	Silver chloride electrode
BES	Bioelectrochemical system
CE	Counter electrode
CP	Carbon paper
CP-MWCNT	Carbon paper coated with multi-walled carbon nanotubes
CV	Cyclic Voltammetry ($V.s^{-1}$)
D	Diffusivity ($m^2.s^{-1}$)
DCM	Dichloromethane
ECN	Electrochemical noise
ee	Enantiomeric excess
EFC	Enzymatic fuel cell
FAD	Flavin adenine dinucleotide
FDH	Formate dehydrogenase
FMN	Flavin mononucleotide
FNR	Ferredoxin $NADP^+$ reductase
FNR@CP-MWCNT	FNR immobilized on CP-MWCNT
GDE	Gas diffusion electrode
GDL	Gas diffusion layer
Ha	Hatta number
Hyd-1	*Aquifex aeolicus* Hydrogenase I
I	Current (A)
k	Rate constant ($m^3.mol^{-1}.s^{-1}$)
k_L	Mass transfer coefficient ($m.s^{-1}$)

LDH	L-lactate dehydrogenase
LDH@CP-MWCNT	LDH immobilized on CP-MWCNT
LSV	Linear sweep voltammetry ($V.s^{-1}$)
MWCNT	Multi-walled carbon nanotubes
$MWCNT_{NH2}$	Multi-walled carbon nanotubes functionalized with amine function
$MWCNT_{ox}$	Oxidized multi-walled carbon nanotubes
N212	Nafion membrane
NAD^+	Nicotinamide adenine dinucleotide (oxidised)
NADH	Nicotinamide adenine dinucleotide hydride (reduced)
$NADP^+$	Nicotinamide adenine dinucleotide phosphate (oxidised)
NADPH	Nicotinamide adenine dinucleotide phosphate hydride (reduced)
NMP	N-Methyl-2-pyrrolidone
OCP	Open-circuit potential (V)
OCV	Open-circuit Voltage (V)
P450	Cytochrome P450
PEMFC	Proton exchange membrane fuel cell
PVDF	Polyvinylidene fluoride membrane filter
Q	Charge (A.s)
Ref	Reference electrode
Rh@CP-MWCNT	Rh complex immobilized on CP-MWCNT
TN	Turnover number (h^{-1})
TOF	Turnover frequency (h^{-1})
TTN	Total turnover number
WE	Working electrode

ZRA	Zero Resistance Amperometry

Résumé étendu

L'hydrogène s'intègre comme le vecteur énergétique du futur. H_2 a une densité énergétique massique bien supérieure à celle du méthane et du pétrole.[1] En outre, H_2 est un agent réducteur bon marché, respectueux de l'environnement et efficace. L'hydrogène peut être produit à l'aide de procédés bien connus, par exemple le reformage des hydrocarbures ou l'électrolyse de l'eau. Avec cette dernière voie, l'énergie électrique requise peut provenir de sources d'énergie renouvelables telles que l'énergie solaire et électrique.[2,3]

L'hydrogène joue un rôle clé dans les procédés chimiques de synthèse d'une large gamme de produits chimiques spécialisés/finis, dans la plupart des cas dans des réactions gaz-liquide. Souvent à des niveaux de pression bien supérieurs à la pression ambiante, ces réactions ont traditionnellement été réalisées dans des réacteurs discontinus (en batch), soit en injectant la phase gazeuse dans la phase liquide (c'est-à-dire par barbotage) pour augmenter la surface interfaciale, soit par un mélange excessif dans la phase liquide pour augmenter la turbulence locale entre les deux phases.[4] Alors que le barbotage de gaz dans les réacteurs discontinus peut facilement permettre l'apparition de réactions gaz-liquide grâce à sa facilité d'accès et d'assemblage, il présente souvent une limitation du transfert de masse gaz-liquide en raison des faibles surfaces interfaciales spécifiques.[5] Outre des problèmes de sécurité accrus, ces limitations du transfert de masse entraînent des temps d'expérimentation plus longs et des cinétiques de réaction limitées par le transfert de masse, ce qui freine le développement des procédés gaz-liquide.[5]

La « chimie en flux » peut être définie comme une réaction chimique réalisée dans un système présentant des conditions d'écoulement structurées et bien définies. Au cours de la dernière décennie, la chimie en flux s'est imposée comme une approche efficace pour les études fondamentales et appliquées des processus gaz-liquide.[4–6] Comme souligné plus loin, l'écoulement des fluides peut être mis en œuvre avec succès dans une configuration

submillimétrique pour favoriser la perturbation locale de l'écoulement, ce qui pourrait entraîner une intensification des phénomènes de transfert. En outre, la combinaison de la chimie des flux et de l'électrochimie peut apparaître comme l'option la plus viable pour jeter un pont entre les deux secteurs, en particulier dans le domaine de la synthèse (bio)organique.

Dans sa configuration la plus simple et la plus typique, une cellule à écoulement électrochimique se compose de deux électrodes à plaque se faisant face, la solution réactionnelle s'écoulant dans un canal créé par des entretoises isolantes. Dans cette configuration, les électrodes de la cellule à écoulement sont parallèles. Sa large applicabilité pour l'électrosynthèse organique est le résultat de sa fabrication simple et de la distribution uniforme du potentiel et du courant due à la configuration d'électrodes parallèles. [7] Des progrès significatifs ont récemment été réalisés dans les procédés électrochimiques organiques tels que le microécoulement, c'est-à-dire les réacteurs électrochimiques submillimétriques,[8–10] et l'électrochimie bipolaire.[11]

Pour réaliser l'électrosynthèse, le courant électrique est évidemment fourni par une source d'énergie électrique dans des cellules électrolytiques. Cependant, le réacteur d'électrosynthèse n'étant pas relié à une source d'énergie électrique, des réactions aux électrodes peuvent se produire spontanément. Ces réactions spontanées peuvent se produire dans deux cas principaux. Premièrement, pour des raisons thermodynamiques, avec des variations globales négatives de l'enthalpie libre entre les produits générés aux électrodes et les réactifs consommés, comme dans les piles à combustible par exemple. Deuxièmement, par l'existence d'un potentiel d'écoulement généré par un flux laminaire d'électrolyte comme énergie motrice pour les réactions aux électrodes. Le potentiel d'écoulement est causé par un gradient de pression passant par des canaux aux parois chargées. Il s'agit d'un phénomène électrocinétique qui intervient dans l'analyse des potentiels zêta des matériaux et des surfaces colloïdales.[12]

Sur la base des nouvelles technologies liées au couplage de la chimie en flux et de l'électrochimie, des réactions gaz-liquide, et de l'émergence de l'H_2 comme source d'énergie propre, l'idée de ce travail est de coupler l'oxydation de l'hydrogène à la réduction du $NAD(P)^+$ dans un réacteur hybride combinant la technologie des piles à combustible et le dispositif d'écoulement redox comme le montre la **figure 1**. L'idée est de compartimenter ces deux réactions catalysées électrochimiquement par des catalyseurs redox, chimiques ou biologiques, et de les coupler séparément. Le NAD(P)H régénéré peut ensuite être couplé à une réaction dépendante du NAD(P), par exemple la biosynthèse d'un alcool par réaction entre une fonction carbonyle et le NAD(P)H catalysée par une alcool déshydrogénase, comme dans la réaction illustrée en **figure 1**.

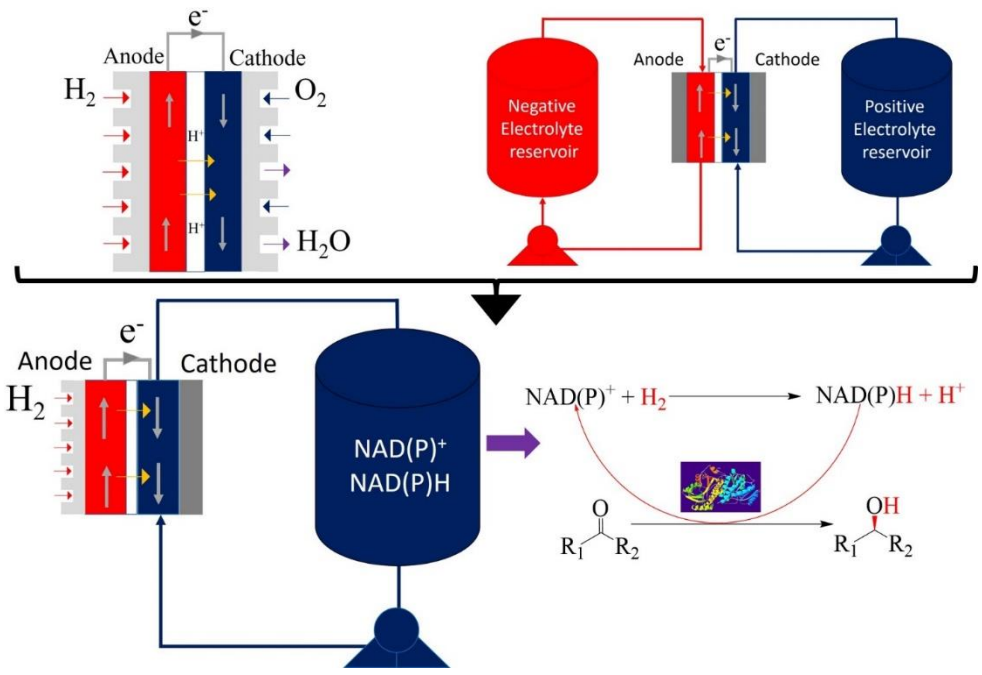

Figure 1. Bioréacteur à flux hybride couplant la technologie des piles à combustible et le dispositif en flux redox pour la régénération du cofacteur NAD(P)H.

En tenant compte du fait que les potentiels redox standards entre l'oxydation de l'hydrogène et le biocatalyseur de régénération du NAD(P) sont proches, des travaux antérieurs ont rapporté la régénération sans courant du NAD(P)H dans des systèmes où tous les catalyseurs sont co-

immobilisés sur les mêmes particules conductrices, *par exemple* des particules de carbone. Malgré les bons résultats obtenus, qui prouvent la simplicité des particules recouvertes de deux catalyseurs,[13] la reproductibilité du système lorsqu'il est couplé à une réaction enzymatique avec des niveaux élevés de TTNs (de l'ordre de 10^5 pour le catalyseur électroenzymatique) même dans des systèmes à flux, [14] combinant les deux types de catalyseurs sur le même support peut souffrir de certaines limitations. Par exemple, pour l'oxydation couplée de l'hydrogène par l'hydrogénase et la réduction du $NADP^+$ par la ferredoxine $NADP^+$ réductase (FNR), on a constaté que l'hydrogénase est active sur les nanotubes de carbone fonctionnalisés par des fonctions amine[15] tandis que la FNR est active sur une électrode ITO, comme l'ont rapporté précédemment Armstrong et ses collaborateurs.[16] Par conséquent, le couplage de ces deux catalyseurs sur la même électrode semble impossible.

D'autre part, la désactivation d'un des deux biocatalyseurs, hydrogénase ou NAD^+ réductase, placés sur la même électrode peut conduire à une perte de l'électrode ou à la nécessité de séparer les deux catalyseurs sur leur support afin de récupérer le catalyseur actif. De plus, bien que la régénération du NADH soit possible sur une surface d'électrode avec du platine et du complexe de rhodium[17] pour l'oxydation de l'hydrogène et la réduction du $NAD(P)^+$ respectivement, la récupération de l'électrode après désactivation sur un catalyseur sera impossible puisque la surface de l'électrode a été modifiée par la fonctionnalisation. Il semble d'après ces exemples que l'immobilisation des deux catalyseurs sur la même électrode soit techniquement non viable.

En outre, il a été démontré que l'interaction entre un catalyseur chimique tel que le complexe de rhodium et un catalyseur biologique tel que le NAD(P)H dépendant utilisé dans la synthèse de composés chimiques sur la même électrode, contribue à une désactivation du catalyseur biologique.[18] Une désactivation de l'hydrogénase pourrait se produire lorsqu'elle est immobilisée sur la même électrode avec un complexe chimique pour la régénération du NAD(P)H, par exemple le complexe de Rh[17]. Compte tenu des éventuels inconvénients

susmentionnés de l'utilisation des deux catalyseurs pour coupler l'oxydation de H_2 à la régénération du NAD(P)H, nous pensons que la séparation des deux catalyseurs est plus avantageuse.

Cette thèse présente une étude hiérarchique rapportant des voies pour la régénération efficace du cofacteur NAD(P)H couplée à l'oxydation de l'hydrogène dans un réacteur hybride en flux.

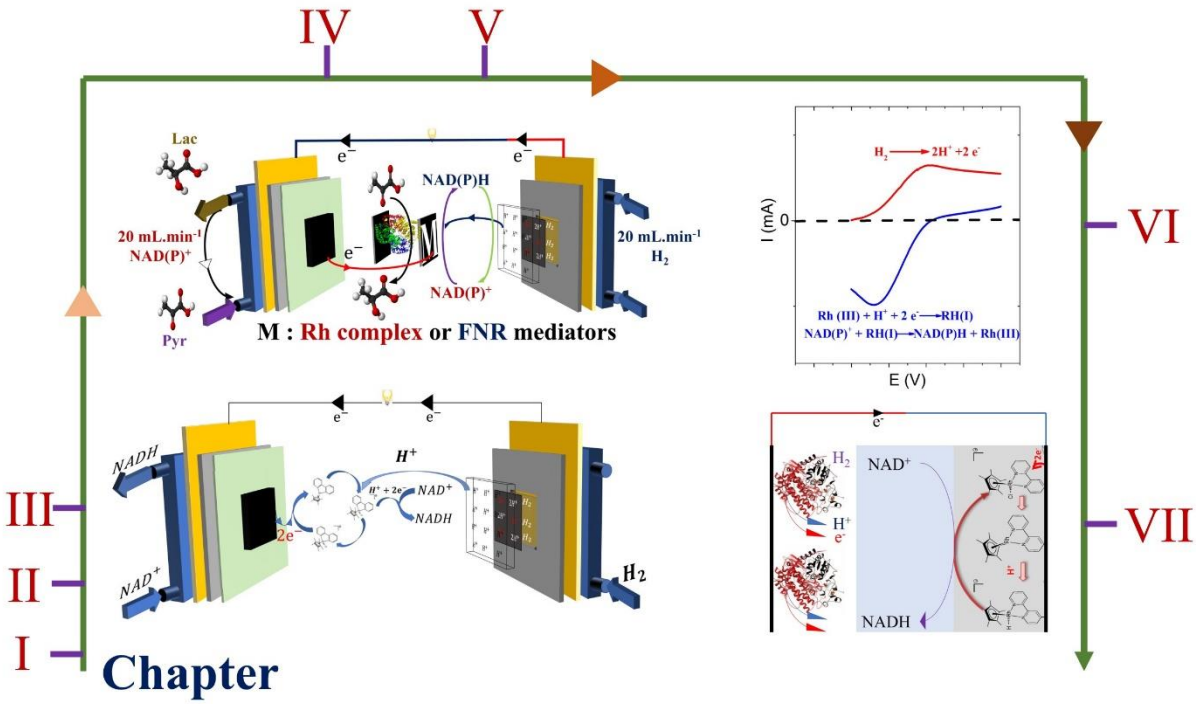

Le manuscrit commence par une étude bibliographique dans le **chapitre I** qui présente le contexte de la biocatalyse et ses avantages par rapport à la synthèse organique conventionnelle, les cofacteurs enzymatiques et leurs méthodes de régénération, les stratégies récentes pour étendre la catalyse redox dans les applications de biosynthèse, les technologies des piles à combustible, l'électrochimie en flux et les approches rapportant la régénération électrochimique des cofacteurs en flux.

Dans les **Chapitres II et III,** nous avons démontré le plein potentiel d'un réacteur bioélectrochimique de 16 cm² de surface externe pour la régénération du NADH qui couple efficacement l'oxydation de l'hydrogène à la réduction du NAD^+ médiée par un complexe de

rhodium : une activité élevée avec un TN de 370 h^{-1} pour une valeur de TTN proche de 40 pour le complexe de rhodium a été démontrée.

La régénération efficace du NADH, avec une conversion complète et un rendement faradique élevé, peut être obtenue en fixant différents paramètres du réacteur utilisé à leurs valeurs optimales : débits d'hydrogène et de solution (20 $mL.min^{-1}$), rapport de concentration entre NAD^+ et $[Cp^*Rh(bpy)Cl]^+$ (40), pH (proche de la neutralité, pour éviter la dégradation du NADH et du NAD^+).

Sur la base de ces paramètres optimisés pour la régénération du cofacteur NADH, l'ajout d'une réaction enzymatique pour la bioconversion du pyruvate en lactate par la LDH-CP-MWCNT a montré sa grande efficacité et stabilité avec un TTN élevé pour la régénération électrochimique du cofacteur et la réaction enzymatique de 2000 et $6.3*10^6$, respectivement. En outre, aucune désactivation du complexe de rhodium et de la LDH n'a été observée ici (une désactivation possible est signalée dans la littérature[18]).

Bien que les performances concernant le TN et le TTN du catalyseur au rhodium en solution soient supérieures à celles rapportées dans la littérature, il faut savoir que le TN et le TTN du catalyseur sont toujours inférieurs à l'électrogénération enzymatique associée à l'immobilisation de surface.[16,19] De plus, le TTN du cofacteur dans la synthèse électroenzymatique reste largement inférieur à ceux des études les plus récentes avec un catalyseur enzymatique étroitement confiné et immobilisé à la surface d'électrodes poreuses.[20]

Ensuite, la modélisation de l'efficacité des réactions électrochimiques médiées menées à un potentiel fixe, en termes de densité de courant et de taux de conversion, en utilisant l'approche développée dans l'absorption gaz-liquide accompagnée d'une réaction chimique du gaz dissous, a été étudiée. La méthode reposant ici sur le processus électrochimique contrôlé par diffusion et appliquée à la régénération du NADH médiée par un complexe de Rh, a permis d'estimer la

constante de vitesse des réactions chimiques entre Rh(I) et NAD^+, par rapport au coefficient de transfert de masse à la surface de l'électrode. De plus, comme il a été démontré que le processus chimique est suffisamment rapide, c'est-à-dire qu'il se produit presque uniquement dans le film de diffusion, la conversion électrochimique du NAD^+ en NADH à un potentiel fixe peut être modélisée comme si le NAD^+ était directement réduit à la surface de la cathode.

La validité de cette approche simple dépend néanmoins de la validité des hypothèses formulées et liées, d'abord au processus électrochimique contrôlé par diffusion, puis à la réaction chimique rapide entre le substrat B et les espèces générées A_1. Dans le cas où la réaction n'est pas assez rapide (Ha < 3), le modèle pour le processus électrochimique par lots doit être modifié en insérant le terme chimique dans le bilan massique correspondant. De plus, il faut prendre soin de vérifier le mécanisme cinétique du processus chimique dans les conditions de fonctionnement étudiées.

L'immobilisation du complexe Rh et le couplage de la régénération de NADH à la conversion de pyruvate catalysée par le lactate déshydrogénase a été étudiée dans le **chapitre IV**. Grâce à l'immobilisation effective des différents catalyseurs et à des optimisations fines, le réacteur électrochimique à flux continu présenté présente des performances remarquables pour l'hydrogénation catalytique de produits chimiques purs par régénération du NADH. Le travail porte sur différents défis tels que le choix du matériau de la cathode, l'immobilisation du catalyseur redox et des enzymes, leur association ou séparation, le rapport molaire entre chacun d'entre eux, et l'utilisation de faibles quantités du cofacteur enzymatique (10 µM).

Différents aspects doivent être pris en considération pour coupler la régénération électrochimique efficace du cofacteur NADH à la bioconversion enzymatique de produits chimiques :

- L'immobilisation du complexe de Rh sur du papier carbone avec des MWCNT, et le pressage à 40 bars de cette couche catalytique avec une membrane GDE et Nafion

ont conduit à un système actif pour la régénération électrochimique efficace du système cofacteur NADH avec une stabilité de plus de 5 jours sous flux continu.

- La réduction de la distance entre le complexe de Rh et la LDH en immobilisant chacun d'entre eux sur des couches séparées et empilées a conduit à une boucle active pour la régénération continue du cofacteur et la bioconversion du pyruvate.
- Le rapport entre le complexe de Rh immobilisé et les unités d'enzymes doit être au moins égal à 10 afin d'atteindre l'efficacité faradique (79 %), la productivité (1,08 $\mu mol.cm^{-2}.h^{-1}$) et la TTN les plus élevées pour le cofacteur (2500), le catalyseur au rhodium (18000) et l'enzyme (180000).
- Enfin, les débits d'hydrogène et de solution peuvent être fixés à 20 $mL.min^{-1}$ dans la cellule de banc comme décrit précédemment[21] et le potentiel d'électrolyse appliqué à -0,3 V réf. (H_2). De plus, la cellule à écoulement a été construite avantageusement en utilisant une électrode en feutre de graphite permettant une distribution uniforme de la solution dans le compartiment cathodique et assurant un contact électrique entre les couches fonctionnelles et le collecteur de courant de la cellule.

Dans le **chapitre V,** nous avons démontré le plein potentiel d'un réacteur électroenzymatique à flux qui couple efficacement la régénération de NAD(P)H à l'oxydation de l'hydrogène où la FNR, Ferrédoxine $NADP^+$ réductase, a été immobilisé sur du papier carbone recouvert de MWCNT oxydés. L'électrode préparée de FNR@CP-$MWCNT_{ox}$ a montré son activité avec le temps pendant plus de 6 jours sous électrolyse et flux continus.

De plus, dans l'ensemble des expériences présentées, le FNR montre son activité non seulement pour la régénération du cofacteur NADPH, mais aussi pour le cofacteur NADH, ce qui n'a pas été rapporté dans les travaux précédents. La régénération électroenzymatique du NADH par la

FNR a été couplée à la bioconversion du pyruvate et a montré que la forme active du NADH a été régénérée (1,4-NADH).

Dans ce travail, les techniques expérimentales, à savoir l'immobilisation de FNR sur des MWCNT oxydés, l'immobilisation de FNR et de LDH sur des couches CP-MWCNT superposées mais distinctes, ainsi que les conditions opératoires, *par exemple* une température de 35°C et un rapport FNR : LDH proche de 5, ont été largement améliorées. Dans des conditions optimales, le système de bioconversion du pyruvate en lactate avec de faibles quantités de cofacteur (10 µM) a obtenu des niveaux élevés de TTNs pour la FNR, le NAD^+ et la LDH avec 1,2 x 10^5 , 10^4 et 6 x 10^5 respectivement, avec une efficacité faradique de 88 % et une productivité de 156 $nmol.h^{-1}$ .cm^{-2} .$nmol^{-1}$ FNR. La mise à l'échelle du système de 60 mL à 600 mL s'est avérée réussie avec un niveau de productivité élevé conservé (113 $nmol.h^{-1}$ .cm^{-2} .$nmol^{-1}$ FNR), des niveaux élevés de TTNs pour FNR, NAD^+ , et LDH de 1,82 x 10^5 , 9200, et 9,2 x 10^5 respectivement, et une efficacité faradique de 83 %. Ces résultats suggèrent que l'exploration linéaire à 5L de solution, par exemple, pourrait être possible avec l'application de cascades d'électrodes à la fois de FNR@CP-$MWCNT_{ox}$ et de LDH@CP-MWCNT supportées par des quantités élevées d'enzymes.

Dans le **chapitre VI,** nous avons pu coupler l'oxydation de l'hydrogène à la régénération du NADH en tirant avantage des potentiels standard proches de l'hydrogène et du complexe Rh.

Avec l'électrode combinée (Rh@GDE), à un pH de 7,2 (50 mM PBS), une réduction totale

du NAD^+ a été obtenue, mais conduisant à une forme inactive malgré la capacité du complexe Rh à régénérer la forme active du NADH comme indiqué précédemment. [17,22]

D'autre part, le couplage de l'oxydation de l'hydrogène sur un GDE à la régénération du NADH sur une électrode Rh@CP-MWCNT dans le réacteur à flux a montré une régénération totale du NADH sous une forme active à 0 V avec les conditions suivantes :

- pH = 7,2 et débits d'hydrogène et de solutions égaux à 20 mL.min^{-1} [21] et l'immobilisation du complexe Rh sur CP-MWCNT[23]

- La séparation entre les compartiments anodique et cathodique avec une grille en plastique au lieu d'une membrane Nafion pour diminuer la résistance du système.

- Le rapport entre le complexe de Rh et le Pt doit être égal à 2,07 nmol de complexe de Rh actif/mg de Pt.

Ces résultats montrent qu'il est nécessaire de séparer les catalyseurs pour régénérer efficacement le NADH actif. Cela ouvre la voie à une biosynthèse globale basée sur le NADH sans apport d'énergie externe.

Le NADH pourrait alors être couplé à une réaction enzymatique, par *exemple* la bioconversion du pyruvate en lactate catalysée par la LDH ou la bioréduction du CO_2 catalysée par la formate déshydrogénase, avec l'application de faibles quantités de NAD^+ (10 µM) comme indiqué précédemment.[23]

Dans le **Chapitre VII**, le présent travail a conduit à la conception d'un système de régénération électrochimique du cofacteur NADH reposant sur l'oxydation de l'hydrogène catalysée par une hydrogénase tolérante à l'O_2 (Hyd-1) et la réduction du NAD^+ médiée par un complexe de rhodium dans un système en batch.

En sélectionnant des MWCNT aminés comme support électroactif pour l'immobilisation de l'hydrogénase, différents paramètres du système ont été optimisés pour une oxydation enzymatique efficace de l'hydrogène sur une couche de diffusion gazeuse, à savoir le dépôt de MWCNT et de Hyd-1 sur la surface du MPL, les quantités de MWCNT et d'hydrogénase (1 pmol Hase : 2,5 µL MWCNT) et la température (40 °C).

Le couplage de l'oxydation de l'hydrogène à la réduction du NAD^+ a montré une différence de potentiel entre les deux couches catalytiques supérieure à 0,12 V. Afin de surmonter ce

problème et de permettre une éventuelle régénération spontanée du cofacteur sans potentiel appliqué, des développements supplémentaires doivent encore être réalisés, notamment par :

- la diminution de l'écart entre les électrodes - actuellement près de 2 mm.

- l'augmentation de la taille des électrodes et/ou les quantités de $MWCNT_{NH2}$ -Hyd-1 sur GDL et le complexe Rh immobilisé de manière covalente CP-MWCNT. Nous avons récemment observé que l'augmentation de la quantité de complexe Rh en utilisant deux électrodes Rh@CP-MWCNT empilées au lieu d'une seule, déplace positivement le potentiel de réduction.[23]

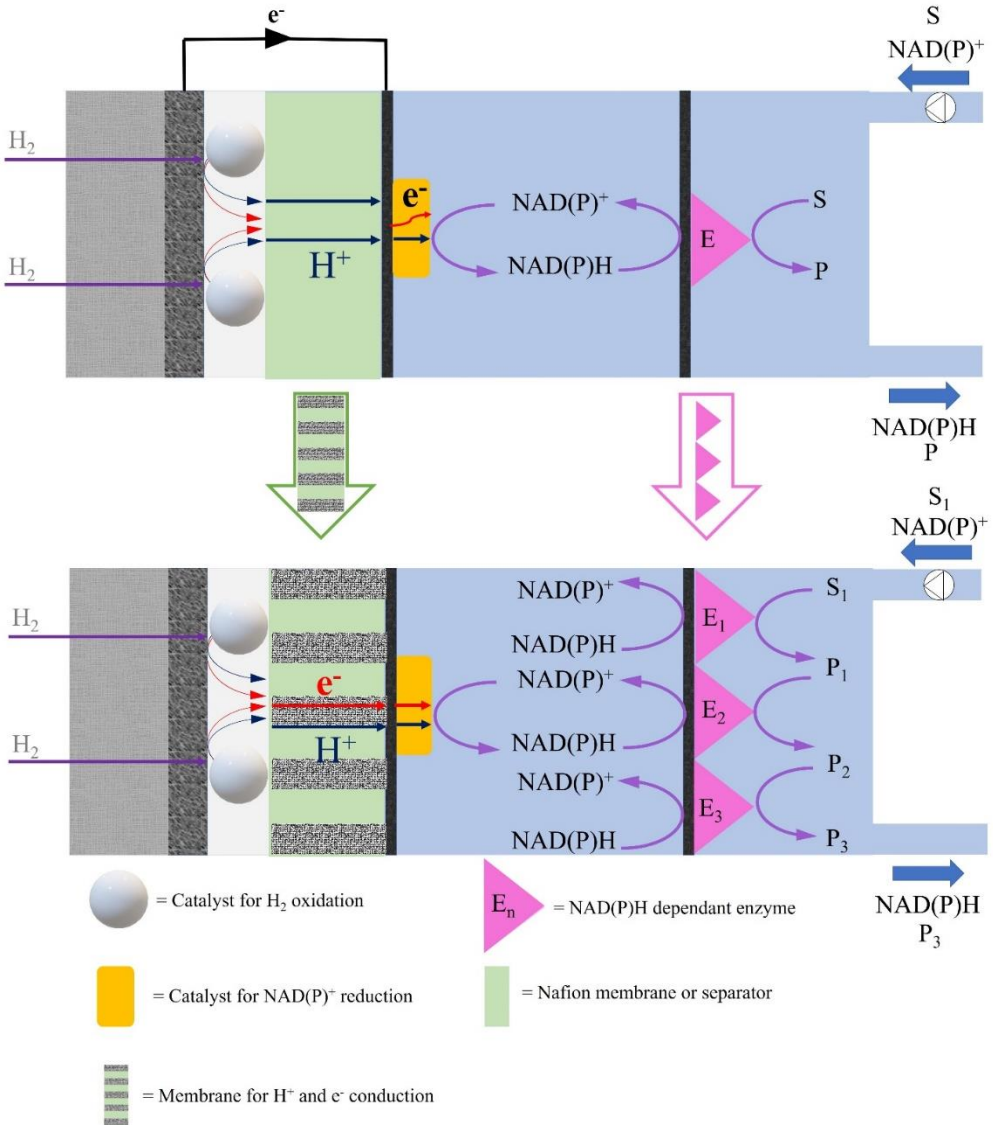

Schéma 1. Représentation cartographique du réacteur bioélectrochimique mis au point pour coupler l'oxydation de H_2 à la régénération du NADH, avec perspectives d'avenir.

Le système présenté montre le couplage du NAD(P)H régénéré à une réaction mono NAD(P) dépendante. Dans des travaux ultérieurs, le système de régénération des cofacteurs pourrait être couplé à une cascade de réactions enzymatiques comme le montre le **schéma 1**. Les cascades biocatalytiques permettent de contourner l'isolement des intermédiaires de réaction, ce qui permet d'économiser du temps et des réactifs. En outre, il est possible de synthétiser des produits chimiques avec des intermédiaires instables, car il est inutile d'isoler les intermédiaires.[24]

L'un des exemples de réactions enzymatiques en cascade est la bioconversion du CO_2. Kuk et al. ont développé un système photoélectrochimique pour la production de méthanol à partir de CO_2 par une cascade multienzyme ,un système de cascade à trois déshydrogénases, et la régénération efficace de NADH à l'aide de la lumière visible.[25]

Pour approfondir l'étude, la séparation des compartiments anodique et cathodique peut être explorée en remplaçant le séparateur par une membrane présentant une conductivité protonique et électronique, par exemple, une membrane MWCNT imprégnée de dérivés époxydiques [26] ou la fabrication d'une membrane copolymère pour l'échange de protons et d'anions (Nafion-polyaniline). Cette membrane améliorerait la connexion et le transport de charge du compartiment anodique à la chambre cathodique, comme le montre la partie inférieure du **schéma 1**.

Références

[1] L. Lauterbach, O. Lenz, *Curr. Opin. Chem. Biol.* **2019**, *49*, 91–96.

[2] B. Konkena, I. Sinev, S. Piontek, O. Khavryuchenko, J. P. Dürholt, R. Schmid, H. Tüysüz, M. Muhler, W. Schuhmann, U.-P. Apfel, others, *Nat. Commun.* **2016**, *7*, 1–8.

[3] E. Ture, in *Assess. Hydrog. Energy Sustain. Dev.*, Springer, **2007**, pp. 135–146.

[4] T. Noël, V. Hessel, *ChemSusChem* **2013**, *6*, 405–407.

[5] C. J. Mallia, I. R. Baxendale, *Org. Process Res. Dev.* **2016**, *20*, 327–360.

[6] F. M. Akwi, P. Watts, *Chem. Commun.* **2018**, *54*, 13894–13928.

[7] M. Atobe, H. Tateno, Y. Matsumura, *Chem. Rev.* **2017**, *118*, 4541–4572.

[8] M. Elsherbini, T. Wirth, *Acc. Chem. Res.* **2019**, *52*, 3287–3296.

[9] K. Mitsudo, Y. Kurimoto, K. Yoshioka, S. Suga, *Chem. Rev.* **2018**, *118*, 5985–5999.

[10] J. Yoshida, A. Shimizu, R. Hayashi, *Chem. Rev.* **2017**, *118*, 4702–4730.

[11] S. Iwai, T. Suzuki, H. Sakagami, K. Miyamoto, Z. Chen, M. Konishi, E. Villani, N. Shida, I. Tomita, S. Inagi, *Commun. Chem.* **2022**, *5*, 1–7.

[12] Á. V Delgado, F. González-Caballero, R. J. Hunter, L. K. Koopal, J. Lyklema, *J. Colloid Interface Sci.* **2007**, *309*, 194–224.

[13] J. A. Cracknell, K. A. Vincent, F. A. Armstrong, *Chem. Rev.* **2008**, *108*, 2439–2461.

[14] X. Zhao, S. E. Cleary, C. Zor, N. Grobert, H. A. Reeve, K. A. Vincent, *Chem. Sci.* **2021**, *12*, 8105–8114.

[15] E. Lojou, *Electrochim. Acta* **2011**, *56*, 10385–10397.

[16] B. Siritanaratkul, C. F. Megarity, T. G. Roberts, T. O. M. Samuels, M. Winkler, J. H. Warner, T. Happe, F. A. Armstrong, *Chem. Sci.* **2017**, *8*, 4579–4586.

[17] L. Zhang, M. Etienne, N. Vilà, T. X. H. Le, G.-W. Kohring, A. Walcarius, *ChemCatChem* **2018**, *10*, 4067–4073.

[18] F. Hildebrand, S. Lütz, *Chem. - A Eur. J.* **2009**, *15*, 4998–5001.

[19] M. Yuan, M. J. Kummer, R. D. Milton, T. Quah, S. D. Minteer, *ACS Catal.* **2019**, 5486–5495.

[20] C. F. Megarity, B. Siritanaratkul, R. S. Heath, L. Wan, G. Morello, S. R. FitzPatrick, R. L. Booth, A. J. Sills, A. W. Robertson, J. H. Warner, N. J. Turner, F. A. Armstrong, *Angew. Chemie - Int. Ed.* **2019**, *58*, 4948–4952.

[21] W. El Housseini, F. Lapicque, A. Walcarius, M. Etienne, *Electrochem. Sci. Adv.* **2021**, 1–11.

[22] B. Tan, D. P. Hickey, R. D. Milton, F. Giroud, S. D. Minteer, *J. Electrochem. Soc.* **2015**, *162*, H102–H107.

[23] W. El Housseini, F. Lapicque, S. Pontvianne, N. Vilà, I. Mazurenko, A. Walcarius, M. Etienne, *ChemElectroChem* **2022**, *9*, e202200463.

[24] J. H. Schrittwieser, S. Velikogne, M. Hall, W. Kroutil, *Chem. Rev.* **2018**, *118*, 270–348.

[25] S. K. Kuk, R. K. Singh, D. H. Nam, R. Singh, J. K. Lee, C. B. Park, *Angew. Chemie - Int. Ed.* **2017**, *56*, 3827–3832.

[26] G. A. Pilgrim, J. W. Leadbetter, F. Qiu, A. J. Siitonen, S. M. Pilgrim, T. D. Krauss, *Nano Lett.* **2014**, *14*, 1728–1733.

Scientific production

Papers in peer-reviewed journals

1. **El Housseini**, W., Lapicque, F., Pontvianne, S., Vilà, N., Mazurenko, I., Walcarius, A., & Etienne, M. (2022). Hybrid flow bioreactor with all catalysts immobilized for enzymatic electrosynthesis. ChemElectrochem, 9(16), e202200463.

2. **El Housseini, W**., Lapicque, F., Walcarius, A., & Etienne, M. (2021). A hybrid electrochemical flow reactor to couple H_2 oxidation to NADH regeneration for biochemical reactions. *Electrochemical Science Advances*, e202100012.

3. Berrada, N., **El Housseini, W.**, Desforges, A., Gleize, J., Ghanbaja, J., Etienne, M., & Vigolo, B. Multiwalled Carbon Nanotube Purification Probed by Electrochemistry: Low Temperature Chlorine Gas Treatment Meets High Temperature Annealing. ChemnanoMat. accepted.

4. **El Housseini, W**., Lapicque, F., Walcarius, A., & Etienne, M. (2021). A hybrid electrochemical flow reactor to couple H_2 oxidation to NADH regeneration for biochemical reactions. *Electrochemical Science Advances*, e202100012.

Oral and poster presentations

1. **Wassim El Housseini,** François Lapicque, Elisabeth Lojou, Neus Vila, Alain Walcarius, Mathieu Etienne., "Efficient Electrochemical Regeneration of the NAD(P)H cofactor", *Accepted for oral presentation at French Group of Bioelectrochemistry 2022, Saint-Dié- des-Vosges, France.*

2. **Wassim El Housseini**, François Lapicque, Elisabeth Lojou, Nicolas Rouhier, Neus Vila, Alain Walcarius, Mathieu Etienne. "NAD(P)H Cofactor Electroenzymatic Regeneration for Selective Biocatalytic Reductions in a Hybrid Flow Reactor" *Accepted for oral presentation at ISE online meeting 2022, Xiamen,China.*

3. **Wassim El Housseini,** Mathieu Etienne, Elisabeth Lojou, Alain Walcarius, François Lapicque. "Modelling of a hybrid bioelectrocatalytic flow reactor combining NADH cofactor regeneration by immobilized rhodium mediator for pyruvate bioconversion", *Accepted for oral presentation at Electrochemistry Day 2022, Mons,Belgium.*

4. **Wassim El Housseini,** François Lapicque, Elisabeth Lojou, Alain Walcarius, Mathieu Etienne. "Gas-Liquid reactor design for cofactors regeneration", *Accepted for Poster presentation at Summer school of flow chemistry, Lille, France.*

5. **Wassim El Housseini**, François Lapicque, Elisabeth Lojou, Nicolas Rouhier, Neus Vila, Alain Walcarius, Mathieu Etienne. "Comparative study between the electrochemical and the electroenzymatic regeneration of the NADPH cofactor" *Accepted for oral presentation at ISE online meeting 2021, Jeju Island, Korea.*

6. **Wassim El Housseini,** François Lapicque, Elisabeth Lojou, Nicolas Rouhier, Neus Vila, Alain Walcarius, Mathieu Etienne., "Electroenzymatic Regeneration of NAD(P)H cofactor", *Accepted for oral presentation at French Group of Bioelectrochemistry online meeting 2021, France.*

7. **Wassim El Housseini,** François Lapicque, Elisabeth Lojou, Neus Vila, Alain Walcarius, Mathieu Etienne., "Efficient Electrochemical Regeneration of the NAD(P)H cofactor", *Accepted for oral presentation at Bioelectrochemical Society online meeting 2021, Cluj, Romania.*

8. **Wassim El Housseini,** François Lapicque, Elisabeth Lojou, Neus Vila,Alain Walcarius, Mathieu Etienne., "Optimized bioreactor for coupling efficiently H_2 oxidation to NADH regeneration", *Accepted for oral presentation at ISE online meeting 2020,Belgrade,Serbia.*

9. **Wassim El Housseini,** François Lapicque Elisabeth Lojou, Ievgen Mazurenko, Neus Vila, Alain Walcarius, Mathieu Etienne., "Optimized bioreactor for coupling efficiently H_2 oxidation to NADH regeneration", *Accepted for poster presentation at SMCBS 2019, Poland.*

General Introduction

Hydrogen, H_2 – also denamed dihydrogen- is integrating as the energy carrier of the future. H_2 has a much greater energy density per weight than methane and petroleum.[1] Moreover, H_2 is a cheap, environmentally friendly, and effective reducing agent. In addition, hydrogen can be produced using well known processes *e.g.*, hydrocarbon reforming or water electrolysis. With this later route, the electrical energy required can originate from renewable energy sources such as solar and electrical energy.[2,3]

Hydrogen has a key role in chemical processes for the synthesis of a wide range of specialty/fine chemicals, in most cases in gas–liquid reactions. Often at pressure levels far above the ambient one, these reactions have traditionally been carried out in batch (flask-based) reactors, either by sparging the gas phase into the liquid phase (i.e., bubbling) to increase the interfacial area or by excessive mixing within the liquid phase to enhance the local turbulence between the two phases.[4] While gas bubbling in batch reactors can easily allow the occurrence of gas–liquid reactions by its ease of access and assembly, it often exhibits a gas–liquid mass transfer limitation due to low specific interfacial areas.[5] Aside from increased safety concerns, such mass transfer limitations result in longer residence time and slower overall reaction kinetics, stifling further development of important gas–liquid reactions.[5]

Flow chemistry can be defined as chemical reactions carried out in systems with well-defined, structured flow conditions. Flow chemistry has emerged as an effective approach for fundamental and applied studies of gas–liquid processes over the last decade.[4–6] As emphasized later, flow of fluids can successfully be implemented in submillimetric configurations to promote flow disruption, which could result in intensification of transfer phenomena. In addition, combination of flow chemistry and electrochemistry may appear to be the most viable option for bridging the two sectors, in particular in the area of (bio)organic synthesis.

In its simplest and most typical configuration, an electrochemical flow cell would consist of two plate electrodes facing each other, with the reaction solution flowing through a channel created by isolating spacers. In this configuration, the electrodes of the flow cell are parallel. Its wide applicability for organic electrosynthesis is a result of its simple fabrication and uniform potential and current distribution due to the configuration of parallel electrodes. [7] Significant progress has recently been made in organic electrochemical processes such as microflow, i.e. submillimetric electrochemical reactors,[8–10] and bipolar electrochemistry.[11]

For completion of electrosynthesis, the electric current is clearly supplied by an electric power source in electrolytic cells. However, if the electrosynthesis reactor is not connected to an electric power source, reactions at the electrodes may occur spontaneously. These spontaneous reactions can occur in two main cases. First, for thermodynamic reasons, with negative overall variations of the free energy between the products generated at the electrodes and the reactants consumed, as is fuel cells for instance. Secondly, by the existence of a streaming potential generated by a laminar flow of electrolyte as a driving energy for electrode reactions. Streaming potential is caused by a pressure gradient passing through channels with charged walls. This is a electrokinetic phenomenon which occurs in the analysis of zeta-potentials of materials and colloid surfaces.[12]

On the basis of novel technologies related to coupling flow chemistry and electrochemistry, gas-liquid reactions, and emergent H_2 as a clean source of energy, the idea in this work is to couple the oxidation of hydrogen to the reduction of $NAD(P)^+$ in a hybrid reactor combining fuel cell technology and redox flow device as shown in **Figure 1**. The idea is to compartmentalize these two reactions electrochemically catalyzed by redox catalysts, chemical catalysts or biological ones, and to couple them separately. Regenerated NAD(P)H can be then coupled to a NAD(P) dependent reaction *e.g.*, the biosynthesis of an alcohol by reaction

between a carbonyl function and NAD(P)H catalyzed by an alcohol dehydrogenase as in the reaction shown in **Figure 1**.

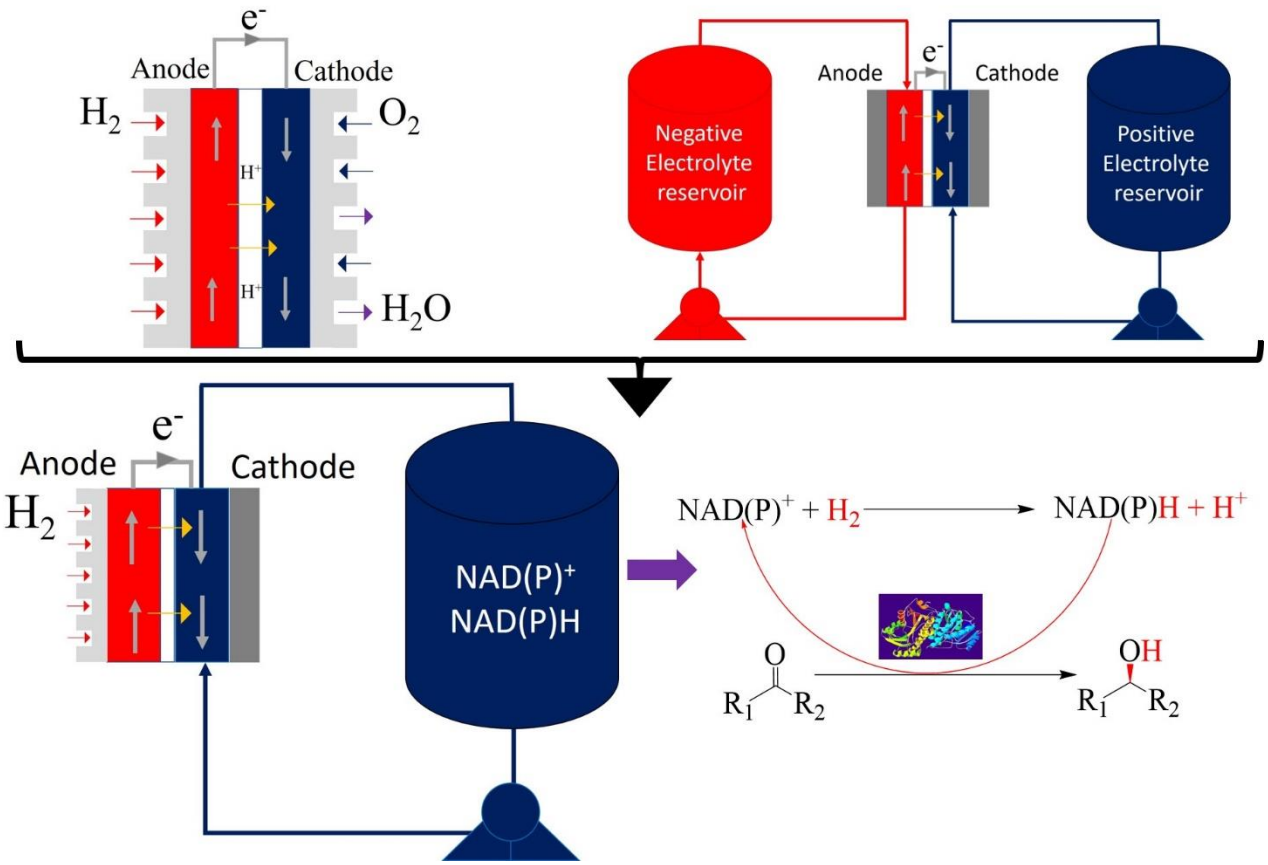

Figure 1. Hybrid flow bioreactor coupling fuel cell technology and redox flow device for the regeneration of the NAD(P)H cofactor.

Taking into consideration that the standard redox potentials between hydrogen oxidation and NAD(P) regeneration biocatalyst are close, former works report on the electroless regeneration of NAD(P)H in systems where all catalysts are co-immobilized on the same conductive particles *e.g.*, activated carbon particles. Despite the successful results obtained, that prove the simplicity of the two-catalyst-coated particles,[13] the reproducibility of the system while coupled to an enzymatic reaction with high levels of TTNs even in flow systems,[14] combining the two types of catalysts on the same support, may suffer from some limitations. For instance, for coupled hydrogen oxidation by hydrogenase and $NADP^+$ reduction by ferredoxin $NADP^+$

reductase (FNR), it was found that hydrogenase is active on carbon nanotubes functionalized by amine functions[15], whereas FNR is active on an ITO electrode as reported previously by Armstrong and co-workers.[16] Therefore, the coupling of these two catalysts on the same electrode appears impossible.

On the other hand, the deactivation of one of the two biocatalysts, hydrogenase or NAD^+ reductase, placed on the same electrode can lead to a loss of the electrode or to the necessity to separate the two catalysts on their support in order to recover the active catalyst. Moreover, although the regeneration NADH would be possible on an electrode surface covered with platinum and rhodium complex[17] covalently immobilized for the oxidation of hydrogen and the reduction of $NAD(P)^+$ respectively, the recovery of the electrode after deactivation on one catalyst will be impossible since the electrode surface had been modified by the functionalization. It seems from these examples that the immobilization of both catalysts on the same electrode is technically not viable.

In addition, it has been shown that the interaction between a chemical catalyst such as the rhodium complex and a biological catalyst such as NAD(P)H dependent used in the synthesis of chemical compounds on the same electrode, contributes to a deactivation of the biological catalyst.[18] A possible deactivation of hydrogenase can occur while casted on the same electrode with a chemical complex for NAD(P)H regeneration e.g., Rh complex[17] and cobaltocene.[19] Because of the possible aforementioned drawbacks of using both catalysts for coupling H_2 oxidation to NAD(P)H regeneration, we believe that the separation of both catalysts is more advantageous.

This thesis presents a hierarchized study reporting ways for the efficient regeneration of NAD(P)H cofactor coupled to the oxidation of hydrogen in a hybrid flow reactor.

The manuscript starts with a bibliographical study in **Chapter I** which lays out the background on biocatalysis and its advantages over conventional organic synthesis, enzymatic cofactors and

their regeneration methods, recent strategies for extending redox catalysis in biosynthetic applications, fuel cells and biofuel cells technologies, flow electrochemistry, and approaches reporting cofactors electrochemical regeneration in flow.

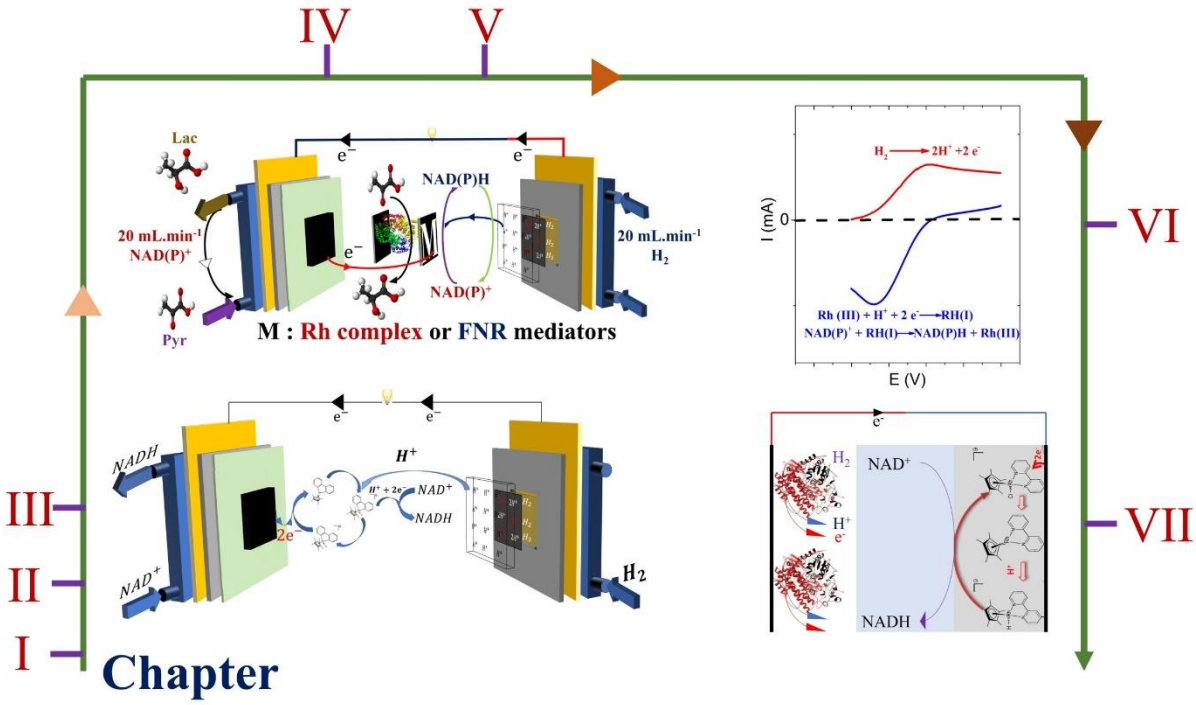

Chapter II reports the combination of the electrochemical regeneration of NADH mediated by a rhodium complex dissolved in the liquid phase, the application of the continuous flow reaction, and hydrogen oxidation on a gas diffusion layer (GDE). The proposed process has been optimized by varying the concentrations of rhodium complex and NAD^+, the pH, and the cell's operating conditions. After inserting an enzymatic module in series with the electrochemical reactor, the conversion of pyruvate to lactate by lactate dehydrogenase (LDH) was performed to test the activity of the in-situ regenerated NADH cofactor. This study's objective is to assess the effect of this redox flow technology on the performance of NADH regeneration using a well-described rhodium electrocatalyst. **Chapter III** reports the development of a model suggested by gas-liquid absorption with chemical reaction, for calculation of the concentration profiles in the vicinity of the electrode surface based on the

operating conditions and rate constant k for the redox reaction between the reduced Rh complex form and NAD^+ species.

In view to using the immobilized complex for NADH electrochemical regeneration, **Chapter IV** investigates two crucial aspects. First, the method for immobilization of the rhodium complex $[Cp^*Rh(bpy)Cl]^+$ relies upon carbon-based supports to obtain Rh-grafted matrices with high stability and activity in the redox flow reactor. Then, LDH was immobilized and placed closely to Rh complex system to facilitate the rapid transfer of NAD^+/NADH from the molecular catalyst to the enzymatic catalyst.

In **Chapter V,** Rhodium complex was replaced by an electroenzymatic catalyst, FNR. The objective of this study was to compare the behaviors of Rh complex and FNR in a flow reactor and to test the activity and the stability of FNR immobilized on carbon support with time. FNR was then coupled to the bioconversion of pyruvate to lactate. Then, a second enzyme, which could be any of several hundred NADP(H)-dependent dehydrogenases, has been immobilized on a second CP-MWCNT. In this study, lactate dehydrogenase (LDH) was chosen for the bioconversion of pyruvate to lactate.

The coupling of hydrogen oxidation to NADH regeneration in an overall electroless system, i.e., with no power consumption or production, was investigated in **Chapter VI** using two different approaches. The first relied on the presence of both catalysts on the same electrode, whereas the second relied on the immobilization of both catalysts on separate electrodes. Secondly, the activity of regenerated NADH was determined by coupling it to pyruvate bioconversion using lactate dehydrogenase catalysis.

The exchange of platinum by hydrogenase for hydrogen oxidation was finally investigated in **Chapter VII.**

References

[1] L. Lauterbach, O. Lenz, *Curr. Opin. Chem. Biol.* **2019**, *49*, 91–96.

[2] B. Konkena, I. Sinev, S. Piontek, O. Khavryuchenko, J. P. Dürholt, R. Schmid, H. Tüysüz, M. Muhler, W. Schuhmann, U.-P. Apfel, others, *Nat. Commun.* **2016**, *7*, 1–8.

[3] E. Ture, in *Assess. Hydrog. Energy Sustain. Dev.*, Springer, **2007**, pp. 135–146.

[4] T. Noël, V. Hessel, *ChemSusChem* **2013**, *6*, 405–407.

[5] C. J. Mallia, I. R. Baxendale, *Org. Process Res. Dev.* **2016**, *20*, 327–360.

[6] F. M. Akwi, P. Watts, *Chem. Commun.* **2018**, *54*, 13894–13928.

[7] M. Atobe, H. Tateno, Y. Matsumura, *Chem. Rev.* **2017**, *118*, 4541–4572.

[8] M. Elsherbini, T. Wirth, *Acc. Chem. Res.* **2019**, *52*, 3287–3296.

[9] K. Mitsudo, Y. Kurimoto, K. Yoshioka, S. Suga, *Chem. Rev.* **2018**, *118*, 5985–5999.

[10] J. Yoshida, A. Shimizu, R. Hayashi, *Chem. Rev.* **2017**, *118*, 4702–4730.

[11] S. Iwai, T. Suzuki, H. Sakagami, K. Miyamoto, Z. Chen, M. Konishi, E. Villani, N. Shida, I. Tomita, S. Inagi, *Commun. Chem.* **2022**, *5*, 1–7.

[12] Á. V Delgado, F. González-Caballero, R. J. Hunter, L. K. Koopal, J. Lyklema, *J. Colloid Interface Sci.* **2007**, *309*, 194–224.

[13] J. A. Cracknell, K. A. Vincent, F. A. Armstrong, *Chem. Rev.* **2008**, *108*, 2439–2461.

[14] X. Zhao, S. E. Cleary, C. Zor, N. Grobert, H. A. Reeve, K. A. Vincent, *Chem. Sci.* **2021**, *12*, 8105–8114.

[15] E. Lojou, *Electrochim. Acta* **2011**, *56*, 10385–10397.

[16] B. Siritanaratkul, C. F. Megarity, T. G. Roberts, T. O. M. Samuels, M. Winkler, J. H. Warner, T. Happe, F. A. Armstrong, *Chem. Sci.* **2017**, *8*, 4579–4586.

[17] L. Zhang, M. Etienne, N. Vilà, T. X. H. Le, G.-W. Kohring, A. Walcarius, *ChemCatChem* **2018**, *10*, 4067–4073.

[18] F. Hildebrand, S. Lütz, *Chem. - A Eur. J.* **2009**, *15*, 4998–5001.

[19] M. Yuan, M. J. Kummer, R. D. Milton, T. Quah, S. D. Minteer, *ACS Catal.* **2019**,

5486–5495.

Chapter I. Literature survey

Flow biocatalytic processes that combine several cascade reactions leading to the synthesis of molecules of interest in various industrial fields, particularly the pharmaceutical and food industries, are currently of great interest. The NAD(P)H cofactor plays a crucial role in biological systems and can also be used as an electron carrier in enzymatic systems that catalyze stereo- and regioselective reactions with significant biotechnological potential (dehydrogenases, cytochrome P450, etc.). Due to the high cost of NAD(P)H, its regeneration is required for its use in biosynthesis. Coupling efficiently hydrogen oxidation to NAD(P)H cofactor regeneration in a hybrid flow reactor was the big theme of the work in this PhD.

This literature survey covers five major parts:

The first part is an introduction covering biocatalysis and its advantages over conventional organic synthesis.

The second part reports cofactors and their regeneration methods as well as the involvement of NAD(P)H cofactor in enzymatic reactions catalyzed by NAD(P)-dependent enzymes.

Then, the third part covers recent approaches in extending redox catalysis in biosynthetic application. After a small introduction about this topic, the bibliographic research will be majorly focusing on modular approaches related to wiring the hydrogen oxidation to the regeneration of the NAD(P)H cofactor and its advantages.

The fourth part of this literature survey gives an overview about this project related to compartmentalizing and linking NAD(P)H cofactor regeneration to hydrogen oxidation in hybrid flow reactor. This section defines all technologies involved in this project such as fuel cell and biofuel cell, flow electrochemistry, approaches reporting cofactors electrochemical regeneration in flow, and carbon material electrodes.

The final part focalizes on concepts and methodologies in this work as well as a hierarchization of different included chapters for coupling hydrogen oxidation to NAD(P)H cofactor regeneration.

I.1 Introduction to biocatalysts

The processes that use enzymes or other biological catalysts (whole cells, cell extracts, etc.) to perform chemical reactions[1] are referred to as biocatalysis or biotransformation. In recent years, biocatalysis has received increasing interest from both academia and industry.[2] Humans have utilized biocatalysis as a technique for thousands of years. Our ancestors had acquired the biocatalysis techniques necessary to produce beer, cheese, and other foods and beverages in antiquity. In Mesopotamia, the Sumerians used brewer's yeast to produce alcoholic beverages over 6,000 years ago.[3] Not until the 19th century did scientists realize that it is the components of living organisms that catalyze the desired biochemical reactions. In 1814, Kirchhoff discovered that a glutinous wheat component could convert starch to sugar.[4] In the past, plant or microbial extracts were utilized to catalyze chemical reactions. In the early 20th century, scientists determined that a specific type of proteins, enzymes, was responsible for catalyzing chemical reactions, and people began to use purified enzymes to speed up chemical reactions.

There are six primary categories of enzymes, namely hydrolases, oxidoreductases, transferases, lyases, isomerases, and ligases, classified based on their functions.[5] 60 % of all industrial biotransformations are currently carried out by hydrolases responsible for hydrolysis reactions using H_2O, making them the most prevalent enzymes in biotechnology. Oxidoreductases, applied in oxidation and reduction reactions, account for 20 % of all biotransformations, placing them in second place.

By the nature of the catalyst, biocatalysts can be divided into three categories for industrial and academic use: isolated enzymes, cell extracts, and whole cell catalysts.[6] Isolated enzymes are purified target enzymes that do not contain any other protein or cell component, are simple to use to catalyze specific reactions, and frequently generate extremely pure products compared to other types of biocatalyst.[7] However, isolated enzymes are difficult to purify and manipulate which substantially increases the cost of manufacturing and storing the biocatalyst. Due to their

low cost, cell extracts containing overexpressed target enzymes are preferred in practical applications. Two types of biocatalysts can be created from cell extracts used in biocatalysis: cell lysates and crudely purified enzymes. Cell lysates are cells that have been directly lysed and contain all cellular components, including target enzymes. Cell lysate contains crudely purified enzymes. Cell extracts may have lower activity per unit weight due to the presence of numerous other proteins and cell components. Other cellular components may inhibit or impede the desired enzymatic reactions.[7] Other enzymes in the extracts may also cause side reactions and by-products, making downstream processing and purification difficult and expensive. Whole cell catalysis is gaining more and more attention recently, particularly when a desired product molecule requires a complex cascade of enzymatic reactions. Numerous molecules, especially active pharmaceutical ingredients (APIs) or drug precursors, involve extremely complex biosynthesis pathways that require the production of a group of enzymes.[8] In such a case, the entire target metabolic biosynthesis pathway is cloned and expressed in a host cell, and the entire host cell serves as a catalyst for the reactions.[9] The whole-cell catalyzed biofuel production[10,11] also makes use of the cell's native metabolic pathways, supplemented with heterogeneously expressed enzymes from other species.[6] However, the whole cell catalysis can also be hindered by side reactions and byproducts produced by other enzymes and cellular components. Some substrates or products are not membrane permeable, reducing the conversion rate or necessitating the destruction of the cells in order to harvest the products.[12] Whole cell catalysis is less effective when the substrates, solvent, or products are toxic to the cell.[12]

By the form of the catalyst, biocatalysts can also be divided into two categories namely immobilized biocatalysts and non-immobilized biocatalysts.[13] Immobilized enzymes circumvent some of the limitations of the aforementioned catalysts. By preventing enzyme denaturation brought on by organic solvents or extreme conditions such as high temperature

and extreme pH, immobilization frequently renders enzymes more stable and re-usable. Enzyme cascade reactions, in which multiple enzymes are immobilized together to carry out a series of reactions, are also more efficient when enzymes are immobilized, because intermediates do not need to diffuse into the bulk solution before being used by the next enzyme. By their methods of immobilization, biocatalysts can be further divided into three categories (**Figure I.1**): binding to a support, entrapment, and cross-linking. Through covalent bonds, ionic bonds, or van der Waals interactions, biocatalysts can bind to a physical support. Entrapment refers to the incorporation of an enzyme within a polymer network, such as polyacrylamide, silica sol–gel, or a membrane structure. Cross-linking is the linking of enzymes to form macroparticles without carriers. In this study, the majority of biocatalysts are non-covalently immobilized enzymes on carbon-based particles.

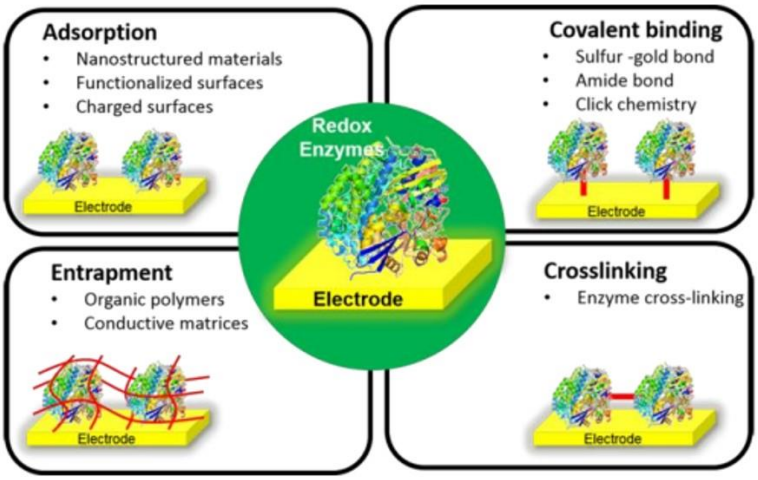

Figure I.1. Illustration of redox enzymes immobilization techniques.[14]

In general, enzymes and other biological components are less stable than conventional chemical catalysts, especially in harsh conditions such as extreme temperature or pH, organic solvent, or high concentrations of organic substrates or products. In real-world applications of chemical synthesis, enzymes typically do not act on their native substrates, so the activity of enzymes for the desired reactions may be low. In recent years, as molecular biology techniques have

advanced, directed evolution has been used to overcome these limitations in biocatalysis.[15] Directed evolution involves iterative cycles of random amino acid substitutions and rationally designed mutagenesis in a protein, followed by selection or screening of the resulting variant libraries to target a number of enzymatic properties, such as activity, substrate specificity, thermal stability, tolerance for organic solvent and extreme conditions, and chiral selectivity.[16]

Despite these limitations, enzymatic catalysis has advantages as discussed below over conventional organic synthesis methods, making it useful and in some cases irreplaceable in certain fields, particularly in pharmaceutical industry.

Why biocatalysis is more advantageous than conventional organic synthesis?

Biocatalysis has several advantages over conventional methods of organic synthesis.[17] Environmentally-friendly enzymatic catalysis requires no precious metals. In conventional organic synthesis, reduction or oxidation reactions frequently require complex catalysts containing a center of a transition metal or precious metal as well as a number of large, complex ligands. For instance, Johnson Matthey's alcohol dehydrogenase 105 catalyzes the reduction of acetophenone to (S)-1-phenylethanol with over 99 % ee at room temperature and in an aqueous phase (**Figure I.2A**). While for conventional approaches to stereo-selective hydrogenation, the use of Noyori's second generation catalyst namely ruthenium-[(S)-PPhosRuCl$_2$(S)-DAIPEN] complex,[18] of a troublesome synthesis ,[19–21] is a popular option (**Figure I.2B**).

Generally, organic methods require organic solvents and may require a strong acid or base to facilitate reactions. All of these are potentially environmentally hazardous. In contrast, biocatalysis takes a greener approach.[22] The catalysts are biomaterials produced by living organisms that are environmentally safe. Typically, the reaction conditions for biocatalysis are considerably more benign: room temperature, neutral pH, atmospheric pressure, and aqueous phase. Biocatalysis is thus not only more environmentally friendly, but also more energy

efficient.[23] As environmental factors and carbon emissions become a greater concern for the general public, biocatalysis becomes increasingly attractive to the business sector.[24]

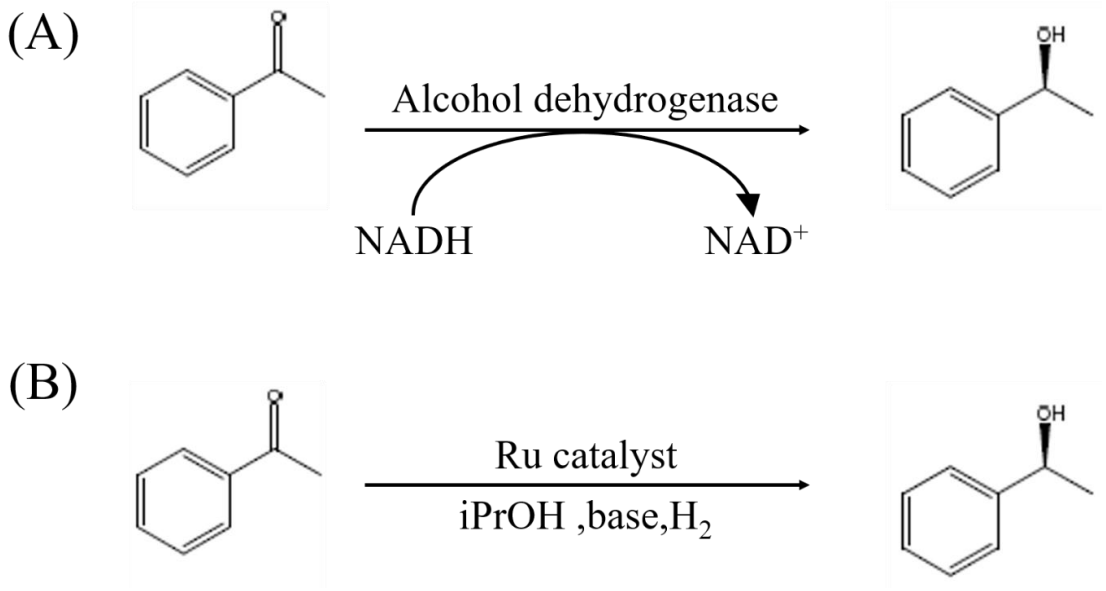

Figure I.2. The acetophenone reduction to S-phenylethanol using (A) alcohol dehydrogenase and NADH as its redox equivalent in Bis-Tris buffer (50 mM, pH 6.0) at room temperature or (B) the second generation of Noyori's catalyst, (S)-PPhos RuCl2 (S)-DAIPEN complex with a Ruthenium center and several chiral ligands, in an organic solvent containing isopropanol and a strong base, is one way to perform conventional organic synthesis.

Moreover, compared to conventional methods, enzymatic catalysis is highly stereo- and regio-selective, making it particularly useful in the pharmaceutical industry, where the majority of active compounds are chiral molecules. Enzymes can also distinguish identical functional groups in different positions of a complex molecule and target the desired group, whereas conventional synthesis requires multiple protection and de-protection steps in order to achieve chemo- or regio- selectivity.

For the production of bulk chemicals, conventional chemical methods are still used at present. Nevertheless, enzymatic catalysis has been adopted by numerous industries. Even in the bulk and fine chemical industries, biocatalysis techniques are already competing with conventional organic synthesis techniques. For instance, nitrile hydratase is utilized in the production of

acrylamide, an essential chemical commodity. Numerous hydrolases are utilized in food industry for the hydrolysis of biological macromolecules such as starches, cellulose, and proteins. Biocatalysis is receiving the most interest in pharmaceutical industry. Several pharmaceutical companies have already utilized enzymes or genetically modified bacteria to create novel antibiotics and other medications. The majority of pharmaceutical companies are also developing enzyme libraries, and biocatalysis is extensively utilized in R&D.

Biosynthesis of boceprevir,[25] a clinical drug for chronic hepatitis C infections,[26] developed by Merck, and multi-enzyme processing of hydroxynitrile,[27] a key intermediate for atorvastatin,[28] developed by Pfizer, are two examples of successful biocatalysis applications in the pharmaceutical industry.

I.2 Cofactors

Numerous enzymatic processes need the presence of cofactors. Therefore, cofactors are crucial to commercial biocatalysis. A cofactor is a non-protein chemical molecule that is necessary for the protein's biological activity. Cofactors are essential for the functioning of enzymes and are required by the majority of oxidoreductases utilized in biocatalysis. Cofactors can be inorganic ions, such as $Fe^{2+,}$ Mg^{2+}, Mn^{2+}, and Zn^{2+}, iron-sulfur clusters, or complex organic or metallo-organic compounds known as coenzymes. Coenzymes are ephemeral transporters of certain functional groups, the majority of which are produced from vitamins, which are organic micronutrients necessary in modest amounts in our diet. A cofactor that is very firmly or even covalently linked to an enzyme is referred to as a prosthetic group.[29] Nicotinamide adenine dinucleotide (NAD), nicotinamide adenine dinucleotide phosphate (NADP), flavin mononucleotide (FMN), and flavin adenine dinucleotide (FAD) are cofactors that undergo reversible oxidation and reduction in several electron-transfer events inside living organisms. NAD and NADP are plentiful and move freely inside cells, but FMN and FAD are often

attached to enzymes as prosthetic groups. This bibliographic study involves a variety of cofactors, which will be addressed in detail below.

I.2.1 NADH/NADPH

Nicotinamide adenine dinucleotide hydride (NADH) and Nicotinamide adenine dinucleotide phosphate hydride (NADPH) are constituted of two nucleotides connected by a phosphoanhydride link via their phosphate groups. The nicotinamide ring undergoes reversible redox reactions with both cofactors. In this process, NAD^+ or $NADP^+$ (**Figure I.3A**) takes one proton and two electrons in order to produce NADH or NADPH. Reduction of $NAD(P)^+$ changes the nicotinamide group's pyridinium ring to dihydronicotinamide (**Figure I.3B**).

NADH and NADPH are both essential reducing equivalents and intermediates in energy conversion in living organisms, although they have distinct functions. In the majority of cells, the overall concentration of NAD^+ and NADH is in the order of 10^{-5} M, while the total concentration of NADP+ and NADPH is closer to 10^{-6} M. Typically, the ratio of NAD^+ to NADH is high, which promotes the conversion of NAD^+ to NADH.[30] The greater concentration of NADPH relative to NADP+ favors the oxidation of NADPH to $NADP^+$. A few enzymes can use both NAD and NADP, but the majority of enzymes in living organisms show a strong preference for one over the other. NADH is often engaged in catabolic processes, such as glycolysis, where glucose is transformed to pyruvate and ATP is generated. During the subsequent phase of glycolysis, the citric acid cycle also produces of NADH. NAD(H) is also involved in fatty acid catabolism and amino acid breakdown, among other catabolic processes. NAD(H) participates in oxidative phosphorylation when NADH is oxidized to NAD^+ and the reductive force is employed to synthesize ATP in the respiration chain. This process creates the majority of the energy cells need, making it essential for the survival of all living species.

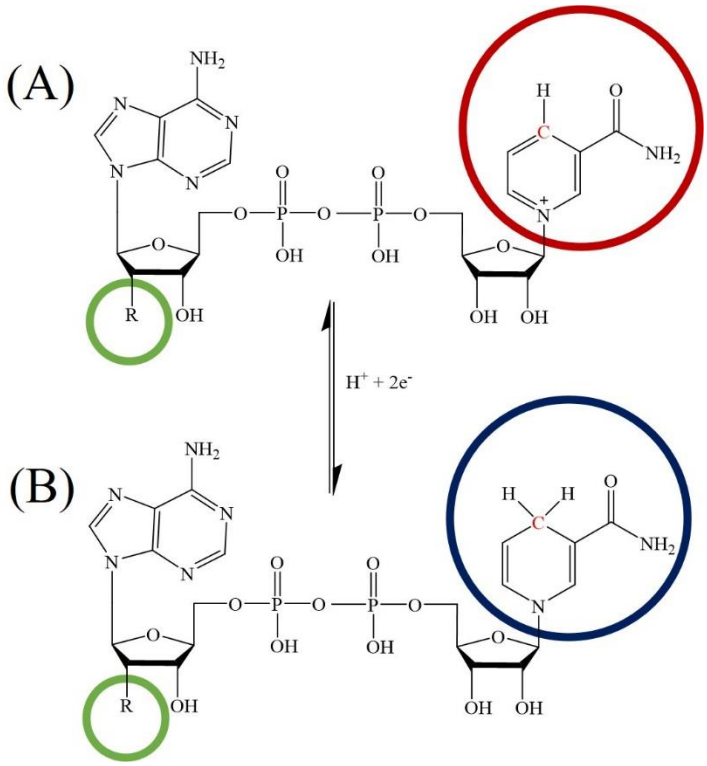

Figure I.3. The structure of (A) $NAD(P)^+$ and (B) its reduction to NAD(P)H by acquiring one proton and two electrons. The structure of NADP+ has an additional phosphate group ($R = PO_3^{2-}$) compared with NAD^+ ($R = OH^-$).

In contrast, NADPH is involved in anabolism, namely photophosphorylation. In the light reaction of photophosphorylation, light-driven H_2O splits into O_2 and reduces $NADP^+$ to NADPH, while in dark conditions, NADPH is oxidized back to $NADP^+$ for carbon-assimilation, where CO_2 is converted into carbohydrates. NADP(H) also participates in the production of lipids, amino acids, and other small molecules. NADP(H) is also engaged in several minor side-pathways of catabolism, such as glucose 6-phosphate metabolism and the pentose phosphate pathway of glucose oxidation, in which NADPH converts glucose 6-phosphate to ribose 5-phosphate, which is used to construct nucleotides, coenzymes, DNA, and RNA. [30]

Most of the oxidoreductases employed in chemical industries are NAD(P)H-dependent enzymes that need $NAD(P)^+$ or NAD(P)H as their redox equivalent. For instance,

dehydrogenases catalyzed reductions of ketones to alcohols need either NADH or NADPH as redox equivalent. Due to the high cost of cofactors, stoichiometric addition of cofactors renders this type of biocatalysis economically impractical. Several cofactor regeneration systems have been developed in this context and will be discussed later.

I.2.2 FMN and FES clusters

Another important cofactor is flavin mononucleotide (FMN). It exists in three forms: oxidised (FMN) (**Figure I.4A**), semi-oxidised (FMNH) (**Figure I.4B**), and reduced (FMNH2) (**Figure I.4C**). It is bound non-covalently as a prosthetic group to a number of oxidoreductases, which are known as flavoproteins.[31,32]

UdhA is another flavoprotein that uses FMN to mediate the transfer of a hydride from NADH to $NADP^+$ or NADPH to NAD^+. FMN collaborates with NAD(P)H in these enzymes to transfer electrons: free NADH binds with FMN in the enzyme and transfers electrons to FMN to form FMNH2, while NADH is oxidized to NAD^+. Reduced FMN either transfers electrons to downstream electron receptors or reduces a substrate directly. A reduced FMN, on the other hand, can pass electrons to NAD^+ and reduce it to NADH.

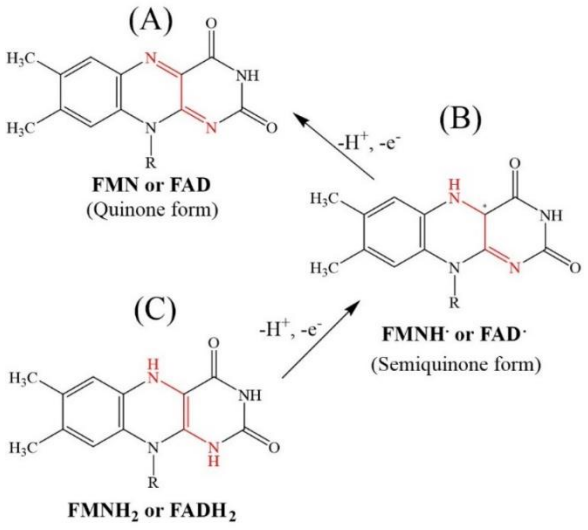

Figure I.4. The structure of (A) flavin mononucleotide (FMN), (B) its semi-oxidized form FMNH and (C) its reduced form $FMNH_2$.

Clusters of iron-sulfur (FeS) is also an essential cofactor. Hydrogenases are among the several enzymes that contain FeS clusters. Iron and sulfur clusters form FeS clusters.[32–37] FeS clusters have vital functions in the biology of living creatures. They serve as relays for electron transport inside proteins. There are typically three primary FeS clusters: the simplest [2Fe-2S] clusters, which contain two iron and two sulfur centres, the cubic [4Fe-4S] clusters, which contain four iron and four sulfur centres, and the [3Fe-4S] clusters, which lack one iron centre relative to the [4Fe-4S] clusters. There are other uncommon FeS clusters, such as the [8Fe-8S] and [7Fe-8S] clusters in nitrogenases and the [4Fe-3S] cluster in hydrogenase (Hyd-1). Coordination of FeS clusters inside proteins is often achieved by cysteine residues covalently linked to cluster iron atoms.

I.2.3 NAD(P)H dependent enzymes

The majority of enzymes used in commercial chemical synthesis are NAD(P)H-dependent (**Figure I.5**). P450 monooxygenases, for instance, employ O_2 and NAD(P)H to insert an O atom into the C-H bond of an organic substrate in order to generate an alcoholic group, producing $NAD(P)^+$ and H_2O in the process.[38] This reaction is very valuable in organic synthesis because it selectively activates a non-activated C-H bond, which is quite difficult to do using traditional methods.[39] P450 monooxygenases are being used in the production of scent molecules and a wide range of other chemical compounds.[40,41] They are also utilized in the pharmaceutical sector to manufacture drug metabolites, since P450 monooxygenase is the initial step in the majority of medications undergoing metabolism in the human body.[42,43]

Many genetically modified commercial alcohol dehydrogenases, such as Johnson Matthey's alcohol dehydrogenase 105, catalyze the selective reduction of pro-chiral ketones to chiral alcohols. To reduce substrates, these alcohol dehydrogenases need NAD(P)H as their redox equivalent.[44–46] Imine reductases (IREDs) are promising catalysts for the production of optically pure secondary cyclic amines, the physiological activities of which are being

investigated and which have enormous application potential in the pharmaceutical industry.[47,48] Most IREDs need NADPH as redox equivalent.[47,48] Other NAD(P)H-dependent enzymes include alkene-reductases that reduce pro-chiral C=C double bonds,[49–53] glucose dehydrogenases that convert reversibly between glucose and glucono-1,5-lactone,[54] and lactate dehydrogenases that convert reversibly between lactate and pyruvate.[55,56] All of these enzymes are very valuable in a wide range of sectors, and they all need a stoichiometric quantity of NAD(P)H as a redox equivalent. As noted above, the cofactors added are sometimes more costly than the products, rendering the biotransformation process economically unviable.

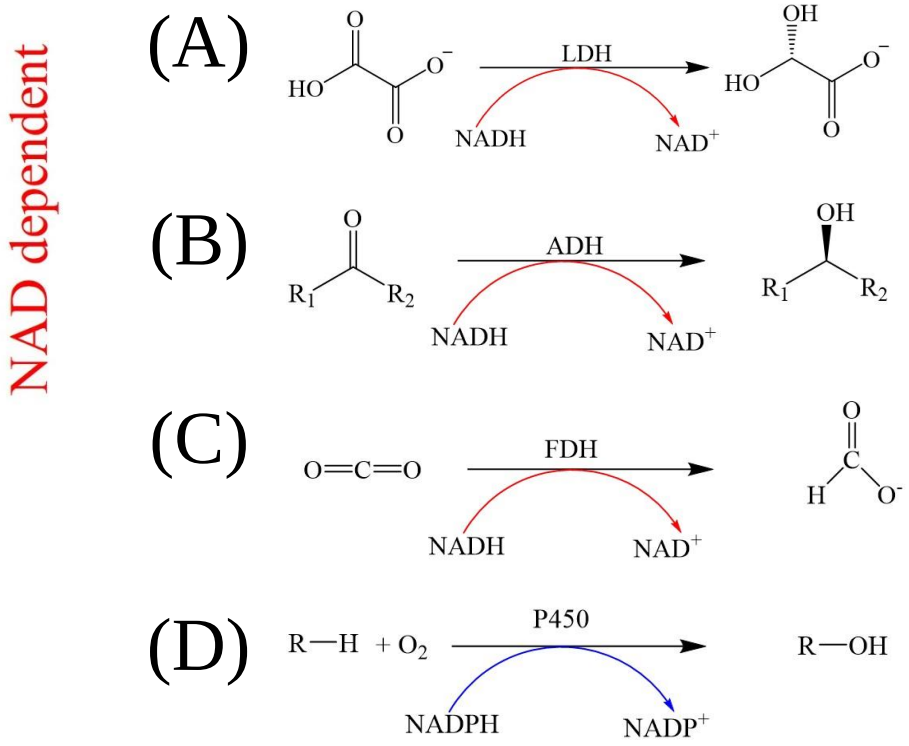

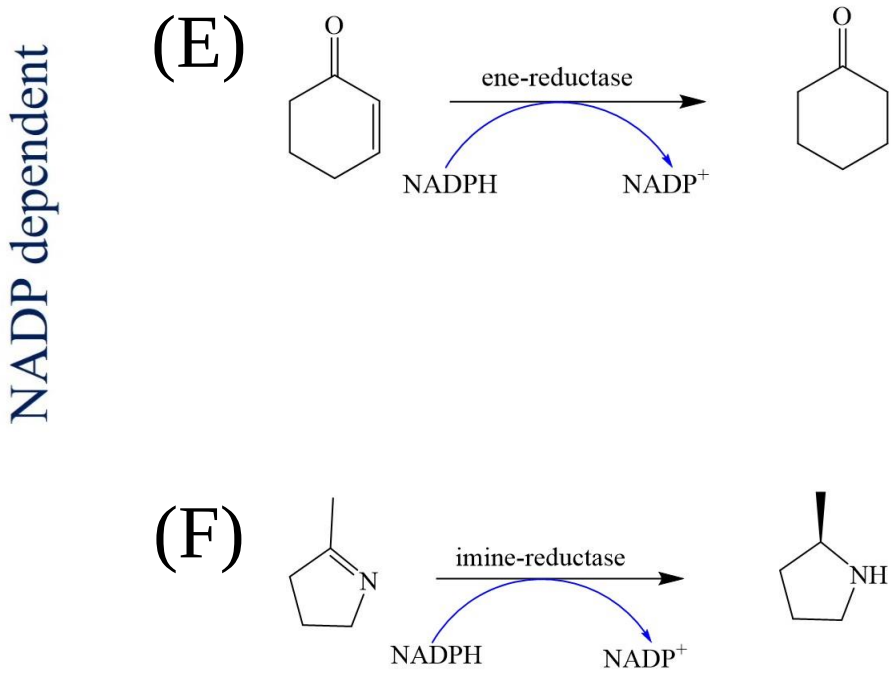

Figure I.5. Examples of Cofactor-dependent enzymes and the reactions that they catalyze. (A) Lactate dehydrogenases use NADH to catalyze the conversion of lactate to pyruvate (involved in this work). (B) Alcohol dehydrogenases use NADH to catalyze the conversion of ketones to alcohols. (C) Formate dehydrogenases use NADH to catalyze the conversion of CO_2 to formate. (D) P450 monooxygenases use O_2 and NADPH to catalyze the insertion of a hydroxyl group into a C-H bond. .(E) Alkene-reductases use NADPH to catalyze the conversion of alkene to alkane. (F) Imine-reductases (IREDs) use NADPH to catalyze the conversion of imines to amines.

I.2.4 NAD(P)H regeneration methods

For large-scale synthetic applications,[57,58] efficient cofactor regeneration and re-use are required. Any method for regenerating cofactors must be practical and allow for a cost-effective and convenient enzymatic process. The regeneration reaction must be high-yielding, and the cofactor's total turnover numbers (TTN), defined in **rel. (1)**, must be as high as possible. Thermodynamically and kinetically advantageous product formation will be aided by cofactor regeneration. The regenerative system's reagents and by-products must not interfere with the desired product's isolation.

$$\mathrm{TTN} = \frac{n_{product}}{n_{cofactor}} \ (1) \ \textit{where n is the molar amounts}$$

To be considered economically feasible, efficient, and industrially sensible, a TTN in the range of 10^3-10^6 is preferred, although the exact efficiency also depends on the cost of the catalysts and cofactors used.[59]

Having a TTN greater than 1,000 is not as simple as it appears. For example, if 50% of the catalytic activity remains after 1,000 successful cycles, the regeneration scheme must have greater than 99.93% efficiency for each cycle.[60] As a result, it is obvious that a successful regeneration scheme must have a fast reaction rate as well as a long lifespan.

The catalysts that regenerate the cofactors can be inorganic, organic, or enzyme-based. The reaction involved in regenerating the cofactors must be coupled with an enzymatic reaction so that the cofactors can continuously switch their redox state back and forth.

Several methods have been developed for the cofactor regeneration and have been gathered in three broad categories: biological and enzymatic regenerations, chemical and photochemical regenerations, electrochemical and electroenzymatic regeneration.

I.2.4.1 chemical and photochemical regenerations

Chemical regeneration

Despite its marginal importance, the chemical and photochemical approaches for NADH regeneration has been the subject of numerous works. The reduction of NAD^+ by sodium dithionite NaS_2O_4 was one of the very first methods implemented. [61] However, this technique has the disadvantage of being very little selective. As a result, sodium dithionite can reduce cofactors as well as enzyme substrates and denature enzymes themselves. Furthermore, the

obtained TTN, near 100, is low. As a result, this method is not suitable for in-situ regeneration during syntheses.

Since the 1980s, numerous studies have investigated the regeneration of NAD(P)(H) using organometallic and biomimetic strategies.[62] Several conditions must be met for these organic compounds to be effective catalysts for NAD(P)(H) regeneration:

- The mediator must be stable in both its oxidized and reduced states.

- The mediators' turnover frequencies should be high.

- The mediator must be soluble in the experiment's working phase.

- The mediator must be involved in a specific reaction with the cofactors.

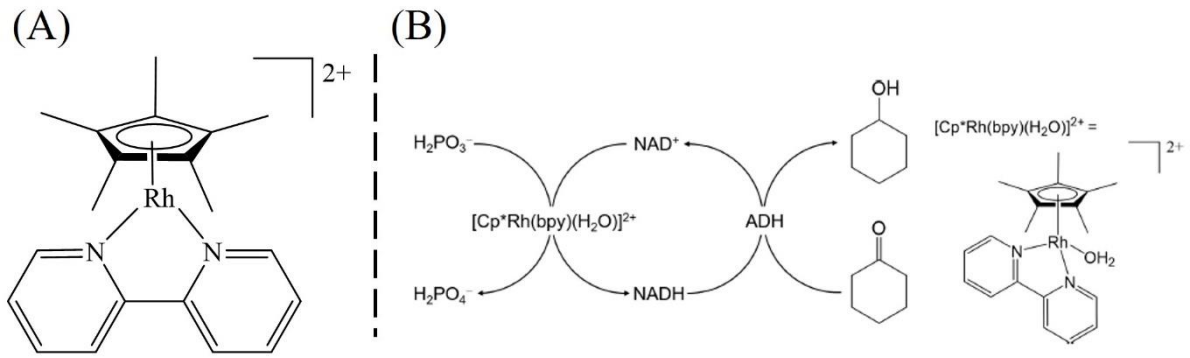

Figure I.6. (A) $[Cp^*Rh(bpy)]^{2+}$ structure. (B) NADH regeneration scheme with ADH (alcohol dehydrogenase) and phosphite as a sacrificial reagent.

Common mediators include organometallic complexes of transition metals such as Rh, Ru, Ir, Fe, etc.[63] **Figure I.6A** shows the molecular structures of $[Cp^*Rh(bpy)]^{2+}$ ($Cp^* = C_5Me_5$, 2=bpy = 2) that can reduce $NAD(P)^+$ by donating two electrons and one proton from the formate, resulting in the formation of CO_2 and the conversion of $[Cp^*Rh(bpy)]^{2+}$ to $[Cp^*Rh(bpy)H]^+$.[64] Low levels of TTNs in the order of 10 have been reported with the application of Rh complex mediator.

Phosphite is another inexpensive sacrificial substrate. In a NADH recycling system (**Figure I. 6B**), cyclohexanol was produced by combining the system with a thermostable ADH from Thermus sp. ATN1. [65] The mutual inactivation of organometallic catalysts and subsequent enzymes is a drawback that prevents further development of this strategy. [66,67] A possible solution to this problem is to compartmentalize or separate the two entities so that their interaction can be avoided to a large extent.[67,68] Using compartmentalization techniques typically results in slow diffusion problems. However, the overall system's durability can be increased. In addition, the TTN of the mediator-catalyzed regeneration scheme lays significantly behind that of the enzymatic method.[69,70] Also, the requirement of large quantities of the mediators, many of which are noble-metal-based and toxic, is unavoidable in a potential scenario involving scaling up. This is not environmentally or economically beneficial.

On the other hand, NADH photochemical regeneration can be achieved using "semiconductor" powders (CdS, for example) and colloids (TiO2), with formate or mercaptoethanol as electron donors. Methyl viologen serves as a relay in this system for electronic transmission.[71] **Figure I. 7** shows a model of this reaction:

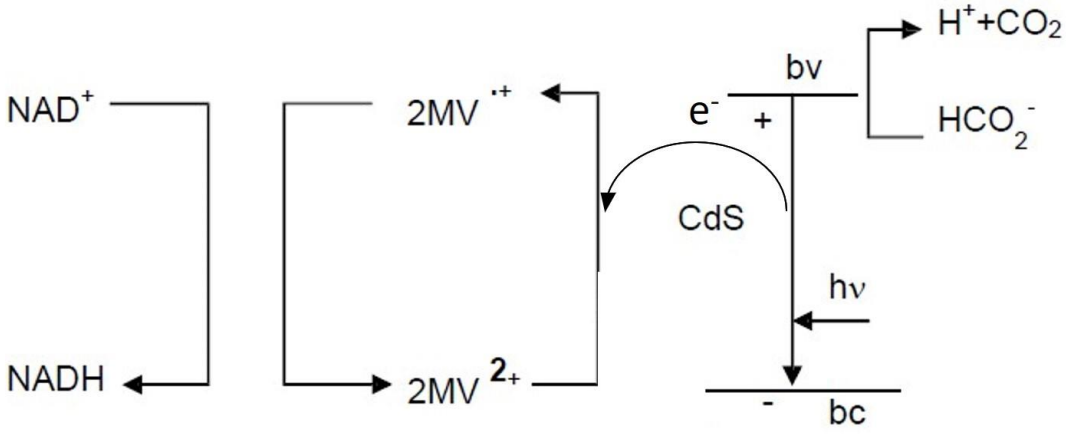

Figure I.7. Photochemical regeneration of NADH

Formic acid serves as an electron donor in this process. The excitation of semi-conductor particles (CdS) by light results in the ejection of negative charges from the electronic

conduction band (bc) to $MV^{2+,}$ whereas the holes in the valence band (bv) are filled by the release of electrons from the oxidation of formic acid. MV^{+} species ensure electron transport. The TTN is in the order of 15.

The use of semi-conductors for cofactor regeneration opens up a new avenue in biotechnology, but it is still in its early stages.

I.2.4.2 Electrochemical and electroenzymatic regeneration of NAD(P)H

Electrochemical or electroenzymatic regeneration of NAD(P)H has been recognized as a promising and efficient technique. While other methods heavily rely on large quantities of co-substrates to donate/accept electrons to/from the NAD(P)(H), it appears that the atom efficiency of the electrochemical method is high because it exchanges mass-free electrons directly or indirectly from the power source.[72,73]

The ability to regenerate the cofactor electrochemically without the use of any other catalyst is intriguing because the resulting method would likely be stable, simple, and inexpensive, especially given current electricity costs.[73] Additionally, if the nicotinamide cofactor could be oxidized or reduced at the electrode surface, no enzymes or other type of catalysts would be required, lowering the overall cost of the process. **Figure I.8A** depicts schematic direct electrochemical regeneration of NAD(P)H.

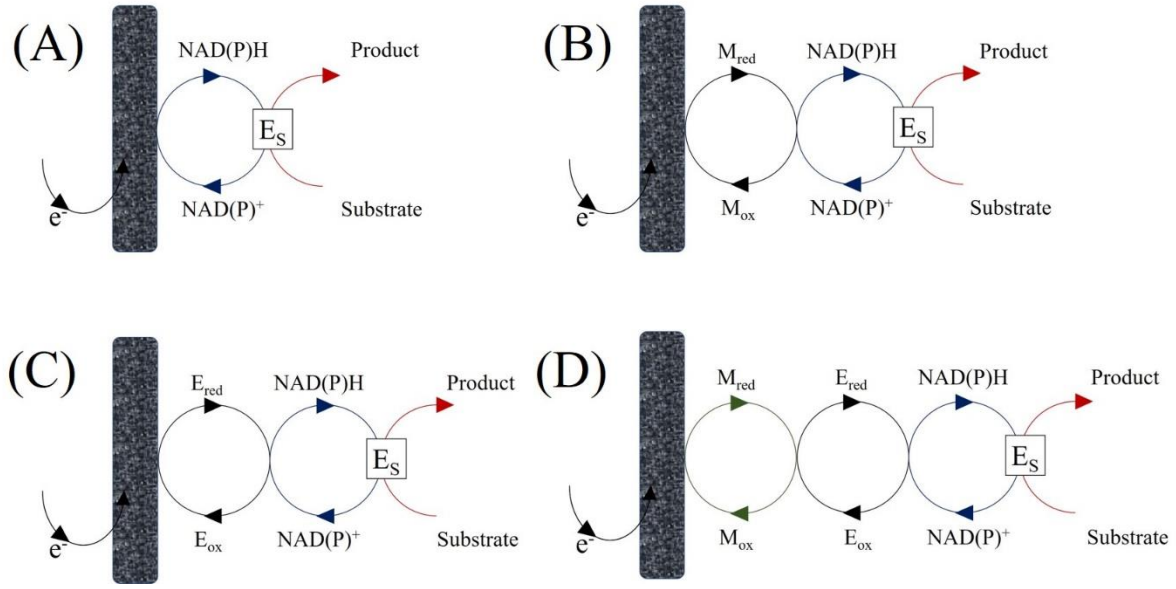

Figure I.8. Schematic representation of NAD(P)H routes. (A) Direct electrochemical regeneration of NAD(P)H, (B) Indirect electrochemical regeneration of NAD(P)H, (C) Direct electroenzymatic regeneration of NAD(P)H, and (D) indirect electroenzymatic regeneration of NAD(P)H. M: electrochemical Mediater; E: Electroenzymatic catalyst; E_s: NAD(P) dependent enzyme.

The nicotinamide cofactor is known to be reduced at the electrode in two steps: first, a radical is formed at –1.1 V vs. SCE, which is then protonated at –1.7 V vs. SCE. The radical species, on the other hand, can dimerize to form NAD(P) dimers, because the protonation step is not selective, it can result in the biologically inactive forms of 1,2-NAD(P)H, 1,6-NAD(P)H, and $NAD(P)_2$ dimer.[63,74] Low selectivity would make any application of the system impossible, as the system's overall efficiency would drop dramatically after a few regeneration cycles. This would hinder any industrial process relying solely on direct electrochemical regeneration.

Indirect electrochemical regeneration of NAD(P)H

Electrochemical mediators can reduce the required overpotential to oxidize/reduce NAD(P)H. As shown in **Figure I.8B**, the reduced form of the mediator behaves as an $NAD(P)^+$ reductant. Compared to the typical situation in which catalysts monomers are present in solution, catalysts

anchored on the electrode surface via covalent bonding reduce the difficulty of product purification and waste disposal and NAD(P) dependent deactivation as reported.[75]

In electrochemistry, the two electron transfer can effectively avoid the problems caused by one-electron radicals, such as formation $NAD(P)_2$, as mentioned in the previous section.[76–78]

$Rh(bpy)_3$ was the first rhodium-based mediator employed in the indirect electrochemical regeneration of NADH. The synthesis of cyclohexanol from cyclohexanone catalyzed by alcohol dehydrogenase in the presence of this mediator was conducted,[79] and the electropolymerized form of cyclohexanol on an electrode was also examined.[80] The incorporation of the pentamethyl cyclopentadienyl (Cp*) ligand substantially increased the mediator's selectivity to 99 %. After the initial electroenzymatic synthesis from pyruvate to lactate in the presence of $[Cp^*Rh(bpy)Cl]^+$ catalyzed by D-Lactate dehydrogenase, it was later combined with alcohol dehydrogenase for the synthesis of various products such as cyclohexanol,[81] (S)-4-phenyl-2-butanol,[82] L-malate,[77] and D-sorbitol.[78] In addition, $[Cp^*Rh(phen)Cl]^+$ with a 1,4-phenanthroline ligand as opposed to a 2,2-bipyridine ligand was shown to be effective in the electroenzymatic synthesis of L-glutamate.[83] The faradaic efficiency of a system mediated by Rh complex was in the average of 80 %.

The advantages of using these catalysts are that they can be used with both NAD^+ and $NADP^+$, expanding the scope of the system. (ii) They are stable over a wide pH range (pH 4 to 7) and temperature range (up to 70°C) for various chemical products, and (iii) they successfully stop the formation of NAD dimers. However, due to complexation with the enzyme, they are reported to inactivate the biocatalyst over the course of the reaction. For that, several immobilization routes have been investigated e.g., the immobilization of the Rh complex on a bucky paper covered with carbon nanotubes,[78] or on a graphite felt electrode.[84] The immobilization of the Rh complex following a recent reported work and its coupling to lactate biosynthesis in a flow reactor was further explored in the **chapter IV** of this thesis.

Direct Electroenzymatic regeneration of NAD(P)H (Figure I.8C)

Numerous oxidoreductases can transfer electrons to the electrode without an exogenous electron shuttle. With these enzymes, direct electron transfer is accomplished by intramolecular and intermolecular electron transfer via redox-active centres, such as heme, ferredoxin adenine dinucleotide (FAD), Mo pterin, and relays, such as iron-sulphur ([FeS]) clusters.[85–87]

Although many oxidoreductases are capable of direct electron transfer with the electrode, including hydrogenase, laccase, carbon monoxide dehydrogenase (CODH), FDH, and bilirubin oxidase,[88,89] direct electroenzymatic regeneration of nicotinamide cofactor is still uncommon.

Cantet et al. discovered that the NADH-producing hydrogenase from Alcaligenes eutrophus H16 adsorbed on a platinum electrode could directly reduce NAD^+ in the presence of H_2.[90]

This regeneration system was coupled with GLDH, and L-glutamate production was detected.[91]

Indirect electroenzymatic regeneration of NAD(P)H

Enzymes can accelerate electron transfer between electron mediators and NAD(P)(H) (**Figure I. 8D**). This is particularly useful when the active site of an enzyme is deeply buried within its tertiary structure.[92]

A common mediator is the one-electron N,N'-dimethyl-4,4'-bipyridinium dichloride (methyl viologen, MV^{2+}), and its primary relay enzymes are diaphorase, FNR, and AMAPORs (artificial mediator accepting pyridine nucleotide oxidoreductase).[93,94] Since this iron-sulphur protein is the natural electron mediator of FNR, ferredoxin (Fd) can replace methyl viologen when FNR is utilized.[57]

The system mediated by $MV^{2+/}MV^+$ is stable and efficient, but toxic. The natural cofactor FAD is an alternative to methyl viologen that is also effective.[95–97]

Ferredoxin NADP$^+$ reductase

FNR (ferredoxin NADP$^+$ reductase) is a monomeric protein found in all phyla.[98]This enzyme is important in the Calvin cycle of photosynthetic organisms because it catalyzes NADP$^+$ reduction when it interacts with reduced Fd (**Equation I**). In heterotrophs, the reaction is more favorable to Fd reduction, and it is involved in several anabolic reactions such as amino acid and deoxyribonucleoside synthesis, as well as fatty acid desaturation.[99]

Ferredoxin is a small iron-sulfur protein (13 kDa in C. reinhardtii) that can carry one electron, whereas NADP$^+$ reduction requires two electrons. The reaction is made possible by the presence of a non-covalently bound FAD (flavin adenine dinucleotide) within FNR.

$$2\ Fd_{red} + NADP^+ + H^+ \xrightarrow{FNR} 2\ Fd_{ox} + NADPH \qquad (I)$$

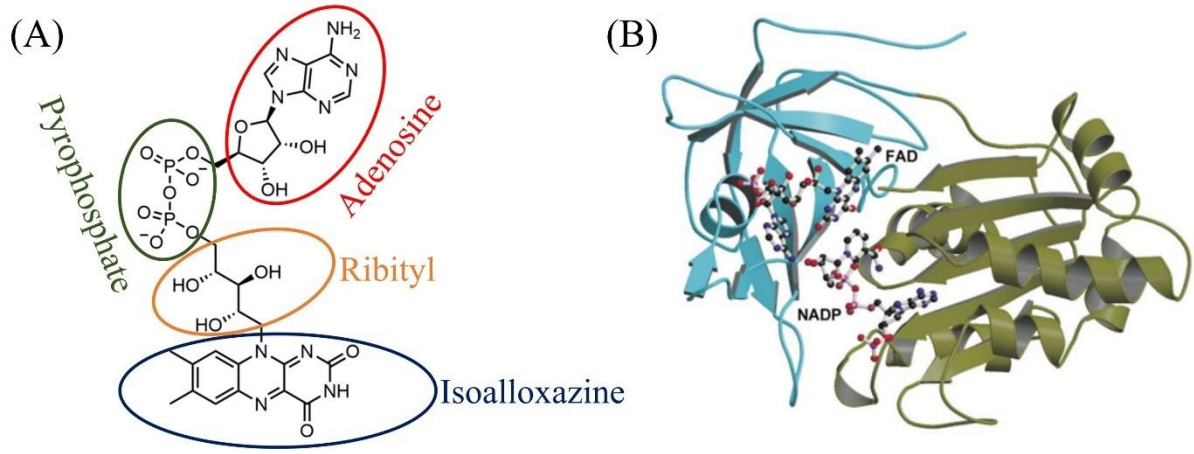

Figure I.9. (A) Structure of FAD where the chemical active part is Isoalloxazine. (B) The FNR:NADP complex's overall structure and enzyme–coenzyme interactions. Ribbon diagram of the FNR:NADP complex, with the FAD prosthetic group and NADP coenzyme represented as balls and sticks, respectively, and the protein-binding domains for each cofactor colored in cyan and green.[100]

Adenosine bound to pyrophosphate and a ribityl moiety comprise the FAD group (**Figure I. 9A**). The isoalloxazine ring undergoes redox reactions. This cofactor can be found in three

different forms: quinone, radical semiquinone, and fully reduced hydroquinone (**Figure I. 4**). FNR creates a unique environment for FAD reduction. Not only does it shift the two-electron reduction potential by 160 mV from –0.22 V to –0.38 V vs. SHE (pH 8), but it also partially stabilizes the semiquinone radical, which would otherwise immediately disproportionate towards the stable forms.The potentials for FAD reduction in FNR are mildly crossed, which means that adding the first electron is slightly less favorable than adding the second, allowing the radical state to be trapped.[101–103]

FNR has two domains: the N-terminal is the FAD binding domain, which also interacts with Fd, and the C-terminal is the $NADP^+$ binding domain (**Figure I.9B**).[101] FNR from C. reinhardtii was used in this thesis.

$NADP^+$'s adenine moiety is linked to the phosphorylated sugar moiety, where the negative charge interacts with positively charged amino acids (lysine, for example). Furthermore, for efficient hydride transfer from FAD to $NADP^+$, the nicotinamide moiety of $NADP^+$ and the isoalloxazine ring of FAD must be coplanar. To achieve this aligned conformation, a tyrosine residue in the C-terminus that is blocking it must be displaced. The electrostatic attraction between $NADP^+$'s 2'-phosphate group and positively charged residues, acts as an anchor, allowing $NADP^+$ to remain bound while the tyrosine is displaced.

As for FNR, the positively charged Fd binds to a positively charged patch.[104] Thus, electrostatic forces are generated to ensure interaction between Fd and FNR. The electrostatically driven binding between Fd and FNR as described facilitates the close alignment of the [2Fe-2S] cluster in Fd with the FAD in FNR, which is approximately 6 A°.[104]

The proposed steps of the catalytic mechanism for FNR, which involves a ternary complex, are as follows:[104,105]

* $NADP^+$ binds to FNR.

* Two reduced Fd_{red} molecules sequentially donate their single electron, thereby reducing FNR (FAD in the hydroquinone state $FADH_2$).

* NADPH regeneration takes place. Hydride transfer occurs via the N_5 of the reduced FADH2 of FNR and the C_4 of the nicotinamide ring of $NADP^+$.

* NADPH is liberated from FNR.

The immobilization route of FNR for its application in the electroenzymatic regeneration of NAD(P)H is further developed in **chapter V**.

I.2.4.3 Enzymatic regeneration of NAD(P)H

Enzyme-based methods for cofactor regeneration are not only the most effective, but also the only ones used on a large scale.[106]

Figure I.10 depicts the most commonly reported enzyme-based systems in the literature. In a nutshell, they are divided into two types: systems with a single enzyme driving both the reaction under investigation and the recycling of the cofactor (**R = E_1**), and systems with two separate enzymes (**R = E_2**). For example, depending on the main reaction under investigation, alcohol dehydrogenases (ADHs) can be used both for the main reaction and for cofactor regeneration by using a co-substrate such as an alcohol or a ketone. The use of a single catalyst in the regeneration system reduces overall costs; however, optimizing enzyme activity for both reactions is difficult, and very high concentrations of co-substrates are required to drive the reaction towards the product. Furthermore, a large amount of waste is usually generated.[107]

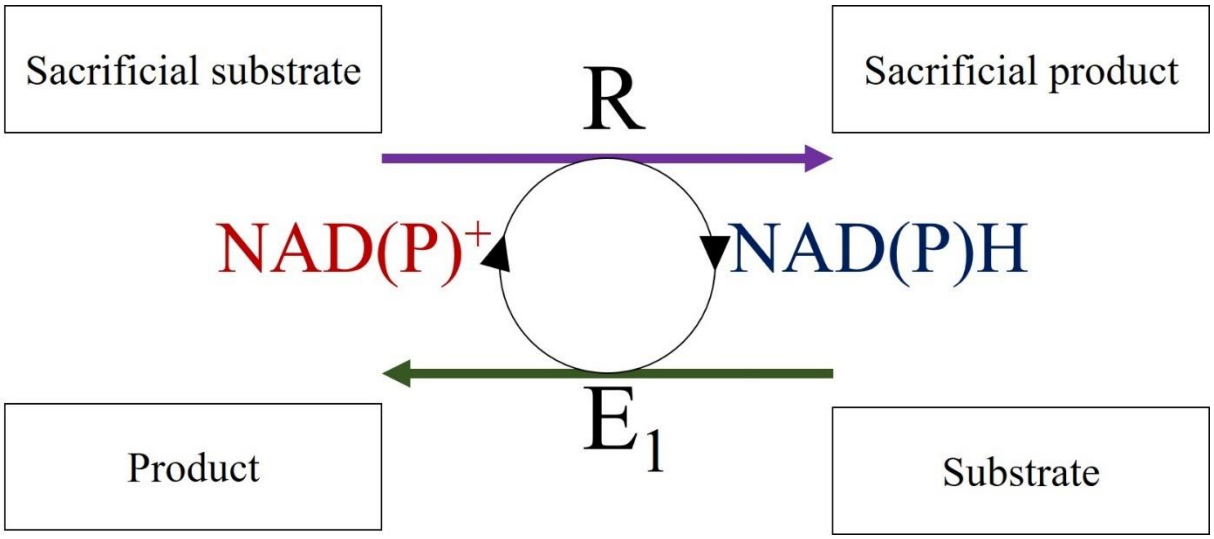

Figure I.10. enzyme-based cofactor regeneration systems with R = E1 for single enzyme driving both reactions and R = E_2 for two enzymes driving each reaction.

The most common method is to use a secondary enzyme, such as formate dehydrogenase (FDH), which reduces the cofactor by oxidizing formic acid to CO_2. GDH, which oxidizes glucose to gluconolactone, can also recycle the cofactor. The primary advantage of using FDH is that the coproduct, CO_2, does not interfere with the product recovery; however, the enzyme is not very active, and CO_2 production gradually acidifies the reaction mixture. While GDH is widely used, excess glucose is required to shift the reaction towards the product, making product recovery difficult and system atom efficiency low.[107]

I.3 Extending redox catalysis in synthetic biochemistry

The generation of co-products from a sacrificial substrate is a drawback shared by all of the aforementioned enzymatic techniques. This is not atom-efficient and reduces the eco-friendliness of biocatalysis. In addition, the separation from undesirable co-products is frequently expensive and time-consuming, making it less likely to be commercialized.

In recent years, H_2 has emerged as a carbon-neutral, clean, and renewable alternative energy source, as traditional energy sources, primarily gasoline derived from fossil fuels, are expected to run out in the near future and emit greenhouse gas. As global warming becomes an

increasingly urgent issue, both academia and industry pay a great deal of attention to H_2. In 2015, Toyota introduced the first commercially available hydrogen fuel cell vehicle. H_2 serves as a sacrificial substrate, and the entire process produces no byproducts, making it completely atom-efficient.

I.3.1 Coupling redox catalysts for the cofactor regeneration and chemicals biosynthesis

Protein film electrochemistry has emerged as an efficient method for controlling, probing, and utilizing enzyme catalysis of redox half-reactions. In this method, enzyme molecules are immobilized on an electrode so that they can directly exchange electrons with the electrode. In the simplest procedures, the enzyme can be directly adsorbed onto a graphite (or other carbon material) electrode; in other examples, carbon or metal electrodes are modified with chemical monolayers to facilitate enzyme attachment.[108,109]

Coupling biological systems rely upon connecting redox half-reactions with much closer potential difference in addition to a facilitated channeling of protons and electrons generated from half-reaction of oxidation.

Armstrong and co-workers explored the combination of two enzyme-catalyzed half-reactions on graphite platelet particles by the discovery that enzyme-modified graphite electrodes are efficient electrocatalysts for a wide variety of redox half-reactions. The graphite particle serves as a sink for electrons from the oxidation half reaction and as a donor to the enzyme catalyzing a reduction reaction, and can therefore be viewed as a "wire" connecting the two redox enzyme moieties. This was demonstrated for particles modified with both a NiFe hydrogenase (from Allochromatium vinosum) and the E. coli nitrate reductase moiety shown schematically in **Figure I.11**.[110]

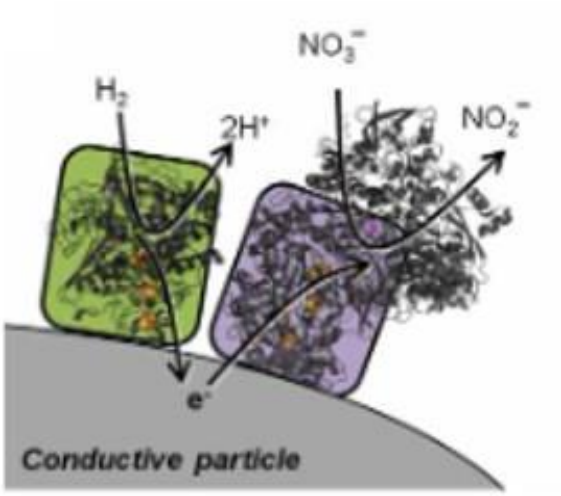

Figure I.11. Enzyme redox catalysis on conductive graphite platelets developed by Armstrong and co-workers. Hydrogenase and nitrate reductase co-immobilized on graphite.[111]

Besides, Mertens and co-workers proposed a typical H_2-driven cofactor regeneration system using hydrogenase I from Pyrococcus furiosus.[112] Hydrogenase I reduces $NADP^+$ to NADPH and oxidizes H_2.[113,114]

Hydrogenase I, however, is a hyperthermophilic enzyme whose activity peaks at 80 °C. This environment is not suitable for the majority of enzymes. In addition, hydrogenase I is not very stable and is sensitive to oxygen, which further restricts the applicability of this method.[115]

By genetically engineering Pseudomonas putida KT244090, Lenz and co-workers developed a whole-cell H_2-driven NADH regeneration system. The necessary gene clusters for the soluble NAD^+-reducing hydrogenase (SH) from Ralstonia eutropha were transferred into the host cell Pseudomonas putida KT2440, along with cytochrome CYP153A and its accessory enzymes, and their expression was induced accordingly. Consequently, the H_2-driven NADH regeneration system in the whole cell can allow the production 1-octanol from n-octane when bubbling with H_2.[116] The whole-cell approach solves the hydrogenase instability problem, as proteins are typically more stable in their native state within the cellular environment. However,

the whole cell approach still has several drawbacks, such as by-product formation and substrate permeability.

I.3.2 Modular approaches in coupling H_2 oxidation to NADH regeneration

Vincent and co-workers have developed the modular H_2-driven NADH regeneration system presented in **Figure I.12A** including a carbon particle and two enzymes: Hydrogenase 2 (Hyd-2) from E. coli and the NAD^+-reductase part of Ralstonia eutropha H16 both co-immobilized on a carbon particle.

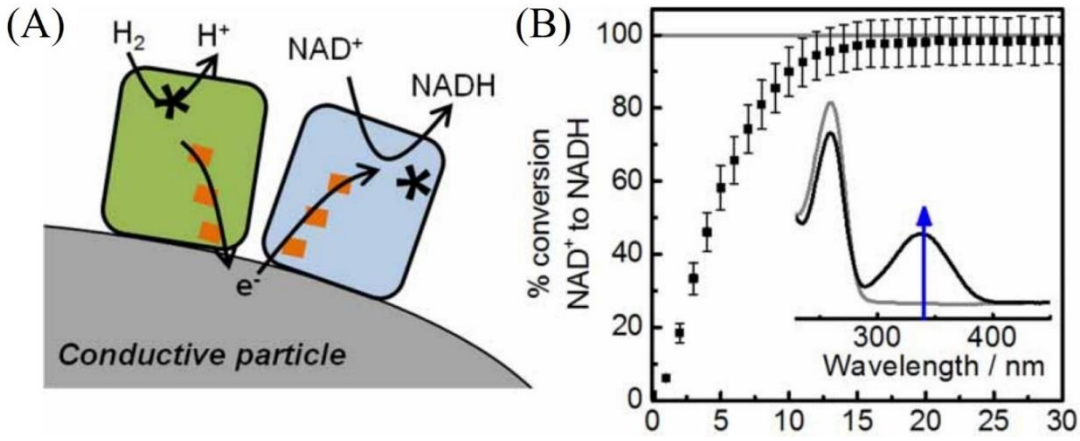

Figure I.12. H_2 oxidation combined with NAD^+ reduction on carbon particles. (A) Illustration of enzyme-modified particles for H_2-driven NADH production. (B) NADH regeneration kinetics evaluated through UV-visible.[111]

Furthermore, along with the other two enzymes, a third catalytic enzyme that requires cofactor as a co-substrate can be immobilized on the carbon particle. Hydrogenase oxidizes H_2 into two protons and two electrons during the reaction. The electrons from the hydrogenase pass through the carbon support to the NAD^+-reductase, which takes up the electrons and protons to reduce NAD^+ to NADH (**Figure I.12B**). The regenerated NADH will be provided for a third enzyme required for the NADH-dependent redox reaction to occur. Carbon support is critical in this system because it serves as both a support for enzyme immobilization and a conductor for

electron transfer between the hydrogenase and the NAD^+-reductase. Polysaccharides, silicas, and zeolites, which are commonly used for enzyme immobilization, are not suitable for this system because they act as insulators, preventing electron transfer between the hydrogenase and the NAD^+-reductase.

On the other hand, organometallic catalysts for H_2-mediated NAD^+ reduction have also been reported. Early examples relied on H_2-driven reduction of electron carriers (such as pyruvate and Safranine) that then reduced $NAD(P)^+$.[117]

Recently, homogeneous organometallic complexes have been used to produce NADH under H_2 without the need for mediators.[118] However, it is known that these complexes have biocompatibility issues when used in one-pot reactions with enzymes that consume NADH (e.g. alcohol dehydrogenases).[68]

Besides, Wang and co-workers used platinum nanoparticles (NPs) supported on carbon or metal oxides for NAD^+ reduction driven by H_2 (**Figure I.13A**). [119,120] To overcome the activation energy for Pt-catalyzed NAD^+ reduction, elevated temperatures and pressures were utilized; however, side-products (e.g., over-reduction of the pyridine ring) were produced in addition to the desired 1,4-NADH. Under milder conditions used to provide 1,4-NADH to an alcohol dehydrogenase, low levels of TTNs after 100 h of reaction where reached, indicating that further catalyst development would be highly required.[119]

As a further work explored by Vincent and co-workers, hydrogenase was exchanged by a metal catalyst. For direct H_2-driven NAD^+ reduction, commercially available carbon-supported metal (metal/C) catalysts e.g., Rh/C, Pd/C, Pt/C,Ir/C, and Ru/C, were investigated. Then, specific metal/C catalysts used for H_2 oxidation, and electrons are transferred from the conductive carbon support material to NAD^+ reductase for NAD^+ reduction (**Figure I. 13B**). Compared to metal/C catalysts presented in **Figure I. 13A**, these chemo-bio catalysts (**Figure I. 13B**) exhibit

greater activity and selectivity for the production of bioactive NADH under ambient reaction conditions.

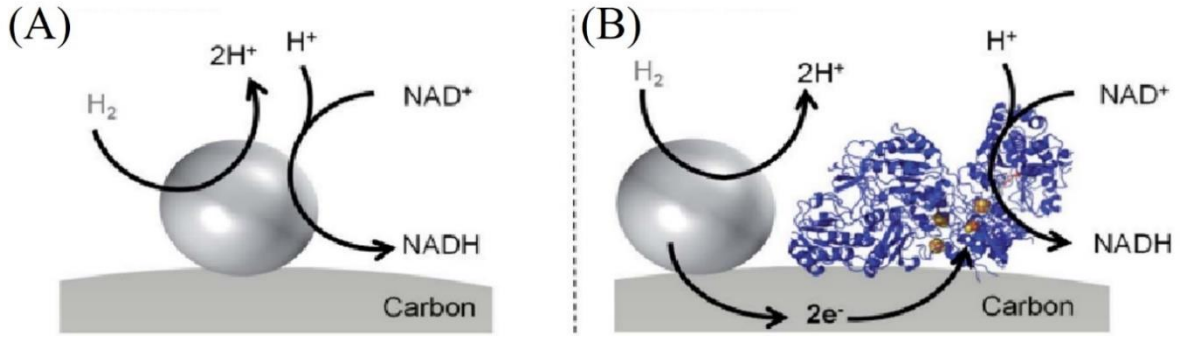

Figure I.13. H_2-driven NADH regeneration approaches using metal nanoparticles supported by carbon. (A) Both H2 oxidation and NAD^+ reduction must occur at the metal. (B) Metal-catalyzed H_2 oxidation is coupled to co-immobilized NAD^+ reductase for NADH regeneration.[121]

The optimized chemo-bio catalysts, Pd/C-NAD^+ reductase, were then used to supply NADH to an alcohol dehydrogenase for enantioselective (>99% ee) ketone reductions, resulting in high cofactor turnover rates and Pd and NAD^+ reductase activities of 441 h^{-1} and 2347 h^{-1}, respectively.

I.3.3 Presented H_2-driven NADH regeneration's advantages

This innovative regeneration system offers numerous benefits. [107,121] First, H_2 is a low-cost sacrificial substrate that is easily separated from the reaction system, making downstream purification much simpler than when using a carbon-based sacrificial substrate. Second, protons generated from H_2 oxidation are incorporated into the reduced product, resulting in an atom efficiency of 100 %. Thirdly, due to the modularity of this system, each enzyme and even the carbon particle can be easily modified to meet specific needs and conditions. To achieve different reactions, the cofactor-dependent enzyme, can be changed to a variety of enzymes including alcohol dehydrogenase, imine-reductase, alkene-reductase, and P450

monooxygenase. If the reaction must be conducted at a high temperature, the NAD^+ reductase from Thermus thermophilus, suitable for higher temperatures, can be substituted.

I.4 Towards compartmentalizing and linking NAD(P)H cofactor regeneration to hydrogen oxidation in a hybrid flow reactor

In this PhD work, we propose to develop a bioelectrode architecture for efficiently coupling hydrogen oxidation to the regeneration of the cofactor NAD(P)H. The plan is to compartmentalize these two redox processes while electrically connecting them in a hybrid reactor that combines a fuel cell and a redox flow device.

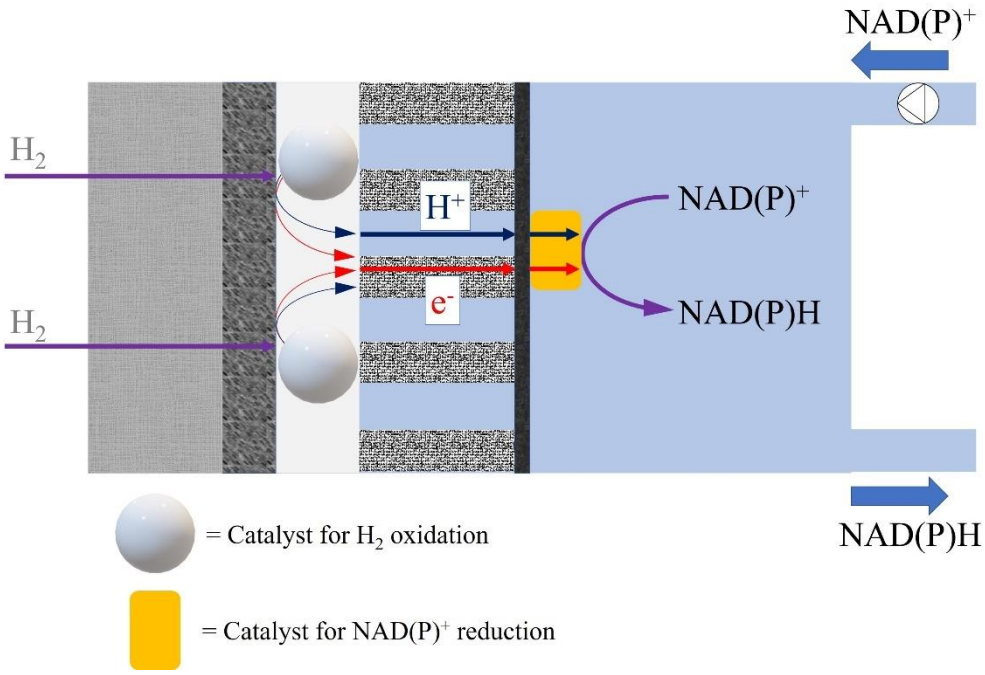

Scheme I.1. Cartoon representation of the thesis project.

The paths chosen by several teams today (**presented in section I.3**) do not consider the physical separation of these two reactions, and we believe that this is a wise entry point for stimulating research. **Scheme I.1** shows a cartoon representation of the work in this proposed project in this thesis. Hydrogen is oxidized at the anodic compartment based on fuel cell technology (presented in **section I.4.1**) while the solution containing the cofactor circulates in the cathodic

compartment at an optimized flow rate whose advantages presented in **section I.4.2**. Catalysts for both half-reactions are immobilized on suitable electrodes. Electrochemical catalysts *e.g.*, Pt and Rh complex and electroenzymatic catalysts *e.g.*, Hydrogenase and FNR are involved in this work. The separation between both compartments plays an important role in driving the electric force of the reaction. We propose here as indicated in **scheme 1** to increase the connection between the center of the anodic catalyst and the center of the cathodic catalyst by minimizing the distance between them and reducing the resistivity of the system. NADH regenerated can be coupled to an enzymatic reaction as previously described (**section I.2.2**). Different themes involved in the efficient electrochemical or electroenzymatic regeneration of NAD(P)H coupled to hydrogen are discussed in this section. The final part gives an orientation towards the hierarchization of implemented factors.

I.4.1 Fuel cell technology

I.4.1.1 Brief history about fuel cells

The concept of fuel cells emerged at the beginning of the 19th century when Volta discovered that electrochemical cells can be manufactured by placing two different metals in an aqueous salt solution.[122,123]

Nicholson and Carlisle were the first to propose using electricity to split water into hydrogen and oxygen in their publication.[124] Faraday coined the term electrolysis (as "lysein" means "to break" in ancient Greek) in 1834 for the process of using electricity to separate water into anions and cations. [123]

Subsequently, in 1838, Grove demonstrated the first simple design of fuel cells; his design consisted of a series of platinum electrodes fed with hydrogen and oxygen and dipped into a dilute sulfuric acid solution, resulting in the birth of a new type of energy source; today, we call

it a hydrogen fuel cell.[125–127] After this significant breakthrough, Mond and Lange coined the term fuel cell in 1889.[128,129]

In 1932, an English engineer named Francis Bacon laid the groundwork for future developments in the field of fuel cells. Although he briefly investigated H_2/O_2 fuel cells, he primarily focused on alkaline electrolyte fuel cells (AFC) because, in his opinion, hydrogen-oxygen fuel cells will not be commercially viable due to the expensive and rare platinum catalyst.[130] Prior to 1950-1960, fuel cell research grew steadily, but after the United States and Russia (USSR at the time) launched their space exploration programs, fuel cell development grew exponentially.[131] Two scientists employed by General Electric, Grubb and Niedrach, invented PEM fuel cell technology. Unlike conventional alkaline fuel cells, it was compact, with the only disadvantage being a higher cost due to a high platinum requirement as a catalyst.[128]

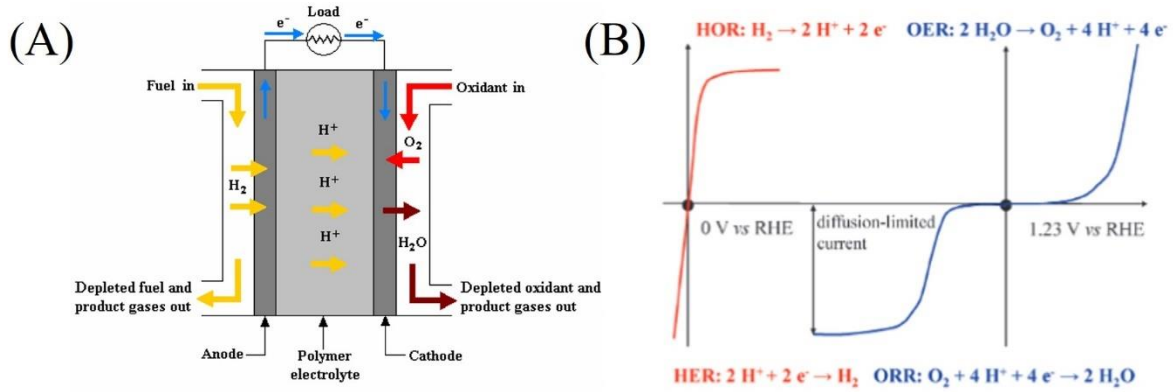

Figure I.14. (A) Illustration of a fuel cell with oxidation of hydrogen at the anode and reduction of oxygen at the cathode. Both compartments separated by proton exchange membrane. (B) An illustration of the distinct oxidation and reduction half reactions of a fuel cell as a function of potential.

Fuel cells operate with a two-electrode configuration: an anode where fuel oxidation occurs and a cathode where oxidant reduction occurs (**Figure I.14A**). The relationship between potential and current when measuring the polarisation curves of anode and cathode reactions separately is depicted in **Figure I.14B**. The open circuit voltage (OCV) reflects the potential difference

when no net current flows between two electrodes when the corresponding polarisation curves are superimposed on a current vs. potential or I-V plot. As its name suggests, OCV value should ideally be measured when the switch is set to OFF. The cell voltage is the working voltage of the cell, and its value is less than the OCP because some driving force is required for the flow of current due to the polarization behavior of both electrodes and the charge transfer in the fuel cell components.

Table I.1. Fuel cells classification[128–132]

Fuel cell type	Temperature (°C)	Fuel	Mobile ion	Application
Proton exchange membrane (PEMFC)	30-150	H_2	H^+	Vehicles Transport Portable
Direct methanol (DMFC)	20-90	Methanol	H^+	Portable electronic systems
Alkaline (AFC)	50-200	OH^-	H_2	Space vehicles Transport
Enzymatic (EFC)	10-50	H^+	Pure H_2, glucose	Under development
Microbial (MFC)	Ambient temperature	H^+, Other ions	Glucose, Dissolved organics	Under development
Solid Oxide (SOFC)	500-1000	O^{2-}	Impure H_2, various hydrocarbon fuels	All CHP systems from 2 kW to MW

There are a few fundamental technical issues with hydrogen fuel cells, including a sluggish oxygen reduction reaction, durability, and hydrogen availability. To address these problems, scientists have been developing and evaluating various types of fuel and catalysts. The fuel cells are categorized according to their operating temperature and electrolyte type. **Table I.1** provides a comprehensive classification of the various types of electrolytes and fuels operating at a temperature range between 20 °C and 1000 °C.

In spite of the above drawbacks, the use of hydrogen fuel cells is gaining popularity due to its advantages over primary conventional batteries, which include: (1) high energy efficiency (some developers have achieved 80% energy efficiency with co-generation), (2) high power density and compact size, (3) reliability and durability, and (4) relatively cleaner source of energy as expressed previously. In this PhD work, hydrogen oxidation is achieved with a half-PEMFC and a half-EFC. The cathodic compartment is for in the indirect electrochemical or electroenzymatic regeneration of NAD(P)H.

I.4.1.2 Proton Exchange Membrane Fuel Cell (PEMFC)

Composition and operational system

The PEMFC operates at low temperatures, and its performance is determined by reactions that occur on either the cathode or the anode. Hydrogen is oxidized at the anode, releasing electrons and the hydrogen cation H^+; at the cathode, oxygen accepts electrons and the hydrogen cations to form water. The individual and overall electrode reactions are as shown in **reaction II** and the current through the external load is made up of free electrons. [129,132]

At the anode:	$H_2 \longrightarrow 2\,H^+ + 2e^-$	(i)
At the cathode:	$0.5\,O_2 + 2\,e^- + 2\,H^+ \longrightarrow H_2O$	(ii)
Global reaction:	$H_2 + 0.5\,O_2 \longrightarrow H_2O + \text{heat}$	(II)

PEMFC use flow plates to feed hydrogen at the anode and oxygen -often from the air- at the cathode. The flow plates, also known as bipolar plates, have gas channels on one side of the plate and water circulation channels on the other for temperature control of the fuel cell (FC).

The membrane electrode assembly (MEA) is an important component of the PEM fuel cell, consisting of (i) a proton exchange membrane (PEM) coated with positive and negative electrodes on both sides, (ii) catalyst layers (CL), and (iii) gas diffusion layers (GDL) sandwiched between two flow plates.[133] Furthermore, in most commercially available membrane electrode assemblies, the catalyst layer is typically deposited on the membrane alongside the electrodes.

Proton exchange membrane

Because of its proton exchanging properties, the membrane separating the two electrodes can only allow proton transport (H^+); thus, it is known as a proton exchange membrane (PEM).[132] This ability to conduct only protons from the anode to the cathode forces electrons to take the external route to the cathode, resulting in current through the external load and a potential difference across the external load, i.e. cell voltage.

The electrolytes used in the early stages of NASA's development and use of PEMFCs were polystyrene sulfonic acid (cationic ionomer). They encountered some difficulties, such as internal cell contamination and oxygen leakage through the membrane, which General Electric resolved. However, in order to be safe, NASA chose Alkaline Fuel cell (AFC) for its space program.[131] Following that, in 1967, DuPont successfully introduced to the world a new and novel fluorinated polymer based on polytetrafluoroethylene (PTFE) (**Figure I. 15A**).[133,134]

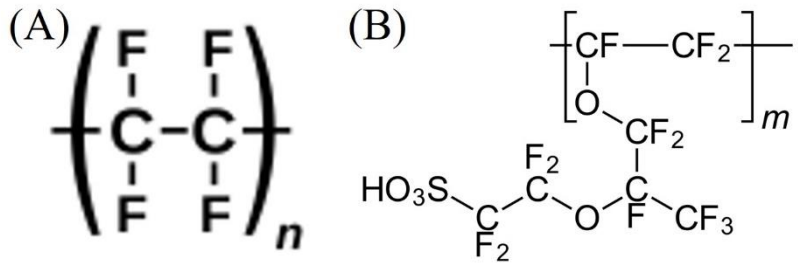

Figure I.15. Formulas of (A) PTFE and (B) Nafion™

Today, PTFE is used as the backbone of Nafion, often with the addition of a sulfonic group at the end of the side chain. It is commonly referred to as Nafion™ (**Figure I.15B**).[134] The invention of Nafion™ resulted in a significant advancement in PEMFC development. Nafion™ has many advantages, including its high resistance to chemical attacks, mechanical strength despite its thinness, acidic nature, ability to absorb large amounts of water, very good proton conductivity under suitable hydration conditions, and with a hydrophobic backbone. However, it has some drawbacks, such as being expensive to produce and requiring proper hydration to allow efficient H^+ transport, which is why it can only operate below 90-100 °C.[134]

Catalyst layer

Platinum (Pt) is commonly used as a catalyst in PEMFCs. Platinum has a high catalytic activity for both anodic and cathodic reactions, as it is one of the most effective catalysts for hydrogen oxidation and the extremely sluggish oxygen reduction reaction. The catalyst is coated on both electrodes at similar or different amounts.[134]

Previously, it was believed that the Pt catalyst, along with flow plates and Nafion, is one of the largest contributors to the cost of PEMFCs, since platinum is a highly sought-after, valuable metal and early PEMFCs required high platinum loading for acceptable energy production. In the initial stages of PEMFC development, the platinum loading had to be as high as 28 $mg.cm^{-2}$ of electrode surface area. It was believed that the PEMFC technology would never be commercially viable for the same reason.[129,132]

In subsequent decades, however, extensive research and development led to a dramatic decrease in the platinum loading on the electrode surface. Even at the cathode, modern commercialized PEMFCs require less than 0.2 mg cm^{-2} of catalyst loading. Lower platinum loadings, as low as 10 µg.cm^{-2}, have also been suggested and tested in the past, but were found to have significantly a lower durability.[129,133] Other catalysts, such as platinum mixed with other metals or alternative materials, are currently in development, despite the fact that platinum is a widely used catalyst currently.[135,136]

Gas diffusion Layer (GDL)

The gas diffusion layer (GDL) is the outermost portion of the MEA that is in direct contact with the flow plates. One of the primary functions of the GDL is to serve as a dispersion medium to facilitate the diffusion of reactants and products to and from the catalyst layer.[137] Moreover, it effectively transports the produced water away from the catalyst layer and prevents corrosion of the catalyst layer caused by water flooding.[138,139]

In addition, they form an electrical connection between the catalyst layer and the bipolar plate to facilitate the flow of electrons; finally, GDLs support the MEA and shield the thin catalyst layer. This conductivity is allowed by that of conducting porous carbon-based materials like carbon paper or carbon felt.[140]

Most GDL comprise two layers: the microporous layer (MPL) and the macroporous substrate (MPS). GDL has an average thickness of 200 to 350 µm with it, MPS being from 150 to 300 µm thick, and thinner MPL (30 to 50 µm). In general, the MPL has pores 30-100 times smaller than the MPS, but this varies greatly depending on the type of GDL. [137]

The MPL is formed by deposition of thinner carbon-based particles, fillers, and hydrophobic resins on top of the MPS, which accounts for its significantly smaller pore size and porosity.[140] The GDL is frequently treated with an adequate amount of PTFE in both MPL and MPS to

render it sufficiently hydrophobic while maintaining optimal membrane hydration. Since the GDL is exposed to bipolar plates, it suffers mechanical damage from compression and corrosion from water flow, which has a significant impact on fuel cell performance.[140]

PEMFC involvement in this project

Besides the performances that depicts PEMFC, a half-PEMFC for hydrogen oxidation is included in this project. For that, a platinum catalyst layer is used in the anodic compartment in addition to the separator. The GDL macroporous substrate is placed on a graphite bipolar plate for hydrogen introduction and distribution towards the catalyst clusters (Pt) through the MPL and the catalytic layer. This electrode is called gas diffusion electrode (**Figure I.16A**).

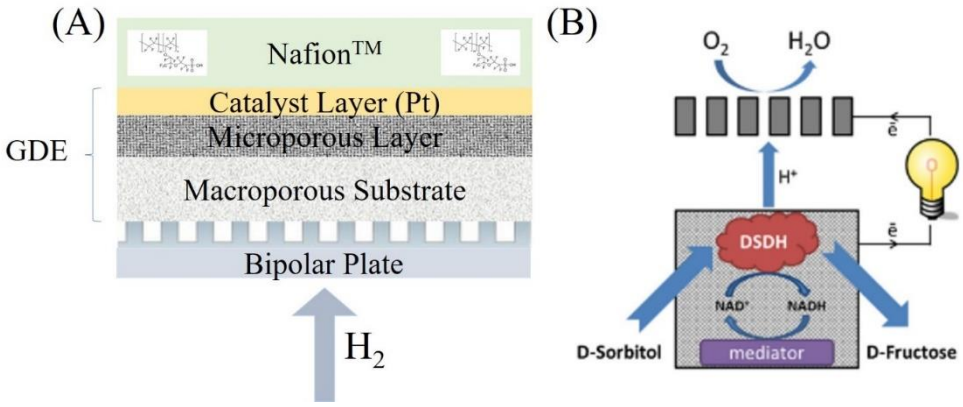

Figure I.16. (A) Representation of cross-section of the anodic compartment with gas diffusion electrode and Nafion membrane (not to be scaled). (B) Example about application of GDE in a flow bioreactor using D-sorbitol dehydrogenase (DSDH) immobilized as bioanode and a GDE as cathode for the simultaneous production of D-Fructose and energy.[141]

Bioelectrochemical systems provide the opportunity to develop novel processes that are efficient and sustainable for the production of a number of valuable products by combining the benefits of biological components (such as reaction specificity and self-replication) with electrochemical techniques. These systems offer the chance to develop novel processes. The performance of bioelectrochemical systems is strongly influenced by the material that is utilized

for the electrodes. In addition to the redox process that occurs at the electrodes, it is necessary to take into account the interactions that biocatalysts have with the electrodes. Some examples of these interactions include enzyme denaturation and biofouling. Gas diffusion electrodes, also known as GDEs, have established themselves as very desirable electrodes for use in bioelectrochemical processes in recent years. GDEs are porous electrodes that have a large three-phase boundary surface. The electrochemical reaction that takes place between the gaseous and liquid phases is supported by a solid catalyst at this interface. GDEs can be applied in microbial and enzymatic fuel cells, for microbial electrolysis, in biosensors, and for electroenzymatic synthesis reactions.[142]

In addition, for applications in gas-liquid phase, GDEs have been suggested to improve current density by overcoming the poor solubility of hydrogen in aqueous electrolytes and minimizing gas-liquid mass transfer constraints.[143]

Figure I.16B illustrates an example for the application of GDE in combined bioelectrochemical synthesis and energy production.[141] The regioselective conversion of D-sorbitol to D-fructose by D-sorbitol dehydrogenase as a model reaction was used to demonstrate the proof of concept for enzymatic electrosynthesis with simultaneous energy production. The flow bioreactor had two electrodes: a carbon felt bioanode modified with multi-walled carbon nanotubes (MWCNT) containing D-sorbitol dehydrogenase immobilized in a silica matrix and a GDE as cathode for oxygen reduction. The NAD^+ cofactor was electrochemically regenerated at the bioanode using a poly(methylene green) mediator electrodeposited on the carbon felt-MWCNT electrode. The conversion rate was 1.18 $mg.day^{-1}.cm^{-3}$, and the energy power output reached 14.6 $\mu W.cm^{-3}$ at 0.1 V.

I.4.1.3 Enzymatic fuel cell (EFC)

EFC: An alternative source of energy of PEMFC under development

While all types of fuel cells adhere to the same electrochemical principles, the enzyme-based fuel cell has unique characteristics due to the intrinsic properties of redox enzymes (**Figure I. 17**), which have both advantages and disadvantages.

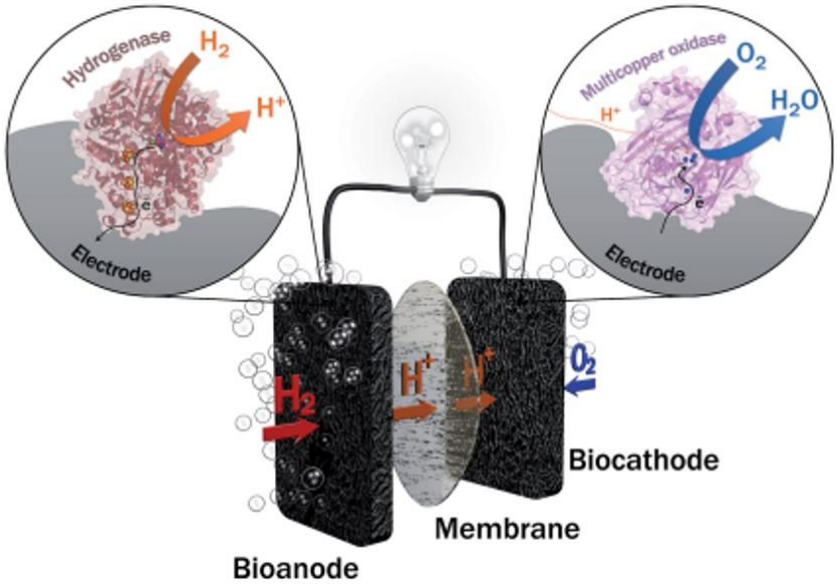

Figure I.17. Schematic illustration of the H_2/O_2 EFC. At the anode, the enzyme responsible for H_2 oxidation is hydrogenase. At the cathode, multicopper oxidases (BOD) reduces O_2 to water.[144]

Advantages of EFC

- First, enzymes are highly efficient and selective catalysts. For instance, lactate dehydrogenases (LDH) used in this study are especially active on pyruvate and have no activity on other components. Hydrogenase enzymes, as their name implies, exclusively utilize hydrogen or protons, a characteristic that results in a simpler and much less expensive fuel cell because it eliminates the need for an ion-exchange membrane barrier because the cross-contamination of fuel and oxidant is no longer a concern.[145,146]

- Second, enzymes are also kinetically efficient. Numerous enzymes can significantly reduce the overpotential required to initiate a reaction.[147,148] Fully reversible and quasi-reversible

reactions are common when using electroactive enzymes as electrocatalysts. For example, the interconversion of the $2H^+/H_2$ couple catalyzed by [NiFe]-hydrogenase. Even the slow four-electron reduction of O_2 can be achieved at high rates by the enzyme bilirubin-oxidase, which only needs an overpotential of 0.3 V. This is better than the well-known Pt.[149]

- Third, as previously described, enzymes are environmentally friendly electrocatalysts. Currently, the primary component of conventional electrocatalysts is transition noble metals such as platinum, iridium, and ruthenium. In contrast, C, H, O, N, and S make up the majority of the skeleton of enzymes. Trace elements such as Ni, Fe, and Zn are also occasionally required as cofactors. For instance, the active site of [NiFe]-hydrogenase contains both Ni and Fe.

- Fourth, the separation of the anode and cathode by proton exchange membrane, if needed, leads generally to a deactivation of enzymes.[150]

Disadvantages of EFC

- Despite the fact that enzymes are more active than many other electrocatalysts in terms of reaction rate per unit of catalyst, they are macromolecules with molecular weights in the range 20-500 kDa range. Therefore, the number of enzyme molecules (catalytic units) to be loaded onto an electrode is restricted.

- Second, many enzymes are sensitive to changes in temperature, pH, or organic solvent. This could make it harder for enzymes to be used in fuel cells in the future.

- Third, not all redox enzymes are electroactive, and some of the electroactive ones show inefficient intramolecular or interfacial electron transfer when they are attached to an electrode surface. For example, the transfer of electrons from the electrode surface to the heme group of chicken liver sulphide oxidase is very fast. However, intramolecular electron transfer is slow because the Mo pterin active site is not close enough to the heme group.[151] Also, some enzyme

molecules when immobilized on an electrode may not be in the best shape for the heme to act as a relay to the active site when they are stuck to an electrode.

- Fourth, purification process of enzymes can be time consuming and of a high cost.

There are methods for overcoming the aforementioned issues. Introducing electrode materials with a large effective surface area is a solution for boosting enzyme loading as reported by Lojou and co-workers. [152]

In addition, the immobilization of enzymes can improve the overall performance and longevity of an enzyme-modified electrode.[153,154]

As for insufficient interfacial electron transfer, the exploitation of electron mediator would work by introducing an intermediary to channel electrons, although this may also complicate the process. Finally, by optimizing the purification protocol and scaling up, the expense of the enzyme purification procedure can be significantly reduced.[155]

BFC involvement in this project

As previously described in section **I.4.1.2**, the fuel cell concept is involved in this project in hydrogen oxidation half-reaction. Hydrogenase is the alternative of platinum usually involved in hydrogen oxidation.

Hydrogenases

The reversible oxidation of hydrogen gas to two protons and two electrons is catalyzed by hydrogenases. They play a crucial role in the energy metabolism of a diverse array of microorganisms. Hydrogenase (**Figure I.18**) can also be divided into three classes based on their catalytic centers: Fe, FeFe, and NiFe.[156–158] [FeFe]-hydrogenases are O_2-sensitive hydrogenases that are inhibited by oxygen. [FeFe]-hydrogenases contain a di-iron catalytic core

and are primarily responsible for H_2 evolution. Only one iron is present in the catalytic center of [Fe]-hydrogenases for H_2 oxidation.

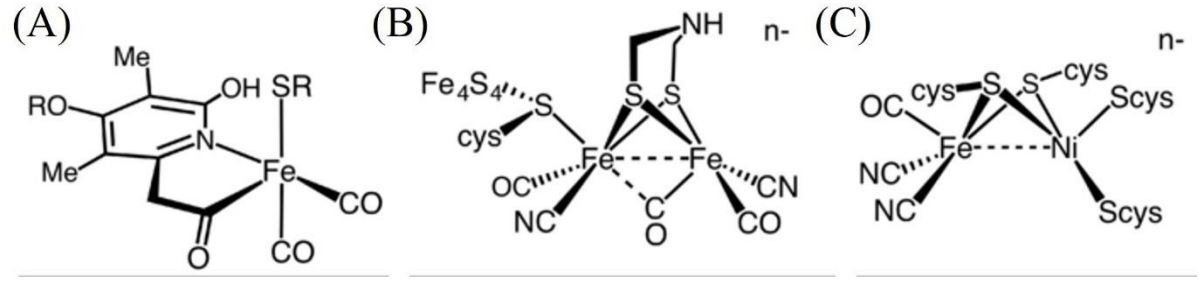

Figure I.18. Structures of (A) [Fe] hydrogenase, (B) [Fe-Fe] hydrogenase, and (C) [Fe-Ni] hydrogenase.[156–158]

[NiFe] hydrogenases are the most robust hydrogenases with a heterodinuclear Ni-Fe active site, and they are typically involved in H_2 uptake. The majority of [NiFe] hydrogenases are O_2-tolerant hydrogenases that remain active in the presence of oxygen, making them potentially useful for industrial applications.

Hydrogenase 1 (Hyd-1) and Hydrogenase 2 (Hyd-2) are periplasmic membrane-bound enzymes responsible for H_2-uptake. Hyd-1 is O_2-tolerant, whereas Hyd-2 is an O_2-sensitive, reversibly inhibited enzyme. Hyd-1 requires an overpotential of approximately 0.05 V for H_2 oxidation, whereas Hyd-2 catalyzes H_2 oxidation at the thermodynamic potential, according to electrochemical experiments. As Hyd-1 is more efficient in an aerobic environment than Hyd-2, Hyd-1 is applied in this thesis.

Immobilization of hydrogenase onto an electrode

Recent studies emphasize the importance of hydrogenase immobilization onto electrodes for efficient H_2 enzymatic oxidation. First, the immobilized hydrogenase on an electrode has to exhibit much stability with time. Another goal is to develop high surface area and nanostructured electrodes capable of increasing the amount of directly connected enzymes so that the bioanode can compete with platinum-based electrodes. Another concept is emphasized,

which has only recently considered for hydrogenases but providing new insight into the control of electron transfer processes (i.e. direct or mediated electron transfer processes), is the search for an interface that allows control of the enzyme's orientation. The most efficient immobilization of hydrogenase will most likely be a balance of these three concepts.

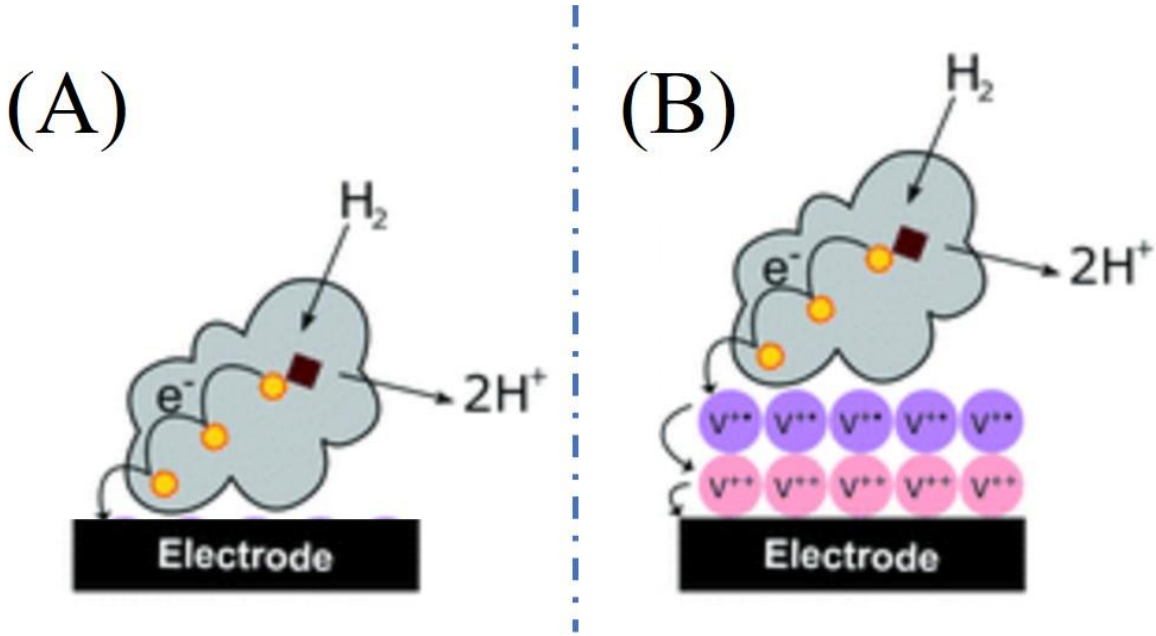

Figure I.19. Cartoon representation of hydrogen oxidation by hydrogenase with (A) direct electron transfer (DET and (B) mediated electron transfer (MET) by methyl viologen.[159]

There are two types of electron transfer mechanisms between enzymes and electrodes: mediated electron transfer (MET) (**Figure I.19B**) and direct electron transfer (DET) (**Figure I.19A)**.[87,160] In a MET-type system, extrinsic redox-active compounds such as methyl viologen are used as redox mediators to transfer electrons between hydrogenase and the electrode.[159,161] Small and low molecular weight electron mediators that require low overpotentials can be advantageous because they enable rapid electron transfer rates with low power losses between an enzyme and an electrode.[161] However, cost, stability, selectivity, and ability of such mediators to exchange electrons in the immobilized state must also be considered.

In contrast, in a DET system, rapid electron transfer occurs via an intrinsic electron relay system.[109,162]

Because of lower overpotentials and less interference, the direct electron transfer process may be advantageous for biofuel cell applications, as well as eliminating the need for co-immobilization of a redox mediator.[144]

I.4.2 NAD(P)H regeneration in a flow reactor

I.4.2.1 Flow electrochemistry

Despite the fact that continuous flow processes have been around for decades and are the foundation of the petrochemical industry in extracting crude material, refining it, and synthesizing bulk products, the use of flow cells for organic synthesis has only recently gained attraction in academia. The incentive of flow chemistry can be attributed to the search for innovative and sustainable chemical processes in organic synthesis, as various electrochemical reactions exhibit high selectivity and reproducibility while reducing costs, energy and solvent consumption, and carbon footprint.[163]

Academic researchers are appreciating flow synthesis for its inherent advantages of enhanced mass and heat transfer, dependable scalability, and inherent safety. As a result, academic institutions and industries are increasing their efforts to adopt this technology. Consequently, a combination of two emerging technologies in organic synthesis — flow chemistry and electrochemistry — may appear to be the option for bridging the two sectors.

In its simplest and most common configuration, an electrochemical flow cell would have two plate electrodes facing one another, and the reaction solution would flow through a channel created by isolating spacers. A flow cell in this configuration has electrodes that are parallel. Its broad applicability for organic electrosynthesis is a result of its simple fabrication and

uniform potential and current distribution attributable to the parallel electrodes configuration.[164]

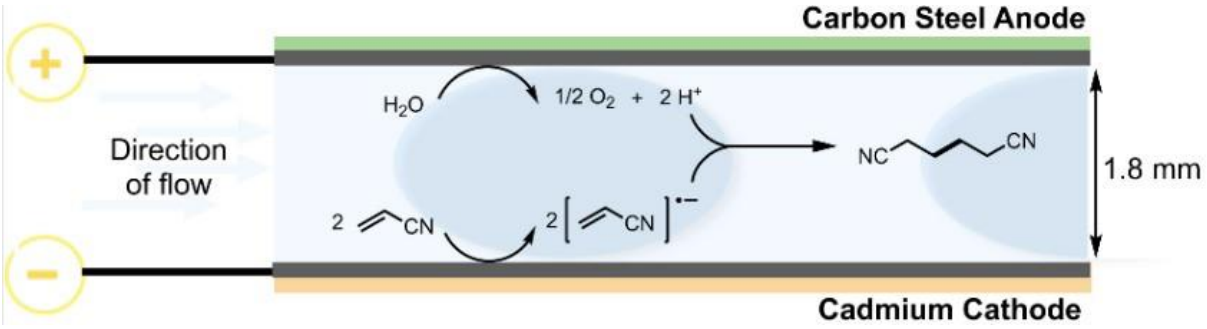

Figure I.20. The « new Mosanto » process for the electrosynthesis of adiponitrile.

The "new Monsanto" process for the electrosynthesis of adiponitrile (**Figure I.20**) is illustrative of the high industrial potential of flow electrosynthesis.[59] The Monsanto process involves the electrochemical hydrodimerization of acetonitrile into adiponitrile, a precursor to nylon 6,6. In 2010, 0.34 million tons per year were produced, making it the largest industrial electrochemical process. In 1965, the first batch process utilized a divided cell with lead/lead oxide electrodes and a catholyte mixture of 16% acetonitrile, 16% adiponitrile, 40% tetraethylammonium ethylsulfate, and 28% water. Each cell was supplied with 12 V, which led to a cathode current density of 0.4–0.6 A/cm^2 and a selectivity of 92% for adiponitrile. The annual production of 900 tons consumed 6,700 kWh per ton. In 1984, the second-generation or "new Monsanto" process, which enables comparable selectivity and employs an undivided flow cell with electrodes made of carbon steel sheets and cadmium-plated faces, was developed through multiple stages of refinement. The reaction mixture consists of an emulsion of acetonitrile and adiponitrile in water with 0.4% hexamethylene-bis(ethyl dibutylammonium) and 15% disodium hydrogen phosphate. The interelectrode gap has been reduced from 7 mm to 1.8 mm, resulting in a significant reduction in the amount of supporting electrolyte required (from 40 % to 15.4 %) and its type, allowing for easier isolation by simple extraction followed by distillation.

Currently, adiponitrile production exceeds 300,000 tons per year, and this flow process has reduced energy consumption by 37 % to 2500 kWh/ton.[59]

In conclusion, under flow condition and with an optimized arrangement of electrodes, mass transfer, ohmic drop, and selectivity are issues that typically arise in batch electro-organic systems that are circumvented by flow electrosynthesis.

I.4.2.2 Cofactor electrochemical regeneration in flow reactors

Recently, the regeneration of enzymatic cofactors in electrochemical flow reactors has gained more interest. Yoon et al. prepared an electrochemical laminar flow microreactor to regenerate NADH in the synthesis of chiral L-lactate from the achiral substrate pyruvate (**Figure I.21A**). For this purpose, gold electrodes were deposited on the inner wall of a Y-shaped reactor, with two separate streams, one with the buffer and the second with reagents (FAD, NAD^+, enzymes and substrate), with the flow directed to the cathode. The reduced cofactor, $FADH_2$ was produced at the cathode and used for the reduction of NAD^+ to NADH, resulting in a 41 % yield of L-lactate.[165]

$FADH_2$ was electrochemically regenerated using a filter-press microreactor with semi-cylindrical channels on the electrode surface resulting in large surface areas (**Figure I.21B**).[96]

As the electrochemical cofactor regeneration must, by definition, take place at the surface of the electrode, scaling up reactions is likely to result in diffusion limitations that reduce reaction rates.[166] Using three-dimensional electrodes in continuous flow reactors can solve this problem. Kochius et al designed a system for the efficient electrochemical regeneration of NAD^+ based on three-dimensional electrodes with a high working surface area of 24 m^2. Two cathodes (titanium net) surrounded the anode, which was comprised of a dense bed of glassy carbon particles. Using ABTS as a mediator, NADH was oxidized at turnover rates of 1860 h^{-1} and 93 h^{-1} for the mediator and cofactor, respectively, which were significantly higher than

those previously reported. For the three-dimensional electrochemical reactor, a space-time yield of 1,4 g L^{-1}. h^{-1} was achieved, which is greater than that of the two-dimensional cell (**Figure I.21 C**).[167]

Ruinatscha et al. constructed a reactor with three-dimensional porous carbon electrodes that have a surface area to volume ratio of near 19.7 $m^2.m^{-3}$ (**Figure I.21D**).

The reactor was used to generate $FADH_2$, which was then coupled with styrene monooxygenases to produce styrene oxide. In this system, the rate of mass transfer increased, and FAD was reduced at a rate of 93 $mM.h^{-1}$ while styrene oxide was produced at a rate of 1.3 $mM.h^{-1}$.[168]

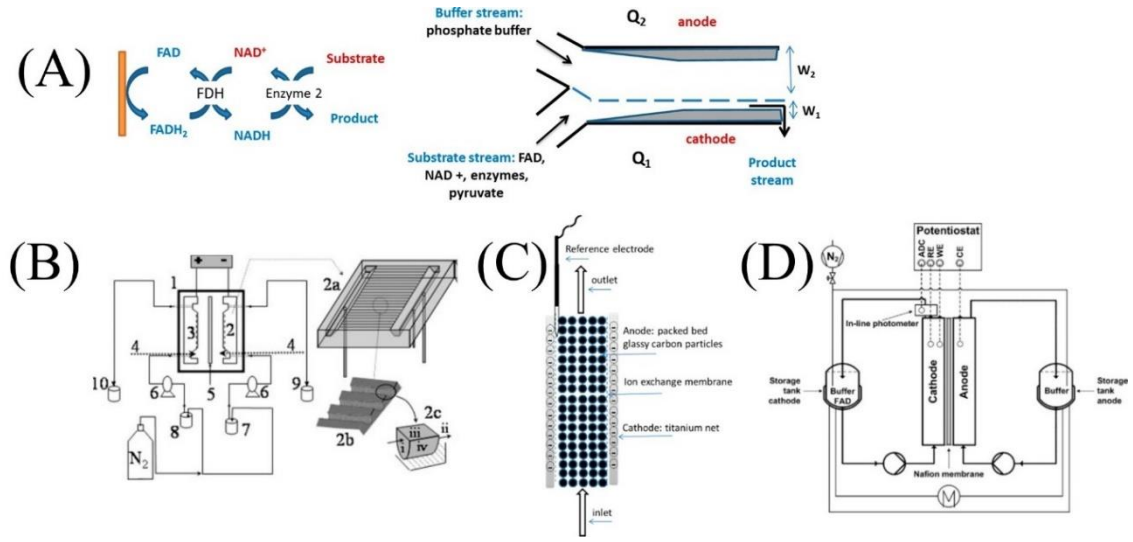

Figure I.21. Examples about applied electrochemical reactors in cofactors regeneration. (A) NADH regeneration in Y shaped electrochemical reactor.[165] (B) Electrochemical filter-press microreactor.[96] (C) 3D schematic electrode.[167] (D) Schematic representation of the applied electrochemical reactor for FAD regeneration.[168]

Besides, Rodriguez-Hinestroza et al. created an electrochemical filter press microreactor for the direct anodic regeneration of NAD^+ through the horse-liver alcohol dehydrogenase-catalyzed synthesis of alanine. The platinum and gold electrodes utilized had a high surface area of 250

cm^2 and 150 microchannels. The direct oxidation of NADH at the gold electrode resulted in a 92 % conversion of NADH to NAD^+. The NAD^+ produced was utilized in the enzymatic oxidation of carboxybenzyl aminopropanol.[169]

Mazurenko et al. conducted poly(methylene green)-mediated NAD^+ regeneration in a flow reactor for the synthesis of D-fructose from D-sorbitol using D-sorbitol dehydrogenase (**Figure I.16 B**).[141]

In the present work, we coupled the electrochemical or the electroenzymatic regeneration of NAD(P)H in flow to the oxidation of hydrogen for the bioconversion of pyruvate catalyzed by lactate dehydrogenase. This efficient coupling between both half reactions can be favored in the presence carbon electrode materials which increases the electroactive surface.

I.4.3 Carbon based electrode materials

Carbon materials have been utilized extensively in the modification of electrodes.[170–172] Carbon nanotubes have special characteristics like high conductivity and high surface areas. A simple method for modifying electrodes with carbon nanotubes and enzymes involves placing a droplet of an enzyme and carbon nanotube suspension on the surface of the electrode.[173] Electrode modification with carbon nanotubes can facilitate direct electron transfer between the electrode and enzymes such as hydrogenase,[109] and fructose dehydrogenase,[174] leading to the production of efficient biofuel cells.[175,176] Jourdin et al. utilized multiwalled carbon nanotubes to enhance the performance of a microbial system for carbon dioxide bioreduction. Compared to graphite plate electrodes, multiwalled carbon nanotube electrodes increased the rate of electron transfer between the electrode and microorganisms by 1.65-fold and the rate of acetate production by 2.60-fold.[177] Using a vitreous carbon electrode modified with multi-walled carbon nanotubes,[178] describes the microbial electrosynthesis of acetate from CO_2. Bulutoglu et al. immobilized alcohol dehydrogenase on multi-walled carbon nanotubes for electrocatalytic

oxidation of 2,3-butanediol.[179] Bucky papers are flexible, lightweight carbon nanotube-based materials [147,166].[180,181] Zhang et al. developed a bioelectrode for electroenzymatic synthesis by immobilizing $[Cp^*Rh(bpy)Cl]^+$ on a bucky paper electrode as a mediator for the regeneration of NADH. The regeneration of NADH attained a turnover frequency of 1.3 s^{-1} and the system was utilized for the preparation of D-sorbitol from D-fructose using immobilized D-sorbitol dehydrogenase.[78]

The high porosity of 3D graphene materials permits greater enzyme loadings, thereby enhancing the performance of electrodes. Choi et al. utilized graphitic carbon nitride and reduced graphene oxide as an effective cathode for O_2 reduction. The peroxygenase-catalyzed selective hydroxylation of ethylbenzene to (R)-1-phenylethanol was catalyzed by the H_2O_2 produced at the cathode surface.[182] Through the controlled functionalization of graphene, enzymes can be covalently bonded to graphene hybrid electrodes, resulting in increased stability. Effective conjugation of enzyme and graphene can pave the way for direct electron transfer at the electrode surface. Seelajaroen et al. utilized enzyme–graphene hybrids for the electrochemical synthesis of methanol from CO_2 utilizing NAD(P)-linked enzymes such as formate dehydrogenase, formaldehyde dehydrogenase, and alcohol dehydrogenase. Enzymes were covalently bonded to the carboxylate-modified surfaces of graphene.[183]

I.5 Concepts and Methodologies for this work

As the importance of sustainability grows in chemical and pharmaceutical industries, new technologies that reduce energy demands, use renewable resources, and aid productivity and automation, becoming increasingly important.[184,185]Continuous processes and biocatalysis are two key examples of technologies that can fill these aforementioned gaps.

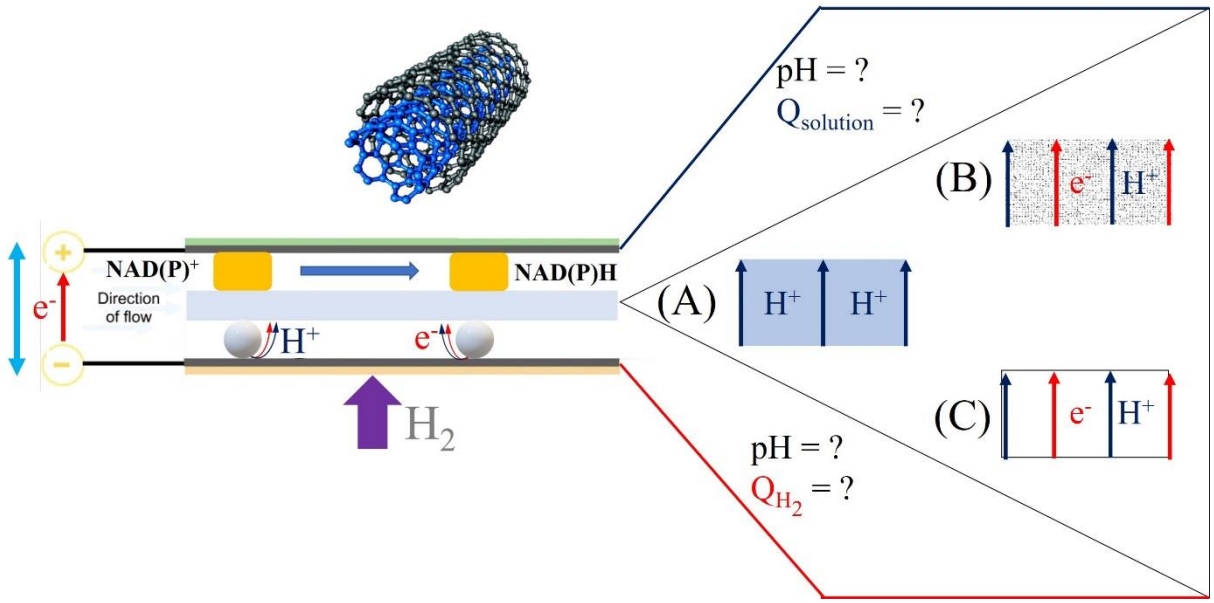

Figure I.22. Schematic view of the flow bioelectrochemical reactor for coupling hydrogen oxidation to NAD(P)H regeneration. Different parameters were taken into consideration in this work e.g., electrode material, pH, distance between anodic and cathodic compartments, and hydrogen and solution flow rates. Separation between anodic and cathodic compartments is one of the main principles and can be based on three possible configurations: (A) Nafion membrane, (B) polymeric separator, and (C) membraneless system.

Biocatalysis, on the other hand, allows for the replacement of finite resource, toxic metal catalysts with renewable alternatives while also enabling high productivities under mild reaction conditions. One area where these advantages may coincide, is the incorporation of redox biocatalysts into continuous processes for the asymmetric reduction of C=X bonds in the synthesis of molecules.[184] One of the difficulties in implementing C=X bond reduction biocatalysts is that the relevant dehydrogenase enzymes rely on hydride transfer from expensive organic cofactors, most commonly NADH or NADPH. In consequence, these cofactors have to be regenerated as discussed above.

Aside from electricity generation, another application for fuel cells is biosynthesis, which uses the driving force of redox reactions. **Figure I.23** depicts two overlaid LSVs **(linear sweep**

voltammetry). The red and blue traces represent the H^+/H_2 and the Rh (III)/Rh(I) complexes half-reactions respectively.

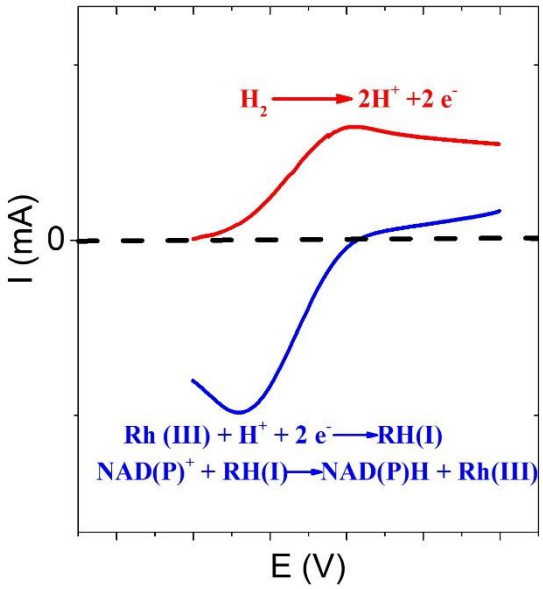

Figure I.23. Linear sweep voltammetry showing the overlaying between hydrogen oxidation and Rh(III) reduction.

While the experimental details of these CVs will be discussed later (**chapter VI**), the point of this overlaid plot is to show that combining any two of these traces is possible and can lead to the indirect regeneration of the NAD(P)H cofactor after valuable optimizations in the flow reactor.

Two main focuses are the basics to reach the objective of the work: the efficient regeneration of the NAD(P)H cofactor and the minimization of the system resistivity.

In this PhD project, the efficient regeneration of the cofactor in the hybrid flow reactor relies on a panel of optimizations such as the hydrogen and solution flow rates, the hydrogen gas fed condition (humidified or non-humidified) (**chapter II**), the amount of catalysts and the procedure for their immobilization, the electrode material e.g., graphite felt and MWCNT that assures a uniform distribution of the solution and increases the electroactive surface area respectively, and the pH in both compartments. Once the efficient regeneration will be reached,

testing the activity of the regenerated cofactor (**1,4-NAD(P)H**) and its coupling to one of the NAD(P) dependent reactions will be the most important criteria that denotes the process viability. For instance, the distance between the electrochemical or the electroenzymatic catalysts and the NAD(P) dependent enzyme and the amount of each of them plays an important role in the productivity of the system as it will discussed in **chapter II and IV**.

In addition to working under flow conditions that increases mass transport between species, coupling hydrogen oxidation to NAD(P)H regeneration requires a minimum resistivity of the overall system. In other words, to couple both oxidation and reduction half-reactions, increasing the interconnection between anodic and cathodic catalysts centers is a requirement. The first requirement to make that possible is to minimize the distance between both compartments as illustrated in the example of « new Mosanto » process for the electrosynthesis of adiponitrile ($d < 2$ mm). Here in our system, the distance between both compartments depends on the thickness of the separator (<1.5 mm). The transport of protons is possible through a Nafion membrane (**Figure I.22A**) that allows a uniform and selective passage of protons from the anodic to the cathodic compartment.

The resistivity of the system can be minimized by replacing the Nafion membrane by a polymeric separator (**Figure I. 22 (B)**), **Chapter VI**, or by using a membraneless system as applied in biofuel cells (**Figure I. 22 (C)**). Nevertheless, the simplicity as well as the robustness and the low-cost of the system are all required.

The overall system consists of a flow reactor inspired from redox flow batteries. The produced cofactor by this hybrid reactor will be used in the biosynthesis of useful molecules. All these concepts have been explored in this work with both electrochemical catalysts *e.g.*, platinum and rhodium complex and electroenzymatic catalysts *e.g.*, Hydrogenase (**Chapter VII**) and Ferredoxin $NAD(P)^+$ reductase (FNR) (**Chapter V**).

Apart from this bibliographic survey (**Chapter I**), this thesis is composed of 6 other chapters. **Chapter II and III** reports the experimental work and a modelling part related to NADH regeneration electrochemically mediated by a Rh complex, dissolved in solution, carried out in a redox flow bioreactor that is also equipped with a gas diffusion electrode for hydrogen oxidation. The reactor was initially optimized for rhodium complex and NAD^+ concentrations, hydrogen gas humidification, flow rates of both H_2 gas and electrolytic solution, and solution pH.

Chapter IV reports the stability and the performances of the combined electrochemical regeneration of the NADH cofactor mediated by the rhodium complex covalently immobilized on MWCNTs with hydrogen oxidation for the bioconversion of pyruvate.

Chapter V focuses on highlighting the performances of the system while coupling NAD(P)H regeneration catalyzed by FNR to hydrogen.

Chapter VI discusses the development of an electroless system for coupling hydrogen oxidation to NADH regeneration.

Chapter VII focuses on the exchange of platinum at the GDE by hydrogen oxidation by hydrogenase.

References

[1] U. T. Bornscheuer, K. Bucholz, *Eng. Life Sci.* **2005**, *5*, 309–323.

[2] A. Schmid, J. S. Dordick, B. Hauer, A. Kiener, M. Wubbolts, B. Witholt, *Nature* **2001**, *409*, 258–268.

[3] V. F. Dr. Vladimir, *Gastron. ecuatoriana y Tur. local.* **1967**, *1*, 5–24.

[4] J. M. Thomas, *Angew. Chemie Int. Ed. English* **1994**, *33*, 913–937.

[5] A. G. McDonald, K. F. Tipton, *FEBS J.* **2014**, *281*, 583–592.

[6] C. C. C. R. De Carvalho, *Biotechnol. Adv.* **2011**, *29*, 75–83.

[7] R. C. Willson, M. R. Ladisch, ACS Publications, **1990**.

[8] D. J. Pollard, J. M. Woodley, *Trends Biotechnol.* **2007**, *25*, 66–73.

[9] R. Leon, P. Fernandes, H. M. Pinheiro, J. M. S. Cabral, *Enzyme Microb. Technol.* **1998**, *23*, 483–500.

[10] K. Ban, M. Kaieda, T. Matsumoto, A. Kondo, H. Fukuda, *Biochem. Eng. J.* **2001**, *8*, 39–43.

[11] H. Fukuda, S. Hama, S. Tamalampudi, H. Noda, *Trends Biotechnol.* **2008**, *26*, 668–673.

[12] Y. Ni, R. R. Chen, *Biotechnol. Bioeng.* **2004**, *87*, 804–811.

[13] S. Sheldon, R. A.;van Pelt, *Chem. Soc. Rev.* **2013**, *42*, 6223–6235.

[14] X. Xiao, H. Xia, R. Wu, L. Bai, L. Yan, E. Magner, S. Cosnier, E. Lojou, Z. Zhu, A. Liu, *Chem. Rev.* **2019**, *119*, 9509–9558.

[15] C. Engineering, *Chem. Eng. Sci.* **1996**, *51*, 5091–5102.

[16] O. Kuchner, F. H. Arnold, *Trends Biotechnol.* **1997**, *15*, 523–530.

[17] R. Ciriminna, M. Pagliaro, *Org. Process Res. Dev.* **2013**, *17*, 1479–1484.

[18] K. Mashima, K. Kusano, N. Sato, Y. Matsumura, K. Nozaki, H. Kumobayashi, N. Sayo, Y. Hori, T. Ishizaki, *J. Org. Chem.* **1994**, *59*, 3064–3076.

[19] J. X. Gao, T. Ikariya, R. Noyori, *Organometallics* **1996**, *15*, 1087–1089.

[20] A. Zanotti-Gerosa, W. Hems, M. Groarke, F. Hancock, *Platin. Met. Rev.* **2005**, *49*, 158–165.

[21] R. Noyori, S. Hashiguchi, *Acc. Chem. Res.* **1997**, *30*, 97–102.

[22] J. M. Woodley, *Trends Biotechnol.* **2008**, *26*, 321–327.

[23] R. A. Sheldon, *Green Chem.* **2007**, *9*, 1273–1283.

[24] R. A. Sheldon, *Chem. Commun.* **2008**, 3352–3365.

[25] C. K. Savile, J. M. Janey, E. C. Mundorff, J. C. Moore, S. Tam, W. R. Jarvis, J. C. Colbeck, A. Krebber, F. J. Fleitz, J. Brands, P. N. Devine, G. W. Huisman, G. J. Hughes, *Science (80-.).* **2010**, *329*, 305–309.

[26] T. Li, J. Liang, A. Ambrogelly, T. Brennan, G. Gloor, G. Huisman, J. Lalonde, A. Lekhal, B. Mijts, S. Muley, L. Newman, M. Tobin, G. Wong, A. Zaks, X. Zhang, *J. Am. Chem. Soc.* **2012**, *134*, 6467–6472.

[27] J. A. Pollock, K. M. Clark, B. J. Martynowicz, M. G. Pridgeon, M. J. Rycenga, K. E. Stolle, S. K. Taylor, *Tetrahedron Asymmetry* **2007**, *18*, 1888–1892.

[28] S. K. Ma, J. Gruber, C. Davis, L. Newman, D. Gray, A. Wang, J. Grate, G. W. Huisman, R. A. Sheldon, *Green Chem.* **2010**, *12*, 81–86.

[29] R. R. Breaker, G. F. Joyce, *J. Mol. Evol.* **1995**, *40*, 551–558.

[30] A. L. Lehninger, *New York Worth* **1993**.

[31] W.-D. Lienhart, V. Gudipati, P. Macheroux, *Arch. Biochem. Biophys.* **2013**, *535*, 150–162.

[32] T. A. Rouault, W. H. Tong, *Trends Genet.* **2008**, *24*, 398–407.

[33] T. A. Rouault, W.-H. Tong, *Nat. Rev. Mol. Cell Biol.* **2005**, *6*, 345–351.

[34] M. K. Johnson, *Curr. Opin. Chem. Biol.* **1998**, *2*, 173–181.

[35] D. C. Johnson, D. R. Dean, A. D. Smith, M. K. Johnson, *Annu. Rev. Biochem.* **2005**, *74*, 247–281.

[36] H. Ogino, S. Inomata, H. Tobita, *Chem. Rev.* **1998**, *98*, 2093–2121.

[37] S. Bandyopadhyay, K. Chandramouli, M. K. Johnson, *Biochem. Soc. Trans.* **2008**, *36*, 1112–1119.

[38] C. J. C. Whitehouse, S. G. Bell, L.-L. Wong, *Chem. Soc. Rev.* **2012**, *41*, 1218–1260.

[39] C. Jia, T. Kitamura, Y. Fujiwara, *Acc. Chem. Res.* **2001**, *34*, 633–639.

[40] G. Grogan, *Curr. Opin. Chem. Biol.* **2011**, *15*, 241–248.

[41] R. Bernhardt, *J. Biotechnol.* **2006**, *124*, 128–145.

[42] R. Zuber, E. Anzenbacherová, P. Anzenbacher, *J. Cell. Mol. Med.* **2002**, *6*, 189–198.

[43] S. A. Wrighton, J. C. Stevens, *Crit. Rev. Toxicol.* **1992**, *22*, 1–21.

[44] W. Kroutil, H. Mang, K. Edegger, K. Faber, *Curr. Opin. Chem. Biol.* **2004**, *8*, 120–126.

[45] K. Goldberg, K. Schroer, S. Lütz, A. Liese, *Appl. Microbiol. Biotechnol.* **2007**, *76*, 249–255.

[46] A. Weckbecker, W. Hummel, *Biocatal. Biotransformation* **2006**, *24*, 380–389.

[47] S. Hussain, F. Leipold, H. Man, E. Wells, S. P. France, K. R. Mulholland, G. Grogan, N. J. Turner, *ChemCatChem* **2015**, *7*, 579–583.

[48] K. Mitsukura, M. Suzuki, K. Tada, T. Yoshida, T. Nagasawa, *Org. Biomol. Chem.* **2010**, *8*, 4533–4535.

[49] K. Mitsukura, M. Suzuki, S. Shinoda, T. Kuramoto, T. Yoshida, T. Nagasawa, *Biosci. Biotechnol. Biochem.* **2011**, *75*, 1778–1782.

[50] B. V Adalbjörnsson, H. S. Toogood, A. Fryszkowska, C. R. Pudney, T. A. Jowitt, D. Leys, N. S. Scrutton, *ChemBioChem* **2010**, *11*, 197–207.

[51] J. Pietruszka, M. Schölzel, *Adv. Synth. Catal.* **2012**, *354*, 751–756.

[52] D. Mangan, I. Miskelly, T. S. Moody, *Adv. Synth. Catal.* **2012**, *354*, 2185–2190.

[53] Y. Fu, K. Hoelsch, D. Weuster-Botz, *Process Biochem.* **2012**, *47*, 1988–1997.

[54] J. A. Duine, J. F. Jzn, J. K. Van Zeeland, *FEBS Lett.* **1979**, *108*, 443–446.

[55] W. Adam, M. Lazarus, C. R. Saha-Möller, P. Schreier, *Tetrahedron: Asymmetry* **1998**, *9*, 351–355.

[56] S. Zhou, K. T. Shanmugam, L. O. Ingram, *Appl. Environ. Microbiol.* **2003**, *69*, 2237–2244.

[57] A. Weckbecker, H. Gröger, W. Hummel, in *Biosyst. Eng. I*, Springer, **2010**, pp. 195–242.

[58] R. Wichmann, D. Vasic-Racki, *Technol. Transf. Biotechnol.* **2005**, 225–260.

[59] K. Aoki, K. Tokuda, H. Matsuda, *J. Electroanal. Chem. interfacial Electrochem.* **1987**, *217*, 33–47.

[60] H. K. Chenault, E. S. Simon, G. M. Whitesides, *Biotechnol. Genet. Eng. Rev.* **1988**, *6*, 221–270.

[61] A. L. Lehninger, *Ann. N. Y. Acad. Sci.* **1969**, *147*, 816–823.

[62] F. Hollmann, B. Witholt, A. Schmid, *J. Mol. Catal. B Enzym.* **2002**, *19*, 167–176.

[63] X. Wang, T. Saba, H. H. P. Yiu, R. F. Howe, J. A. Anderson, J. Shi, *Chem* **2017**, *2*, 621–654.

[64] R. Ruppert, S. Herrmann, E. Steckhan, *J. Chem. Soc. Chem. Commun.* **1988**, 1150–1151.

[65] M. M. Grau, M. Poizat, I. W. C. E. Arends, F. Hollmann, *Appl. Organomet. Chem.* **2010**, *24*, 380–385.

[66] R. Ruppert, S. Herrmann, E. Steckhan, *Tetrahedron Lett.* **1987**, *28*, 6583–6586.

[67] Z. J. Wang, K. N. Clary, R. G. Bergman, K. N. Raymond, F. D. Toste, *Nat. Chem.* **2013**, *5*, 100–103.

[68] V. Köhler, Y. M. Wilson, M. Dürrenberger, D. Ghislieri, E. Churakova, T. Quinto, L. Knörr, D. Häussinger, F. Hollmann, N. J. Turner, others, *Nat. Chem.* **2013**, *5*, 93–99.

[69] T. Quinto, V. Köhler, T. R. Ward, *Top. Catal.* **2014**, *57*, 321–331.

[70] M. Poizat, I. W. C. E. Arends, F. Hollmann, *J. Mol. Catal. B Enzym.* **2010**, *63*, 149–156.

[71] Z. Goren, N. Lapidot, I. Willner, *J. Mol. Catal.* **1988**, *47*, 21–32.

[72] C. Kohlmann, W. Märkle, S. Lütz, *J. Mol. Catal. B Enzym.* **2008**, *51*, 57–72.

[73] F. Hollmann, A. Schmid, *Biocatal. Biotransformation* **2004**, *22*, 63–88.

[74] F. Hollmann, I. W. C. E. Arends, K. Buehler, *ChemCatChem* **2010**, *2*, 762–782.

[75] W. Liu, P. Wang, *Biotechnol. Adv.* **2007**, *25*, 369–384.

[76] R. Ruppert, S. Herrmann, E. Steckhan, *Tetrahedron Lett.* **1987**, *28*, 6583–6586.

[77] B. Tan, D. P. Hickey, R. D. Milton, F. Giroud, S. D. Minteer, *J. Electrochem. Soc.* **2015**, *162*, H102.

[78] L. Zhang, M. Etienne, N. Vilà, T. X. H. Le, G.-W. Kohring, A. Walcarius, *ChemCatChem* **2018**, *10*, 4067–4073.

[79] R. Wienkamp, E. Steckhan, *Angew. Chemie Int. Ed. English* **1982**, *21*, 782–783.

[80] M. Beley, J.-P. Collin, *J. Mol. Catal.* **1993**, *79*, 133–140.

[81] K. Delecouls-Servat, R. Basseguy, A. Bergel, *Bioelectrochemistry* **2002**, *55*, 93–95.

[82] E. Steckhan, in *Electrochem. V*, Springer, **1994**, pp. 83–111.

[83] J. S. Lee, S. H. Lee, J. Kim, C. B. Park, *J. Mater. Chem. A* **2013**, *1*, 1040–1044.

[84] L. Zhang, N. Vilà, G. W. Kohring, A. Walcarius, M. Etienne, *ACS Catal.* **2017**, *7*, 4386–4394.

[85] C. Cadoux, R. D. Milton, *ChemElectroChem* **2020**, *7*, 1974–1986.

[86] R. D. Milton, S. D. Minteer, *J. R. Soc. Interface* **2017**, *14*, 20170253.

[87] A. L. Ghindilis, P. Atanasov, E. Wilkins, *Electroanalysis* **1997**, *9*, 661–674.

[88] A. Bassegoda, C. Madden, D. W. Wakerley, E. Reisner, J. Hirst, *J. Am. Chem. Soc.* **2014**, *136*, 15473–15476.

[89] C. Léger, S. J. Elliott, K. R. Hoke, L. J. C. Jeuken, A. K. Jones, F. A. Armstrong, *Biochemistry* **2003**, *42*, 8653–8662.

[90] J. Cantet, A. Bergel, M. Comtat, J.-L. Séris, *J. Mol. Catal.* **1992**, *73*, 371–380.

[91] J. Cantet, A. Bergel, M. Comtat, *Enzyme Microb. Technol.* **1996**, *18*, 72–79.

[92] M. Yuan, M. J. Kummer, R. D. Milton, T. Quah, S. D. Minteer, *ACS Catal.* **2019**, 5486–5495.

[93] M. Schulz, H. Leichmann, H. Günther, H. Simon, *Appl. Microbiol. Biotechnol.* **1995**, *42*, 916–922.

[94] H. Günther, K. Walter, P. Köhler, H. Simon, *J. Biotechnol.* **2000**, *83*, 253–267.

[95] E. Katz, I. Willner, *J. Am. Chem. Soc.* **2003**, *125*, 6803–6813.

[96] K. Cheikhou, T. Tzedakis, *AIChE J.* **2008**, *54*, 1365–1376.

[97] A. Bergel, M. Comtat, *J. Electroanal. Chem. interfacial Electrochem.* **1991**, *302*, 219–231.

[98] N. Carrillo, E. A. Ceccarelli, *Eur. J. Biochem.* **2003**, *270*, 1900–1915.

[99] M. A. Musumeci, E. A. Ceccarelli, D. L. Catalano-Dupuy, *Adv. Photosynth. Asp. Najafpour, M., Ed.; InTech Rijeka, Croat.* **2012**, 539–562.

[100] J. A. Hermoso, T. Mayoral, M. Faro, C. Gómez-Moreno, J. Sanz-Aparicio, M. Medina, *J. Mol. Biol.* **2002**, *319*, 1133–1142.

[101] A. Aliverti, V. Pandini, A. Pennati, M. de Rosa, G. Zanetti, *Arch. Biochem. Biophys.* **2008**, *474*, 283–291.

[102] B. Siritanaratkul, C. F. Megarity, T. G. Roberts, T. O. M. Samuels, M. Winkler, J. H. Warner, T. Happe, F. A. Armstrong, *Chem. Sci.* **2017**, *8*, 4579–4586.

[103] M. A. Musumeci, H. Botti, A. Buschiazzo, E. A. Ceccarelli, *Biochemistry* **2011**, *50*, 2111–2122.

[104] G. Kurisu, M. Kusunoki, E. Katoh, T. Yamazaki, K. Teshima, Y. Onda, Y. Kimata-Ariga, T. Hase, *Nat. Struct. Biol.* **2001**, *8*, 117–121.

[105] C. J. Batie, H. Kamin, *J. Biol. Chem.* **1984**, *259*, 11976–11985.

[106] S. Fukuzumi, Y.-M. Lee, W. Nam, *J. Inorg. Biochem.* **2019**, *199*, 110777.

[107] L. Lauterbach, O. Lenz, K. A. Vincent, **2013**, *280*, 3058–3068.

[108] S. Belkin, I. Endo, S. O. Enfors, W. S. Hu, B. Mattiasson, J. Nielsen, G. Stephanopoulos, G. T. Tsao, R. Ulber, A. P. Zeng, others, *Biotechnology* **2010**, *123*.

[109] E. Lojou, *Electrochim. Acta* **2011**, *56*, 10385–10397.

[110] K. A. Vincent, X. Li, C. F. Blanford, N. A. Belsey, J. H. Weiner, F. A. Armstrong, *Nat. Chem. Biol.* **2007**, *3*, 761–762.

[111] H. A. Reeve, P. A. Ash, H. Park, A. Huang, M. Posidias, C. Tomlinson, O. Lenz, K. A. Vincent, *Biochem. J.* **2017**, *474*, 215–230.

[112] R. Mertens, L. Greiner, E. C. D. van den Ban, H. B. C. M. Haaker, A. Liese, *J. Mol. Catal. B Enzym.* **2003**, *24*, 39–52.

[113] K. Ma, R. N. Schicho, R. M. Kelly, M. W. Adams, *Proc. Natl. Acad. Sci.* **1993**, *90*, 5341–5344.

[114] F. O. Bryant, M. W. Adams, *J. Biol. Chem.* **1989**, *264*, 5070–5079.

[115] K. Ma, M. W. W. Adams, *J. Bacteriol* **1999**, *181*, 1163–1170.

[116] T. H. Lonsdale, L. Lauterbach, S. H. Malca, B. M. Nestl, B. Hauer, O. Lenz, *Chem. Commun.* **2015**, *51*, 16173–16175.

[117] O. Abril, G. M. Whitesides, *J. Am. Chem. Soc.* **1982**, *104*, 1552–1554.

[118] Y. Maenaka, T. Suenobu, S. Fukuzumi, *J. Am. Chem. Soc.* **2012**, *134*, 367–374.

[119] T. Saba, J. Li, J. W. H. Burnett, R. F. Howe, P. N. Kechagiopoulos, X. Wang, *ACS Catal.* **2020**, *11*, 283–289.

[120] X. Wang, H. H. P. Yiu, *ACS Catal.* **2016**, *6*, 1880–1886.

[121] X. Zhao, S. E. Cleary, C. Zor, N. Grobert, H. A. Reeve, K. A. Vincent, *Chem. Sci.* **2021**, *12*, 8105–8114.

[122] V. Alessandro, *Philos. Trans. R. Soc. London* **1800**, *90*, 403–431.

[123] P.-O. Eggen, L. Kvittingen, A. Lykknes, R. Wittje, *Sci. Educ.* **2012**, *21*, 179–189.

[124] W. Nicholson, *J. Nat. Philos. Chem. arts* **1800**, *4*, 179–191.

[125] J. Wisniak, *Indian J. Hist. Sci.* **2015**, *50*, 476–490.

[126] W. R. Grove, *London, Edinburgh, Dublin Philos. Mag. J. Sci.* **1842**, *21*, 417–420.

[127] W. R. Grove, *London, Edinburgh, Dublin Philos. Mag. J. Sci.* **1839**, *14*, 127–130.

[128] C. Spiegel, *PEM Fuel Cell Modeling and Simulation Using MATLAB*, Elsevier, **2011**.

[129] J. Larminie, A. Dicks, M. S. McDonald, *Fuel Cell Systems Explained*, J. Wiley Chichester, UK, **2003**.

[130] F. T. Bacon, *Electrochim. Acta* **1969**, *14*, 569–585.

[131] M. Warshay, P. R. Prokopius, in *Grove Anniv. Fuel Cell Symp.*, **1989**.

[132] M. Poux, P. Cognet, C. Gourdon, *Green Process Engineering: From Concepts to Industrial Applications*, CRC Press, **2015**.

[133] S. Litster, G. McLean, *J. Power Sources* **2004**, *130*, 61–76.

[134] C. Hartnig, C. Roth, *Polymer Electrolyte Membrane and Direct Methanol Fuel Cell*

Technology: Volume 2: In Situ Characterization Techniques for Low Temperature Fuel Cells, Elsevier, **2012**.

[135] O. Savadogo, K. Lee, K. Oishi, S. Mitsushima, N. Kamiya, K.-I. Ota, *Electrochem. commun.* **2004**, *6*, 105–109.

[136] H. Yang, J. Liu, J. Wang, C. K. Poh, W. Zhou, J. Lin, Z. Shen, *Electrochim. Acta* **2016**, *216*, 246–252.

[137] F. Lapicque, M. Belhadj, C. Bonnet, J. Pauchet, Y. Thomas, *J. Power Sources* **2016**, *336*, 40–53.

[138] J. T. Gostick, M. W. Fowler, M. D. Pritzker, M. A. Ioannidis, L. M. Behra, *J. Power Sources* **2006**, *162*, 228–238.

[139] B. D. Cunningham, J. Huang, D. G. Baird, *Int. Mater. Rev.* **2007**, *52*, 1–13.

[140] L. Cindrella, A. M. Kannan, J. F. Lin, K. Saminathan, Y. Ho, C. W. Lin, J. Wertz, *J. Power Sources* **2009**, *194*, 146–160.

[141] I. Mazurenko, M. Etienne, G.-W. Kohring, F. Lapicque, A. Walcarius, *Electrochim. Acta* **2016**, *199*, 342–348.

[142] A. E. W. Horst, K.-M. Mangold, D. Holtmann, *Biotechnol. Bioeng.* **2016**, *113*, 260–267.

[143] J. W. Ager, A. A. Lapkin, *Science* **2018**, *360*, 707–708.

[144] I. Mazurenko, X. Wang, A. De Poulpiquet, E. Lojou, *Sustain. Energy Fuels* **2017**, *1*, 1475–1501.

[145] L. Xu, F. A. Armstrong, *RSC Adv.* **2015**, *5*, 3649–3656.

[146] S. Calabrese Barton, J. Gallaway, P. Atanassov, *Chem. Rev.* **2004**, *104*, 4867–4886.

[147] C. F. Megarity, B. Siritanaratkul, R. A. Herold, G. Morello, F. A. Armstrong, *J. Chem. Phys.* **2020**, *153*, 225101.

[148] F. A. Armstrong, J. Hirst, *Proc. Natl. Acad. Sci.* **2011**, *108*, 14049–14054.

[149] L. Dos Santos, V. Climent, C. F. Blanford, F. A. Armstrong, *Phys. Chem. Chem. Phys.* **2010**, *12*, 13962–13974.

[150] C. Artner, B. Bohrer, L. Pasquini, I. Mazurenko, N. Lahrach, D. Byrne, A. De Poulpiquet, **2022**, 1–26.

[151] C. Kisker, H. Schindelin, A. Pacheco, W. A. Wehbi, R. M. Garrett, K. V Rajagopalan, J. H. Enemark, D. C. Rees, *Cell* **1997**, *91*, 973–983.

[152] I. Mazurenko, K. Monsalve, P. Infossi, M. T. Giudici-Orticoni, F. Topin, N. Mano, E. Lojou, *Energy Environ. Sci.* **2017**, *10*, 1966–1982.

[153] L. B. Wingard Jr, C. H. Shaw, J. F. Castner, *Enzyme Microb. Technol.* **1982**, *4*, 137–142.

[154] S. D. Minteer, P. Atanassov, H. R. Luckarift, G. R. Johnson, *Mater. Today* **2012**, *15*, 166–173.

[155] K. Bych, M. H. Mikš, T. Johanson, M. J. Hederos, L. K. Vigsnæs, P. Becker, *Curr. Opin. Biotechnol.* **2019**, *56*, 130–137.

[156] T. Burgdorf, O. Lenz, T. Buhrke, E. Van Der Linden, A. K. Jones, S. P. J. Albracht, B. Friedrich, *Microb. Physiol.* **2005**, *10*, 181–196.

[157] G. Berggren, A. Adamska, C. Lambertz, T. R. Simmons, J. Esselborn, M. Atta, S. Gambarelli, J.-M. Mouesca, E. Reijerse, W. Lubitz, others, *Nature* **2013**, *499*, 66–69.

[158] J. C. Fontecilla-Camps, A. Volbeda, C. Cavazza, Y. Nicolet, *Chem. Rev.* **2007**, *107*,

4273–4303.

[159] A. A. Oughli, M. Vélez, J. A. Birrell, W. Schuhmann, W. Lubitz, N. Plumeré, O. Rüdiger, *Dalt. Trans.* **2018**, *47*, 10685–10691.

[160] S. Cosnier, A. J. Gross, A. Le Goff, M. Holzinger, *J. Power Sources* **2016**, *325*, 252–263.

[161] K. Kano, T. Ikeda, *Anal. Sci.* **2000**, *16*, 1013–1021.

[162] J. Cracknell, K. Vincent, F. Armstrong, *Chem. Rev.* **2008**, *108*, 2439–61.

[163] D. Pletcher, R. A. Green, R. C. D. Brown, *Chem. Rev.* **2017**, *118*, 4573–4591.

[164] M. Atobe, H. Tateno, Y. Matsumura, *Chem. Rev.* **2017**, *118*, 4541–4572.

[165] S. K. Yoon, E. R. Choban, C. Kane, T. Tzedakis, P. J. A. Kenis, *J. Am. Chem. Soc.* **2005**, *127*, 10466–10467.

[166] J. Britton, S. Majumdar, G. A. Weiss, *Chem. Soc. Rev.* **2018**, *47*, 5891–5918.

[167] S. Kochius, J. B. Park, C. Ley, P. Könst, F. Hollmann, J. Schrader, D. Holtmann, *J. Mol. Catal. B Enzym.* **2014**, *103*, 94–99.

[168] R. Ruinatscha, K. Buehler, A. Schmid, *J. Mol. Catal. B Enzym.* **2014**, *103*, 100–105.

[169] R. A. Rodriguez-Hinestroza, C. López, J. López-Santin, C. Kane, M. D. Benaiges, T. Tzedakis, *Chem. Eng. Sci.* **2017**, *158*, 196–207.

[170] S. A. Kumar, S.-M. Chen, *Sensors* **2008**, *8*, 739–766.

[171] J. J. Gooding, *Electrochim. Acta* **2005**, *50*, 3049–3060.

[172] Z. Zhu, L. Garcia-Gancedo, A. J. Flewitt, H. Xie, F. Moussy, W. I. Milne, *Sensors* **2012**, *12*, 5996–6022.

[173] N. D. J. Yates, M. A. Fascione, A. Parkin, *Chem. Eur. J.* **2018**, *24*, 12164–12182.

[174] P. Bollella, Y. Hibino, K. Kano, L. Gorton, R. Antiochia, *Acs Catal.* **2018**, *8*, 10279–10289.

[175] A. J. Gross, X. Chen, F. Giroud, C. Abreu, A. Le Goff, M. Holzinger, S. Cosnier, *Acs Catal.* **2017**, *7*, 4408–4416.

[176] H. J. Sim, D. Y. Lee, H. Kim, Y.-B. Choi, H.-H. Kim, R. H. Baughman, S. J. Kim, *Nano Lett.* **2018**, *18*, 5272–5278.

[177] L. Jourdin, S. Freguia, B. C. Donose, J. Chen, G. G. Wallace, J. Keller, V. Flexer, *J. Mater. Chem. A* **2014**, *2*, 13093–13102.

[178] R. Barin, D. Biria, S. Rashid-Nadimi, M. A. Asadollahi, *J. CO2 Util.* **2018**, *28*, 117–125.

[179] B. Bulutoglu, F. C. Macazo, J. Bale, N. King, D. Baker, S. D. Minteer, S. Banta, *ACS Appl. Mater. Interfaces* **2019**, *11*, 20022–20028.

[180] N. Mano, *Curr. Opin. Electrochem.* **2020**, *19*, 8–13.

[181] A. J. Gross, M. Holzinger, S. Cosnier, *Energy Environ. Sci.* **2018**, *11*, 1670–1687.

[182] D. S. Choi, H. Lee, F. Tieves, Y. W. Lee, E. J. Son, W. Zhang, B. Shin, F. Hollmann, C. B. Park, *ACS Catal.* **2019**, *9*, 10562–10566.

[183] H. Seelajaroen, A. Bakandritsos, M. Otyepka, R. Zboril, N. S. Sariciftci, *ACS Appl. Mater. Interfaces* **2019**, *12*, 250–259.

[184] C. Jiménez-González, P. Poechlauer, Q. B. Broxterman, B. S. Yang, *Dell'Orco, H. Noorman, S. Yee, R. Reintjens, A. Wells, V. Massonneau, J. Manley, Org. Process Res. Dev* **2011**, *15*, 900–911.

[185] D. J. C. Constable, P. J. Dunn, J. D. Hayler, G. R. Humphrey, J. L. Leazer Jr, R. J. Linderman, K. Lorenz, J. Manley, B. A. Pearlman, A. Wells, others, *Green Chem.* **2007**, *9*, 411–420.

Chapter II and III. Optimization of a hybrid electrochemical flow reactor coupling H_2 oxidation to NADH regeneration

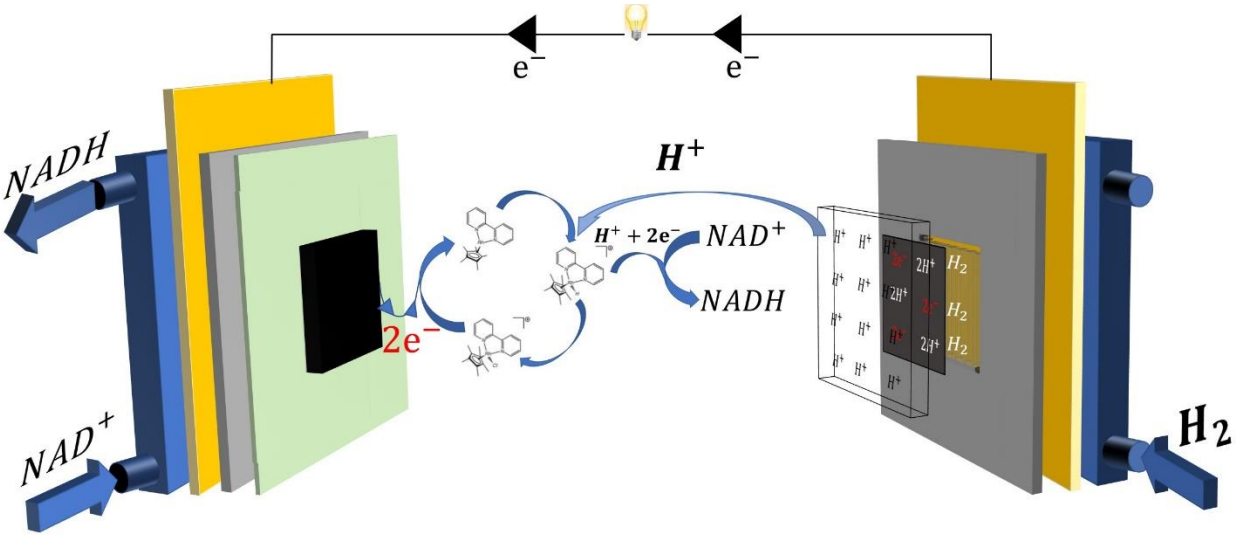

Schematic view of the flow electrochemical reactor. Solution flow is on the left side and hydrogen flow is on the right side. A proton-conducting Nafion membrane is separating the gas diffusion electrode, for hydrogen oxidation, from the graphite felt electrode, for NADH production by electrocatalytic reduction of NAD^+ with $[Cp^*Rh(bpy)Cl]^+$ complex.

Objective of the study in Chapter II

In the present study, we combined the electrochemical regeneration of NADH mediated by a rhodium complex, the application of continuous flow reaction, and hydrogen oxidation using a GDE, in a single reactor with electrolytic solution recirculation. This method relies on the electrochemical reactor efficiently coupling the reduction of NAD^+ to the oxidation of hydrogen at the anode. The proposed process has been optimized with respect to varying operating factors such as rhodium complex and NAD^+ concentrations, pH, the activation procedure for the carbon-based electrode, and cell operating conditions. After inserting an enzymatic module in series with the electrochemical reactor, the conversion of pyruvate to lactate by L-lactic dehydrogenase (LDH) was performed to test the activity of the in-situ regenerated NADH cofactor. This study's objective is to assess the effect of this redox flow technology on the performance of NADH regeneration using a well-described rhodium electrocatalyst.

Article published in Electrochemical science advances

El Housseini, W., Lapicque, F., Walcarius, A., & Etienne, M. (2021). A hybrid electrochemical flow reactor to couple H_2 oxidation to NADH regeneration for biochemical reactions. *Electrochemical Science Advances*, e202100012.

Chapter II. A hybrid electrochemical flow reactor to couple H_2 oxidation to NADH regeneration for biochemical reactions

Abstract

Beta-nicotinamide adenine dinucleotide (NAD^+/NADH) is an important enzymatic co-factor that can be efficiently regenerated using a rhodium-based catalyst as electron transfer mediator (*i.e.* $[Cp^*Rh(bpy)Cl]^+$, where Cp* = pentamethylcyclopentadienyl and bpy = 2,2-bipyridine). Here, the above mediated regeneration of NADH is implemented in a redox flow bioreactor hybridized with a gas diffusion electrode for hydrogen oxidation. The reactor was initially optimized with respect to rhodium complex and NAD^+ concentrations, humidification of the hydrogen gas, flow rates of both H_2 gas and electrolytic solution, and solution pH. The integration of an enzymatic reaction consuming the generated NADH was then investigated in a flow process, combining in series the electrochemical reactor to a biochemical cell with immobilized L-lactic dehydrogenase for the conversion of pyruvate to lactate. A high activity was achieved with a turnover number up to 370 h^{-1} for NADH regeneration. Coupled electrochemical regeneration to enzymatic reaction led to total turnover number values of 2000 and $6.3*10^6$ for NADH electrochemical regeneration and bioconversion, respectively.

II.1 Introduction

NAD^+/NADH cofactor and its phosphorylated derivative ($NADP^+$/NADPH) are important biological cofactors that play a critical role as electron shuttles in biological systems.[1] They can also be applied as an electron carrier in enzymatic systems catalyzing stereo- and regioselective reactions having a great biotechnological potential, *e.g.* dehydrogenases or cytochrome P450.[2] However, NADH and its derivatives in enzymatic systems are expensive,[1] so the regeneration of the enzymatically-active reduced form of the cofactor is strongly required.

Four methods for regeneration of the NAD(P)H cofactor can be employed: (i) chemical and photochemical regenerations, (ii) biological regeneration, (iii) enzymatic regeneration, (iv) electrochemical regeneration or electroenzymatic regeneration.[3] To quantify and compare the efficiency of each method, two criteria are usually defined: the turnover number (TN in h^{-1}) and the total turnover number (TTN). TN, which is homogeneous to a frequency, expresses the velocity at which the cofactor is regenerated. TTN provides information on the number of moles of product formed per mole of cofactor during the entire synthesis reaction of the targeted product.[2]

The average TTN of the enzymatic cofactor in the different regeneration methods has been reported to be in the order of 105 using chemical regeneration,[4] 21 with photochemical regeneration,[5] between 100 000 and 150 000 using enzymatic regeneration,[6–8] and between 101 and 3760 by electrochemical regeneration.[9–11] The difference between the TTN values obtained in enzymatic and electrochemical regenerations appears to be due to the nature of the

[1] NAD^+ 88.2 €/g, NADH 206 €/g, $NADP^+$ 355 €/g, NADPH 1330 €/g (A chemical provider catalog consulted the 12/12/2020)

catalytic reaction that is used, i.e. homogeneous versus heterogeneous, and of the mediator used in enzymatic and indirect electrochemical regenerations respectively.

A technique for the regeneration of NADH – or NADPH – cofactor must allow TTN larger than 1000 in order to be economically viable.[12,13] However, the technique that enables to reach the highest TN or TTN is not always the most economical due to the loss of the cofactor, or its thermal, chemical, or photochemical degradation.[13]

In fact, none of the regeneration methods cited above appear to offer a fully satisfactory solution to the problem of NADH regeneration that fulfils economic and environmental criteria for its application.[12] It is often reported that the cost of the technology or the products used for the regeneration of this cofactor (particularly enzymes used in enzymatic regeneration) are in the same order of magnitude or even higher than the cost of the cofactor and present problems related to their possible inhibition effects.[14] Therefore, TTN is not the only criterion for the economic evaluation of the process. The optimization of the reactor design, the limitation of the formation of by-products such as the inactive form of NADH, and the prevention of the NADH degradation during the process, all play an important role in the regeneration of NADH.[15]

The regeneration of NADH through electrochemical techniques is one of the most promising and controllable approaches that are used for the reduction of NAD^+.[2,16,17] It offers an easy separation of products of the reaction, if catalysts are immobilized, and it allows as well the control of the potential and the progress of the reaction.[18] The direct regeneration of NADH at bare electrodes only occurs at very negative potentials leading to the inactive dimerized form of NADH formed through one electron transfer instead of two electrons exchanged in the indirect regeneration of the NADH cofactor.[19] The usage of a mediator leads to the active form NADH with a potential lower than the potential needed in the direct regeneration.

$[Cp^*Rh(bpy)Cl]^+$ (chloro(2,2′-bipyridyl) (pentamethylcyclopentadienyl)-rhodium (III)) acting as a redox mediator has been shown to be the best non-enzymatic catalyst for the selective regeneration of NADH.[9,20,21]

The mechanism of NADH regeneration consists first in the reduction of the $[Cp^*Rh(bpy)Cl]^+$ **(M_{ox})** complex to $[Cp^*Rh(bpy)]$ **(M_{red1})** through two electron transfers,[22] which can be globally written as:

$$[\mathrm{Cp}*\mathrm{Rh(bpy)Cl}]^+ + 2\,e^- \rightleftharpoons [\mathrm{Cp}*\mathrm{Rh(bpy)}] + Cl^- \quad (1)$$

The reduced complex is protonated to rhodium hydride complex ($[Cp^*Rh(bpy)H]^+$, **M_{red2}**): [22]

$$[\mathrm{Cp}*\mathrm{Rh(bpy)}] + H^+ \rightleftharpoons [\mathrm{Cp}*\mathrm{Rh(bpy)H}]^+ \qquad k_2 = 10.6\ \mathrm{s}^{-1}\ \text{at pH} = 7.5 \quad (2)$$

NAD^+ can then reduce to 1,4-NADH with the hydride form of the complex (**M_{red2}**) acting as a mediator:[23]

$$NAD^+ + [Cp*Rh(bpy)H]^+ + Cl^- \xrightarrow{k3} NADH + [Cp*Rh(bpy)Cl]^+ \quad (3)$$

Development of continuous flow reactors has occupied a wide range of interest by chemical engineers for over one decade due to their high efficiency when being compared with batch reactors.[24] In continuous flow reactors, reactants are continuously fed into the reactor and emerge as a continuous stream of products.[25] These continuous flow reactors are more and more used by chemists for the synthesis of fine chemicals such as NADH.[26] Electrochemical developments in continuous flow reactors have contributed to the reduction in energy consumption, to the improvement of material transport, and to increased conversion and selectivity[27] through more refined cell design and technology. It is anticipated that the synthesis in flow will be coupled in the future with new analytical techniques for online monitoring of the process and speeding up the isolation and the purification.[28]

As shown in equations (2) and (3), the reactions are associated with proton transfer. The oxidation of hydrogen on platinum appears attractive for the generation of protons required at the biocathode for electrochemical synthesis offering the possibility to be applied as a reducing agent in a hybrid reactor combining a fuel cell and a redox flow device. This reaction is highly selective, producing no toxic or hazardous species.[29]

The electrochemical regeneration of fine chemicals, *e.g.* NADH, by indirect electrochemical reaction coupled with the oxidation of hydrogen is limited by the solubility of hydrogen in the electrolyte.[30] Gas diffusion electrodes (GDEs) have proven to boost current density by overcoming the poor solubility of hydrogen in aqueous electrolytes[31] and reducing gas-liquid mass transfer constraints.[31] Recently, GDEs have been applied to bioelectrochemical synthesis in continuous flow reactors[32,33] and evaluated for anodic NAD^+ regeneration coupled with energy production.[34]

While being compared to chemical catalysts, enzymes are known as efficient biocatalysts offering high competitive processes and becoming well recognized in organic synthesis and biotechnology.[35,36] The electrochemical regeneration of the NADH cofactor through a rhodium complex mediator can be coupled to a bioconversion for the synthesis of fine chemicals and to assess whether the regenerated NADH cofactor is in its active form.[18] Besides, for the sake of long term stability and reusability, enzymatic catalysts have to be immobilized[37] as for example by adsorption on carbon materials.[38]

In the present work, we combined the above approaches, namely the electrochemical regeneration of NADH mediated by a rhodium complex, the application of continuous flow reaction, and hydrogen oxidation using a GDE, in a single reactor with recirculation of the electrolytic solution. This approach relies upon the electrochemical reactor coupling efficiently the reduction of NAD^+ to the anode oxidation of hydrogen. The proposed process has been

optimized by varying operating factors, *e.g.* the concentrations of rhodium complex and NAD^+, the pH, the activation procedure for the carbon-based electrode, as well as the cell operating conditions. Finally, the conversion of pyruvate to lactate by L-lactic dehydrogenase (LDH) has been carried out in the process after insertion of an enzymatic module in series with the electrochemical reactor, to check the activity of the in-situ regenerated NADH cofactor. The purpose of this study is to evaluate the contribution of this redox flow technology on the performance of NADH regeneration with a well described rhodium electrocatalyst.[9]

II.2 Materials and methods

II.2.1 Chemical and reagents

β-nicotinamide adenine dinucleotide (NAD^+, >98%) and β-nicotinamide adenine dinucleotide reduced dipotassium salt (NADH, >97%), K_2HPO_4 (99%), KH_2PO_4 (99%), HCl (37 %), Tris HCl (99 %), L-lactic dehydrogenase (LDH) from bovine heart (≥ 250 units/mg protein, 144,000 Da.), pyruvate (98 %) and lactate (98 %) were from Sigma-Aldrich. Phosphate buffer (0.1 M) was used to investigate the electrocatalytic properties of the rhodium complex towards NAD^+ reduction and was reported to be the most appropriate for such experiments[39]. Multiwall carbon nanotubes (MWCNT, NC7000™ series) were from Nanocyl (Belgium) and carbon papers (SpectraCarb 2050L-0550 Carbon Paper) were acquired from Fuel Cell Store (USA). MWCNT were dispersed in a solution of ethanol (96 %). All solutions were prepared with high purity water (18 MΩ cm) from a Purelab Option water purification system.

II.2.2 Rhodium complex synthesis

$[Cp^*Rh(bpy)Cl]^+$ complex was prepared in a $CHCl_3$ solution after stoichiometric reaction between the 2,2-bipyridine and the pentamethylcyclopentadienyl rhodium(III) chloride dimer $(RhCp^*Cl_2)_2$. After addition of the reagents, the solution has been stirred for three hours under

air and at room temperature then allowed to settle overnight at 8 °C. The solid complex was recovered by filtration by Buchner filtration.[18]

II.2.3 Electrode pretreatment

A piece of graphite felt (GFD4.6EA, SGL, Germany) being 4 cm x 4 cm x 0.4 cm in dimensions was used as cathode in the reactor (flow cell in Scheme 1). The as-received material is hydrophobic which can limit the good distribution of solution in the reactor. The graphite felt (GF) piece was treated to provide a suitable wettability using washing in successive solutions:[40] the GF piece was first immersed in ethanol and submitted to ultrasounds for 15 minutes at 25 °C, then, the process was repeated with 80:20, 60:40, 40:60 and 20:80 ethanol-water solutions and ending with pure water.

II.2.4 Enzymatic carbon paper with MWCNT (LDH-CP-MWCNT) preparation

A piece of SpectraCarb carbon paper being 1.5 cm x 1.5 cm x 0.05 cm was used as the enzyme support for the conversion of pyruvate to lactate using L-lactate dehydrogenase. The MWCNT-containing CP was prepared following the same process for a bucky paper electrode preparation reported in literature.[41] 10 mg MWCNT were dispersed in 50 mL ethanol by ultrasonication for 5 h. Afterwards, the suspension was decanted and vacuum filtered using the CP as filter. Then, the material was dried at 60 °C overnight. This process has been repeated three times to obtain the desired number of MWCNT layers. Finally, an LDH enzyme was adsorbed on the MWCNT surface by depositing 50 µL suspension of LDH (500 units, *i.e.*, 2 mg) and keeping for 2 hours at a temperature of 3°C.

II.2.5 Electrochemical reactor

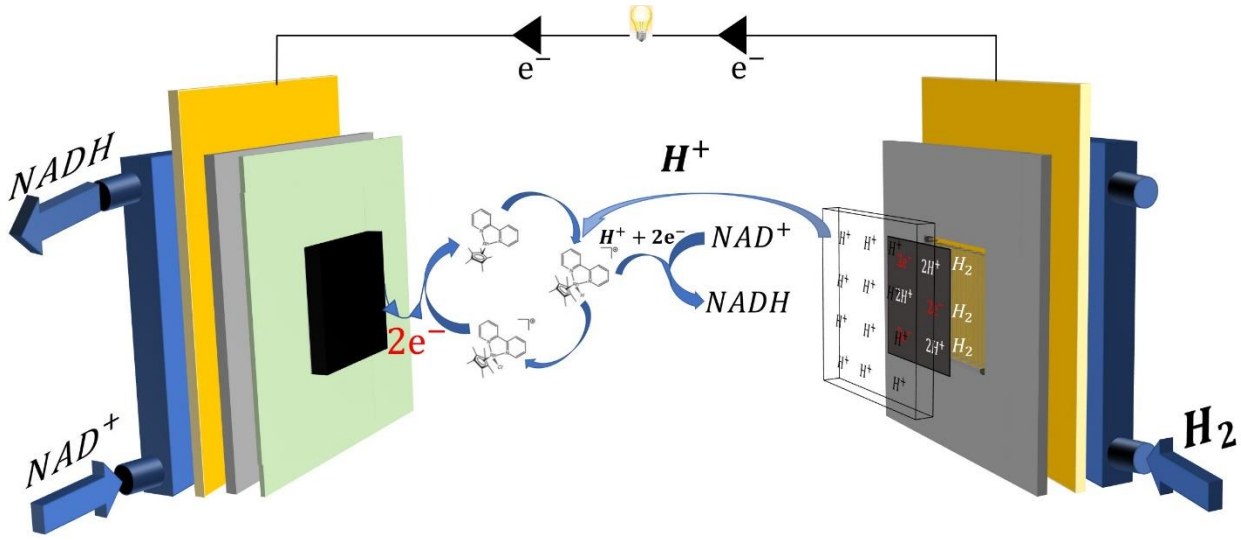

Scheme II.1. Schematic view of the flow electrochemical reactor. Solution flow is on the left side and hydrogen flow is on the right side. A proton-conducting Nafion membrane is separating the gas diffusion electrode, for hydrogen oxidation, from the graphite felt electrode, for NADH production by electrocatalytic reduction of NAD^+ with $[Cp^*Rh(bpy)Cl]^+$ complex.

Scheme II.1 shows the electrochemical reactor used in this study. A Pt/C gas diffusion electrode (Paxitech France) with a Pt content at 0.2 $mg.cm^{-2}$, was used as anode and installed on a graphite bipolar plate, with grooved 1 x 1 mm^2 channels forming three channel clusters for continuous hydrogen introduction and distribution in the anode chamber. The gas diffusion electrode allows uniform and constant production rates of protons and electrons for a given flow rate of hydrogen. 40 mL of reaction solution, containing 0.1 M phosphate buffer and various amounts of NAD^+ and $[Cp^*Rh(bpy)Cl]^+$, were introduced to the glass storage tank. Temperature was at ambient level and unless specified otherwise, the initial pH was adjusted to 7.2. The solution was circulating continuously using a peristaltic pump through a graphite felt (4 cm x 4 cm x 0.4 cm), known as a good electrical conductor and acting as a three-dimensional cathode, with homogeneous distribution of the solution: this configuration is expected to be more efficient than a carbon foil as used in former works.[9] A Nafion membrane

(N-212) was placed between the two electrodes for separation of the two compartments – in particular to avoid anode flooding from the solution treated at the cathode – and to permit a uniform proton transport rate from the anode to the cathode. Two copper ending plates allowed mechanical cohesion of the cell and electrical connection to the potentiostat (Bio-Logic VSP3). Continuous nitrogen bubbling was allowed in the storage tank using a sintered glass sparging system for saturating the gas with water at ambient temperature to avoid undesired evaporation of water during the NADH production tests.[42] Both nitrogen and hydrogen flow rates were controlled by mass flowmeters (Brooks).

Cyclic voltammograms and batch electrolysis were performed in a two-electrode configuration, the hydrogen anode acting also as reference electrode. The usage of a two-electrode configuration where the anode acts as reference can be considered here because of the very low polarization of gas diffusion anode with current densities below 10 mA cm^{-2}. All potentials are thus given versus H^+/H_2 couple, noted ref. (H_2). Potential scan rate was fixed 5 mV s^{-1}. In electrolysis tests, the solution was sampled at regular intervals (each 5 or 10 minutes) and the conversion of NAD^+ to NADH was followed by UV absorption at 340 nm after suitable dilution (10 times). For the production of NADH, two protons are produced by hydrogen oxidation while one proton is consumed by NAD^+ reduction, according to the stoichiometry of both reactions. In consequence, the pH slightly decreased during electrosynthesis, but owing to the buffer concentration, the pH change was never larger than 0.4 unit. The biological activity of the cofactor was then confirmed by reaction with a lactate dehydrogenase immobilized in the enzymatic cell.

II.2.6 Enzymatic cell

Scheme II.2 shows the enzymatic cell used for the conversion of pyruvate to lactate connected in series with the electrochemical reactor (**Scheme II.1**).

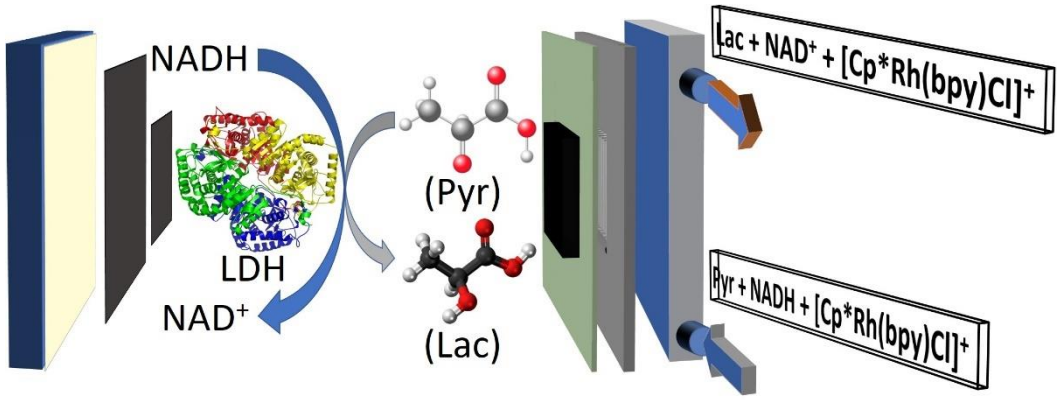

Scheme II.2. Schematic view of the enzymatic cell. Solution flows from the right side.

The solution containing the rhodium complex, NADH, and the pyruvate was fed to the enzymatic cell through a graphite plate with grooved 1 x 1 mm^2 channels forming three channel clusters for its homogeneous distribution. The solution then percolated through a carbon felt that maintains the stability of the enzymes immobilized on the MWCNT-CP, which was put in contact with the felt. A gas diffusion layer, known as hydrophobic, has been placed in contact with the rear side of the LDH-MWCNT-CP preventing the adsorption of the solution, thus ensuring the stability of the enzymes even at high solution flow rates. The whole assembly was stacked between two polymeric (PMMA) plates for mechanical cohesion and to prevent solution leakage. The solution leaving the enzymatic cell with a higher lactate content, was pumped to the glass storage provided by N_2 degassing before returning to the electrochemical reactor. Samples taken at regular intervals were analyzed by HPLC using a Laminex separation column with 0.05 M H_2SO_4 as eluant.

II.3 Results and discussion

II.3.1 Evidence of electrochemical NADH Regeneration

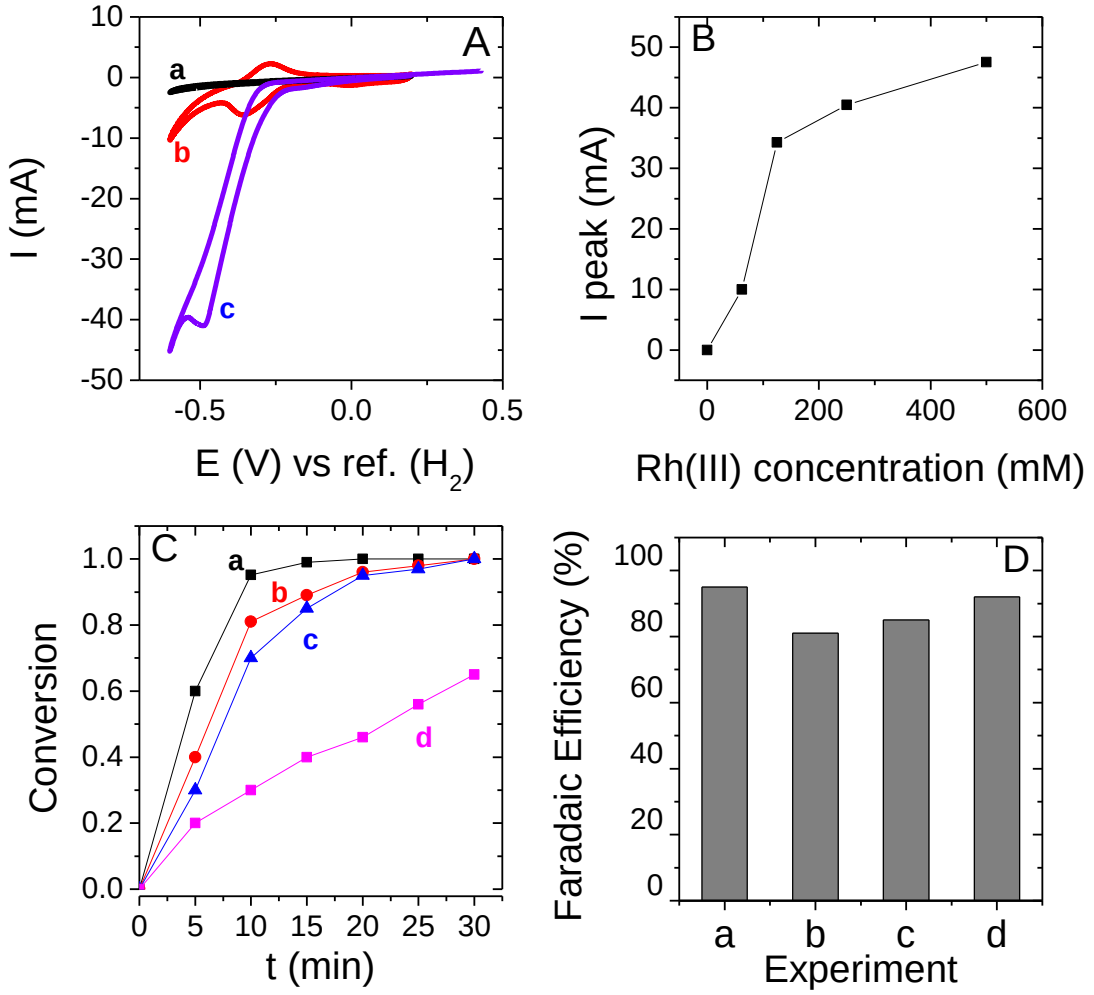

Figure II.1. (A) Cyclic voltammograms recorded at 5 $mV.s^{-1}$ successively with the graphite felt electrode in (a) buffer solution (b) after addition of 250 µM $[Cp^*Rh(bpy)Cl]^+$ and (c) after addition of 2.5 mM NAD^+. (B) Influence of the rhodium complex concentration on the cathodic current peak measured by CV. (C and D) Influence of the catalyst concentration and the electrolysis potential on (C) the conversion rate of 2.5 mM NAD^+ to NADH and (D) the faradaic efficiency; (a) 62.5 µM $[Cp^*Rh(bpy)Cl]^+$ at -0.5 V vs ref. (H_2); (b) 250 µM $[Cp^*Rh(bpy)Cl]^+$ at -0.4 V vs ref. (H_2); (c) 125 µM $[Cp^*Rh(bpy)Cl]^+$ at -0.4 V vs ref. (H_2); (d) 62.5 µM $[Cp^*Rh(bpy)Cl]^+$ at -0.4 V vs ref. (H_2). All experiments were carried out in 0.1 M phosphate buffer solution at pH 7.2 under nitrogen atmosphere with a solution and hydrogen flow rates of 20 $mL.min^{-1}$ each.

The catalytic response of the GF electrode for the NADH regeneration was evaluated by cyclic voltammetry (**Figure II.1A**). In the presence of 250 µM $[Cp^*Rh(bpy)Cl]^+$ (**curve b**), a redox signal is observed, showing a cathodic peak at -0.39 V and an anodic peak at -0.27 V. The intensity of the cathodic peak is approximately double that of the anodic peak. The latter corresponds to the oxidation of the reduced active form of the rhodium complex I ($[Cp^*Rh(bpy)H]^+$: M_{red2}). However, the first reduced form remains inactive ([Cp*Rh(bpy)]: M_{red1}) and unsuitable for redox reactions. Addition of 2.5 mM NAD^+ to the above solution (curve c) led to a large increase in the cathodic peak caused by the electrocatalytic reduction of NAD^+ by $[Cp^*Rh(bpy)H]^+$ and not by the direct reduction of NAD^+ which is observed at much cathodic potential values (and usually gives non-active forms of the cofactor, *i.e.* dimers).[19,43] The cathodic peak was observed at a potential slightly more negative (-0.45 V) than that observed with the reduction of the complex only. The cause of this potential shift can be a limitation associated to the electron transfer kinetics on the graphite felt electrode[18] or to other ohmic losses in the configuration of the system.

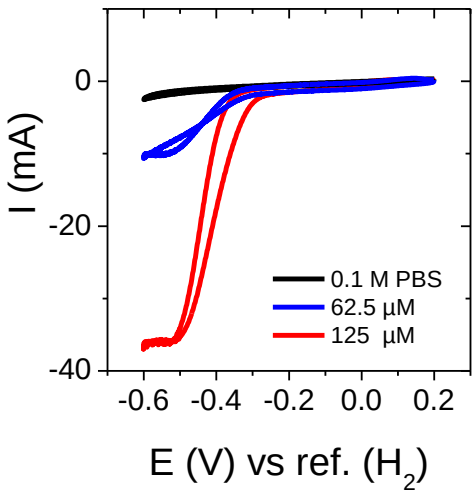

Figure II.2. Cyclic voltammograms recorded with the graphite felt electrode in the presence of 2.5 mM NAD^+ (black line), and in the presence of 62.5 µM (blue line) and 125 µM $[Cp^*Rh(bpy)]^+$. All experiments were done in 0.1 M phosphate buffer solution at pH 7.2 under nitrogen atmosphere with a solution and hydrogen flow rates of 20 $mL.min^{-1}$ each, and with graphite felt treated in hydro-alcoholic solution.

The effect of the rhodium complex concentration on the intensity of the cathodic peak has been investigated at a fixed concentration of NAD^+ (2.5 mM); it shows that this intensity increases steeply with the mediator concentration before levelling off at higher concentrations (**Figure II.1B**). The corresponding CV responses are presented in **Figure II.2**.

The rhodium complex concentration and the cathode potential in electrolysis tests are important operating parameters that should be adjusted for optimizing the process of the regeneration of NADH. The performance of an electrochemical process is based on two criteria: conversion X measured by UV-visible absorption for NADH regeneration (**Figure II.1C**), and the faradaic efficiency Φ expressing the fraction of electrons involved in the key electrochemical reaction (**Figure II.1D**).

$$X = \frac{[NADH]_t}{[NAD^+]_0} \qquad \Phi = \frac{Q_{experimental}}{Q_{\ theorical}} = \frac{n_{e^-} \times F \times [NAD^+]_0 \times V \times X}{I \times t} \times 100 \qquad = \frac{7720 \times [NAD^+]_0 \times X}{I \times t} \times 100$$

;

n_{e^-} = 2; F=96500 C/mol; V = 40 mL

At -0.4 V vs ref. (H_2) and with an initial concentration of NAD^+ of 2.5 mM, the NADH was totally regenerated within 30 min for a rhodium complex concentration of 125 µM (**curve c**) and 250 µM (**curve b**). However, while decreasing the concentration of the rhodium complex to 62.5 µM, the conversion was limited to 0.62 after this lapse of time (**curve d**). At this potential, the faradaic efficiency is higher, attaining 92% by using the lowest concentration of the rhodium complex (62.5 µM) and 80 % with 250 µM of rhodium complex (**data b-d in Figure II.1D**). In order to increase the conversion with a rhodium complex concentration of 62.5 µM with 2.5 mM NAD^+, tests were made at -0.5 V vs ref. (H_2). Total conversion was observed within 20 min (**see curve a in Figure II.1C**), with a faradaic efficiency of 96 % (**data a in Figure II.1D**) which is actually far larger than the values usually reported in the relevant literature in the range 50-70 %,[9] indicating the high selectivity and production rate of the

process. Working at -0.5 V seems thus to be very promising based on the total conversion within an optimal time and the high faradaic efficiency. One explanation of these better performances can be found in **Figure II.2** (**blue curve**). The maximum cathodic current was observed around -0.5 V.

Applying -0.5 V vs ref. (H_2), led thus to the highest conversion rate. On the contrary, applying -0.4 V vs ref. (H_2) led to a much lower current and consequently to a lower conversion rate. Note that the ratio between rhodium complex and NAD^+ was also found critical to reach complete conversion, as doubling the cofactor concentration to 5 mM with 62.5 µM $[Cp^*Rh(bpy)Cl]^+$ led to incomplete conversion (**Figure II.3**).

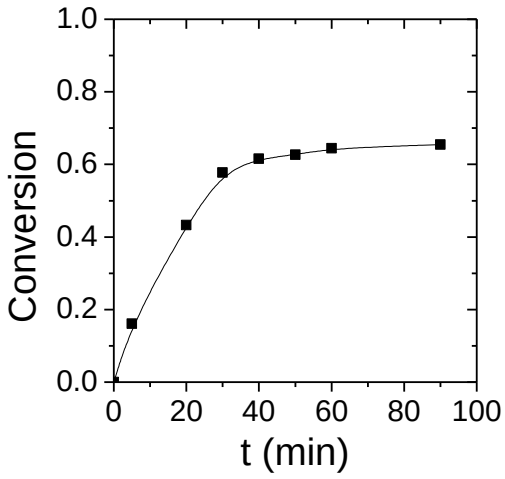

Figure II.3. Electrochemical conversion of 5 mM NAD^+ with 62.5 µM $[Cp^*Rh(bpy)Cl]^+$ (concentration ratio = 80). The experiment was conducted at -0.5 V vs ref. (H_2) in 0.1 M phosphate buffer solution at pH 7.2 under nitrogen atmosphere, with a solution and hydrogen flow rates of 20 $mL.min^{-1}$ each, and with graphite felt pre-treated in solution.

We suppose that a high concentration of NADH is hindering the catalytic activity of the rhodium catalyst for NAD^+ reduction. Actually, we do not know if this effect is reversible or irreversible. In any case, high concentration of cofactor is not meaningful for the electrosynthetis application targeted here.

Finally, to validate that the total regeneration of 2.5 mM of NADH was achieved in the presence of 62.5 µM of the rhodium complex and at a potential of -0.5 V vs ref, the biochemical conversion of 2.5 mM pyruvate to lactate was carried out in the presence of lactate dehydrogenase in the solution. Results are reported in **Figure II.4**, they show that indeed 2.5 mM lactate were produced within 200 min.

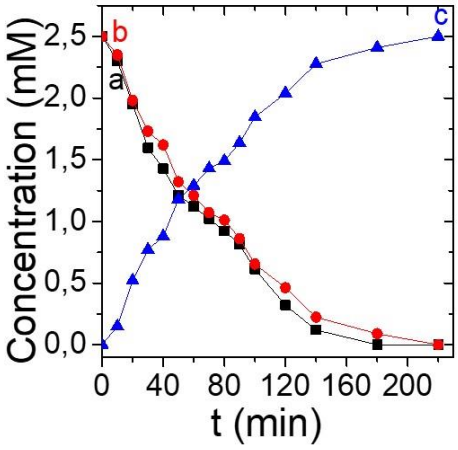

Figure II.4. Bioconversion of 2.5 mM of regenerated NADH (40 mL) in the enzymatic cell. (a) NADH measured by UV-Visible spectroscopy, (b) pyruvate and (c) lactate measured with HPLC. Experiments were done in 0.1 M phosphate with 2.5 mM pyruvate, 62.5 µM $[Cp^*Rh(bpy)Cl]^+$, and with LDH-MWCNT-CP system (500 U) under nitrogen atmosphere, with a solution flow rate of 20 $mL.min^{-1}$, and at pH 7.2.

After the complete production of 2.5 mM NADH (40 mL) with 62.5 µM of the rhodium complex and at -0.5 V vs ref. (H_2), the bioconversion was studied in the presence of 2.5 mM pyruvate through the enzymatic reaction (with 500 U LDH). The NADH concentration (**data a in Figure II.4**) and pyruvate concentration (**data b in Figure II.4**) decrease with time with an increase in the concentration of lactate (**data c, Figure II.4**) until reaching a total pyruvate bioconversion to lactate after 200 min. This experiment clearly shows that the electrochemical regeneration of NADH with the rhodium complex in solution and with a ratio of 40 between

the cofactor and the rhodium complex is total and leads to the active form of NADH (1,4-NADH).

II.3.2 Optimization of hydrogen and solution flows

Flow of hydrogen in the anodic compartment and solution flow through the cathode chamber represent also important operating conditions in the electrochemical regeneration of NADH.

The used nitrogen was humidified as expressed above. In addition, it is noted that in operation of membrane fuel cells, the reacting gases are often humidified to improve the membrane conductivity and protons transport in the vicinity of the Pt clusters.[44] In consequence, the hydrogen used in first tests has been humidified as well.

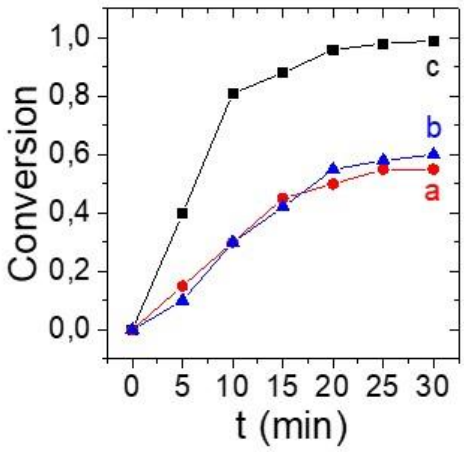

Figure II.5. Influence of humidified hydrogen on the production of NADH at -0.4 V vs ref. (H_2) All experiments were done in 0.1 M phosphate buffer solution at pH 7.2 in the presence of 2.5 mM NAD^+ and 250 µM $[Cp^*Rh(bpy)Cl]^+$ under nitrogen atmosphere with a solution flow rate of 20 mL.min^{-1} and (a) humidified hydrogen with a flow rate of 20 mL.min^{-1}, (b) humidified hydrogen with a flow rate of 10 mL.min^{-1}, (c) non-humidified hydrogen with a flow rate of 20 mL.min^{-1} .

Figure II.5. shows the effect of hydrogen humidification on the conversion of 2.5 mM NAD^+ with 250 µM rhodium complex, at -0.4 V vs ref. (H_2). With humidified hydrogen, the conversion at room temperature, was observed to be limited to 0.55 and 0.50 with 10 (**Figure**

II.5, curve b) and 20 mL.min^{-1} H_2 respectively (**Figure II.5, curve a**) after 30 min conversion. Dismantling the cell and examination of its components showed that the GDE catalyst was soaked, thus not suitable anymore for H_2 oxidation. With fully humidified hydrogen, the water activity in the ionomer becomes very large which may favor water flux from the (liquid phase) cathode medium, resulting in severe flooding of the anode.

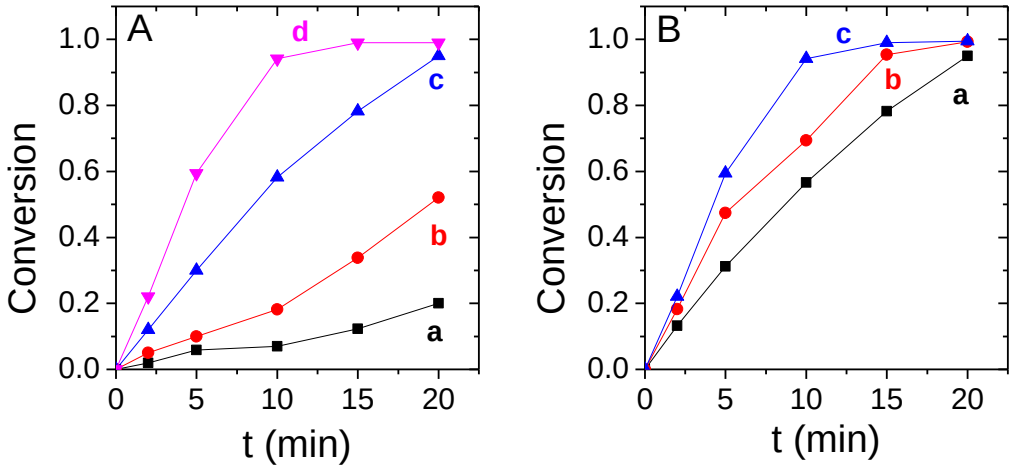

Figure II.6. Influence of (A) hydrogen flow rate ((a) 1 (b) 5, (c) 10 and (d) 20 mL.min^{-1}) and (B) solution flow rate ((a) 4, (b) 10 and (c) 20 mL.min^{-1}) on the conversion of NAD^+. Experiments were carried out in 0.1 M phosphate buffer solution at pH 7.2 in the presence of 1 mM NAD^+ and 25 µM $[Cp^*Rh(bpy)Cl]^+$, under nitrogen atmosphere, at an operating potential of -0.5 V vs Ref. (H_2) with either (A) a constant solution flow rate or (B) a constant hydrogen from rate of 20 mL.min^{-1} each.

The effect of the non-humidified hydrogen flow rate in the anodic compartment was then examined in a series of experiments using increased flow rates of pure hydrogen from 1 mL.min^{-1} to 20 mL.min^{-1} at -0.5 V vs ref. (H_2). As shown by **Figure II.6A**, higher conversion was actually allowed upon increased hydrogen flow rate. The conversion was very low with 1 mL.min^{-1} H_2 (**curve a**, 0.12 after 15 min), but was total within the same time period upon 20 mL.min^{-1} hydrogen (**curve d**). As a matter of fact, the amount of hydrogen consumed at the anode is far lower than 1 cm^3.min^{-1} after Faraday's law. Therefore, the lower performance of the cell at flow rates below 20 mL.min^{-1} is presumably due to small leakage in the hydrogen

circuit and in the flow cell, with possible maldistribution of the fuel gas in the bipolar plate channel at too low flow rates. Besides, the faradaic efficiency of NADH regeneration remains unchanged at approx. 96% for all tested hydrogen flow rates, partly owing to 100 % current efficiency for hydrogen oxidation on a GDE and because this faradaic efficiency is certainly controlled by the conditions applied in the cathodic compartment, i.e., flow, potential and concentrations. The main limitation comes from the anodic side being the amount of hydrogen that can be oxidized at the GDE to provide all electrons needed for the regeneration of NADH.

To confirm this hypothesis, the effect of the solution flow rate on the conversion was also followed with a positive effect on the conversion rate as shown in **Figure II.6B**. Larger solution flow rates favor its uniform distribution within the porous electrode and mass transport between species, thus improving the overall conversion rate. The conversion was 0.78, with an average reaction rate of 7.08 $mmol.L^{-1}.s^{-1}$, after 15 min of electrolysis with the solution flowing at 4 $mL.min^{-1}$ (**curve a**); however, the conversion at the same time with a solution flow rate of 10 $mL.min^{-1}$ attained 0.93 with an average reaction rate of 8.16 $mmol.L^{-1}.s^{-1}$ (**curve b**). In contrast with what was observed with the effect of hydrogen flow rate, the faradaic efficiency of the reaction increased with the solution flow rate, passing from 83 % at 4 $mL.min^{-1}$ to 96 % at 20 $mL.min^{-1}$ (**curve c**). These data clearly show that the faradaic efficiency is also controlled by flow conditions in the cathodic compartment.

II.3.3 Effect of pH on NADH regeneration

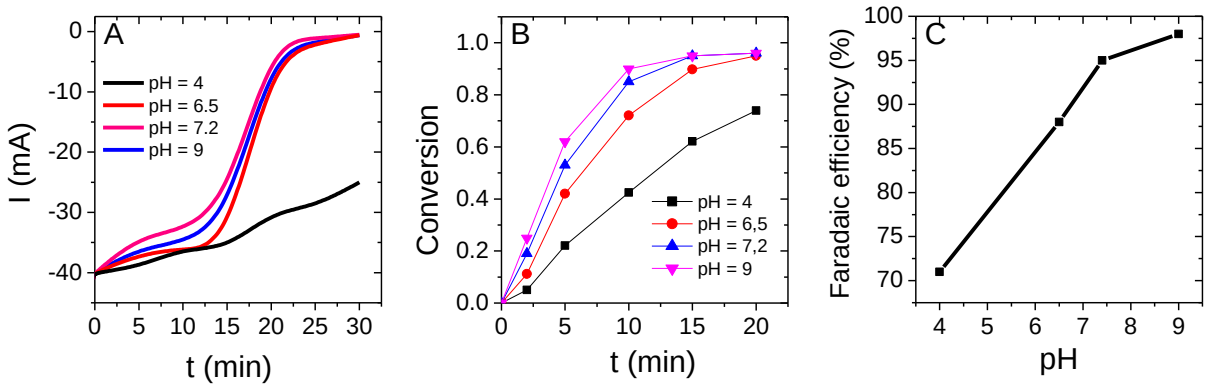

Figure II.7. Influence of the solution pH on (A) the current, (B) the conversion and (C) the faradaic yield for the mediated transformation of NAD^+ to NADH. All experiments were performed in 0.1 M phosphate buffer solution in the presence of 1 mM NAD^+ and 25 µM $[Cp^*Rh(bpy)Cl]^+$ under nitrogen atmosphere with solution and hydrogen flow rates of 20 $mL.min^{-1}$ each.

The effect of pH on the NADH regeneration was studied in 0.1 M of phosphate buffer with different ratio of K_2HPO_4 (99%) and KH_2PO_4 (99%) for pH between 4 and 7.2 and upon addition of 0.1 M of tris-HCl for the pH of 9. The current variations (**Figure II.7A**) have very similar profiles for pH 6.5, 7.2, and 9 featuring an asymptote after 15 min operation corresponding to nearly complete conversion. However, at pH 4 the current decreases far less in absolute value than in neutral or slightly alkaline media. The conversion (**Figure II.7B**) and the faradaic efficiency (**Figure II.7C**), in relation with the current variations (**Figure II.7A**), are increasing with the solution pH. In the acidic medium, the conversion attained 60% after 20 min, with a faradaic efficiency near 72 %. By contrast, full conversion was obtained within 20 min for all other pH values, whereas the faradaic efficiency increased from 87 % at pH 6.5 to 98 % at pH 9 showing the increased selectivity of the electrocatalytic reaction when proton concentration is lowered. It is also reported in the literature that NADH is unstable in acidic environment while NAD^+ is unstable in alkaline media.[45] Thus, as a compromise between

stability of the molecules and acceptable faradaic efficiency, the optimal pH for NADH regeneration was taken in the range 6.5 - 7.2.

II.3.4 Turnover number

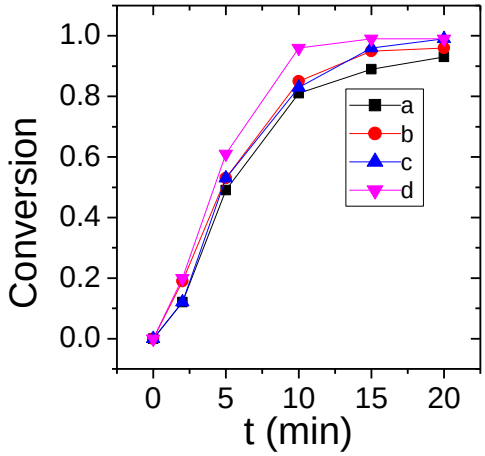

Figure II.8. Studying the reduction of NAD^+ using the same ratio of NAD^+ and $[Cp^*Rh(bpy)Cl]^+$ (40) and the electrolysis potential (-0.5 V vs H_2 oxidation) using different concentrations of NAD^+ and $[Cp^*Rh(bpy)Cl]^+$: (a) 2.5 mM NAD+ and 62.5 µM $[Cp^*Rh(bpy)Cl]^+$, (b) 1.25 mM NAD^+ and 31.25 µM $[Cp^*Rh(bpy)Cl]^+$, (c) 1 mM NAD^+ and 20 µM $[Cp^*Rh(bpy)Cl]^+$, (d) 0.5 mM NAD^+ and 12.5 µM $[Cp^*Rh(bpy)Cl]^+$. All experiments were performed in 0.1 M phosphate buffer solution at pH 7.2 under nitrogen atmosphere with solution and hydrogen flow rates of 20 $mL.min^{-1}$ each.

Regeneration of NADH using the same NAD^+ over Rh concentration ratio was carried out at various concentration levels, at -0.5V vs ref. (H_2). For a $[NAD^+]/[Rh]$ ratio of 40, as shown in **Figure II.8**, very similar conversion rates were observed for Rh complex concentrations ranging from 12.5 to 62.5 µM, with differences in average reaction rates below 13%. For example, the average rate of the reaction using 2.5 mM NAD^+ and 62.5 µM $[Cp^*Rh(bpy)Cl]^+$ is $8.16*10^{-4}$ $mol.L^{-1}.s^{-1}$ fairly similar to the average reaction rate with 0.5 mM NAD^+ and 12.5 µM $[Cp^*Rh(bpy)Cl]^+$ ($7.8*10^{-4}$ $mol.L^{-1}.s^{-1}$). Measured in the first 5 min of the reaction, TN is in this case 370 h^{-1}, far larger than that reported in the literature, at room temperature (25 °C), for rhodium complex in solution from 0.68 to 6.3 h^{-1}. [9,46] While applying the chemical

regeneration of the NADH cofactor with this rhodium complex, reduced by action of phosphite species,[47] the TN obtained was equal to 21 h^{-1} using the same operational conditions of temperature and pH.

In such conditions, the conversion is total in all studied cases and the ratio between $[NAD^+]$ and $[Cp^*Rh(bpy)Cl]^+$ corresponds to the TTN. This TTN can only be increased here if the regenerated cofactor is consumed continuously by an enzymatic reaction, a development briefly examined in this study and described in the next section with lactate dehydrogenase as example. Enzymatic systems applied continuously with the electrochemical regeneration of the NADH depend on the amount of enzymes used, in relation to the quantity of substrate to be converted, which rules the time required for given bioconversion.

For that purpose, it was important to evaluate the stability of the regenerated NADH with time. Results showed that 98 % of the regenerated NADH after 72 hours were still stable and active as shown in **Figure II.9**.

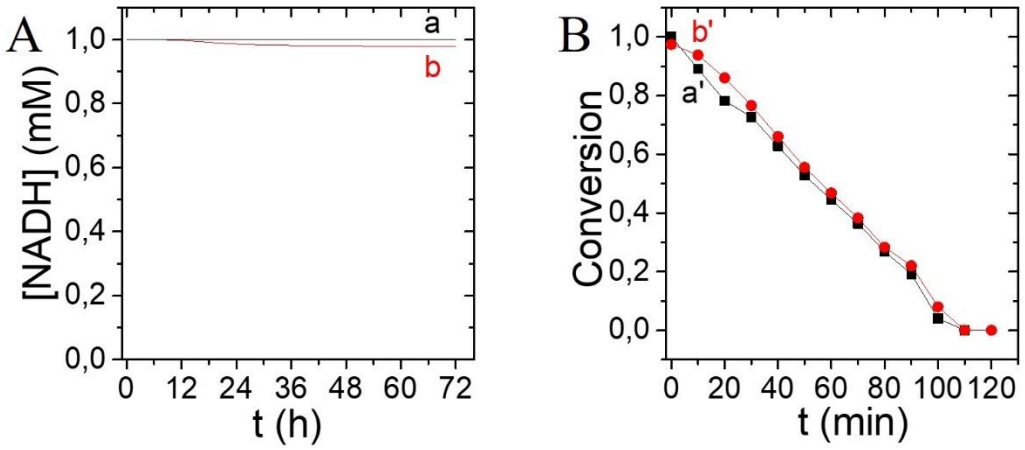

Figure II.9. (A) Storage of NADH stability test after a conversion of 1 mM NAD^+ at room temperature measured by UV-visible spectroscopy: (a) theoretical and (b) experiment values. (B) Online monitoring of the oxidation of 1mM regenerated NADH after the addition of 50 U LDH and 1 mM pyruvate in a 3 mL cuvette: (a') directly after

conversion (b') 72 hours after conversion. The two experiments were done in the presence of 25 µM $[Cp^*Rh(bpy)Cl]^+$ and 0.1 M PBS. The regeneration of NADH was carried out at -0.5 V vs ref. (H_2).

II.3.5 Application of regenerated NADH in an enzymatic reaction

After having determined the optimal parameters for the efficient regeneration of NADH in the flow electrochemical reactor, integrating an enzymatic reaction in the process was attempted to validate the production of the active form of the NADH cofactor regenerated in the above mediated redox process. This is indeed important for the practical application of such bioelectrocatalytic system[18] and for the evaluation of its possible use in the production of fine chemicals as expected from biocatalysis in biotechnology.[35] For this purpose, Lactate dehydrogenase was used here since it is a widely available NAD-dependent enzyme, whose substrate and products can be easily analyzed. The first step in this work was to demonstrate the stability and the selectivity of LDH enzymes immobilized on the chosen support in the presence of dissolved rhodium complex and NAD^+/NADH species (**Figure II.10**).

The second step was to prove that NADH was regenerated with a high purity and exhibiting a high activity towards the bioconversion of pyruvate to lactate in comparison to the commercial one (**reported in Figures II.11 to II.14**). The third step was the application of the regenerated NADH for the conversion of pyruvate to lactate in the presence of the rhodium complex. It was assumed that the bioconversion occurs at the surface of the LDH-MWCNT-CP. For this reason, it was important to evaluate the optimal amount of LDH that has to be added on MWCNT. 500 units LDH were found sufficient (> 200 U/cm² CP-MWCNT) for the efficient bioconversion of pyruvate to lactate). In a previous report from the literature, 1400 U LDH were added to a 50 mL solution containing 2 mM NAD^+ and 20 mM pyruvate.[9]

II.3.5.1 LDH-CP-MWCNT stability and selectivity tests

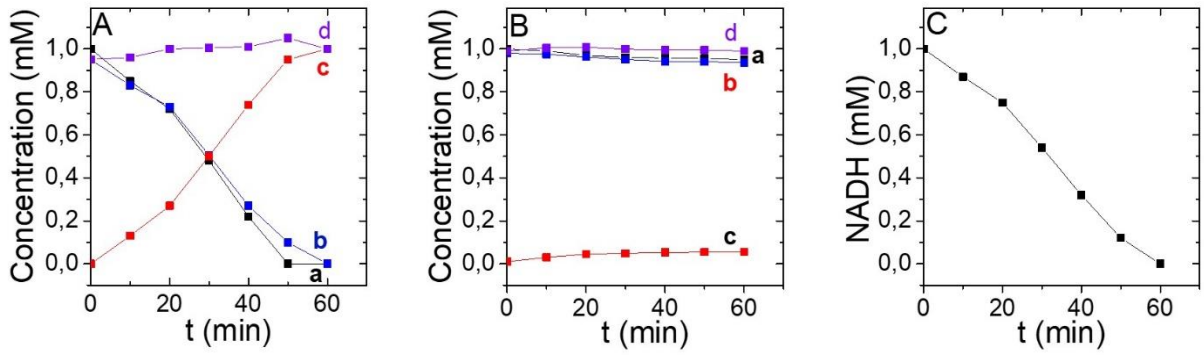

Figure II.10. (A) LDH immobilization on MWCNT-CP: stability and selectivity toward pyruvate conversion tests in the enzymatic flow cell. Time variations of concentrations: (a) NADH, (b) pyruvate, (c) lactate, and (d) sum of pyruvate and lactate. (B) Stability of the solution recovered after stage A, after addition of 1 mM NADH and 1 mM pyruvate: (a) NADH, (b) pyruvate, (c) lactate, and (d) sum of pyruvate and lactate. (C) NADH concentration vs. time in the enzymatic cell after 24 hours storage. All experiments were done in 0.1 M phosphate with 1 mM NADH, 1 mM pyruvate, 25 µM $[Cp^*Rh(bpy)Cl]^+$, and with LDH-MWCNT-CP system (except for stage B) under nitrogen atmosphere, with a solution flowing at 20 $mL.min^{-1}$, and at pH 7.2.

In a first stage (A), 40 mL solution containing 25 µM $[Cp^*Rh(bpy)Cl]^+$, 1 mM NADH, and 1 mM pyruvate was continuously recirculated at 20 $mL.min^{-1}$ in the enzymatic cell for one hour, where 500 units of LDH were immobilized on the MWCNT-CP. At the end of this first stage, 1 mM NADH and 1 mM pyruvate have been added to the remaining solution in the glass vessel, and the solution was circulated in the electrochemical reactor for one hour in the electroless **stage B** under the same recirculation conditions as in **stage A**. Finally, the first enzymatic stage was repeated (**stage C**) after 24 hours: in the meanwhile, the LDH-MWCNT-CP had been stored at 2°C.

For evaluation of the effectiveness of LDH immobilization on the CP-MWCNT, Figure II.10A shows that the NADH concentration decreased regularly to nearly zero after 50 min conversion. This proved the activity of the enzymes confined in the MWCNT-CP support and the non-deactivation of LDH enzymes, contrary to what has been reported in the literature.[48] Besides,

the selectivity of the supported enzymes was shown excellent, with the regular formation of lactate over time (**Fig. II.10A, curve (b)** and the fact that the sum of pyruvate and lactate concentrations remained equal to the initial pyruvate concentration within 5 %. Moreover, the presence of the rhodium complex in the solution does not affect the enzyme selectivity.

On the other hand, testing the solution recovered after stage A upon addition of 1 mM NADH and 1 mM pyruvate (**Figure II.10B**) with continuous flow in the electrochemical reactor operated electroless, revealed that the NADH concentration (**Fig. II.10B, curve a**) slightly decreased, reaching 0.95 mM after 60 min. In the meanwhile, the pyruvate concentration decreased accordingly, attaining 0.935 mM at 60 min (**Fig. II.10B, curve b**), and with corresponding lactate formation. As observed in stage A, lactate formation corresponds well to pyruvate consumption. This stage also indicates that a small quantity of LDH desorbed from the MWCNT-CP support. On the other side, LDH in direct contact with the dissolved rhodium complex was not been deactivated.

Finally, in order to test the stability of the prepared LDH-MWCNT-CP, **Stage C**, **Stage A** was repeated. LDH-MWCNT-CP assembly appeared quite stable, as indicated by its activivity and selectivity towards the bioconversion of pyruvate to lactate, with a conversion rate identical within 8% to that obtained 2 hours after enzyme introduction into the assembly. As observed in **Figure II.10C**, curve a, the NADH concentration decreased with a profile very similar to that in **Stage A**, leading to a total consumption after 60 min. Hence, LDH enzymes immobilized on the MWCNT-CP were observed to be still active after 24 hours.

II.3.5.2 Test of regenerated NADH purity

II.3.5.2.1 Enzymatic evaluation of the purity of the regenerated NADH

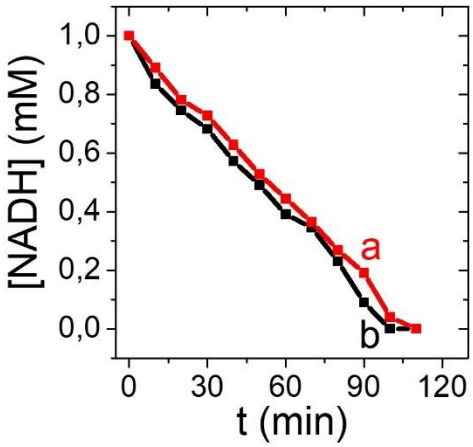

Figure II.11. Online monitoring of the reduction of 1mM of NADH after the addition of 50 U LDH and 1 mM pyruvate in a 3 mL cuvette containing (a) 1 mM of commercial NADH and (b) 1 mM of regenerated NADH. The two experiments were done in the presence of 25 µM $[Cp^*Rh(bpy)Cl]^+$ and 0.1 M PBS. The regeneration of NADH was carried out at -0.5 V vs ref. (H_2).

The study of the reduction of 1 mM NADH, in the presence of 50 U LDH and 1 mM pyruvate in a 3 mL quartz cuvette, related to the bioconversion of 1 mM pyruvate to lactate was evaluated by UV-visible spectroscopy at 340 nm. Results for both tests showed that the NADH concentration decreased with time. With the commercial NADH (**curve a, Figure II.11**), the NADH reduction rate is similar as for regenerated NADH (**curve b, Figure II.11**) showing the purity and the activity of the regenerated NADH are very close. For more information on the purity of the regenerated NADH, tests with NMR were done (next section).

II.3.5.2.2 ^{1}H NMR of regenerated NADH

To perform the NMR analysis on the electrochemically produced NADH, the solution was filtered using a filter paper in order to remove potential impurities. The solution was lyophilized under nitrogen overnight. Then, the obtained powder was mixed with 10 mL of methanol and

stirred for half an hour at room temperature. PBS and the rhodium complex are not soluble in methanol, but NADH is. After that, the mixture was filtered and the liquid solution having a yellow color referred presumably to the NADH color was lyophilized for 5 hours.

Figure II.12. Regenerated NADH powder after lyophilization. Regeneration experiment was done in the presence of 2.5 mM of NAD^+ (40 mL) and 62.5 µM of the Rh complex and carried out at -0.5 V vs ref under the optimized parameters.

A product of mass 0.0562 g, having a yellow color as shown in **figure II.12**, was recovered and represented 71 % of initial mass of cofactor introduced in the solution. The same protocol was applied for mixtures after 5 and 15 min of conversion.

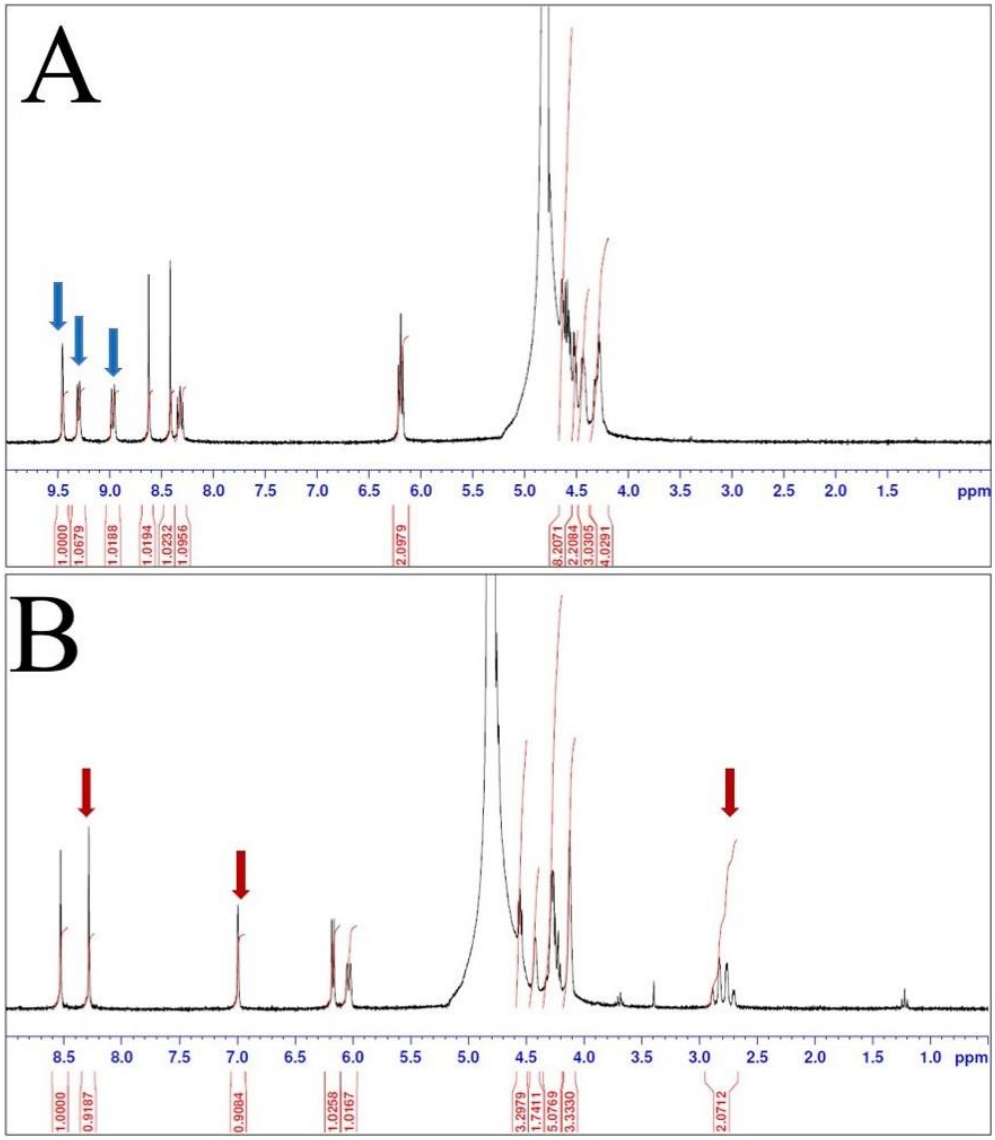

Figure II.13. ^{1}H NMR of commercial (A) NAD^+ and (B) NADH. The NAD^+ (A) and the NADH (B) characteristic peaks are indicated with blue and red arrows, respectively. NAD^+ and NADH were dissolved in D_2O.

As shown in **figure II.13A**, the characteristic peaks of the NAD^+ cofactor are found at 9 ppm, 9.3 ppm, and 9.5 ppm. The characteristic peaks of NADH (B) are found at 2.75 ppm, 7 ppm, and 8.2 ppm.

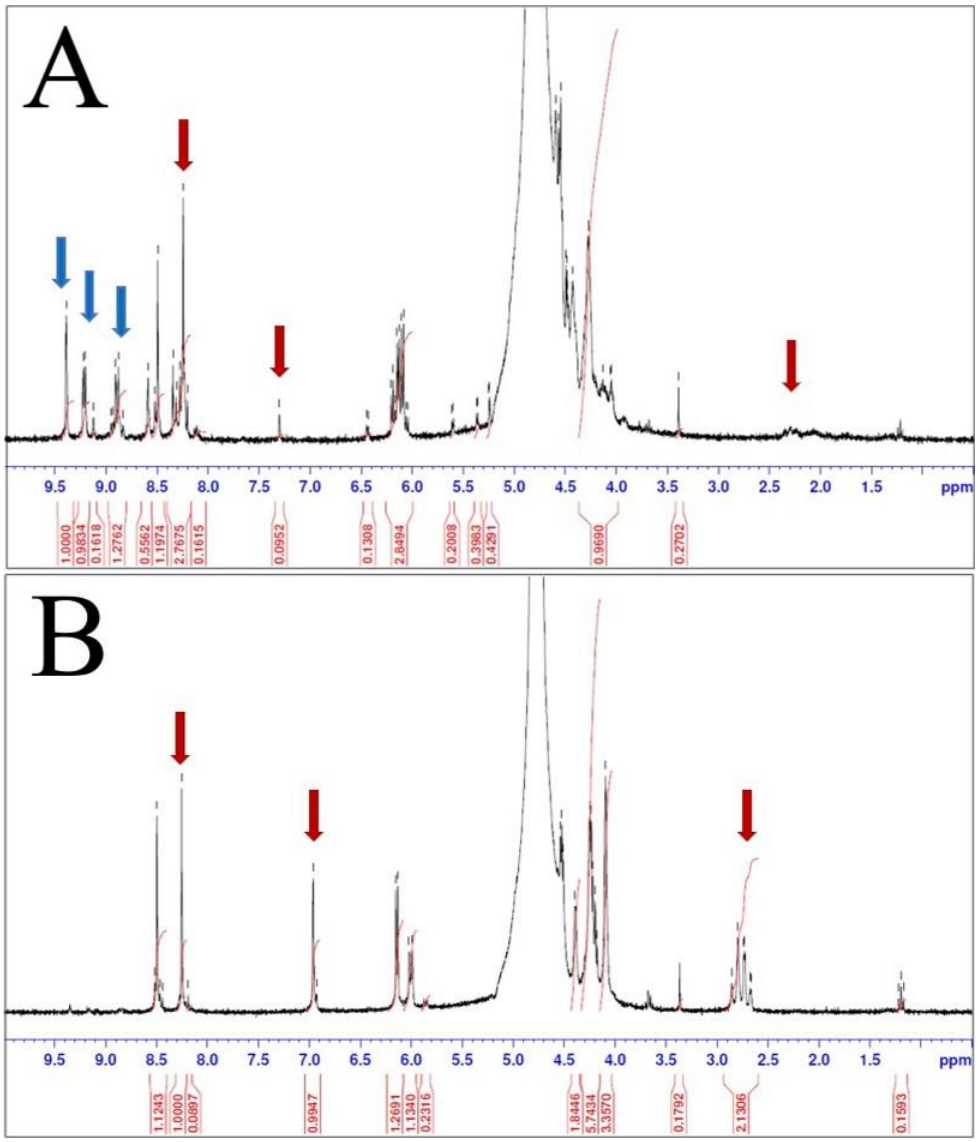

Figure II.14. ^{1}H NMR samples after (A) 5 min and (B) 15 min of conversion. The NAD^{+} (A) and the NADH (B) characteristic peaks are indicated with blue and red arrows respectively. Regeneration experiment was done in the presence of 2.5 mM of NAD^{+} (40 mL) and 62.5 µM of the Rh complex and carried out at -0.5 V vs ref under the optimized parameters. NAD+ and NADH were dissolved in D_2O.

NMR results after 5 min of conversion (**Figure II.14A**) shows characteristic peaks referred to the NAD^{+} and the NADH cofactors when compared with data of **Figure II.13** (commercial NAD^{+} and NADH) where the conversion of NAD^{+} to 1,4-NADH was found to reach 58 % by NMR versus 61 % determined by UV-visible spectroscopy. **Figure II.14A** shows small peaks between 5 ppm and 5.5 ppm that are referred to a slight amount of the buffer in the sample.

In addition, **Figure II.14B** reports the NMR spectra after 15 min of electrolysis that shows a total regeneration of the 1,4-NADH with peaks having the intensity of 2.1, 0.99, and 1 at 2.75 ppm, 7 ppm, and 8.2 ppm, respectively. No singlet pics related to the dimerized form were observed at 2 ppm and 6.85 ppm[49] and no singlet pic was observed at 7.3 referred to 1,6-NADH[50]. In addition, 1,2-NADH cannot be formed due to its instability at neutral pH. [51]

Considering that NADH electrochemically regenerated was totally active, the purity of the regenerated NADH was determined while being compared with purity of the commercial NADH (98%). H^1 NMR pics at 2.8 ppm, 7 ppm, 8.2 are referred to the 1,4-NADH cofactor. The purity of the regenerated NADH was calculated and was found to be equal to 96 %. Slight amounts of soluble phosphate buffer may exist in the sample.

II.3.5.3 Coupling NADH regeneration to pyruvate bioconversion

Scheme II.3 represents the electrochemical reactor in series with the enzymatic cell in the recirculation loop, with the rhodium complex in solution. 40 mL 0.1 M PBS solution at 7.2, containing 0.5 mM NADH, 12.5 µM $[Cp^*Rh(bpy)Cl]^+$, and 25 mM pyruvate, was circulated in the electrochemical reactor, whose cathode was operated at -0.5 V vs ref. (H_2). The carbon-based support of the enzymatic cell was loaded with 500 units LDH. The experiment was carried out under nitrogen degassing, with 20 $mL.min^{-1}$ hydrogen and solution flows (as determined above). For the sake of comparison, another test was made without the enzymatic cell, and with 0.5 mM NAD^+ instead of NADH in the solution.

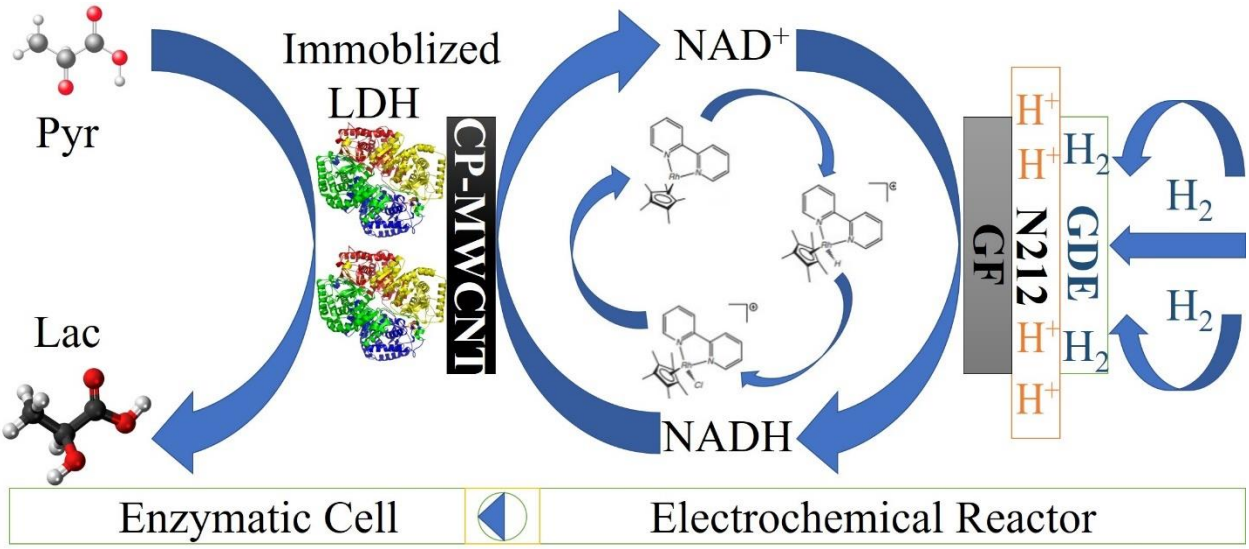

Scheme II.3. Schematic representation of the electrochemical reactor in series with the enzymatic cell including Rh-mediated electrochemical and enzymatic reactions with the LDH-MWCNT-CP system.

As shown in **Figure II.15A** without the enzymatic cell (**curve a**), the cathodic current decreased gradually from 37 to 30 mA (abs. value), then decayed more rapidly after 15 min, corresponding to the large conversion extent of NAD^+ (over 85%). However, with the enzymatic cell in series (**curve b**), a fairly stable current in the order of 21 mA (approx. 1.3 $mA.cm^{-2}$) was observed, revealing indirectly the activity of the rhodium complex toward the regeneration of the NADH consumed in the enzymatic reaction. Contrary to what was observed with test (a), the combined system was operated with balanced NADH enzymatic consumption and electrode regeneration over the 30 min period shown in **Figure II.15A**. The current remained at a comparable level during the combined electro-enzymatic test carried out for 5 hours, with a current regularly decreasing from 21 mA to 16 mA after 5 hours electrolysis (**Figure II.15B**).

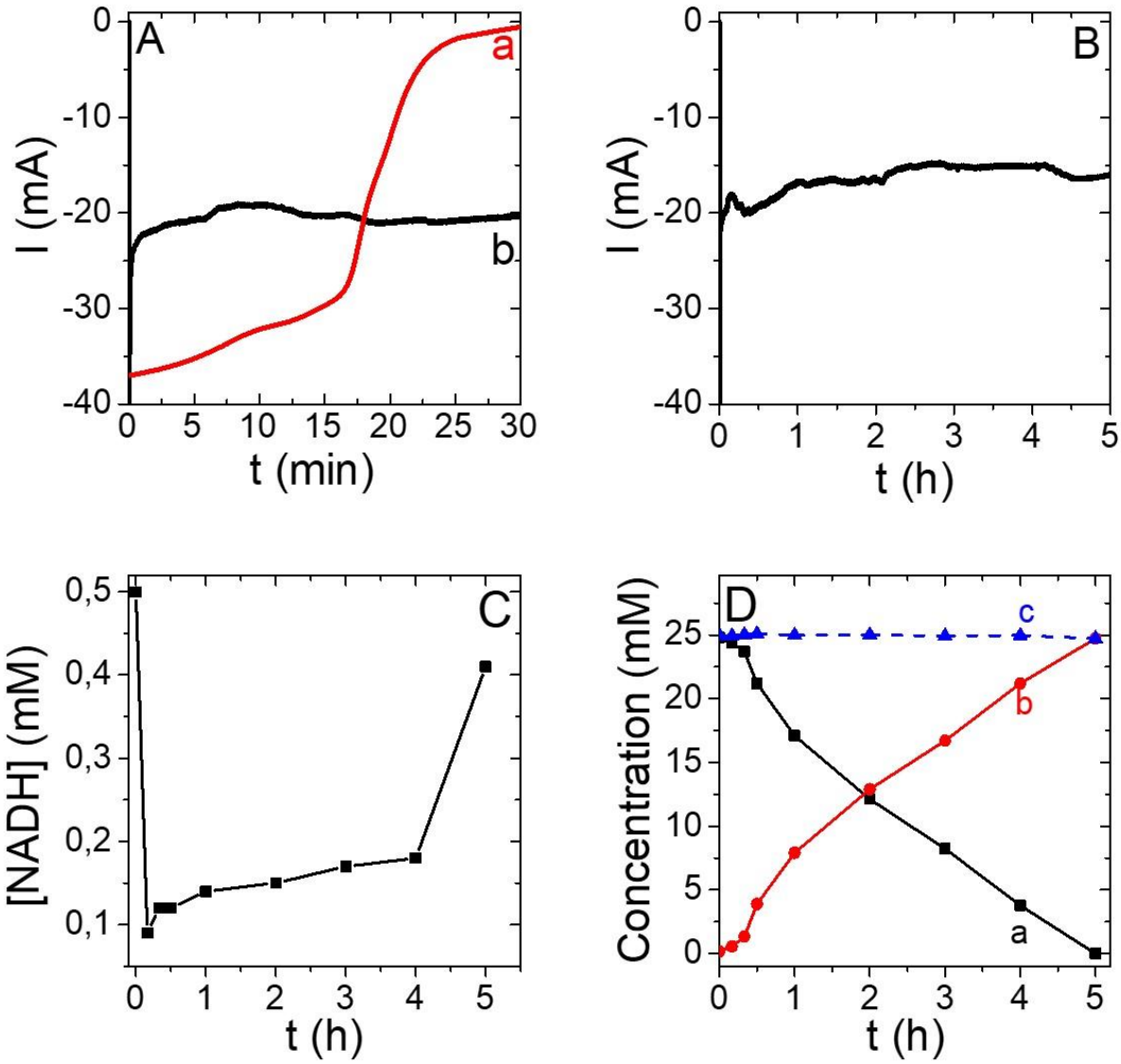

Figure II.15. (A) Current recorded after the addition of 25 mM pyruvate recorded using 12.5 µM $[Cp^*Rh(bpy)Cl]^+$ in solution (a) without the enzymatic cell and with 0.5 mM of NAD^+ and (b) with the enzymatic cell. (B) Current, and (C) NADH evolution recorded with time in test (b). (D) Time variations of the concentrations of (a) pyruvate, (b) lactate, and (c) the sum of pyruvate and lactate, as determined by HPLC. Enzymatic reaction was carried out in 0.1 M PBS solution at pH 7.2, with 0.5 mM NADH and 12.5 µM $[Cp^*Rh(bpy)Cl]^+$ under nitrogen atmosphere, H_2 and solution flow rates at 20 $mL.min^{-1}$ with 500 units of LDH immobilized on MWCNT-CP. In both tests, the cathode potential was at -0.5 V. vs ref. (H_2).

The concentration of the enzymatic cofactor decreased rapidly in the 10 first minutes of the run (**Figure II.15C**) to less than 0.1 mM, due to its quantitative LDH-catalyzed consumption. In

the meanwhile, the lactate concentration raised to 0.56 mM, corresponding to approx.1.12 times of the initial NADH concentration of the NADH cofactor, *i.e.*, with little significant NADH regeneration. Afterward, the NADH concentration slowly increased, attaining 0.17 M after 4 hours, whereas pyruvate was efficiently converted to lactate (**Figure II.15D**), with equilibrated constant rates between electrochemical and enzymatic processes. In the last hour, the lower pyruvate concentration rendered the enzymatic reaction slower, resulting in increased NADH concentration (0.41 mM after 5 hours). Conversion was nearly total after 5 hours, with a 24.7 mM lactate final concentration, corresponding approximately to 50-times of the initial NADH concentration. The faradaic efficiency was higher than 90% during the first hours of reaction, but decreased abruptly during the last hour to 61 %, *i.e.*, below that obtained without enzymes (96 %). Apparently, the decrease in NAD^+ concentration in the flow reactor when NADH was not consumed anymore by LDH (because of the full conversion of pyruvate to lactate), provided more opportunities for side electrochemical reactions, e.g., reduction of oxygen traces or hydrogen evolution.

A total turnover number of more than 2000 was obtained for the rhodium complex after 5 h, which is the highest value ever obtained with rhodium complex in solution, compared with those in former electroenzymatic synthesis tests for the bioconversion at room temperature, reported between 55 and 214.[52],[48] Without the application of an enzymatic reaction, the highest TTN for the rhodium complex applied in the electrochemical regeneration of the NAD(P)H cofactor was 400.[53] In addition, the TN in the period from 1 to 4 hour with enzymes was near 300 h^{-1}, in the same order of magnitude but slightly lower than the value of 370 h^{-1} obtained without enzymes in the presence of a higher concentration of NAD^+ (2.5 mM reported in **Figure II.8** versus 0.5 mM in **Figure II.15**); TTN obtained for the enzymatic reaction was equal to $6.3*10^6$ showing the good stability of the flow device combining the electrochemical reactor and the enzymatic cell. No conversion was observed in the absence of NADH.

The lactate produced by the redox flow bioreactor displayed a very good purity, over 99% as determined by ^{1}H NMR.

^{1}H NMR of produced lactic acid

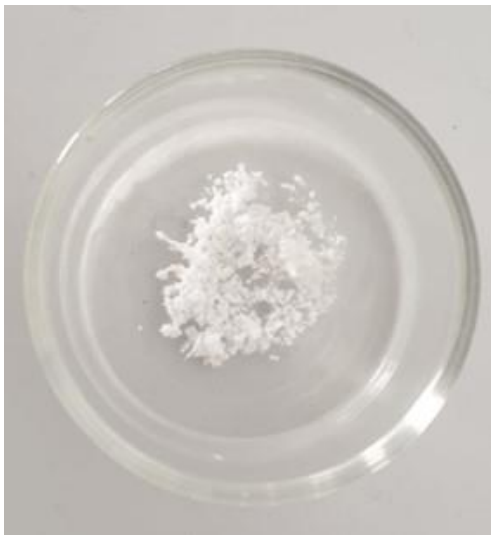

Figure II.16. Lactic acid crystals after product separation.

In order to evaluate the purity of the produced lactate (**Figure II.16**), the post-reaction solution was first filtered using a filter paper in order to remove potential impurities. Decolorization of the solution was then performed by adding 10% mass/vol activated charcoal to the solution and stirred for half an hour. One of the methods used for the recovery of lactic acid is precipitation. 20 mL of the solution containing 24.7 mM of lactate as determined by HPLC were mixed with 20 mL of 25 mM of calcium hydroxide allowing the formation of $Ca(LA)_2$. The solution has been stirred gently at 200 rpm for 6 hours. After, 40 mL of an equivalent solution of sulfuric acid having a concentration of 12 mM was added to the solution allowing the liberation of the lactic acid and the precipitation of calcium sulfate. The solution has been left 2 hours under stirring at a temperature of 90 °C before filtration. The supernatant (65 mL) was recovered by three successive filtration steps and placed under lyophilization, overnight. Lactic acid was then miscible in methanol at a temperature of 18 °C. This step of mixing with 10 mL of methanol may lead to the elimination of PBS, the rhodium complex, and residual amount of sulfate and

calcium that were still in the mixture. The supernatant has been then placed under lyophilization for 5 hours.

The NMR spectrum indicates a purity of over 99% (shown in **Figure II.17**) when compared with the standard ^{1}H NMR of lactic acid. The mass of pure product (0.036 g) represents a recovery rate of approximately 81 % from the product after the bioconversion, which could be improved by further work up.

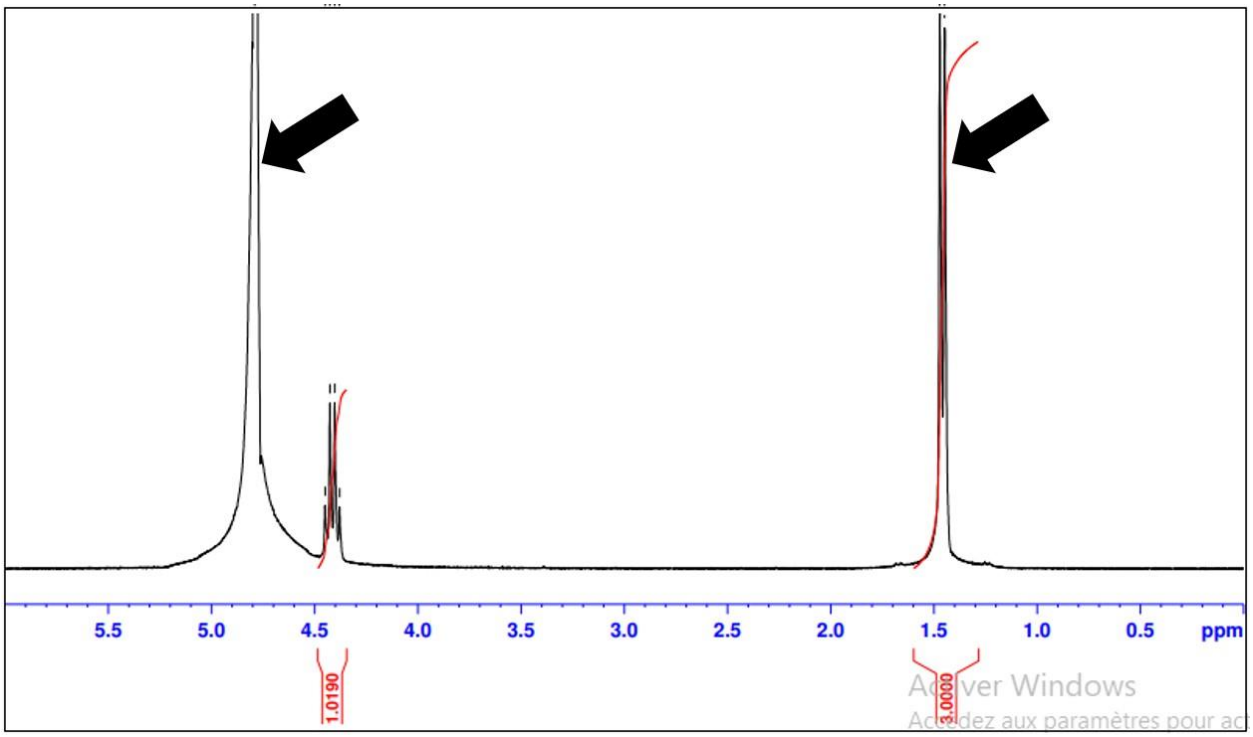

Figure II.17. ^{1}H NMR of recovered lactic acid.

II.4 Conclusion

In summary, we have demonstrated the full potential of a bioelectrochemical reactor for the regeneration of NADH that couples efficiently the oxidation of hydrogen to the reduction of NAD^{+} mediated by a rhodium complex: high activity with a TN of 370 h^{-1} for TTN value near 40 was shown.

The efficient regeneration of NADH featured with a complete conversion and with a high faradaic yield can be reached by fixing different parameters for the used reactor at their optimal values: hydrogen and solution flow rates (20 $mL.min^{-1}$), NAD^+ to $[Cp^*Rh(bpy)Cl]^+$ concentration ratio (40), pH (close to neutrality, to avoid NADH and NAD^+ degradation).

Based on these optimized parameters for the regeneration of the NADH cofactor, adding an enzymatic reaction for the bioconversion of pyruvate to lactate by the LDH-CP-MWCNT showed its high efficiency and stability with a high TTN for the cofactor electrochemical regeneration and the enzymatic reaction of 2000 and $6.3*10^6$, respectively. In addition, no deactivation of both the rhodium complex and the LDH was observed here (a possible deactivation is reported in the literature[48]).

The electrochemical reactor and the enzymatic cell, presented in Schemes 1 and 2 respectively, are in principle scalable. While the performances regarding TN and TTN of the rhodium catalyst in solution are larger than those reported in the literature, one must be aware that TN and TTN for the catalyst are still lower than enzymatic based electrogeneration associated to surface immobilization.[54,55] Moreover, TTN for the cofactor in the electroenzymatic synthesis remain largely lower than the most recent achievements with closely confined enzymatic catalyst also immobilized on the surface of porous electrodes.[56] As a perspective, the immobilization of the rhodium complex allowing much higher TTN (up to 12 000)[20,57] has to be applied for this flow reaction and associated more closely with the enzymatic reaction in order to promote the best cycling of both the catalyst and the enzymatic cofactor and potentially easier purification of the synthesized molecules. In this way, one could promote the application of redox flow technologies in quite relevant industrial topic: dehydrogenases allow for the development of blocks of chiral synthesis comprising various functions e.g. alcohols, hydroxy acids, aldehydes and ketones having a large interest in cosmetics, food, and pharmaceutical industries.[58] Besides, lactate production from lactate dehydrogenase, the illustrative example

considered in this study, is widely used in various applications e.g. food, cosmetics, pharmaceutical, and chemical industries.[59],[60]

References

[1] L. Sorci, O. Kurnasov, D. A. Rodionov, A. L. Osterman, in *Compr. Nat. Prod. II Chem. Biol.*, Elsevier Ltd, **2010**, pp. 213–257.

[2] H. K. Chenault, G. M. Whitesides, *Appl. Biochem. Biotechnol.* **1987**, *14*, 147–197.

[3] L. Zhang, M. Etienne, N. Vilà, A. Walcarius, in *Funct. Electrodes Enzym. Microb. Electrochem. Syst.* (Eds.: N. Brun, V. Flexer), World Scientific, **2017**, pp. 215–271.

[4] B. J. Bryan, W. Sneddon, A. J. Lewis, *J. Chem. Soc. Chem. Commun.* **1972**, 5–6.

[5] G. T. Hçfler, M. Pesic, S. H. Younes, E. Choi, Y. H. Kim, V. B. Urlacher, I. W. C. E. Arends, F. Hollmann, *ChemBioChem* **2018**, *19*, 2344–2347.

[6] C. Virto, I. Svensson, P. Adlercreutz, B. Mattiasson, *Biotechnol. Lett.* **1995**, *17*, 877–882.

[7] G. Xu, H. Yu, Y. Shang, J. Xu, *RSC Adv.* **2015**, *5*, 22703–22711.

[8] K. D. Kulbe, M. W. Howaldt, K. Schmidt, T. R. Rothig, G.- Bioverfahrenstechnik, *Ann. N. Y. Acad. Sci.* **1990**, *613*, 820–826.

[9] R. Ruppert, S. Herrmann, E. Steckhan, *Tetrahedron Lett.* **1987**, *28*, 6583–6586.

[10] E. Siu, K. Won, C. B. Park, *Biotechnol. Prog.* **2007**, *23*, 293–296.

[11] B. Cheng, L. Wan, F. A. Armstrong, *ChemElectroChem* **2020**, *7*, 4672–4678.

[12] H. K. Chenault, E. S. Simon, G. M. Whitesides, *Biotechnol. Genet. Eng. Rev.* **1988**, *6*, 221–270.

[13] H. Zhao, W. A. van der Donk, *Curr. Opin. Biotechnol.* **2003**, *14*, 583–589.

[14] Kane, C. (2005). Application to the Electroenzymatic Regeneration of NADH and

Potentialities in Synthesis (in French) (Doctoral Dissertation, Toulouse 3)., (Doctoral dissertation, Toulouse 3), **2005**.

[15] J. Cantet, (1992). Process for the Regeneration of the NADH Cofactor by the Simultaneous Use of an Electrode and a Hydrogenase (in French) (Doctoral dissertation, Toulouse 3)., University of Toulouse 3, **1992**.

[16] S. Fukuzumi, Y.-M. Lee, W. Nam, *J. Inorg. Biochem.* **2019**, *199*, 110777.

[17] C. F. Megarity, B. Siritanaratkul, B. Cheng, G. Morello, L. Wan, A. J. Sills, R. S. Heath, N. J. Turner, F. A. Armstrong, *ChemCatChem* **2019**, *11*, 5662–5670.

[18] A. Walcarius, R. Nasraoui, Z. Wang, F. Qu, V. Urbanova, M. Etienne, M. Göllü, A. S. Demir, J. Gajdzik, R. Hempelmann, *Bioelectrochemistry* **2011**, *82*, 46–54.

[19] H. Jaegfeldt, *J. Electroanal. Chem. Interfacial Electrochem.* **1981**, *128*, 355–370.

[20] L. Zhang, M. Etienne, N. Vilà, T. X. H. Le, G.-W. Kohring, A. Walcarius, *ChemCatChem* **2018**, *10*, 4067–4073.

[21] B. Tan, D. P. Hickey, R. D. Milton, F. Giroud, S. D. Minteer, *J. Electrochem. Soc.* **2015**, *162*, H102.

[22] E. Steckhan, S. Herrmann, R. Ruppert, E. Dietz, M. Frede, E. Spika, *Organometallics* **1991**, *10*, 1568–1577.

[23] H. C. Lo Leiva, C., Buriez, O., Kerr, J. B., Olmstead, M. M., & Fish, R. H., *Inorg. Chem.* **2001**, *40*, 6705–6716.

[24] A. Goršek, P. Glavič, *Chem. Eng. Res. Des.* **1997**, *75*, 709–717.

[25] T. Noë, Y. Cao, G. Laudadio, *Acc. Chem. Res.* **2019**, *52*, 2858–2869.

[26] W. Ehrfeld, *Microreaction Technology: Industrial Prospects: IMRET 3: Proceedings*

of the Third International Conference on Microreaction Technology, Springer Science & Business Media, **2012**.

[27] J. Britton, S. Majumdar, G. A. Weiss, *Chem. Soc. Rev.* **2018**, *47*, 5891–5918.

[28] R. Porta, M. Benaglia, A. Puglisi, *Org. Process Res. Dev.* **2016**, *20*, 2–25.

[29] M. Wesselmark, B. Wickman, C. Lagergren, G. Lindbergh, *Electrochem. commun.* **2010**, *12*, 1585–1588.

[30] I. Lozano, N. Casillas, C. P. de León, F. C. Walsh, P. Herrasti, *J. Electrochem. Soc.* **2017**, *164*, D184.

[31] J. W. Ager, A. A. Lapkin, *Science* **2018**, *360*, 707–708.

[32] M. Varničić, T. Vidaković-Koch, K. Sundmacher, *Electrochim. Acta* **2015**, *174*, 480–487.

[33] A. E. W. Horst, K.-M. Mangold, D. Holtmann, *Biotechnol. Bioeng.* **2016**, *113*, 260–267.

[34] I. Mazurenko, M. Etienne, G.-W. Kohring, F. Lapicque, A. Walcarius, *Electrochim. Acta* **2016**, *199*, 342–348.

[35] M. T. Reetz, *J. Am. Chem. Soc.* **2013**, *135*, 12480–12496.

[36] G. Roiban, M. T. Reetz, *J. Am. Chem. Soc.* **2013**, *135*, 1665–1668.

[37] S. Sheldon, R. A.;van Pelt, *Chem. Soc. Rev.* **2013**, *42*, 6223–6235.

[38] J. Quinson, R. Hidalgo, P. A. Ash, F. Dillon, N. Grobert, K. A. Vincent, *Faraday Discuss.* **2014**, *172*, 473–496.

[39] U. Koelle, A. D. Ryabov, *Mendeleev Commun.* **1995**, *5*, 187–189.

[40] V. Sivasankar, P. Mylsamy, K. Omine, *Microbial Fuel Cell Technology for Bioelectricity*, Springer, **2018**.

[41] L. Hussein, G. Urban, M. Krüger, *Phys. Chem. Chem. Phys.* **2011**, *13*, 5831–5839.

[42] E. V LaBelle, H. D. May, *Front. Microbiol.* **2017**, *8*, 756.

[43] L. Gorton, E. Dominguez, in *Encycl. Electrochem.*, Wiley-VCH Verlag GmbH & Co. KGaA, Weinheim, Germany, **2007**, pp. 67–143.

[44] S. Goswami, S. Klaus, J. Benziger, *Langmuir* **2008**, *24*, 8627–8633.

[45] L. Rover Júnior, J. C. Fernandes, G. de Oliveira Neto, L. T. Kubota, E. Katekawa, S. H. Serrano, *Anal. Biochem.* **1998**, *260*, 50–55.

[46] S. Lee, H. Choe, D. H. Cho, S. H. Yoon, K. Won, Y. H. Kim, *J. Electrochem. Soc.* **2016**, *163*, G50–G52.

[47] M. M. Grau, M. Poizat, I. W. C. E. Arends, F. Hollmann, *Appl. Organomet. Chem.* **2010**, *24*, 380–385.

[48] F. Hildebrand, S. Lütz, *Chem. - A Eur. J.* **2009**, *15*, 4998–5001.

[49] S. Betanzos-Lara, A. Habtemariam, P. J. Sadler, *J. Mex. Chem. Soc.* **2013**, *57*, 160–168.

[50] P. Stufano, A. R. Paris, A. Bocarsly, *ChemElectroChem* **2017**, *4*, 1066–1073.

[51] J. W. H. Burnett, R. F. Howe, X. Wang, *Trends Chem.* **2020**, *2*, 488–492.

[52] F. Hildebrand, S. Lütz, *Tetrahedron Asymmetry* **2007**, *18*, 1187–1193.

[53] K. Vuorilehto, S. Lu, C. Wandrey, **2004**, *65*, 1–7.

[54] M. Yuan, M. J. Kummer, R. D. Milton, T. Quah, S. D. Minteer, *ACS Catal.* **2019**,

5486–5495.

[55] B. Siritanaratkul, C. F. Megarity, T. G. Roberts, T. O. M. Samuels, M. Winkler, J. H. Warner, T. Happe, F. A. Armstrong, *Chem. Sci.* **2017**, *8*, 4579–4586.

[56] C. F. Megarity, B. Siritanaratkul, R. S. Heath, L. Wan, G. Morello, S. R. FitzPatrick, R. L. Booth, A. J. Sills, A. W. Robertson, J. H. Warner, N. J. Turner, F. A. Armstrong, *Angew. Chemie - Int. Ed.* **2019**, *58*, 4948–4952.

[57] L. Zhang, N. Vilà, G. W. Kohring, A. Walcarius, M. Etienne, *ACS Catal.* **2017**, *7*, 4386–4394.

[58] R. Patel, M. Kula, U. Kragl, *Stereoselective Biocatal.* **2000**, *13*, 839–866.

[59] Y. J. Wee, J. N. Kim, H. W. Ryu, *Food Technol. Biotechnol.* **2006**, *44*, 163–172.

[60] E. T. H. Vink, K. R. Rábago, D. A. Glassner, P. R. Gruber, *Polym. Degrad. Stab.* **2003**, *80*, 403–419.

Objective of the study in Chapter III.

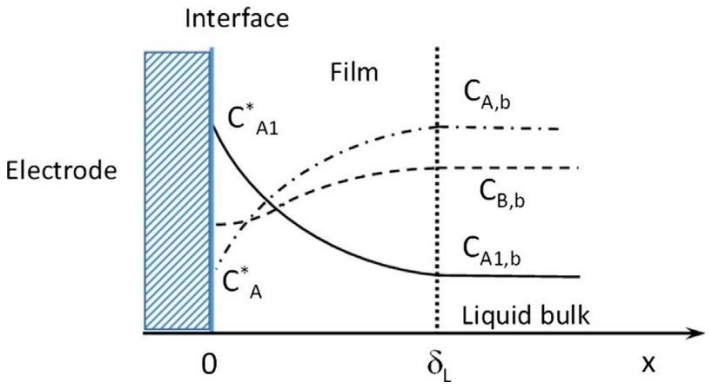

Schematic view of the overall NADH regeneration mediated by Rh complex

In this chapter, a model for calculating concentration profiles near the electrode surface based on operating conditions and the rate constant k of the reaction has been developed. The limiting current density of Rh(III) reduction in the absence of NAD^+ permitted the estimation of this species' mass transfer coefficient. Moreover, based on the experimental values for the current density at various NAD^+ concentrations, the model could be used to estimate the rate constant k. Then, the progression of NAD^+ electromediated conversion in discontinuous tests could be easily predicted by assuming a rapid chemical reaction, with successful comparison to prior data for identified operating conditions.

Article published in Chemical Engineering Science

El Housseini, W., Etienne, M., Walcarius, A., & Lapicque, F. (2022). Multiphase chemical engineering as a tool in modelling electromediated reactions-Example of Rh complex-mediated regeneration of NADH. Chemical Engineering Science, 247, 117055.

Chapter III. Multiphase chemical engineering as a tool in modelling electromediated reactions- Example of Rh complex-mediated regeneration of NADH

Abstract:

On the basis of the electromediated regeneration of beta-nicotinamide adenine dinucleotide hydrate (NADH) by chloro(2,2′-bipyridyl) (pentamethylcyclopentadienyl)-rhodium (III) chloride complex – Rh(III), the manuscript describes a modelling approach inspired by multiphase chemical engineering with gas absorption with chemical reaction. Here, the electrode surface is assimilated to the gas-liquid interface, and the reducing Rh(I) formed at the electrode corresponds to the dissolved gas. This method allows the kinetics of the liquid phase reaction between NAD^+ and Rh(I) to be estimated and the beneficial effect of NAD^+ concentration on the reduction current of Rh(III) to be successfully predicted. Moreover, because of the fast kinetics of the liquid phase reaction, the overall mediated regeneration of NADH by the redox Rh couple can be viewed as occurring as the direct reduction of NAD^+ to NADH. The approach could be applied to other electromediated processes, upon sufficient knowledge of the system physico-chemical specificities.

III.1 Introduction

Beta-nicotinamide adenine dinucleotide hydrate (NAD+/NADH) cofactor and its phosphorylated derivative ($NADP^+$/NADPH) are well-known electron mediators in biological systems, making it possible a number of enzymatic catalysed oxidation and reduction reactions.[1,2] Because of their high costs, these cofactors must be regenerated in order to enable syntheses with oxidoreductases or bio-fuel-cells applications economically viable.[3] In particular, various techniques can be used to regenerate the reducing forms NAD(P)H[4] but electrochemical methods are often employed [5–7] because of their high total turnover number (TTN) allowed and no need of additional sacrificial electron donors. However, great care should be taken to produce only the bioactive 1,4-NADH and avoiding the enzymatically inactive products (such as 1,6-NADH, 1,2-NADH or NAD2 dimers).[8] The direct regeneration of NADH by reduction of NAD^+ at an electrode surface occurs at very cathodic potentials, thus enters in competition with hydrogen evolution and leads to the formation of the inactive dimer of NAD^+.[9] For this reason, redox mediators are usually employed for this purpose.[7,10] These mediators can be chemical species - such as complexes of transition or precious metals cations, or organic molecules e.g. methyl viologen - biological molecules e.g. flavine adenine dinucleotide or ferredoxin $NADP^+$ reductase (FNR). All of them allow the electrochemical reduction to be conducted at lower cathodic potentials and have a very high selectivity towards the regeneration of the active form of the NADH cofactor (1,4-NADH) – a crucial aspect, considering the high cycling rate of NAD^+/NADH in enzymatic processes.

The complex chloro(2,2′-bipyridyl) (pentamethylcyclopentadienyl)-rhodium (III) chloride was shown to be the best non-enzymatic mediator for the regiospecific regeneration of NADH[11,12] when electrochemically reduced into the monovalent rhodium (I) complex form. Using Rh(III) and Rh(I) names to relate to the two mediator forms, NADH regeneration occurs after the

reaction below, with consumption of one proton per NAD^+ ion (which is an accepted simplified view of a multistep process:[13]

$$Rh(III) + 2\ e \rightarrow Rh(I) \quad (1)$$

$$Rh(I) + H^+ + NAD^+ \rightarrow Rh(III) + NADH \quad (2)$$

The principle is shown in **Figure III.1**.

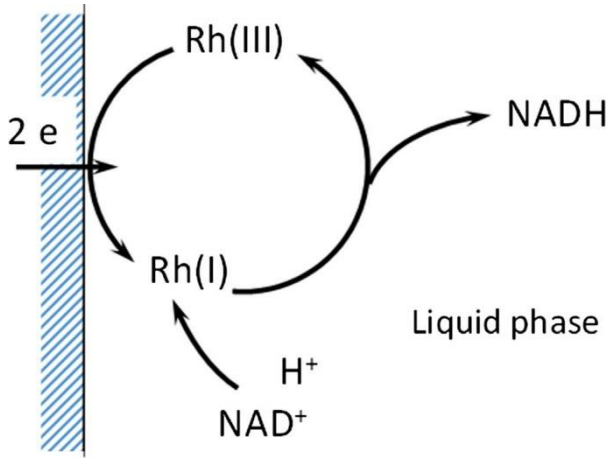

Figure III.1. Principle of the electromediated system investigated here, with occurrence of chemical reaction in the liquid phase.

The rhodium complex can be employed as dissolved in the solution for liquid-phase reaction (2) as reported by Vuorilehto et al.[14] or in a companion paper,[15] or grafted at the electrode surface,[16,17] for possible recycling of this expensive mediator in real bioelectrochemical processes. In both cases, NAD^+ reduction leads to active NADH as shown by ^1H NMR spectroscopy or by integration of an enzymatic reaction e.g. lactate dehydrogenase-catalysed reduction of pyruvate. Experimental measurements related to the mediated regenerations show that: (i) voltammetric curves of Rh(III) reduction exhibit far larger currents (in absolute value) in the presence of NAD^+ in the solution than without. (ii) batch conversion of NAD^+ in the presence of the Rh complex under various concentrations of the two reactants does not simply depend on one of the two concentrations. In addition, for modelling and scale-up of mediated electrochemical processes, the rate constant, k, of reaction (2) needs to be estimated.

Because of its high interest in biochemistry, the regeneration of NADH using bi-pyridines pentamethylcyclopentadienyl (cp)-rhodium complexes has been largely investigated, depending on the nature of the pyridyl functionalized groups,[18,19] and the nature of the Rh(III) reduction process. For this concern, the incorporation of one proton after the two electron transfers from the cathode, has often been chemically emulated by use of hydride donors e.g., sodium formate. According to most published papers dealing with reduction with formate,[20,21] the formation rate of NADH obeys a Michaelis-Menten law involving the concentrations of Rh(III) introduced and formate ions. The low value of inhibition constant K_M related to Rh (III) near 9 µM suggests that for practical applications, NADH formation rate is nearly independent of Rh(III) concentration, contrary to what has been observed with electrochemical reduction. For both chemical and electrochemical ways to generate Rh(I) species, the rate of NADH formation is expressed in terms of turnover frequency of the Rh complex, covering the occurrences of reactions (1) and (2), with – to our state of knowledge - no quantified values for reaction rate k between Rh(I) and NAD^+.

In case that the redox couple is attached to the cathode surface by chemical grafting or adsorption, experimental data – in the form of voltammetric curves in motionless conditions, or under forced convection – are treated using electrochemical models developed for estimation of electrochemical and chemical kinetic parameters.[22–24] When the mediating redox couple is dissolved, other interpretation methods were developed.[25,26] Although not corresponding to mediated electrosynthesis, the case of an electrochemical process followed by a chemical reaction occurring in the liquid bulk has been considered in the past.[27] Modelling of the whole system was shown to successfully benefit from previous works on gas-liquid (G-L) absorption processes with chemical reaction,[28] to calculate the enhancement of gas absorption rate by occurrence of a fast chemical reaction, as it is for the absorption of acidic CO_2 and SO_2 gases in alkaline media.

The aim of this work was to use a comparable method to model the performance of an electrochemical cell for mediated electrosynthesis - in terms of current density and conversion rate of the reactant, on the example of the above Rh/NAD^+ system.[15] In both cases, the approach relies on the existence of a diffusion layer of thickness δ_L near the (G-L or electrode-electrolyte) interface, in which transfer phenomena only occur upon diffusion, i.e. with a negligible liquid velocity.[28] For the above example of electromediated reaction, Rh(III) is named R3, Rh(I) complex, R1, whereas NAD^+ is referred as NAD. In the model (text and equations) for evident chemical meaning, Rh(I), Rh(III) and NAD^+ will still be used as such. The first step of the process is the dissolution of the gas in the liquid or the reduction of Rh(III) species on the cathode surface: in both cases, this interfacial step is assumed to be very fast. R1 formed diffuses from the cathode or reacts with NAD after (2) in the diffusion layer as shown in **Figure III.2**.

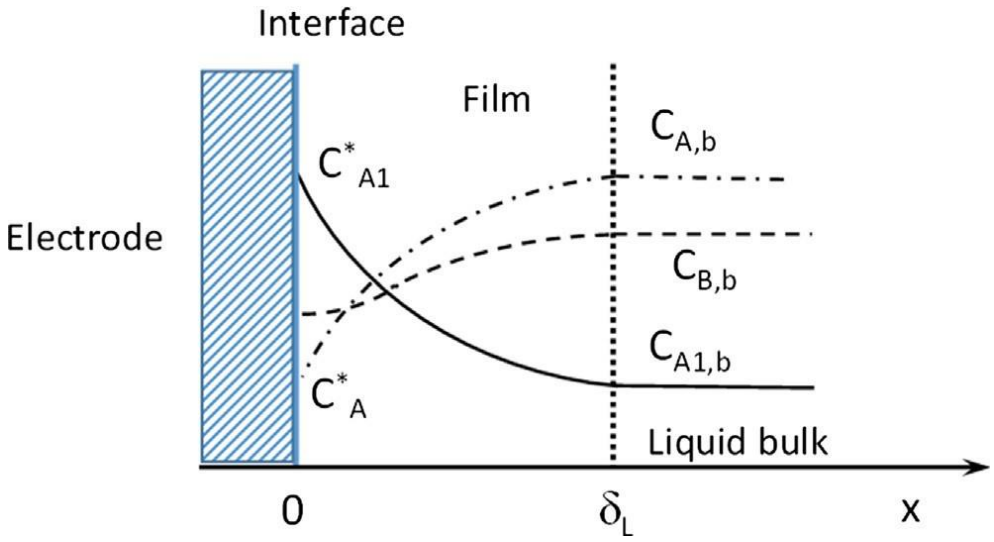

Figure III.2. Schematic view of the overall NADH regeneration mediated by Rh complex: Electrode reduction of R3 forming R1, which chemically reacts with dissolved NADspecies.

On the basis of the above analogy, a model has been developed here for calculation of concentrations profiles in the vicinity of the electrode surface depending on the operating conditions and the rate constant k of the reaction. The limiting current density of Rh(III)

reduction in the absence of NAD^+ allowed mass transfer coefficient of this species to be estimated. Moreover, from the experimental values for the current density at various NAD^+ concentrations, rate constant k could be estimated using the model. Then, progress of NAD^+ electromediated conversion in discontinuous tests could be simply predicted assuming a fast chemical reaction, with successful comparison to previous data for identified operating conditions.

III.2 Materials and methods

The electrochemical reactor depicted in Figure III.3 was formed by two 4 x 4 cm^2 compartments. The anode for hydrogen oxidation into H^+ was a commercial gas diffusion electrode (GDE) (Ion Power) supported by a gas diffusion layer and loaded at 0.2 mg Pt/cm^2 was deposited on a Nafion N-212 membrane. This membrane separated the gas/solid part of the cell from the cathode chamber for NAD^+ mediated reduction. The mediated reduction of NAD^+ was carried out on the surface of a 4 x 4 x 0.4 m^3 graphite felt (GFD4 6EA, SGL, Germany). The material formed from polyacrylonitrile precursor was highly porous (81%) with pores larger than 100 µm. Whereas the anode was fed with a stream of fresh hydrogen (20 $Ncm^3.min^{-1}$), the liquid phase, with a volume of 40 cm^3 was recirculated in the cell at 20 $cm^3.min^{-1}$ in batch NADH runs carried out at a fixed voltage and at ambient temperature. Because of the very low change in potential of the anode GDE operated with current density in the order of 1 $mA.cm^{-2}$, the cathode potential was referred to the hydrogen anode, noted ref. (H_2) in the manuscript.

The two electrode reactions are written as:

$$Rh(III) + 2\ e^- \rightarrow Rh(I) \quad (1)$$

$$\text{with } Rh(I) + H^+ + NAD^+ \rightarrow Rh(III) + NADH \quad (2)$$

$$H_2 \rightarrow 2\ H^+ + 2\ e^- \quad (3)$$

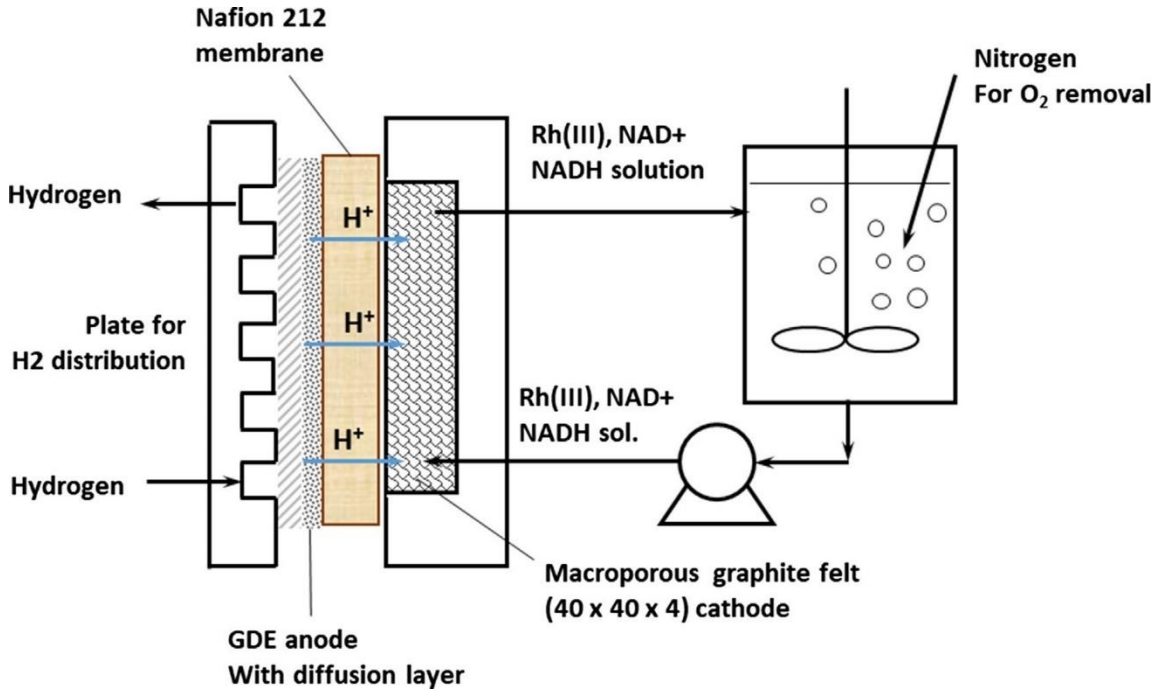

Figure III.3. Electrochemical cell for NADH generation with recirculation of the Rh complex -NAD^+ containing solution

From the above reactions, formation of one NADH molecule is accompanied by one proton gained by the solution. To avoid any visible change in the pH which has to be kept near 7, the solution contained phosphate buffer at 0.1 M.

III.3 Presentation of the model

The model was developed by analogy with G/L absorption with chemical reaction, first to predict the concentration profiles and the enhancement of the limiting current density for Rh(III) reduction by the presence of NAD^+. In this model, the system was assumed at steady state, on the basis of the initial concentrations of the two reactants. In contrast, time dependence was accounted for in modelling NAD^+ conversion in the discontinuous cell.

Concentration profiles near the electrode surface

For the system presented above, one-dimensional mass balances were written at steady state in the diffusion layer, thus neglecting the convective terms;

$$D_{R1}\frac{d^2C_{R1}}{dx^2} = D_{NAD}\frac{d^2C_{NAD}}{dx^2} = kC_{R1}C_{NAD} \quad (4)$$

where x is the coordinate from the electrode surface; D_{R1} and D_{NAD} are the diffusion coefficients of Rh(III) and NAD^+ in the solution, and k the rate constant of the 2nd order kinetic law. The assumptions of the model are listed below:

- Rh(I) species was assumed to be present only in the solution even though Rh(I) was shown to be partially adsorbed on the electrode surface (Vuorilehto et al.), due to the effective solution recirculation. NAD^+ reduction is thus assumed to occur only in the liquid phase which justifies the expression for the kinetic term in equation (4).
- As expressed above, the electrode reduction of Rh(III) is carried out under diffusion control, so its surface concentration $C_{R3,s}$ is zero. The current density is then at its limiting value, i_L.
- Rh(III) and Rh(I) complexes have identical diffusion coefficients. Therefore, since Rh(III) is converted to Rh(I) with a perfect selectivity, it can be shown that:

  $$C_{R3} + C_{R1} = C_{R3,b} \text{ anywhere in the solution.} \quad (5)$$

  where subscript b refers to the solution bulk. $C_{R3,b}$ corresponds to the concentration of Rh complex introduced.
- Consumption of Rh(I) complex by the chemical reaction is assumed to be fast thus occurring only in the diffusion layer. Therefore, two boundary conditions were written:

  $x = 0$, $C_{R1} = C_{R3,b}$ and (6a)

  $x = \delta_L$, $\frac{dC_{R1}}{dx} = 0$ (6b)
- The kinetic law was written regardless of proton concentration. The presence of phosphate buffer and the pH fixed at 7.2 justify this assumption; k value holds for the pH considered.

Since NAD^+ is not formed or consumed at the electrode surface, its gradient at x=0 is zero; moreover, its concentration at δ_L is assumed to be that in the bulk:

$$x = 0, \frac{dC_{NAD}}{dx} = 0 \quad (7a)$$

$$x = \delta_L, C_{NAD} = C_{NAD,b} \quad (7b)$$

Dimensionless length and concentrations were defined:

$$R1 = \frac{C_{R1}}{C_{R3,b}}; \quad X = \frac{x}{\delta_L} \quad (8)$$

According to the diffusion layer film model, mass transfer coefficient k_L of Rh(III) to the electrode is defined as the ratio

$$k_L = \frac{D_{R3}}{\delta_L} \quad (9)$$

Finally, Ha number was finally defined as:

$$Ha = \frac{\sqrt{kD_{R3}C_{NAD,b}}}{k_L} \quad (10)$$

Therefore, relation (4) could yield the two dimensionless differential equations:

$$\frac{d^2R1}{dX^2} = Ha^2 R1.NAD \quad (11a)$$

$$\frac{d^2NAD}{dX^2} = Ha^2 \frac{D_{R3}}{D_{NAD}} \frac{C_{R3,b}}{C_{NAD,b}} . R1.NAD \quad (11b)$$

With the boundary conditions:

$$X=0 \quad R1 = 1, \frac{dNAD}{dX} = 0 \quad (12a)$$

$$X=1 \quad \frac{dR1}{dX} = 0, \ NAD = 1 \quad 12b)$$

According to Danckwerts, the assumption related to a fast reaction i.e. occurring only in the diffusion layer is only valid for Ha ≥ 3, for sufficient value of rate constant k in comparison to mass transfer coefficient k_L, and sufficient concentration in "scavenging" NAD^+ species. Also

introduced in G/L absorption, the enhancement factor E, defined as the ratio of the flux of Rh(III) consumption at the interface in the presence of chemical reaction to the flux without chemical reaction. In the present case, this flux is proportional to the current density, so that for mediated electrosynthesis, E is expressed as:

$$E = \frac{S_{0with\ NAD^+}}{S_{0,without}} = \frac{i_{L,with\ NAD^+}}{i_{L,without}} \quad (13)$$

If S_0 is the concentration gradient of Rh(III) complex at the electrode:

$$S_0 = \frac{dR3}{dX}\Big)_{X=0} \quad (14)$$

Without occurrence of chemical reaction (no NAD^+ added, or k=0), the profile of Rh(III) concentration is linear, so S_0 is equal to -1, and **relation (13)** reduces to

$$E = -S_{0,\text{without}} \quad (15)$$

E is easily deduced from the voltammetric curves by dividing the current at the diffusion plateau for the considered concentration of NAD^+, to the corresponding recorded current without NAD^+. For a postulated value of k, integration of (11) has been carried out by a finite element scheme, considering the boundary conditions (12).

III.4 Results and discussion

III.4.1 Experimental results

Voltammetric curves with Rh have first been recorded at 5 mV/s between 0.2 and -0.6 V/H_2, in the cell containing various concentrations of Rh(III) in the 0.1 M PBS, NAD^+-free solution at pH 7.2. This scan rate was formerly used with this system[15,29]; in other works,[18] the scan rate was larger or equal to 9 mV/s. Although showing the increasing effect of Rh(III) concentration, together with the synergetic action of NAD^+ presence in the reduction current observed, the possible control of mass transfer could not be observed by a well-defined current plateau in all cases.

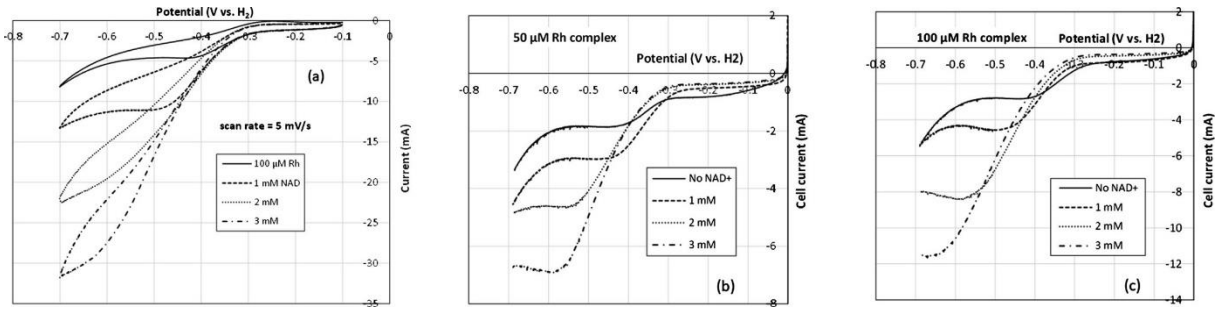

Figure III.4. (a) Cyclic voltammograms recorded at 5 mV s^{-1} (Scan 3) with the graphite felt electrode in the buffer solution with 125 µM $[Cp^*Rh(bpy)Cl]^+$: two replicates. (b and c) Voltammetric curves recorded at 1 mV/s after 4 successive cycles at 5 mV/s for Rh complex solution with increasing amounts of NAD^+: (b) with 50 µM Rh(III), (c) with 100 µM Rh(III) complexes. Experiments were carried out in 0.1 M phosphate buffer solution at pH 7.2 under nitrogen atmosphere with a solution and hydrogen flow rates of 20 mL.min^{-1} each.

As exemplified by **Figure III.4a**, evidence of mass transfer control was observed near -0.25 V vs ref (H_2), either by a current hump peak or on the contrary by a shoulder peak from which the limiting current density could not be estimated with a sufficient accuracy. It was therefore preferred to proceed to four activation cycles at 5 mV/s in the above potential range, before performing a linear scan at 1 mV/s between 0 V and -0.6 V vs. H_2. The conversion of NAD^+ to NADH was estimated by the charge passed to be in the order or below 5%. Because of the above consumption of NAD^+ in the voltammetric experiments, each couple of Rh(III) and NAD^+ concentrations was investigated with a freshly prepared solution. As shown in **Figures 4b and c**, better-defined plateaus of Rh(III) cathodic reduction could be observed at 1 mV/s, with or without NAD^+ present in the solution. Replicate experiments led to deviations in the current plateau lower than 10%. Mass transfer rates of Rh(III) species could be estimated from the curves after graphical subtraction of the residual current. The limiting current with an uncertainty estimated at 10%, was shown to obey a linear function of Rh(III) concentration (**Figure III.5**), however with a constant term. This non-zero current was attributed to a residual current I_{res} not subtracted by the above procedure.

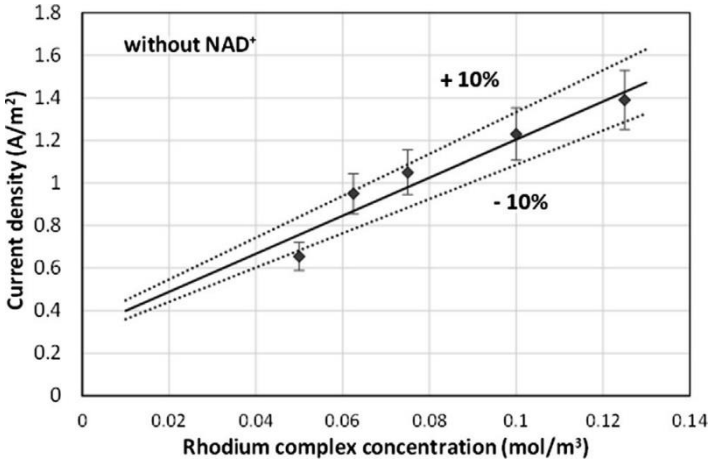

Figure III.5. Variations of the limiting current density estimated from voltammetric curves at 1 mV/s with the Rh(III) solutions. Data are given with a 10% error bar; the liner regression is in solid lines and the two dotted lines are linear variations with a slope 10% higher or lower than the regression slope.

The data obtained for tests with six different Rh concentrations are comprised between two linear variations with a slope respectively equal to the average slope with plus or minus 10%. The slope of the average variation led to mass transfer coefficient k_L, on the basis of two electrons exchanged and the area of the electrode taken as its geometrical area i.e. 16 cm^2 (see Appendix 1). Moreover, diffusivities D_{R3} and D_{NAD} have been estimated as explained in Appendix 2.

$$k_L = 4.6\ 10^{-5}\ m/s \pm 10\%,\ D_{R3} = 3.48\ 10^{-10}\ m^2/s,\ D_{NAD} = 2.4\ 10^{-10}\ m^2/s \qquad (16)$$

III.4.2 Concentration profiles in the diffusion layer

Calculations have been carried out for a Rhodium complex concentration of 50 µM, with 2 mM NAD^+, for rate constant k varying between 20 to 100 $m^3.mol^{-1}$, corresponding to Ha values ranging from 2.9 to 6.47.

For the lowest k value, Rh(I) concentration profile in the film deviates noticeably from the linear profile expected without NAD^+. The concentration gradient at X=0 was found near -2.83. However, R1 is still near 0.06 for X=1 (Figure III.6), expressing the fact that the boundary conditions do not hold perfectly: as a matter of fact, the chemical reaction although relatively

fast, does not only occur in the diffusion layer. This phenomenon is less visible for k = 40 m^3 mol^{-1} s^{-1} for which gradient S_0 is more negative and R1 is slightly below 0.02 at X = 1: calculated concentration profiles are more reliable. For k = 100 m^3 mol^{-1} s^{-1}, R1 is below 0.005 at the edge of the film (**Figure III.6**), and the chemical reaction can be considered as "fast", i.e. occurring only in the film.

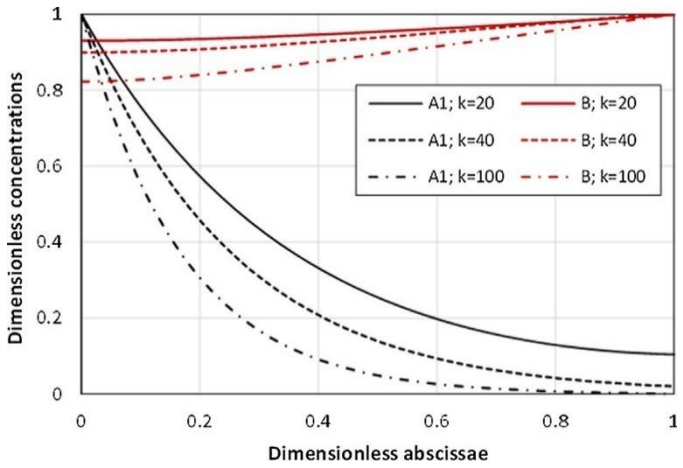

Figure III.6. Dimensionless concentration profiles of species A1 (Rh(I) complex) and B (NAD+) in the diffusion film. Concentration of Rh complex and NAD+ at 50 µM and 2 mM respectively. Effect of the rate constant k in m3.mol-1.s-1.

Because of its large excess in comparison to Rh complex, NAD^+ is little depleted in the diffusion film (**Figure III.6**). Moreover, increasing the rate constant results – as expected - in more significant depletion of NAD^+ near the electrode surface.

These calculations carried out for various k values led to the corresponding values for the concentration gradients at the wall and enhancement factor E, as shown in Figure III.7a below. The value for Ha number deduced from k affects strongly the enhancement factor, as shown in Figure III.7b. In both figures, the curve in dotted line corresponds to Ha number below 3, i.e. for which boundary conditions related to Rh(I) conversion in the film are not fulfilled.

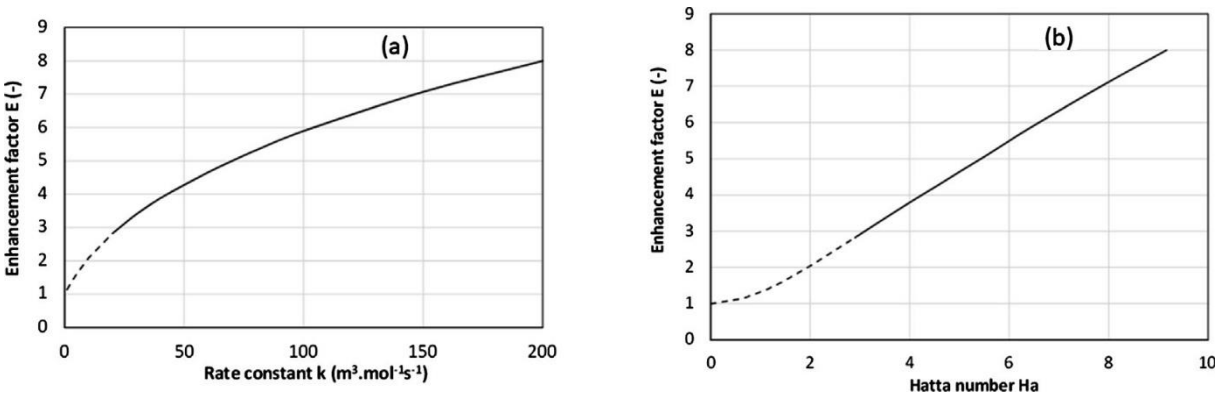

Figure III.7. Enhancement factor E corresponding to occurrence of the chemical reaction. Concentrations of Rh complex and NAD^+ at 50 µM and 2 mM respectively. Fig. 7a): variation of E with rate constant k; Fig. 7b: variation of E with Hatta number Ha.

III.4.3 Estimation of the rate constant from electrochemical data

Residual current density i_{res} evidenced in Figure III.5 was assumed to be constant at 0.3 mA/cm^2 in all voltammetric curves, i.e. for all NAD^+ concentrations. In Rel (13) giving access to enhancement factor E, both limiting current densities $i_{L,without}$ and $i_{L,with\ NAD+}$ had to be corrected for current density i_{res}.

The experimental value for E factor was used for estimation of rate constant k: equations (11) subject to (12) were integrated: the trial-and-error procedure relied on the convergence of gradient S_0, which has to be equal to the opposite of the E value (rel. 15).

III.4.4 Sensitivity analysis

Because of the uncertainty on the limiting current in the order of 10%, sensitivity analysis of the method for k estimation was achieved on the example of 125 µM Rh complex and 2 mM NAD^+. In addition to the E value determined at 3.83, we considered its lower and higher estimates, within 10%. For this experiment example, the estimate for k from the "central" E value was found at 46 m^3.mol^{-1}, and at 35 and 58 m^3.mol^{-1}.s^{-1} from the lower and higher E values respectively. The above values show the strong sensitivity of the electrochemical technique, for which a 10% uncertainty in the limiting current recorded induces a change in k

value in the order of 25%. In the three cases, R1 at the edge of the film was lower than 0.015, validating in an acceptable manner the assumption of fast reaction with complete consumption of Rh(I) in the film. The dimensionless profiles of R1 and NAD are shown in **Figure III.8**.

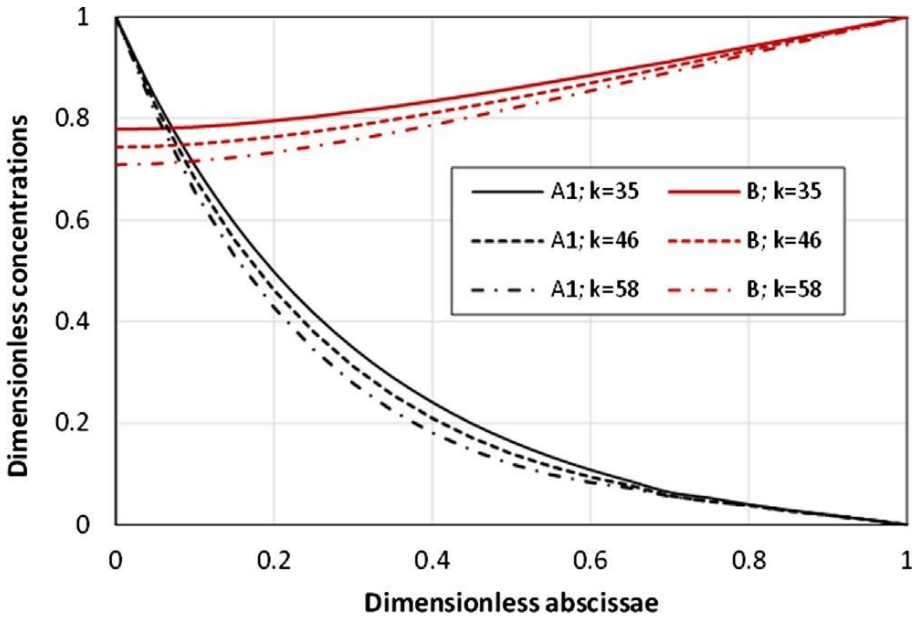

Figure III.8. Dimensionless concentration profiles in the diffusion film for the three estimates of the enhancement factor (± 10%). 125 µM Rh complex and 2 mM NAD^+; E = 3.83. k valuesare in $m^3.mol^{-1}.s^{-1}$.

III.4.5 Determination of rate constant k

The experimental values for the enhancement factor E estimated from CV curves for the various concentrations of NAD^+ and Rh complex, have been treated following the above procedure. Only experiments leading Ha number larger than 3 were shown here. Because of the uncertainties commented above, constant k was evaluated within its confidence interval:

$$k = 47 \pm 20\ m^3.mol^{-1}.s^{-1} \qquad (pH = 7.2) \qquad (17)$$

Comparison between theory and practice has been made on the basis of the enhancement factor. For each experiment treated, the predicted enhancement factor could be estimated from the profile of R1 in the film. As shown in **Figure III.9**, the predicted E values are in accordance with their experimental values within 20%.

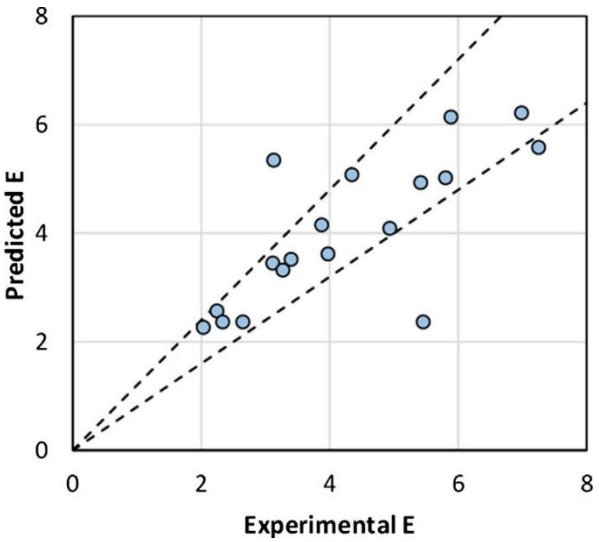

Figure III.9. Enhancement factor calculated for k=50 $m^3.mol^{-1}.s^{-1}$ versus their experimentalvalues; dotted lines correspond to the diagonal ± 20%.

The expression of the Hatta number (rel. 10) clearly shows that the chemical rate constant k is subject to the value for mass transfer coefficient k_L. Because k_L was estimated on the basis the geometrical area of the cathode, i.e. S=16 cm^2 as explained in the Appendix, the estimate for k is also subject to the area assumption. More precisely, k value given in rel. (17) does not have to be considered per se, but in comparison with k_L. On the contrary, dimensionless criterion Ha related to the kinetics of the chemical process, is determinant to examine whether this process can be considered as fast, i.e., occurring exclusively in the diffusion film or not: the various experiments carried out, clearly showed that the reaction could be constant as fast.

III.4.6 Simulating NAD^+ mediated conversion in the cell with H_2 anode

For these tests conducted at a fixed cathode potential corresponding to diffusion control, the solution with a volume V=40 cm^3 was circulated continuously in the cell. Former works dealing with G/L absorption[30] often mention criterion R, which is the ratio of the maximum flow rate of A_1 consumption in the whole solution volume over the maximum mole flow rate of A_1 generated at the interface. R can be then expressed as:

$$R = \frac{kC_{NAD,b}C_{RR3,b}V}{k_L C_{R3,b}S} = \frac{kC_{NAD,b}V}{k_L S} \qquad (18)$$

where S is the geometrical area of the cathode (16 cm^2). Considering k = 47 m^3 mol^{-1} s^{-1} and $C_{NAD,b}$= 2 mM, leads to R near 2.6 10^4, a value expressing that the overall mediated regeneration of NADH is controlled by the rate of Rh(III) reduction. Therefore, modelling of NADH regeneration can be viewed as carried out in a batch (discontinuous) electrochemical reactor with a rate calculated regardless of the occurrence of the chemical reaction, i.e. as if NAD^+ reacts directly at the cathode surface. It can be observed that the nature of the rate-controlling process was the same for the median k values and for its lower and upper estimates.

The mass balance in the simplified discontinuous process carried out at the limiting current is:

$$V\frac{dC_{NAD,b}}{dt} = -\frac{I_L}{nF} = -Sk_{L,B}C_{NAD,b} \quad (19)$$

Coefficient $k_{L,B}$ in the above relation is the mass transfer coefficient for species B: because δ_L is assumed independent of the species nature in the film model, $k_{L,B}$ derives from k_L (related to A_1) after:

$$k_{L,B} = k_L\frac{D_B}{D_A} \quad (20)$$

Integration of rel. (19) yields the usual exponential expression of the concentration expected from the above first order kinetics, from which conversion X_{NAD+} of NAD^+ can be deduced:

$$X_{NAD+} = \frac{(C_{NAD,0}-C_{NAD})}{C_{NAD,0}} = 1 - exp\left(-\frac{Sk_{L,B}}{V}t\right) = 1 - exp(-Kt) \quad (21)$$

It can be observed that according to this simple model, the electromediated conversion of NAD^+ depends neither on Rh complex concentration, nor on NAD^+ initial concentration, thus it might be supposed that the model holds for any value of the concentration ratio $C_{NAD,0}/C_{R3,0}$. Practically, it is often considered to use concentration of Rh complex at least at a few 10^{-5} M for possible observation of a diffusion plateau in voltammetric curves, and NAD^+ concentration not larger than 10 mM.

Data reported in El Housseini et al.[15] obtained with various concentrations of Rh complex and NAD^+ with the same initial C_{NAD}/C_{R3} concentration ratio at 40 and at E = -0.5 V vs. ref.(H_2), could be fairly well modelled by rel. (21) using the above value for mass transfer coefficient k_L, without further adjustment (**Figure III.10**).

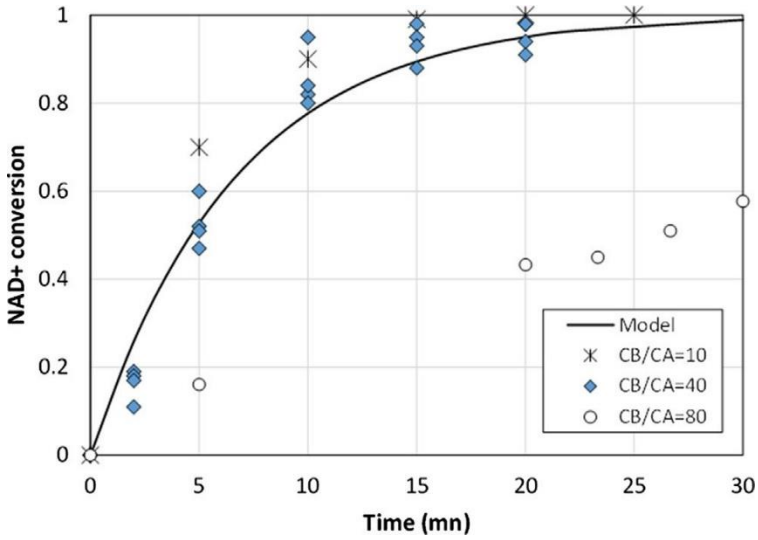

Figure III.10. NAD^+ conversion versus time for various NAD^+-over Rh complex concentration ratio. Rh complex concentrations varied from 12.5 – 62.5 µM. Experimental data (some of them from El Housseini et al.)[15] compared to the model predictions (rel. 21).

Moreover, it can be observed that the various data in the Figure III. correspond to a turnover frequency of Rh complex near 370 h^{-1} for NADH regeneration. Because of the sufficiently fast chemical reaction between Rh(I) and NAD^+, regeneration of NADH can be modelled as though this species is directly reduced at the electrode surface. Additional data with C_{NAD}/C_{R3} ratio at 10 only, follow the above trend, confirming the reaction mechanism. However, for ratio C_{NAD}/C_{R3} at 80, NADH regeneration appears sluggisher (Figure III.10) with a quite slower reaction from 20 minutes; for this ratio value, the conversion could not exceed 62% even after 120 min (data not shown). Obviously, the above simple model does not hold for such case, presumably because the mechanism of mediated electrosynthesis deviates from the simple mechanism considered here for too different concentrations of Rh complex and NAD^+, with

possible effect of the surface reduction of NAD^+ by adsorbed Rh(I), a phenomenon not accounted for in the present model.

III.5 Conclusion

The present work was aimed at modelling the effectiveness of mediated electrochemical reactions conducted at fixed potential in terms of current density and conversion rates, using the approach developed in gas-liquid absorption accompanied by chemical reaction of the dissolved gas. The method relying here upon diffusion-controlled electrochemical process and applied to NADH regeneration mediated by a Rh complex, led to estimates of the rate constant of the chemical reactions between Rh(I) and NAD^+, in comparison to the mass transfer coefficient to the electrode surface. Moreover, because the chemical process was shown to be fast enough, i.e., occurring nearly only in the diffusion film, the electrochemical conversion of NAD^+ to NADH at a fixed potential can be modelled as if NAD^+ was directly reduced at the cathode surface. The method could be successfully applied to other electrochemical processes involving indirect reduction or oxidation, a situation often encountered in electro-organic synthesis or bioelectrochemistry.

The validity of the simple approach is nevertheless dependent on the validity of the assumptions made and related to, first diffusion-controlled electrochemical process, then fast chemical reaction between substrate B and generated A_1 species. In case that the reaction is not fast enough ($Ha < 3$), the model for the batch electrochemical process has to be modified by inserting the chemical term in the related mass balance. Moreover, care has to be taken to check the kinetic mechanism of the chemical process in the operating conditions investigated.

Appendices

1- Experimental estimation of mass transfer coefficient

This coefficient has been estimated from the limiting current for Rh(III) reduction, I_L, was deduced after subtraction of the residual current recorded at the same potential without Rh complex. Mass transfer coefficient was estimated considering the porous graphite felt as a flat, the very large pores of the materials allowing internal diffusion to be not controlling:

$$k_L = \frac{I_L}{nFSC_{R3}} \qquad \text{(A1)}$$

with S= 16 cm^2. For replicate tests for Rh complex concentration in the range 50 – 250 µM, k_L was estimated at 4.6 10^{-5} ± 10% $m.s^{-1}$.

2- Estimation of diffusion coefficients

Most relationships for estimation of the diffusivity of a soluble species in the solvent rely upon the molar volume of this species, V_m, in addition to the temperature and the molecular weight of the solvent. Molecular volumes of the two solutes have been estimated using Le Bas' incremental method [31] at 337.8 cm^3 mol^{-1} for the Rh complex, and 588.8 $cm^3.mol^{-1}$ for NAD^+. For estimation of diffusivities in the aqueous solutions, the reference case of dissolved oxygen was used. Use of Wilke and Chang's relation led to estimates for diffusivities of oxygen and NAD^+ at least two times larger than the expected values, respectively at 1.96 10^{-9} and 2.40 10^{-10} $m^2.s^{-1}$ at 293 K.[32] It was then preferred to consider the diffusivity in a solid as in the form:

$$D \sim V_m^m \qquad \text{(A2)}$$

For the molecular volume of oxygen, 25.6 cm^3. mol^{-1}, the two diffusivity values led to m near -0.67, slightly different from Wilke and Chang's value at -0.6. Finally, the diffusivity of the Rh complex was estimated from either oxygen or NDA^+, the two methods yielding the same value at 3.48 10^{-10} $m^2.s^{-1}$.

References

[1] C. Kohlmann, W. Märkle, S. Lütz, *J. Mol. Catal. B Enzym.* **2008**, *51*, 57–72.

[2] E. Steckhan, in *Electrochem. V*, Springer, **1994**, pp. 83–111.

[3] A. Weckbecker, H. Grçger, **2010**.

[4] L. Zhang, N. Vilà, G. W. Kohring, A. Walcarius, M. Etienne, *ACS Catal.* **2017**, *7*, 4386–4394.

[5] H. K. Chenault, G. M. Whitesides, *Appl. Biochem. Biotechnol.* **1987**, *14*, 147–197.

[6] K. Cheikhou, T. Tzedakis, *AIChE J.* **2008**, *54*, 1365–1376.

[7] S. Immanuel, R. Sivasubramanian, R. Gul, M. A. Dar, *Chem. Asian J.* **2020**, *15*, 4256–4270.

[8] T. Saba, J. Li, J. W. H. Burnett, R. F. Howe, P. N. Kechagiopoulos, X. Wang, *ACS Catal.* **2020**, *11*, 283–289.

[9] H. Jaegfeldt, *J. Electroanal. Chem. Interfacial Electrochem.* **1981**, *128*, 355–370.

[10] M. Yuan, M. J. Kummer, R. D. Milton, T. Quah, S. D. Minteer, *ACS Catal.* **2019**, 5486–5495.

[11] R. Ruppert, S. Herrmann, E. Steckhan, *Tetrahedron Lett.* **1987**, *28*, 6583–6586.

[12] H. C. Lo, O. Buriez, J. B. Kerr, R. H. Fish, *Angew. Chemie Int. Ed.* **1999**, *38*, 1429–1432.

[13] E. Höfer, E. Steckhan, B. Ramos, W. R. Heineman, *J. Electroanal. Chem.* **1996**, *402*, 115–122.

[14] K. Vuorilehto, S. Lütz, C. Wandrey, *Bioelectrochemistry* **2004**, *65*, 1–7.

[15] W. El Housseini, F. Lapicque, A. Walcarius, M. Etienne, *Electrochem. Sci. Adv.* **2021**, 1–11.

[16] B. Tan, D. P. Hickey, R. D. Milton, F. Giroud, S. D. Minteer, *J. Electrochem. Soc.* **2015**, *162*, H102.

[17] L. Zhang, M. Etienne, N. Vilà, A. Walcarius, in *Funct. Electrodes Enzym. Microb. Electrochem. Syst.* (Eds.: N. Brun, V. Flexer), World Scientific, **2017**, pp. 215–271.

[18] R. Ruppert, S. Herrmann, E. Steckhan, *Tetrahedron Lett.* **1987**, *28*, 6583–6586.

[19] V. Ganesan, D. Sivanesan, S. Yoon, *Inorg. Chem.* **2017**, *56*, 1366–1374.

[20] E. Steckhan, S. Herrmann, R. Ruppert, E. Dietz, M. Frede, E. Spika, *Organometallics* **1991**, *10*, 1568–1577.

[21] F. Hollmann, B. Witholt, A. Schmid, *J. Mol. Catal. B Enzym.* **2002**, *19*, 167–176.

[22] K. Kano, T. Ikeda, *Anal. Sci.* **2000**, *16*, 1013–1021.

[23] T. Ikeda, C. R. Leidner, R. W. Murray, *J. Electroanal. Chem. Interfacial Electrochem.* **1982**, *138*, 343–365.

[24] M. E. G. Lyons, *Electroanalysis* **2015**, *27*, 992–1009.

[25] R. Wienkamp, E. Steckhan, *Angew. Chemie Int. Ed. English* **1982**, *21*, 782–783.

[26] T. Shono, *Tetrahedron* **1984**, *40*, 811–850.

[27] P. Labrune, A. Bergel, *Chem. Eng. Sci.* **1992**, *47*, 1219–1227.

[28] P. V. Danckwerts, **1970**.

[29] L. Zhang, M. Etienne, N. Vilà, T. X. H. Le, G.-W. Kohring, A. Walcarius, *ChemCatChem* **2018**, *10*, 4067–4073.

[30] W. P. M. van Swaaij, G. F. Versteeg, *Chem. Eng. Sci.* **1992**, *47*, 3181–3195.

[31] R. C. Reid, J. M. Prausnitz, B. E. Poling, **1987**.

[32] M. Aizawa, R. W. Coughlin, M. Charles, *Biochim. Biophys. Acta (BBA)-General Subj.*

1975, *385*, 362–370.

Objective of the study in Chapter IV

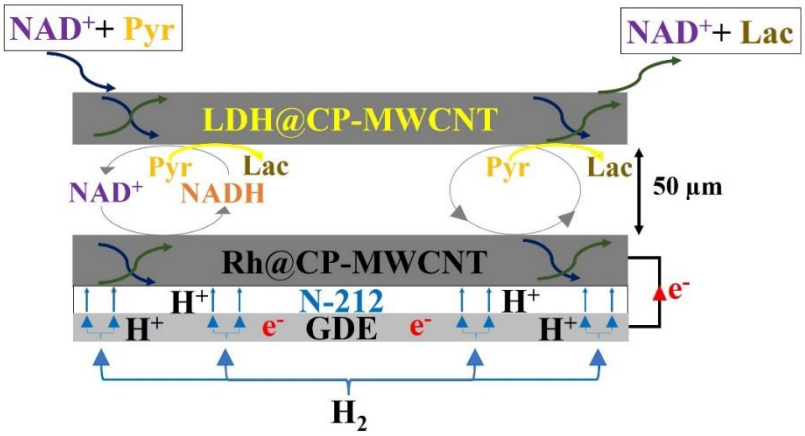

Schematic representation of the flow bioreactor with all catalysts immobilized

Following optimizations in Chapter II and in the context of immobilized rhodium complex for NADH electrochemical regeneration, the present work investigates two crucial aspects. Initially, the method for immobilization of the rhodium complex $[Cp^*Rh(bpy)Cl]^+$ was optimized utilizing carbon-based supports to obtain Rh-grafted matrices with high stability and activity in the redox flow reactor. Because of their low cost, large potential window, relatively inert surface, and active electrochemical properties for redox reactions, carbon materials have been chosen. The lactate dehydrogenase was subsequently immobilized to facilitate the rapid transfer of NAD^+/NADH from the molecular catalyst to the enzymatic catalyst. The optimal cell requires as little as 10 µM NAD^+ to convert pyruvate into lactate.

Article accepted in ChemElectroChem

El Housseini, W., Lapicque, F., Pontvianne, S., Vilà, N., Mazurenko, I., Walcarius, A., & Etienne, M. (2022). Hybrid flow bioreactor with all catalysts immobilized for enzymatic electrosynthesis. *ChemElectroChem*, *9*(16), e202200463.

Chapter IV. Hybrid flow bioreactor with all catalysts immobilized for enzymatic electrosynthesis

Abstract

The electrochemical regeneration of the NADH cofactor was realized in a hybrid flow reactor coupling fuel cell technology and redox flow device, paying attention to the robust immobilization of all catalysts. The rhodium catalyst $Rh(Cp*)(bpy)Cl^{+}$ was covalently immobilized on a MWCNT layer and the association with the gas diffusion electrode was carefully optimized. High stability and activity of the electrochemical system were assessed by cyclic voltammetry and amperometry in the flow reactor. Afterwards, the optimal cofactor regeneration was applied to NADH-dependent biosynthesis using immobilized lactate dehydrogenase for the conversion of pyruvate to lactate in the flow cell in the presence of cofactor concentration as low as 10 µM. 79 % faradaic efficiency was achieved and remarkable total turnover number (TTN) were reached: 2500, 18000, and 180000, for the NADH cofactor, the Rh complex and the LDH enzyme, respectively.

IV.1 Introduction

The catalytic hydrogenation using heterogeneous or homogeneous transition metal catalysts is well set up in industrial fine chemicals synthesis[1] where 10 % to 20 % of chemical steps involves catalytic hydrogenations.[2] Noble metals are highly exploited as catalysts in this area[3,4]. In these processes, high pressures of hydrogen are generally required for the efficient catalytic hydrogenation (>80 bars)[4]. Alternatively, the synthesis of fine chemicals, *e.g.* the reduction of the "C double bond X" in the ketones, alkenes, and imines, requires the use of biological catalysts, *e.g.*, oxidoreductases (known for their high productivity, enantio- and chemo-selectivity).[5] This particularity is valuable in the chemical and pharmaceutical sectors where 90 % of the chiral molecules were sold as racemic mixture before 1993[6] and 75 % of new drugs in 2002 were single enantiomers.[7]

However, oxidoreductases applied in bioconversions cannot use molecular hydrogen directly. Hydrogen can be transferred through enzymatic cofactors such as NADH (*Nicotinamide adenine dinucleotide hydride*) which plays an important role in biological systems and can be applied as electron carrier in enzymatic systems catalyzing stereo- and regio- selective reactions having a great biotechnological potential.[5,8] The use of enzymatic cofactors in biosynthesis applications (bioconversion) requires their regeneration due to their high costs.[9] The NADH cofactor can be indirectly regenerated *in situ* by electrochemistry (using suitable redox mediators), which offers an easy separation of products and a high control of the process.[9,10] Other NAD(P)H regeneration techniques can be applied such as the chemical, photochemical, enzymatic, and biological ones.[11–13] The application of the electrochemical regeneration of the NAD(P)H cofactor requires the use of an electrochemical mediator in order to lower the cathodic overpotentials associated to the reduction of $NAD(P)^+$, thus preventing the formation of the inactive dimer form $(NAD(P))_2$ occurring at more cathodic potential values.[14] One efficient mediator for the electrochemical regeneration of 1,4-NAD(P)H, the active form of

NAD(P)H, is chloro(2,2′-bipyridyl) (pentamethylcyclopentadienyl)-rhodium (III) chloride complex $[Cp*Rh(bpy)Cl]^+$.[15–17] Catalysts applied in the electrochemical or the electroenzymatic regeneration of the NAD(P)H cofactor, either molecular or enzymatic, *e.g.*, the aforementioned rhodium complex or Ferredoxine NADP(+) reductase (FNR), can be immobilized on electrode surfaces,[18][19] which is important for the easy recovery of the products formed (*i.e.*, no need for separation) and the possible re-use of the electrocatalyst.

There is expanding interest in implementing hydrogenation in continuous flow reactors, where reactants are continuously fed to the reactor and emerge as a continuous stream of products.[20,21] Advantages of continuous flow reactors include increased yields of bioconversion due to a high mass transport between reactants and increased selectivity through refined cell design and technology.[22,23] The electrochemical regeneration of the NADH cofactor has been previously reported for biocatalytic hydrogenations and dehydrogenations.[9][24] However, the translation into flow electrochemical reactor has suffered from different constrains such as the reactor design[25] and low conversion efficiencies related to slow kinetics of regeneration of NADH at conventional electrodes[26].

While NAD(P)H dependent enzymes are most frequently used in batch reactors, the development of flow reactors for the biosynthesis of chemicals catalyzed by NADH-dependent enzymes is of increasing interest. Indeed, it can bring significant benefits, such as improved mass and heat transfers, lower costs, and higher yields. The enzymatic regeneration of NADH cofactor was studied in a flow reactor coupling the bioconversion of formate to CO_2 catalyzed by formate dehydrogenase and the biosynthesis of lactate catalyzed by lactate dehydrogenase. The flux density of the produced NADH ranged from 0.14 $mmol.h^{-1}.m^{-2}$ at the beginning to 0.05 $mmol.h^{-1}m^{-2}$ three weeks later.[27] The averaged TTN of the NAD^+ cofactor was found approximately equal to 15 after 24 hours with an initial concentration of NAD^+ of 0.5 mM. [27] On the other hand, the regeneration of enzymatic cofactors in electrochemical flow reactors

gained more interest for the last decade. Yoon et al. designed an electrochemical laminar flow microreactor to regenerate NADH for the biosynthesis of L-lactate. Gold electrodes were deposited on the inside of a Y-shaped reactor, with two separate streams, one with buffer and the other with reagents (FAD (*Flavin adenine dinucleotide*), NAD^+, enzymes, and substrate), and the flow directed to the cathode. The reduced cofactor, $FADH_2$, was produced at the cathode and used in the reduction of NAD^+ to NADH, yielding 41% L-lactate (17.1 $mmol.h^{-1}.m^{-2}$).[26] The turnover frequency was equal to 75.6 h^{-1} which is 28 times higher than the value reported in a batch system.[28] Besides, Vincent and co-workers have succeeded in coupling the oxidation of hydrogen to the regeneration of NADH catalyzed by hydrogenase and NAD^+ reductase respectively in a microflow reactor with a volume of 0.2 mL. Direct use of regenerated NADH to the bioconversion of pyruvate catalyzed by lactate dehydrogenase showed an overall lactate production of 500 $g_{lactate}.g_{catalyst}^{-1}$ and a turnover frequency of 1060 min^{-1} for the NAD^+ cofactor .[29] Because of the usage of a high amount of NAD^+(1.7 mM),TTN for the NAD^+ cofactor and the catalyst for NAD+ regeneration were 35 and 766100 respectively.[29] Finally, photochemical regeneration of NADH using batch reactors was achieved, but with relatively low TTNs[30] which explains that the photochemical regeneration of NADH in a flow reactor is not yet explored. Batch regeneration of NADH using a Rh complex as mediator exhibited a turnover frequency of 0.46 h^{-1}.[31]

Previously, we have described a new modular route to combine efficiently the oxidation of hydrogen to the regeneration of NADH using a mediator in solution.[32] The idea was to couple the two redox reactions in a hybrid reactor that combines a gas diffusion electrode and a redox flow device with the help of an ion-exchange membrane for protons conduction from the anodic to the cathodic compartment. More precisely, the reactor allows the electrochemical regeneration of the NADH cofactor mediated by a rhodium complex in solution at the cathode with continuous flow reaction, and hydrogen oxidation at the gas diffusion anode. Several

parameters were optimized such as hydrogen and solution flow rates (20 mL.min^{-1}), pH (7.2), and the molar ratio between NAD^+ and the rhodium complex.[32] The efficiency of the approach was demonstrated first in H_2-driven NADH production, then to supply an NADH-dependent lactate dehydrogenase immobilized by adsorption on multi-walled carbon nanotubes for reduction of pyruvate to lactate. The lactate dehydrogenase is unable to use electrons directly and, therefore, only operated if supplied with reducing equivalents in the form of NADH regenerated by the rhodium complex mediator added in solution. The next challenge is thus the immobilization of all catalysts, compatible with the use of a sustainable flow bioreactor using low amount of enzymatic cofactor.

In the context of immobilized complex for NADH electrochemical regeneration, two essential aspects have been investigated in the present work. First, the method for immobilization of the rhodium complex $[Cp * Rh(bpy)Cl]^+$ have been optimized using carbon-based supports to obtain Rh-grafted matrices exhibiting high stability and activity in the redox flow reactor. Carbon materials has been selected because of their low cost, large potential window, relatively inert surface, and active electrochemical properties for redox reactions,[33]. Then, the immobilization of the lactate dehydrogenase has been achieved in order to promote rapid transfer of NAD^+/NADH from the molecular catalyst to the enzymatic catalyst. NAD^+ amounts as low as 10 µM were shown sufficient for the bioconversion of 25 mM pyruvate to lactate in the optimal cell. The original design of the cathode chamber led to a total turnover of NADH larger than the best values ever reported in the literature for electrochemical regeneration.[34]

IV.2 Materials and methods

IV.2.1 Chemical and reagents

All chemicals and LDH from porcine heart (250 units/mg protein) used were from Sigma-Aldrich. Multi-walled carbon nanotubes (MWCNT, NC7000™ series) were from Nanocyl (Belgium) and carbon papers (SpectraCarb 2050L-0550 Carbon Paper) were acquired from Fuel Cell Store (USA). MWCNT were dispersed in a solution of ethanol (96 %). High purity water (18 MΩ cm) was used to prepare all solutions.

IV.2.2 Immobilization of $[\boldsymbol{Cp*Rh(bpy)Cl}]^{+}$ on a carbon support electrode

IV.2.2.1 Graphite felt electrode pretreatment

A piece of graphite felt (GFD4.6EA, SGL, Germany) being 4 cm x 4 cm x 0.4 cm in dimensions was used as cathode in the first part of the study. In order to reduce its hydrophobicity, the graphite felt electrode was washed and ultrasonicated with different proportions of ethanol and water at a temperature of 25 °C following the adopted protocol in our previous work.[32]

IV.2.2.2 Carbon paper with MWCNT (CP-MWCNT) preparation

A piece of SpectraCarb carbon paper (CP) (4 cm x 4 cm x 0.05 cm) covered with MWCNT was prepared following a reported work in the literature [46] where 10 mg of MWCNT were ultrasonicated in a solution of ethanol (50 mL) for 5 hours. This suspension was then vacuum filtered on the CP and the resulting material was dried overnight. The CP coated with MWCNT was then denoted CP-MWCNT and was used as cathode for the rhodium complex covalent immobilization and as a support material for the immobilization of L-lactate dehydrogenase.

IV.2.2.3 Carbon support electrode functionalization with $[Cp*Rh(bpy)Cl]^+$

The carbon support was functionalized following a protocol from the literature.[17] 1 mM 4-amino-2,2-bipyridine (synthetized following a reported procedure[17]) was mixed with 2 mM sodium nitrite in 0.5 M HCl under gentle stirring for 5 min in order to generate 2,2-bipyridyl diazonium cations. A negative potential was then applied by running 2 cyclic voltammograms between 0.4 V and -0.8 V (vs Ag/AgCl (3M)) at a scan rate of 20 mV/s. The electrode was then rinsed with ultra-pure water and left to dry.

The functionalized electrode with 2,2-bipyridine moieties was then placed into a solution of DCM containing 0.15 mM of $((RhCp^*Cl_2)_2$ for 4 h with a gentle stirring. The functionalized electrode with the rhodium complex was then rinsed with DCM for 5 min in order to remove the unreacted residues.

IV.2.3 Enzymatic carbon paper with MWCNT (CP-MWCNT-LDH) preparation

CP-MWCNT was prepared following the same protocol applied in the section before (*Carbon paper with MWCNT preparation*). LDH enzyme was adsorbed on the MWCNT surface by depositing 50 µL suspension of LDH and keeping for 2 hours at a temperature of 3°C.

IV.2.4 Electrochemical reactor

Scheme IV.1 shows the bioelectrochemical bioreactor used in this study. The bioreactor has been presented in a previous work.[32] A gas diffusion electrode (4 cm * 4 cm), used as anode, was placed on a grooved graphite bipolar plate allowing the introduction and the distribution of hydrogen in the anodic compartment at flow rate of 20 $mL.min^{-1}$. [32]

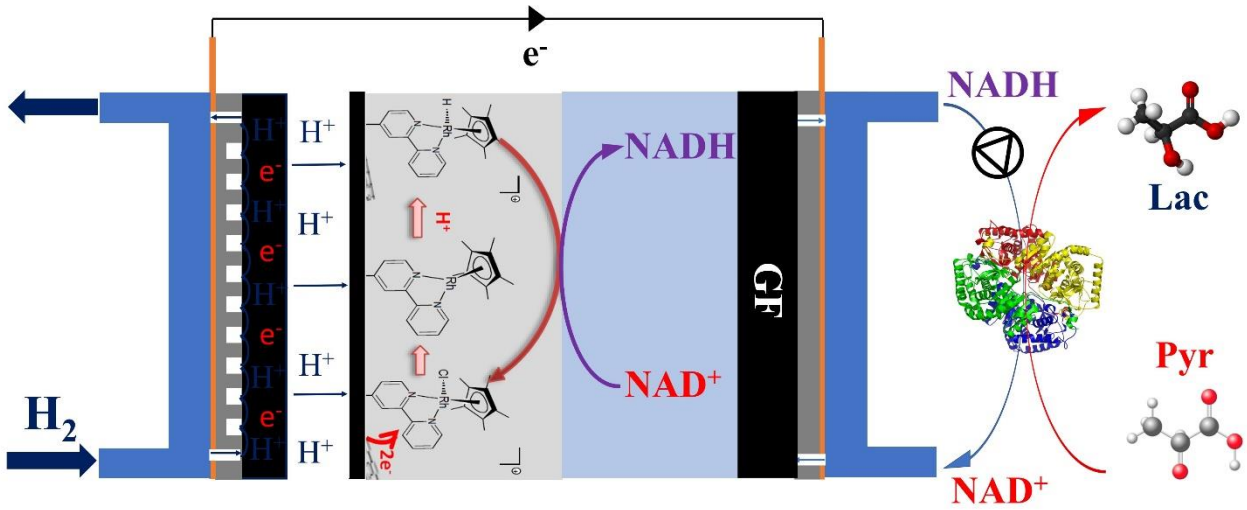

Scheme IV.1. Schematic view of the flow bioelectrochemical reactor. Solution flow is on the right side and hydrogen flow is on the left side. A proton-conducting Nafion membrane is separating the gas diffusion electrode, for hydrogen oxidation, from the graphite felt electrode, for NADH production by electrocatalytic reduction of NAD^+ with $[Cp^*Rh(bpy)Cl]^+$ complex covalently immobilized on a CP-MWCNT.

At the same time, the reaction solution containing 50 mM phosphate buffer (pH = 7.2), NAD^+, and pyruvate was flowed continuously to the cathodic compartment using peristaltic pump at flow rate of 20 $mL.min^{-1}$. [32] A CP-MWCNT on which is immobilized the rhodium complex was used as cathode. On the top of the CP-MWCNT-Rh was placed a graphite felt electrode known as a good electrical conductor and acting as a three-dimensional cathode, with homogeneous distribution of the solution. For pyruvate bioconversion tests, a CP-MWCNT-LDH was placed on the top of the CP-MWCNT-Rh electrode in addition to the graphite felt electrode.

Finally, a nafion membrane (N-212) was placed between the two compartments to separate between them and to transport protons from the anodic to the cathodic compartment.

Cyclic voltammograms and batch electrolysis were performed in a two-electrode configuration, the hydrogen anode acting also as reference electrode. Potential scan rate and electrolysis potential were fixed at 5 mV s^{-1} and -0.3 V vs ref (H_2).

Quantitative analysis of pyruvate bioconversion was performed by High Performance Liquid Chromatography (HPLC), using the Aminex HPX-87H HPLC column (300 mm x 7.8 mm, Phenomenex) thermostated at 45 °C, and a refractive index detector. The aqueous phase was flowed at 0.7 mL.min^{-1}. 200 µL aliquots were taken at different intervals from the reaction mixture. These aliquots were further analyzed by HPLC to determine the pyruvate and lactate concentrations.

IV.3 Results and Discussion

IV.3.1 Immobilization of $[Cp * Rh(bpy)Cl]^+$

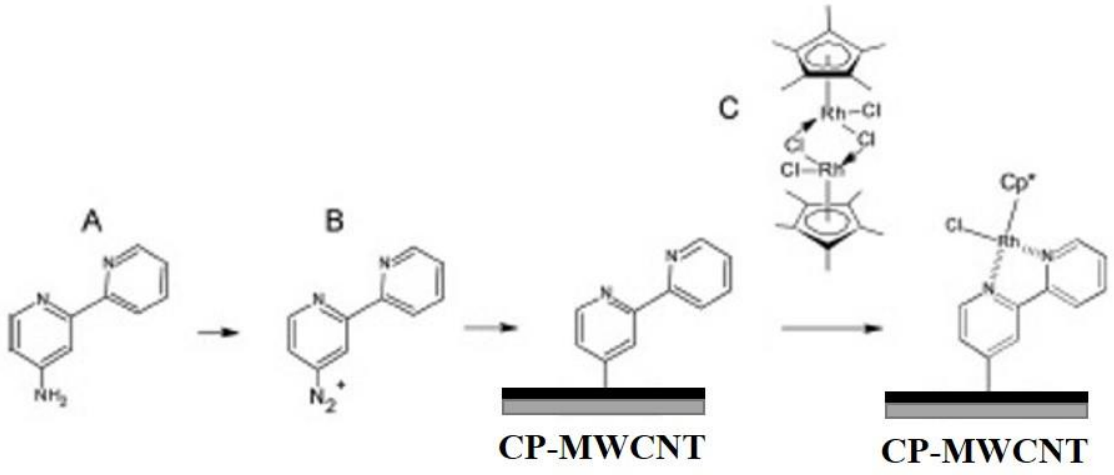

Figure IV.1. Synthetic route followed for the functionalization of the CP-MWCNT with [Cp*Rh(bpy)Cl]$^+$ by combination of diazonium salt electrografting and complexation process.[1]

The immobilization of the rhodium complex on a carbon support involves a two-step process as described in the literature.[17] First, 4-amino-2,2-bipyridine reacts quantitatively in solution to produce bipyridyl diazonium cations. Then, the functionalization of the carbon support with 2,2-bipyridine (bpy) moieties is carried out by cyclic voltammetry, involving the electroreduction of the diazonium cations with concomitant release of dinitrogen and generation of aryl radicals prone to be grafted on the carbon support. The rhodium complex is then formed

after a complexation reaction of $(RhCpCl_2)_2$ with the bipyridyl-functionalized electrode, giving rise to rhodium complexes covalently bonded to the carbon support. **(Figure IV.1)**

IV.3.2 Selection of the carbon electrode material

Multi-walled carbon nanotubes (MWCNTs) can allow significant improvement of the efficiency of the electroenzymatic synthesis system by tuning some electrochemical properties, *e.g.*, by enhancing the electroactive surface area.[35] On the basis of this opportunity, MWCNTs had been identified as suitable supporting materials for Rh complex immobilization.[29,31] Based on the perspective of combination between fuel cell technology and redox flow technique, a carbon paper (CP) coated with MWCNTs (noted CP-MWCNT) was chosen for the construction of the catalytic layer after comparing it with bucky paper and graphite felt electrodes.

Diazonium electrografting on a 16 cm² CP-MWCNT electrode was performed by cyclic voltammetry from 0.4 V to -0.8 V vs Ag/AgCl, as shown in **Figure IV.2A**. During the first scan, an irreversible wave was observed at -0.35 V vs Ag/AgCl (curve a) corresponding to the grafting of 2,2-bipyridine and the release of N_2. A cathodic reduction peak of lower intensity was observed in the second scan (curve b) due to the partial blockage of the CP-MWCNT electrode surface, indicating successful electrografting. The CP-MWCNT electrografted with 2,2-bipyridine moieties was then immersed in a solution of $(RhCpCl_2)_2$ for the formation of rhodium complexes covalently immobilized onto the electrode surface.

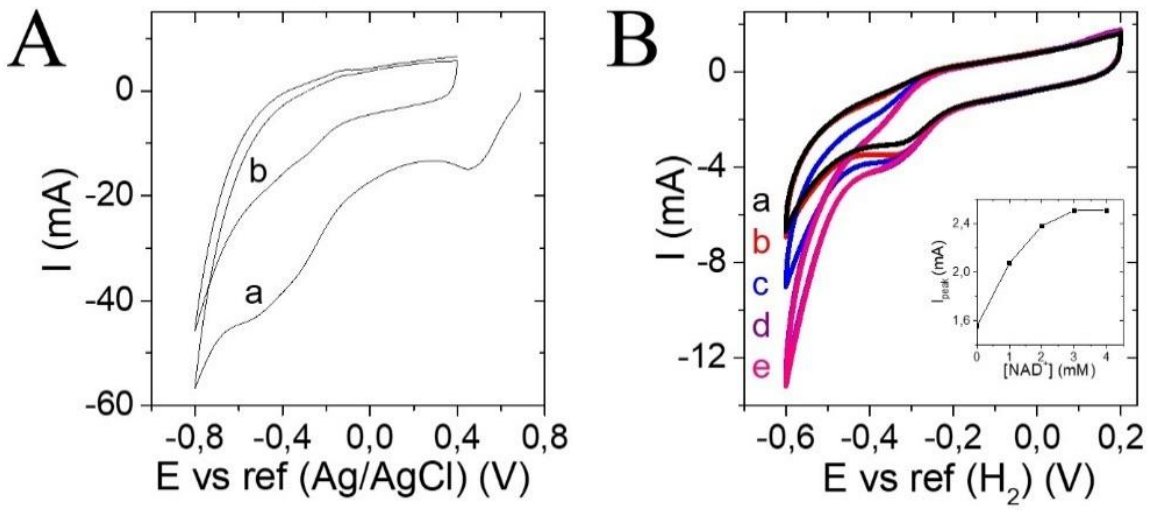

Figure IV.2. (A) (a) first and (b) second cyclic voltammograms for the reduction of diazonium cations generated 'in situ' from 1 mM 4-amino-2,2'-bipyridine and 2 mM $NaNO_2$ in 0.5 M HCl, as recorded on CP-MWCNT electrode at 20 $mV.s^{-1}$. (B) Cyclic voltammograms recorded at a potential scan rate of 5 $mV.s^{-1}$ using a CP-MWCNT-bpy-Rh electrode in 50 mM PBS buffer at pH 7.2 under nitrogen and in the presence of increasing concentrations of NAD^+ (a) 0 mM (b) 1 mM (c) 2 mM (d) 3 mM and (e) 4 mM. The geometric surface area of the electrode was 16 cm^2 and hydrogen and solution flow rates were at 20 $mL.min^{-1}$.

The electrocatalytic behavior of the so-formed CP-MWCNT-bpy-Rh electrode was evaluated through cyclic voltammetry (**Figure IV.2**), in a configuration where the working electrode has been arranged in the redox flow reactor, at a scan rate of 5 $mV.s^{-1}$ in 50 mM phosphate buffer solution (PBS) at pH 7.2, with hydrogen and solutions flow rates of 20 $mL.min^{-1}$. As shown in **scheme IV.1**, a graphite felt (16 cm^2) was placed on the top of the CP-MWCNT-bpy-Rh electrode in order to ensure a uniform distribution of the solution in the cathodic compartment and to maintain good electrical conduction with the graphite bipolar plate. A gas diffusion electrode, allowing hydrogen oxidation was used in the anodic compartment A Nafion membrane (N-212) was placed between the two electrodes for separation of the two compartments and to permit a uniform proton transport rate from the anode to the cathode. In the absence of NAD^+ in the medium, a cathodic current was observed at -0.31 V vs ref. (H_2)

(see curve **a** in **Figure IV.2B**), which was less negative than the potential reported in previous works for the same Rh complex immobilized on a bucky paper (BP) electrode (-0.65 V vs ref. (Ag/AgCl) ≈ -0.45 V vs ref. (H_2))[17] or in solution (-0.4 V vs ref. (H_2)) [32]. This potential shift can be explained by the influence of the electrode material on the electron density of the rhodium complex center [37] or due to the minimized distance between the anodic and the cathodic electrodes separated by the Nafion membrane. The addition of increased amounts of NAD^+, from 1 mM to 4 mM (see curves **b**, **c**, **d** and **e**, in **Figure IV.2B**), led to the increase in the cathodic current showing the mediated electrocatalytic activity of the Rh complex towards NAD^+ reduction. A maximum cathodic current of 2.6 mA was observed at the concentration of 3 mM NAD^+.

Alternatively, for comparison with a previous work where $[\boldsymbol{Cp*Rh(bpy)Cl}]^+$ was reacting on graphite felt,[32] the direct immobilization of the Rh complex on a graphite felt electrode (GF-bpy-Rh) was evaluated. The cathodic current peak observed at -0.35 V vs ref (H_2) decreased with increasing NAD^+ concentrations, expressing a lower electroactive surface of the GF than with MWCNT[38] and indicating the poor stability of the support-Rh complex system under high flow rate conditions (**Figure IV.3A&B**), confirming the advantage of CP-MWCNT-bpy-Rh electrode for the present study.

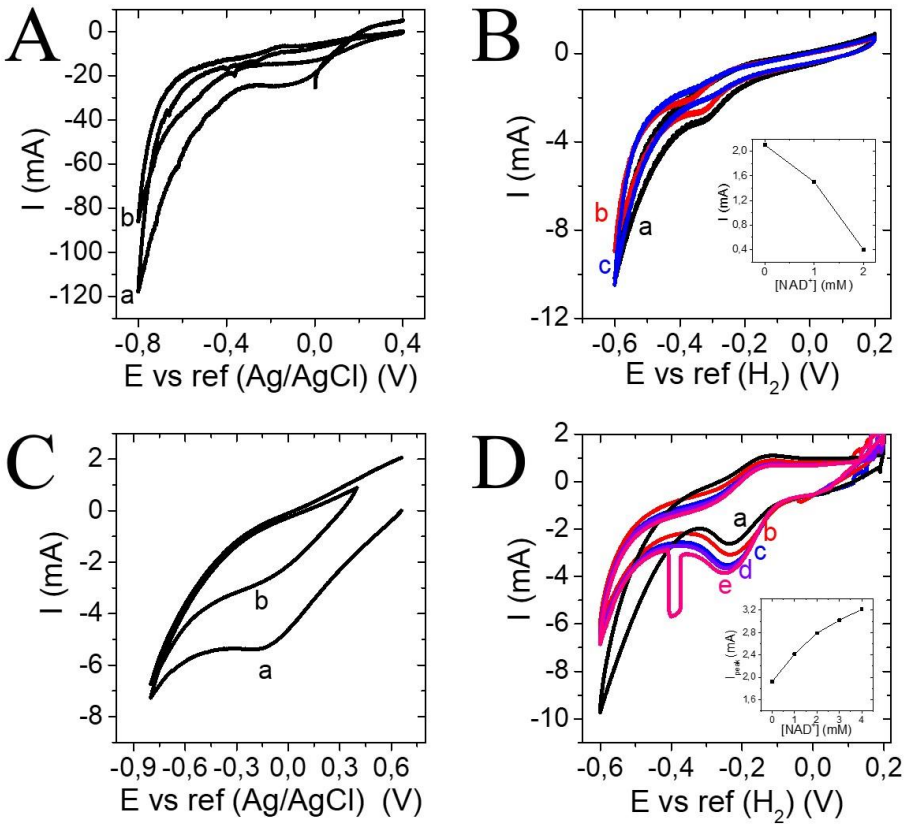

Figure IV.3. (A) and (C) (a) first and (b) second cyclic voltammogram for the reduction of diazonium cations generated 'in situ' from 1 mM 4-amino-2,2'-bipyridine and 2 mM NaNO2 in 0.5 M HCl, as recorded on GF (graphite felt) electrode (A) and (B) BP (bucky paper) electrode at 20 $mV.s^{-1}$. (B)Cyclic voltammograms recorded at a potential scan rate of 5 $mV.s^{-1}$ using a GF-bpy-Rh electrode and with increasing concentrations of NAD^+ (a) 0 mM, (b) 1 mM, and (c) 2 mM. (D) Cyclic voltammograms recorded at a potential scan rate of 5 mV.s-1 using a BP-bpy-Rh and with increasing concentrations of NAD^+ (a) 0 mM, (b) 1 mM, (c) 2 mM, (d) 3 mM and (e) 4 mM. Experiments (B) and (D) were carried out in a 50 mM phosphate buffer solution at pH 7.2 under nitrogen atmosphere and with a solution and hydrogen flow rates of 20 $mL.min^{-1}$ each.

In addition, the catalytic activity of CP-MWCNT-bpy-Rh towards NADH regeneration was also confirmed by amperometry at constant potential (-0.3 V vs ref (H_2)) and the corresponding current variation for the conversion of 1 mM NAD^+ in solution (V=20 mL) is shown in **Figure IV.4A** (curve **a**). Complete conversion of NAD^+ into NADH was observed within 50 min electrolysis (**Figure IV.4B**, curve **a**) with an averaged faradaic efficiency of 71 % (**Figure**

IV.4C, experiment **a)** using the CP-MWCNT-bpy-Rh cathode. The quantification of regenerated NADH was evaluated through UV-visible absorption at 340 nm.

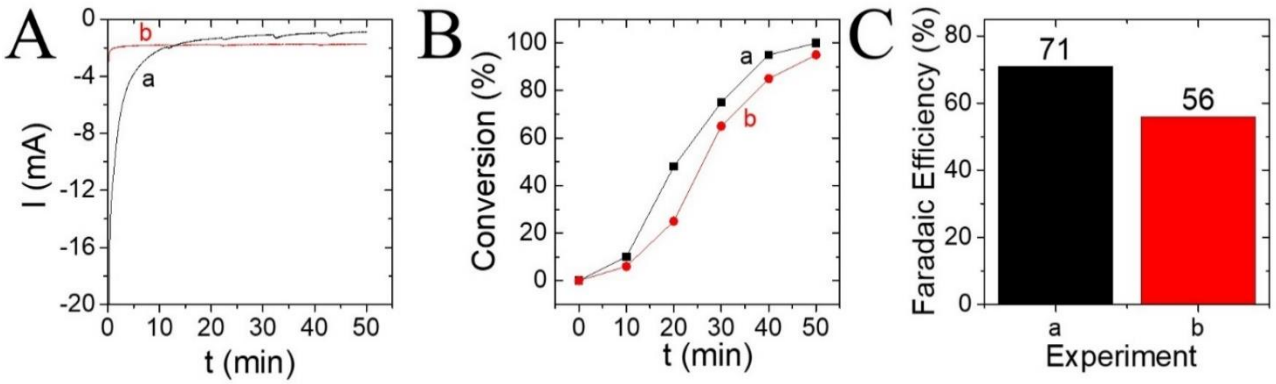

Figure IV.4. Influence of the applied electrode (a: CP-MWCNT-bpy-Rh; b: BP-bpy-Rh) on (A) the recorded current, (B) the conversion, and (C) the faradaic efficiency of the electrochemical regeneration of 1 mM NAD^+ to NADH. Experiments were carried out in 50 mM phosphate buffer solution at pH 7.2 in the presence of 1 mM NAD^+ (V=20 mL), under nitrogen atmosphere, at an operating potential of -0.3 V vs Ref. (H_2) for CP-MWCNT-bpy-Rh system (a) and at -0.26 V vs Ref (H_2) for BP-bpy-Rh system (b), and with a constant solution flow rate and a constant hydrogen flow rate of 20 $mL.min^{-1}$ each.

In addition, the regenerated NADH was totally oxidized after the addition of 250 units of LDH (*L-lactate dehydrogenase*) and 1 mM of pyruvate to NADH solution which indicates that the regeneration method used led to the active form of NADH (1,4-NADH). The amount of rhodium complex on the CP-MWCNT electrode, 4.125 $nmol.cm^{-2}$, was estimated from cyclic voltammetry by integrating the cathodic peak. From that amount, a turnover frequency of 1.7 s^{-1} was calculated during the first 5 min of NADH electrochemical regeneration. This value of turnover frequency is very close to the highest value reported in the literature (3.6 s^{-1}) for an immobilized Rh complex on MWCNTs.[36] Furthermore, total conversion of NAD^+ into NADH was obtained with a ratio of NAD^+ over rhodium complex concentrations in the order of 300, which is much larger than the maximal value achievable with dissolved Rh complex (ratio between NAD^+ and Rh complex not exceeding 40).[32] Such improvement in terms of

performance came in addition to the advantage of CP-MWCNT-bpy-Rh leading to effective NADH regeneration while avoiding the use of dissolved rhodium complex.

To complete this study, bucky paper functionalized by the rhodium complex was also evaluated for the conversion of 1 mM NAD^+ into NADH in the flow bioreactor. Its catalytic activity for NAD^+ reduction was confirmed by cyclic voltammetry (**Figure IV.3D**), and the conversion reached 92 % after 50 min (**Figure IV.4B**, curve **b**) with a faradaic efficiency at only 56 % (**Figure IV.4C**, experiment **b**). However, bucky paper electrode was prepared by filtration of the MWCNT suspension on a PVDF (*Polyvinylidene fluoride*) filter that is not electroactive but on which adsorption of the dissolved $(RhCpCl_2)_2$ was observed (as indicated by the orange color of rhodium dimer) that could not be removed by dissolution in the solvent (DCM) (*Dichloromethane*). On the contrary, the electroactive carbon paper used in the preferred configuration (i.e., CP-MWCNT) was involved in the electrografting reaction and allowed, as well as the MWCNT layer, the formation of the targeted rhodium complex.

Among the three functional electrodes that were tested, a carbon paper modified with a layer of MWCNT and functionalized with $[\boldsymbol{Cp} * \boldsymbol{Rh}(\boldsymbol{bpy})\boldsymbol{Cl}]^+$ (CP-MWCNT-bpy-Rh) was thus selected here as the best one for regeneration of the NADH cofactor.

Stability and sustained activity

In order to ensure the robustness of the CP-MWCNT-bpy-Rh electrode, a cell assembly was prepared by pressing the GDE (*Gas diffusion electrode*), the Nafion membrane (N212), and the CP-MWCNT-bpy-Rh together at 40 bars at room temperature, as illustrated in **Figure IV.5A**. The technique was expected to improve mechanical and electrical contacts in the whole flow cell (anode, membrane and cathodic chamber). CP-MWCNT-bpy-Rh system was characterized by cyclic voltammetry (**Figure IV.5B**) for different times under flow conditions after the electrode preparation: 4 h, 12 h, 24 h, and 120 h. The electrode was left inside the reactor and

was tested each time with a new solution of phosphate buffer (50 mM; pH = 7.2). The very similar cathodic currents observed revealed that the electrode has maintained its activity for more than five days, and more precisely that the rhodium complex remained immobilized under flow conditions ensuring a long-term operational stability of the electrode. After confirming the electrode activity towards NADH regeneration by mediated NAD^+ electroreduction, its application in electroenzymatic biosynthesis was further explored.

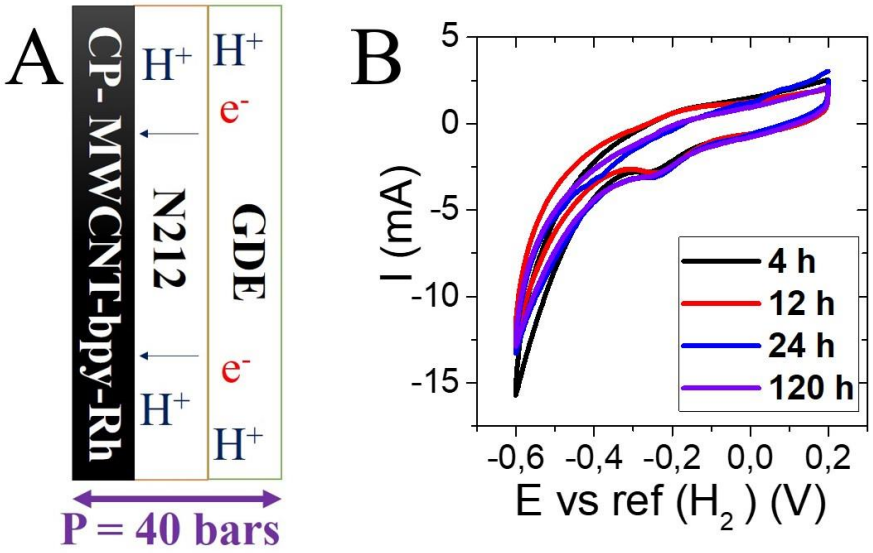

Figure IV.5. (A) Schematic representation of GDE-N212-(Cp-MWCNT-bpy-Rh) system pressed together at 40 bars. (B) Cyclic voltammograms recorded at a potential scan rate of 5 $mV.s^{-1}$ using a $[Cp^*Rh(bpy)Cl]^+$ functionalized CP-MWCNT (using the pressed system in **Figure IV.5A**) electrode in 50 mM PBS buffer at pH 7.2 under nitrogen after 4 h, 12h, 24 h, and 120 h of electrode preparation. The geometric surface area of the electrode was 16 cm^2 and hydrogen and solution flow rates were at 20 $mL.min^{-1}$.

IV.3.3 Application of regenerated NADH in an enzymatic reaction

IV.3.3.1 Parameters optimization for the efficient bioconversion of pyruvate

Coupling an enzymatic reaction to NADH regeneration should allow demonstrating that the active form of NADH (1,4-NADH)[39] was really produced by the redox flow reactor, and would be compatible with the production of fine chemicals with electrochemically regenerated NADH

as a reactant involved in the biocatalytic reduction of the organic substrate. NAD-dependent lactate dehydrogenase LDH was used here as a convenient example (robust enzyme, commercially available, with reliable analytical methods for lactate and pyruvate).

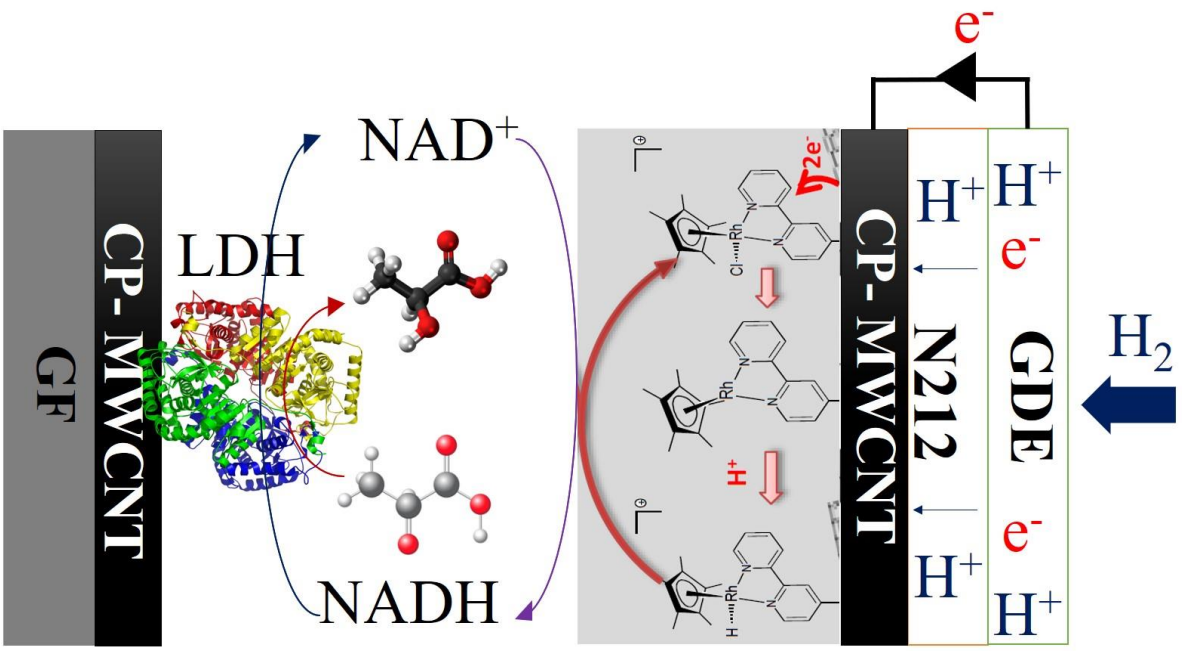

Scheme IV.2. Schematic representation of the electroenzymatic reactor including CP-MWCNT-bpy-Rh electrode and CP-MWCNT-LDH enzymatic system reactions with the LDH-MWCNT-CP system.

Scheme IV.2 illustrates the NADH regeneration on a CP-MWCNT-bpy-Rh electrode coupled to hydrogen oxidation and pyruvate bioconversion. LDHs were immobilized on a second CP-MWCNT layer placed inside the electrochemical cell and stacked to the CP-MWCNT-bpy-Rh as shown in **scheme IV.2**. This design has the great advantage to connect electrically the current collector and the active electrode pressed on the Nafion membrane. The NAD^+ and pyruvate-containing solution was circulated in the cathodic compartment, where NADH was regenerated by the Rh complex, then consumed continuously in the biosynthesis of lactate.

While the cofactor in its oxidized or reduced form is used as an active mediator leading to the bioconversion, we worked with low amounts of the cofactor (10 µM) which is economically

desired and proves the stability of the cofactor with time. In addition, low amounts of cofactor are targeted to reach high TTNs.[40]

IV.3.3.2 Effect of the arrangement of supported Rh complex and LDH in the cell

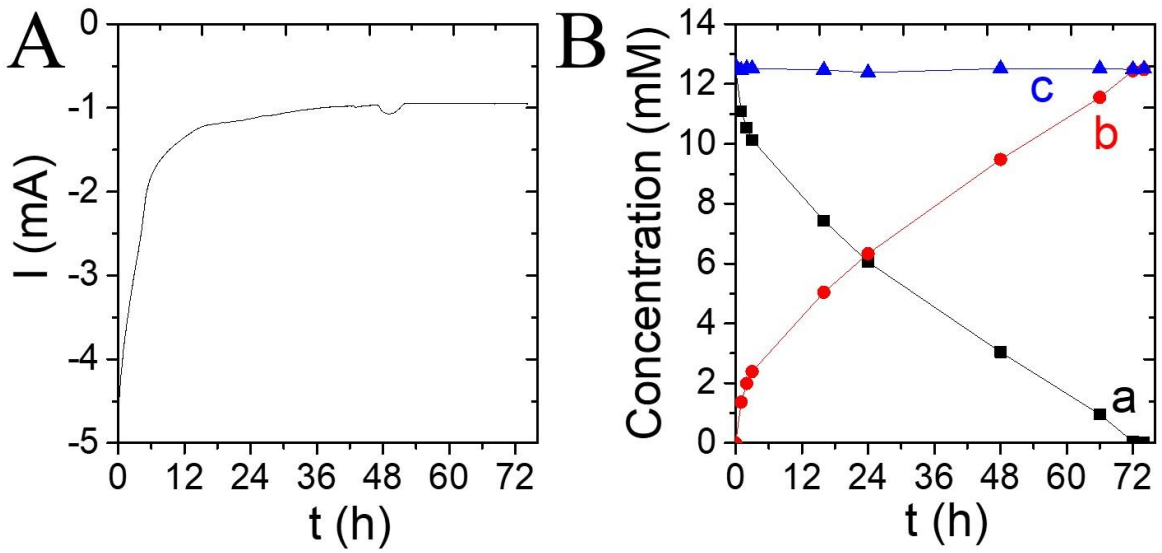

Figure IV.6. (A) Variation of sampled currents with time during the electroenzymatic synthesis of lactate from 12.5 mM of pyruvate in 100 mL solution containing 10 µM NAD^+ (and 50 mM PBS, pH 7.2) in the flow reactor provided with one CP-MWCNT-bpy-Rh electrode and one CP-MWCNT-LDH (250 units) layer. (B) Variation of concentrations with time of (a)Pyruvate, (b) Lactate, and (c) the sum pyruvate and lactate, as determined by HPLC.

The bioconversion of 12.5 mM pyruvate (in 100 mL solution containing 10 µM NAD^+) applying the process described in **Scheme IV.2** was carried out potentiostatically, at -0.3 V vs ref. (H_2) for 72 hours, with the two electrodes CP-MWCNT-bpy-Rh and CP-MWCNT-LDH onto which 250 units of LDH were immobilized (≈ 6.6 nmol). The current near -4 mA in the first instants, decreased gradually to reach -1 mA after 72 hours (**Figure IV.6A**) whereas 100 % of pyruvate introduced was converted to lactate within this period (**Figure IV.6B**). The sum of the two species concentrations was nearly constant at 12.5 mM **(Figure IV.6B)** indicating the high selectivity of the enzymatic reaction.

The faradaic efficiency was equal to 73 %, a value comparable to that of NADH regeneration without enzymatic reaction (**Figure IV.4C**). TTNs of Rh complex, NAD^+, and LDH were respectively larger than 1.8×10^4, 1250, and 1.8×10^5. TTN for the Rh complex is – to our state of knowledge – the highest value with rhodium complex applied in electroenzymatic synthesis.[17,41] The turnover frequency was 0.28 s^{-1} after 3 hours of the bioconversion. This value is higher than the value reported in our previous work,[17] thanks to the flowing system allowing of the performance cofactor regeneration coupled to the bioconversion of pyruvate.

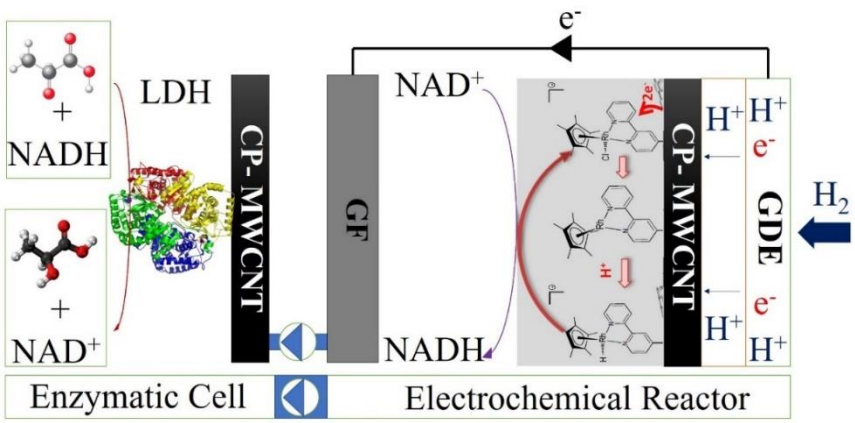

Scheme IV.3. Schematic representation of the electrochemical reactor for NADH electrochemical regeneration in series with the enzymatic cell for pyruvate bioconversion with the system with Cp-MWCNT-LDH.

On the other hand, setting the CP-MWCNT-LDH layer in another reactor downstream of the "electrochemical cell" provided with the CP-MWCNT-bpy-Rh layer for NADH regeneration (**Scheme IV.3**) led to a lower bioconversion of 12.9 % with only 49% faradaic efficiency (**Figure IV.7**), far below the performances obtained with the two modified CP layers (CP-MWCNT-Rh and CP-MWCNT-LDH) stacked in the same cell.

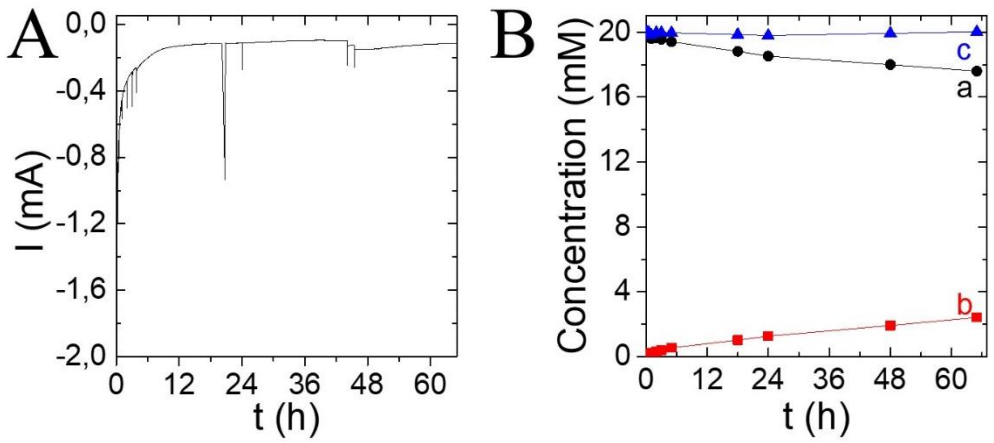

Figure IV.7. Electroenzymatic synthesis of lactate from 20 mM of pyruvate in 50 mL solution containing 20 µM NAD^+ (and 50 mM PBS, pH 7.2) with a combination of electrochemical cell containing a CP-MWCNT-bpy-Rh electrode and the enzymatic cell containing Cp-MWCNT-LDH system under nitrogen degassing, with hydrogen and solution flow rates of 20 $mL.min^{-1}$and at an electrolysis potential of -0.3 V vs ref (H_2). (A) Variations of the current in the run. (B) Variation of concentrations with time of (a) pyruvate, (b) lactate, and (c) the sum pyruvate and lactate, as determined by HPLC.

This reported experiment leads to the conclusion that the bioconversion of pyruvate is facilitated by close interaction between the Rh complex and LDH adsorbed onto different CP-MWCNT layers, separated but closely associated, under flow conditions for efficient mass transport rates, leading to increased overall conversion kinetics.

As a control experiment and following reported works in the literature where both catalysts for the regeneration of the cofactor and the production of fine chemicals were placed on the same electrode, [42]LDH enzymes were adsorbed directly on the Rh-immobilized CP-MWCNT layer forming the cathode. The efficiency of the single layer system, where both the Rh complex and LDH were immobilized on the same CP-MWCNT, was tested by studying the conversion of 20 mM pyruvate (50 mL at pH=7.2) with 500 units LDH adsorbed, in the presence of 0.5 mM NAD^+, at -0.3 V vs ref (H_2). The recorded currents decreased rapidly (in absolute value) from -1.5 mA to -0.25 mA after 5 hours (**Figure IV.8A**). Chemical analysis of the solution showed

that the bioconversion had not occurred (**Figure IV.8B**), whereas NAD^+ was entirely reduced to NADH as revealed by UV-visible measurement at 340 nm.

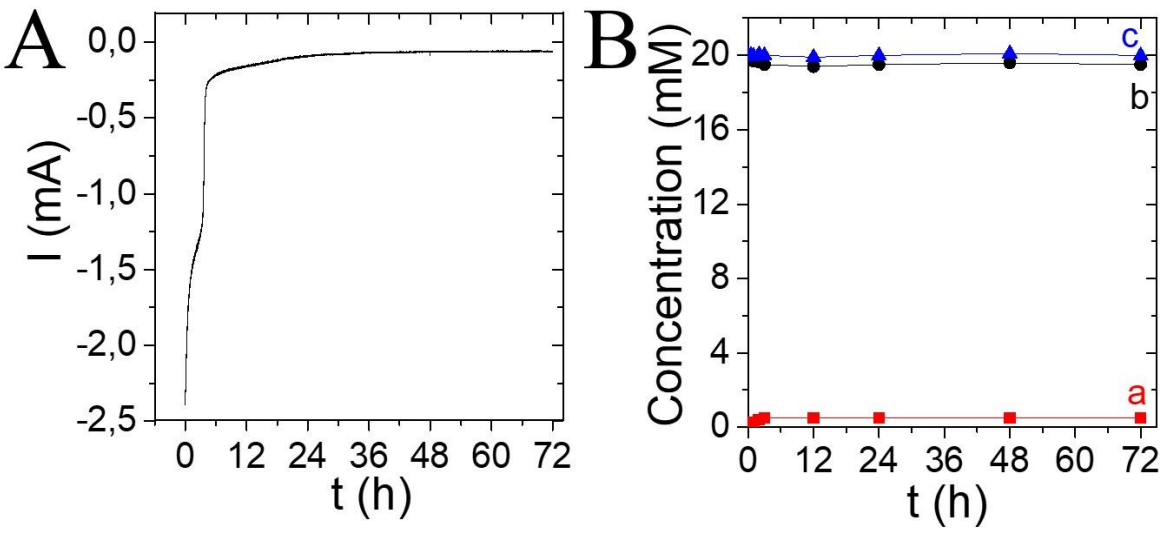

Figure IV.8. *(*A) Electroenzymatic synthesis of lactate from pyruvate in 50 mL solution containing 0.5 mM NAD^+ (50 mM PBS, pH 7.2) with a combination of systems CP-MWCNT-bpy-Rh-LDH on the same electrode (B) Variation of concentrations with time of (a)Pyruvate, (b) Lactate, and (c) the sum pyruvate and lactate, as determined by HPLC. Experiment was done under nitrogen and with hydrogen and solution flow rates of 20 $mL.min^{-1}$ and at an electrolysis potential of -0.3 V vs ref (H_2).

This result suggests that LDH was totally deactivated while being placed in a direct contact with rhodium complex, in agreement with former works reporting deactivation of the rhodium complex or lactate dehydrogenase.[16] In conclusion, the best strategy for optimal activity of these two catalysts, the molecular one and the biological one, is to associate them closely while keeping a small separation between them (few µm) that allows an efficient regeneration of the cofactor as well as an efficient bioconversion of pyruvate but prevent direct molecular interaction (and eventually deactivation), as it is illustrated here with the two catalytic layers.

IV.3.3.3 Towards higher production rate of lactate

Production rate of the designed system (scheme 1) is a quite important criterion to address. For this purpose, four experiments have been designed and carried out, in particular for optimization of the amount of Rh complex in relation to LDH immobilized on the separated CP-MWCNT material. Conditions and results of these tests are reported in Table 1.

Table IV.1. Ratio optimization between Rh complex and LDH for the optimal bioconversion of pyruvate (V = 100 mL). (*) Current efficiency is for lactate production.

Experiment	[Pyruvate] at t=0 (mM)	LDH (nmol)	Rh (nmol)	n_{Rh}/n_{LDH} ratio	[Lactate] after 72 h (mM)	(*) Current efficiency (%)
1	20	13.8	66	5	7.2	76.7
2	12.5	6.6	66	10	12.5	73
3	25	13.8	138	10	25	78
4	25	2.76	138	50	16.5	79

First, in order to evaluate the effect of LDH amount on the productivity, Experiment (1) and Experiment (2) were performed with the same amount of immobilized Rh complex and different amounts of LDH (**Table IV.1**).

The current obtained with the system in Experiment (2), where the ratio between the Rh complex and LDH is equal to 10, led to a total (100 %) bioconversion **(Figure IV.7)** approximately 1.5 times higher than the one obtained in Experiment (1) where the ratio between the Rh complex and LDH is equal to 5 for which the bioconversion was restricted to 59 % (**Figure IV.9**).

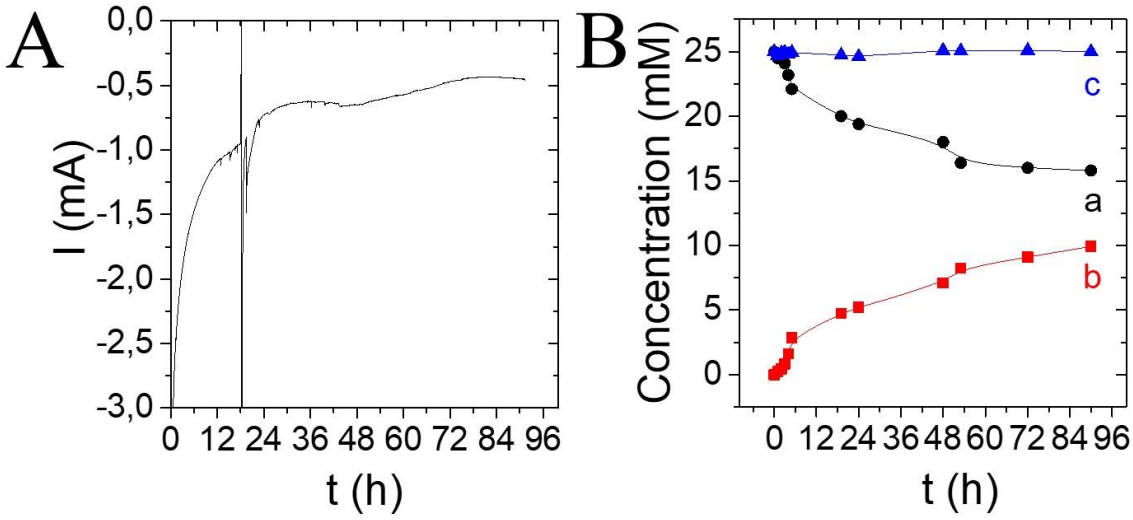

Figure IV.9. Electroenzymatic synthesis of lactate from 25 mM of pyruvate in 100 mL solution containing 10 µM NAD^+ (and 50 mM PBS, pH 7.2) in the flow cell containing one CP-MWCNT-bpy-Rh electrode and one enzymatic CP-MWCNT-LDH layer (500 units) (A) Variations of the current in the run. (B) Variation of concentrations with time of (a) pyruvate, (b) lactate, and (c) the sum pyruvate and lactate, as determined by HPLC.

Faradaic efficiencies for both systems were in the same order of magnitude. This result leads to the consequence that an equilibrium between the regeneration of NADH by the Rh complex and its oxidation by LDH is important in order to reach a total bioconversion within an optimal time.

Later, for the sake of higher lactate production within an optimal time and to obtain a system for the electrochemical regeneration of NADH comparable with the electroenzymatic one involving enzymatic mediators, e.g. FNR,[37,38,39] additional tests (not reported in Table 1) were carried out by inserting two CP-MWCNT-bpy-Rh layers in the electrochemical bioreactor instead of one. As a matter of fact, the immobilization of the Rh complex on the same CP-MWCNT with a larger amount of Rh complex allowed by a larger concentration of 2,2-bipyridine moieties led only to the blockage of the electrode.

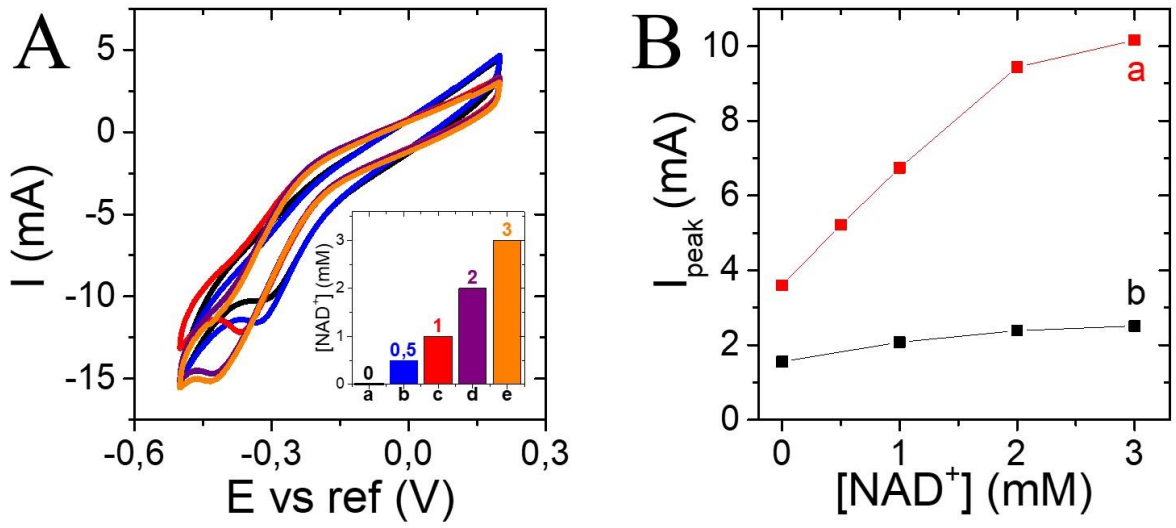

Figure IV.10. (A) Cyclic voltammograms recorded at a potential scan rate of 5 $mV.s^{-1}$ using 2 CP-MWCNT-bpy-Rh electrodes under nitrogen, in 50 mM PBS buffer at pH 7.2 and with increased concentrations of NAD^+ (a) 0 mM, (b) 0.5 mM, (c) 1 mM, (d) 2 mM, and (e) 3 mM. (B) Comparison between cathodic currents recorded at a potential scan rate of 5 $mV.s^{-1}$ with (a) 2 CP-MWCNT-bpy-Rh electrode and (b) 1 CP-MWCNT-bpy-Rh in 50 mM PBS buffer at pH 7.2 and with NAD^+ concentrations between 0 mM and 3 mM. The geometric surface area of each electrode is 16 cm^2 and hydrogen and solution flow rates are 20 $mL.min^{-1}$.

Further, the electrocatalytic activity of the two coupled CP-MWCNT-bpy-Rh electrodes was evaluated by cyclic voltammetry (**Figure IV.10A**). Without NAD^+ in the flow cell, the cathodic peak was located at -0.3 V vs ref. (H_2) and a cathodic current near 3.5 mA was measured, as compared to 1.6 mA with a single CP-MWCNT-bpy-Rh layer (**Figure IV.10B**), in agreement with the higher amount of rhodium complex immobilized in the former case. The calculated surface coverage with the rhodium complex estimated by charge balance and Faraday's law from voltammograms was found equal to 138 nmol.

The surface concentration near 4.3 $nmol.cm^{-2}$ was very close to that exhibited by a single CP-MWCNT-bpy-Rh layer. Then, when adding increasing amounts of NAD^+ in the flow cell, significant increases in the cathodic currents were observed, much larger than for the single CP-MWCNT-bpy-Rh layer (**Figure IV.10B**). In the NAD^+ concentration range investigated, the

cathodic current measured at -0.3 V increased gradually with the increase of NAD^+ until levelling off with NAD^+ concentration higher than 3 mM. The improved activity of the bilayer electrochemical system appears promising for more efficient regeneration of NADH coupled to pyruvate bioconversion.

Two experiments of lactate biosynthesis were performed in the presence of the two layer CP-MWCNT-bpy-Rh electrode associated to one CP-MWCNT-LDH on which distinct amounts of LDH were immobilized (**Table IV.1, Experiment 3 and Experiment 4**).

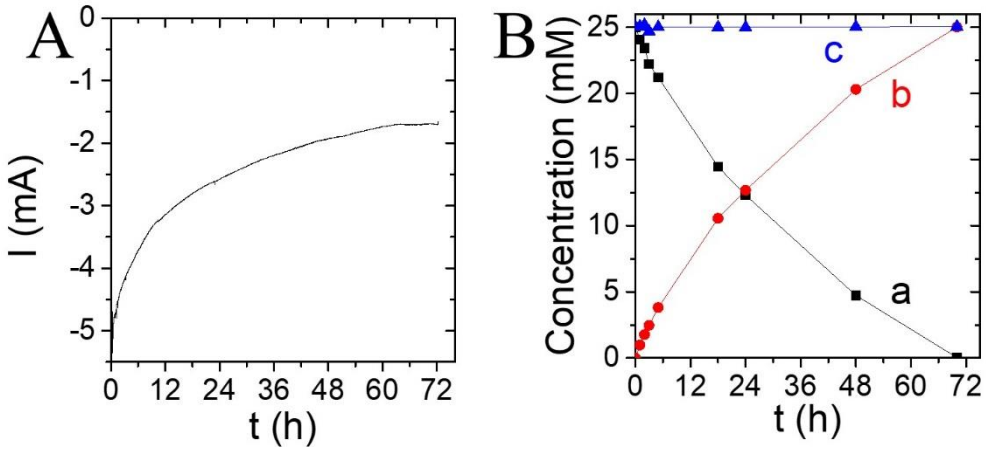

Figure IV.11. Electroenzymatic synthesis of lactate from 25 mM pyruvate in 100 mL solution containing 10 µM NAD^+ (and 50 mM PBS, pH 7.2) in the hybrid flow cell provided with two CP-MWCNT-bpy-Rh electrodes and one enzymatic CP-MWCNT-LDH (500 units) layer (Experiment 3). (A) Variations of the current in the run. (B) Time variations of the concentrations of (a) pyruvate, (b) lactate, and (c) the sum pyruvate and lactate, as determined by HPLC.

Let's first consider the case where 500 units (approximately 13.8 nmol) of enzyme were adsorbed on a CP-MWCNT, corresponding to Rh-over-LDH molar ratio near 10, for which the bioconversion of 100 mL solution of 25 mM pyruvate was carried out in the presence of 10 µM NAD^+, under usual flow and potential conditions (**Experiment 3 in Table IV.1**). The current monitored at -0.3 V vs ref. (H_2) decreased regularly from -5.5 mA to reach a fairly stable current value at -1.8 mA after 72 hours (**Figure IV.11A**). This current was larger than that measured

with a single Rh electrode (**Figure IV.7A**) in correlation with the two-time larger amount of immobilized rhodium complex. Pyruvate was continuously converted along the run, until its disappearance after 72 hours. In the meanwhile, lactate was formed quantitatively (**Figure IV.11B**). These results show the positive impact of increasing the amount of immobilized Rh complex on the overall performance of the regeneration of the cofactor coupled to the enzymatic reaction. Furthermore, these results showed that the regeneration system of NADH coupled to pyruvate bioconversion can be scaled up and can lead to a high bioconversion yield following a ratio of 10 between the rhodium complex and lactate dehydrogenase both immobilized on separated CP-MWCNT. TTNs obtained with the bilayer system for the Rh complex, NAD^+, LDH were respectively calculated at 1.81×10^4, 2.5×10^3 and 1.8×10^5. The TTN for the rhodium complex is in the same order of magnitude as the one reported in the literature for the FNR-mediated regeneration of NADPH.[19] In addition, the TTN obtained for NAD^+ is – to our state of knowledge – the highest value among those reported in the literature.[19,38]

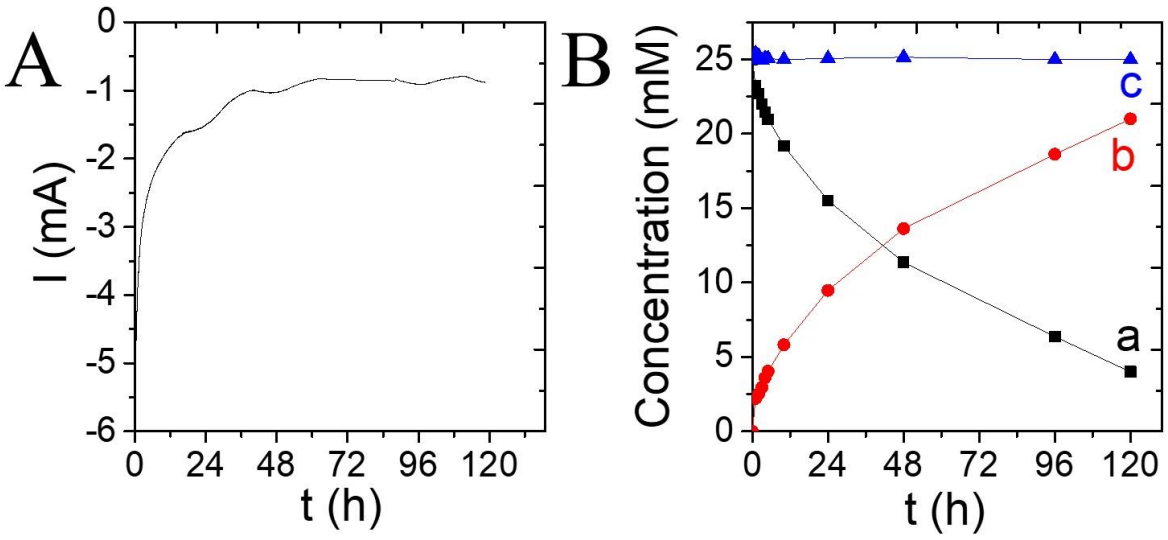

Figure IV.12. Electroenzymatic synthesis of lactate from 25 mM of pyruvate in 100 mL solution containing 10 µM NAD^+ (and 50 mM PBS, pH 7.2) in the flow cell containing two CP-MWCNT-bpy-Rh electrodes and one enzymatic CP-MWCNT-LDH layer (100 units) (A) Variations of the current in the run. (B) Variation of concentrations with time (a) pyruvate, (b) lactate, and (c) the sum pyruvate and lactate, as determined by HPLC.

On the other hand, the bioconversion of the 25 mM lactate in the presence of two CP-MWCNT-bpy-Rh layers, corresponding to 13.8 nmol of immobilized Rh complex, and one CP-MWCNT-LDH layer with only 100 LDH units (2.76 nmol) showed a bioconversion current (Experiment 4 in Table 1) starting near -5 mA and decreasing to -1 mA after 72 h (**Figure IV.12A**). This bioconversion current is lower in absolute value than the one obtained in Experiment 3 with 500 units of LDH. As a consequence, 16.5 mM of lactate were synthetized after 72 h (**Figure IV.12B**) with a faradaic efficiency of 79 %. Moreover, extending the electrosynthesis up to 120 h resulted in the bioconversion of 21.5 mM of pyruvate (**Figure IV.12B**).

To conclude, an optimal ratio between the Rh complex and LDH of 10 allows a total bioconversion of pyruvate within an optimal time (72 hours).

IV.4 Conclusion

Thanks to the robust immobilization of all catalysts and fine optimizations, the presented continuous flow electrochemical reactor shows remarkable performances for catalytic hydrogenation of pure chemicals through NADH regeneration. The work deals with different challenges such as the choice of the cathode material, the immobilization of both the redox catalyst and the enzymes, their association or separation, the molar ratio between each of them, and the use of low amounts of the enzymatic cofactor (10 µM).

Different aspects have to be taken into consideration when coupling efficient electrochemical regeneration of the NADH cofactor to enzymatic bioconversion of chemicals:

1) Immobilizing the Rh complex on carbon paper with MWCNT, and pressing at 40 bars this catalytic layer with a GDE and Nafion membrane led to an active system for the efficient electrochemical regeneration of the NADH cofactor system with a stability of more than 5 days under continuous flow.

2) Reducing the distance between the Rh complex and LDH by immobilizing each of them on separated, stacked layers led to an active loop for the continuous regeneration of the cofactor and pyruvate bioconversion.
3) The ratio between the immobilized Rh complex and enzymes units has to be at least equal to 10 in order to reach the highest faradaic efficiency (79 %), productivity (1.08 $\mu mol.cm^{-2}.h^{-1}$) and TTN for cofactor (2500), rhodium catalyst (18000) and enzyme (180000).
4) Finally, hydrogen and solution flow rates can be fixed at 20 $mL.min^{-1}$ in the bench cell as described previously[32] and the applied electrolysis potential at -0.3 V ref. (H_2). In addition, the flow cell was built advantageously using a graphite felt electrode allowing uniform distribution of the solution in the cathodic compartment and ensuring electrical contact between the functional layers and the current collector of the cell.

Lactate produced from the bioconversion of pyruvate can have a wide range of applications in cosmetics, food, and pharmaceutical industries.[45] Although we have focused on the hydrogenation of a ketone catalyzed by an alcohol dehydrogenase, the approach presented here should be applicable to many other NADH-dependent bioconversions.

References

[1] R. Ciriminna, M. Pagliaro, *Org. Process Res. Dev.* **2013**, *17*, 1479–1484.

[2] F. Nerozzi, *Platin. Met. Rev.* **2012**, *56*, 236–241.

[3] H. U. Blaser, C. Malan, B. Pugin, F. Spindler, H. Steiner, M. Studer, *Adv. Synth. Catal.* **2003**, *345*, 103–151.

[4] R. Noyori, M. Kitamura, T. Ohkuma, *Proc. Natl. Acad. Sci. U. S. A.* **2004**, *101*, 5356–5362.

[5] H. Zhao, W. A. Van Der Donk, *Curr. Opin. Biotechnol.* **2003**, *14*, 583–589.

[6] J.roche, Continuous Regeneration of the NADH Cofactor Catalysed by Formate Dehydrogenase Immobilized in a Filter Press Reactor (in French), Toulouse 3, **2011**.

[7] I. Agranat, H. Caner, J. Caldwell, *Nat. Rev. Drug Discov.* **2002**, *1*, 753–768.

[8] W. Liu, P. Wang, *Biotechnol. Adv.* **2007**, *25*, 369–384.

[9] H. K. Chenault, G. M. Whitesides, *Appl. Biochem. Biotechnol.* **1987**, *14*, 147–197.

[10] S. Fukuzumi, Y.-M. Lee, W. Nam, *J. Inorg. Biochem.* **2019**, *199*, 110777.

[11] J. B. Jones, D. W. Sneddon, W. Higgins, A. J. Lewis, *J. Chem. Soc. Chem. Commun.* **1972**, 856–857.

[12] G. T. Hçfler, M. Pesic, S. H. Younes, E. Choi, Y. H. Kim, V. B. Urlacher, I. W. C. E. Arends, F. Hollmann, *ChemBioChem* **2018**, *19*, 2344–2347.

[13] C. Virto, I. Svensson, P. Adlercreutz, B. Mattiasson, *Biotechnol. Lett.* **1995**, *17*, 877–882.

[14] L. Gorton, E. Domínguez, in *Encycl. Electrochem.*, Wiley-VCH Verlag GmbH & Co. KGaA, Weinheim, Germany, **2007**, pp. 67–143.

[15] H. K. Chenault, G. M. Whitesides, *Appl. Biochem. Biotechnol.* **1987**, *14*, 147–197.

[16] F. Hildebrand, S. Lütz, *Chem. - A Eur. J.* **2009**, *15*, 4998–5001.

[17] L. Zhang, M. Etienne, N. Vilà, T. X. H. Le, G.-W. Kohring, A. Walcarius, *ChemCatChem* **2018**, *10*, 4067–4073.

[18] L. Zhang, M. Etienne, N. Vilà, A. Walcarius, in *Funct. Electrodes Enzym. Microb. Electrochem. Syst.* (Eds.: N. Brun, V. Flexer), World Scientific, **2017**, pp. 215–271.

[19] B. Cheng, L. Wan, F. A. Armstrong, *ChemElectroChem* **2020**, *7*, 4672–4678.

[20] M. Irfan, T. N. Glasnov, C. O. Kappe, *ChemSusChem* **2011**, *4*, 300–316.

[21] P. J. Cossar, L. Hizartzidis, M. I. Simone, A. McCluskey, C. P. Gordon, *Org. Biomol. Chem.* **2015**, *13*, 7119–7130.

[22] A. Goršek, P. Glavič, *Chem. Eng. Res. Des.* **1997**, *75*, 709–717.

[23] T. Noë, Y. Cao, G. Laudadio, *Acc. Chem. Res.* **2019**, *52*, 2858–2869.

[24] B. Siritanaratkul, C. F. Megarity, T. G. Roberts, T. O. M. Samuels, M. Winkler, J. H. Warner, T. Happe, F. A. Armstrong, *Chem. Sci.* **2017**, *8*, 4579–4586.

[25] R. W. Coughlin, M. Aizawa, B. F. Alexander, M. Charles, *Biotechnol. Bioeng.* **1975**, *17*, 515–526.

[26] S. K. Yoon, E. R. Choban, C. Kane, T. Tzedakis, P. J. A. Kenis, *J. Am. Chem. Soc.* **2005**, *127*, 10466–10467.

[27] J. Roche, K. Groenen-Serrano, O. Reynes, F. Chauvet, T. Tzedakis, *Chem. Eng. J.* **2014**, *239*, 216–225.

[28] R. DiCosimo, C.-H. Wong, L. Daniels, G. M. Whitesides, *J. Org. Chem.* **1981**, *46*, 4622–4623.

[29] B. Poznansky, S. E. Cleary, L. A. Thompson, H. A. Reeve, K. A. Vincent, *Front. Chem. Eng.* **2021**, *3*, 1–11.

[30] Z. Goren, N. Lapidot, I. Willner, *J. Mol. Catal.* **1988**, *47*, 21–32.

[31] J. H. Kim, S. H. Lee, J. S. Lee, M. Lee, C. B. Park, *Chem. Commun.* **2011**, *47*, 10227–10229.

[32] W. El Housseini, F. Lapicque, A. Walcarius, M. Etienne, *Electrochem. Sci. Adv.* **2021**, 1–11.

[33] R. L. McCreery, *Chem. Rev.* **2008**, *108*, 2646–2687.

[34] C. F. Megarity, B. Siritanaratkul, R. S. Heath, L. Wan, G. Morello, S. R. FitzPatrick, R. L. Booth, A. J. Sills, A. W. Robertson, J. H. Warner, N. J. Turner, F. A. Armstrong, *Angew. Chemie - Int. Ed.* **2019**, *58*, 4948–4952.

[35] I. Mazurenko, M. Etienne, G.-W. Kohring, F. Lapicque, A. Walcarius, *Electrochim. Acta* **2016**, *199*, 342–348.

[36] B. Tan, D. P. Hickey, R. D. Milton, F. Giroud, S. D. Minteer, *J. Electrochem. Soc.* **2015**, *162*, H102–H107.

[37] E. Steckhan, S. Herrmann, R. Ruppert, E. Dietz, M. Frede, E. Spika, *Organometallics* **1991**, *10*, 1568–1577.

[38] M. Etienne, J. Vivo-vilches, I. Vakulko, C. Genois, L. Liu, M. Perdicakis, R. Hempelmann, A. Walcarius, M. Etienne, J. Vivo-vilches, I. Vakulko, C. Genois, L. Liu, R. Hempelmann, A. Walcarius, *Electrochim. Acta* **2019**, *313*, 131–140.

[39] T. Saba, J. Li, J. W. H. Burnett, R. F. Howe, P. N. Kechagiopoulos, X. Wang, *ACS Catal.* **2020**, *11*, 283–289.

[40] X. Wang, T. Saba, H. H. P. Yiu, R. F. Howe, J. A. Anderson, J. Shi, *Chem* **2017**, *2*, 621–654.

[41] F. Hildebrand, S. Lütz, *Tetrahedron Asymmetry* **2007**, *18*, 1187–1193.

[42] C. F. Megarity, B. Siritanaratkul, B. Cheng, G. Morello, L. Wan, A. J. Sills, R. S. Heath, N. J. Turner, F. A. Armstrong, *ChemCatChem* **2019**, *11*, 5662–5670.

[43] L. Castañeda-Losada, D. Adam, N. Paczia, D. Buesen, F. Steffler, V. Sieber, T. J. Erb, M. Richter, N. Plumeré, *Angew. Chemie - Int. Ed.* **2021**, *60*, 21056–21061.

[44] X. Zhao, S. E. Cleary, C. Zor, N. Grobert, H. A. Reeve, K. A. Vincent, *Chem. Sci.* **2021**, *12*, 8105–8114.

[45] R. Patel, M. Kula, U. Kragl, *Stereoselective Biocatal.* **2000**, *13*, 839–866.

[46] L. Hussein, G. Urban, M. Krüger, *Phys. Chem. Chem. Phys.* **2011**, *13*, 5831–5839.

Objective of the study in Chapter V

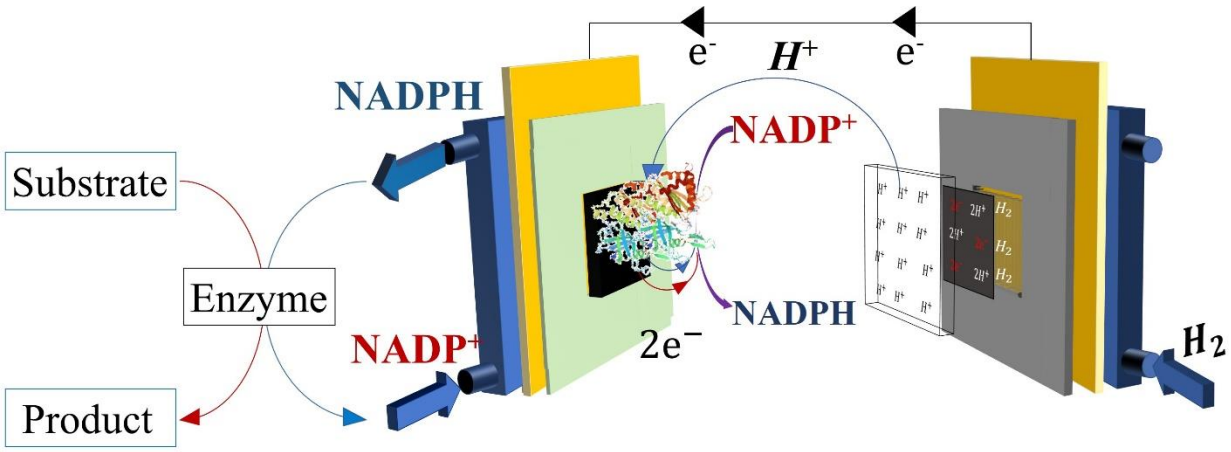

Schematic representation of the flow electroenzymatic bioreactor

The idea in the present work is to replace the rhodium complex by Ferredoxin $NADP^+$ reductase (FNR), an electroenzymatic mediator, known as an electroactive biocatalyst for the regeneration of the NADPH cofactor. In addition to the desire to compare between these two catalysts in terms of stability and activity towards NAD(P)H regeneration under flow conditions, the idea of the work was oriented towards testing the ability of FNR immobilized on carbon materials to regenerate NADH. Then, on another CP-MWCNT, a NADP(H)-dependent dehydrogenase was immobilized following the same arrangement of catalysts adopted in Chapter IV. In this study, lactate dehydrogenase (LDH) was chosen for the bioconversion of pyruvate to lactate.

This manuscript will be submitted later

Chapter V. Electroenzymatic flow bioreactor for the efficient bioelectrocatalytic regeneration of NADH coupled to LDH catalyzed reduction of pyruvate

Abstract:

The electroenzymatic regeneration of the NAD(P)H cofactor using ferredoxin-NADP+ reductase (FNR) as a mediator has gained a large importance constituting a clean, efficient, and enantioselective approach to produce high-value products in chemical and pharmaceutical industries. Here, we coupled the regeneration of the enzymatic cofactor mediated by Chlamydomonas Reinhardtian FNR to the oxidation of hydrogen in flow reactor.

FNR immobilized by adsorption on oxidized carbon nanotubes (FNR@CP-MWCNT$_{ox}$), displayed a constant activity for more than 6 days under high flow rate conditions. Interestingly, FNR@CP-MWCNT$_{ox}$ electrode has shown a high activity not only towards the regeneration of NADPH cofactor but also towards the regeneration of NADH. The optimal cofactor regeneration was then applied to NADH-dependent biosynthesis in the flow cell using immobilized lactate dehydrogenase for the conversion of pyruvate to lactate in the presence of cofactor concentrations as low as 10 µM. The overall system coupled to the enzymatic reaction showed a Total Turnover Number (TTN) of 10^4 for the cofactor and a faradaic efficiency larger than 80 %.

V.1 Introduction

Ferredoxin NADP+ reductase (FNR) is an enzyme found in chloroplasts that contains flavin adenine dinucleotide (FAD). It accepts electrons from ferredoxin (Fd), which is located at the end of the electron transport chain consisting of two light harvesting units, and reduces $NADP^+$ to NADPH. The NADPH produced is then utilized as reducing equivalents in the Calvin cycle, which drives CO_2 assimilation. $NADP^+$ reduction is a two-electron reaction, while ferredoxin carries one electron. The FAD group is capable of existing in three redox states: oxidized, semiquinone (1-electron reduced), and hydroquinone (2-electron reduced). Consequently, it can function as an electron reservoir, and the two ferredoxins must donate electrons in two distinct events.

The vast possibilities for biomaterial design and functionality made possible by mimicking nature continue to push the boundaries of imagination. [1,2] For example, mimicking photosynthesis and energized mitochondria is a long-term method for regenerating NAD(P)H and using it to convert CO_2 and produce pure chemicals is one of the topics that gains a big interest.[3–5] To regenerate efficiently the NAD(P)H cofactor, combining different scientific and non-scientific disciplines, like bioelectrochemistry, chemical engineering, flow chemistry, and eventually architecture, may seem like a good way to bridge the gap between biological systems and systems that look like them.

Among NAD(P)H cofactor regeneration techniques *e.g.*, chemical, photochemical, enzymatic, and biological regenerations, [6–8] the electrochemical and the electroenzymatic regeneration of the NAD(P)H cofactor catalyzed by chemical catalysts e.g., Rh complex and biological ones e.g., FNR and NAD^+ reductase may offer numerous advantages such as the continuous monitoring of the process, the optimization of the number of enzymes loaded on the electrode, and the unnecessary separation process after the reaction between enzymes and products since

enzymes are immobilized.[9,10] In this work, we are interested to the electroenzymatic regeneration of the NAD(P)H cofactor biocatalyzed by FNR.

Use of dissolved enzymes in biosynthesis is an expensive route due to their troublesome separation from reactants downstream of the reaction chamber.[11] Besides, denaturation of enzymes in aqueous solutions is to strongly reduce their activity. [11] For the two above reasons and for large scale applications, enzymes should be immobilized on an electroactive support that maintains or enhances their activity.[12]

Remarkable progresses related to the immobilization of electroenzymatic catalysts e.g., FNR and NAD^+ reductase regarding the maintenance of their activity and stability with time have been reported.[13] Their immobilization can be achieved by following one of the two techniques as below. The first one relies upon the direct electron transfer between the electrode and the biocatalyst immobilized on an electroactive surface *e.g.,* MWCNT, as reported by Vincent and co-workers[14] or ITO electrode, as reported by Armstrong and co-workers.[15] The second one consists on the indirect transfer of electrons using a redox hydrogel wiring between the biocatalyst and the electrode as reported by Minteer and co-workers.[16] While the application of a direct electron transfer between the electrode and the biocatalyst appears easier in a flow reactor,[14] the immobilization of the mediator using a redox hydrogel showed its advantage in enhancing the synthetic output of biohybrid systems.[17]

Flow processes offer significant advantages over the conventional batch processes in biotechnology such as high mass transport and the increased kinetics of the reactor with a highly agitated system favored by the application of high solution flow rates. Despite its inherent industrial concerns, translation of batch electrocatalysis to flow processes induced is more and more considered in industry. More precisely, the electroenzymatic regeneration of the cofactor in a flow reactor represents a challenging idea to solve issues usually encountered in batch

processes such as complex reactor design, insufficient stability of the immobilized mediator, [18] and low conversion efficiencies[19].

For their efficiency and their implementation, bioreactors have to fulfill some prerequisites. First, enzymes must be immobilized on the electrode surface (or another solid support) in order to reduce waste production as much as possible and to reduce the cost. This is also to reduce the number of separation and purification steps of the produced fine chemicals.[20] Second, the immobilization method of enzymes has to permit sustained enzymatic activity so that long-term runs with a high productivity can be envisioned.[21,22] Third, in order to meet with industrial concerns related to high production, large quantities of enzymes have to be loaded on the electrode. For that reason, porous electrodes with high area have to be employed for enzymes immobilization.[21]

Besides, the combination between a gas diffusion electrode, for hydrogen oxidation, and an enzymatic bioelectrode have revealed to be an attractive strategy in reactors designing for bioelectrochemical synthesis.[23] We previously described the combination between hydrogen oxidation and the regeneration of the NAD(P)H electrochemically mediated by a rhodium complex immobilized on a carbon support in a flow reactor.[24]

The idea in the present work is to replace the rhodium complex by an electroenzymatic mediator, FNR immobilized on a carbon paper coated with MWCNT. After development of the immobilization method, FNR@CP-MWCNT electrode has shown here to be active not only towards NADPH regeneration but also towards NADH regeneration. Then, a second enzyme that could be any of hundreds of NADP(H)-dependent dehydrogenases has been immobilized on another CP-MWCNT. Lactate dehydrogenase (LDH) has been chosen in this work for the bioconversion of pyruvate to lactate. The scheme of the whole arrangement is depicted in **Scheme 1**.

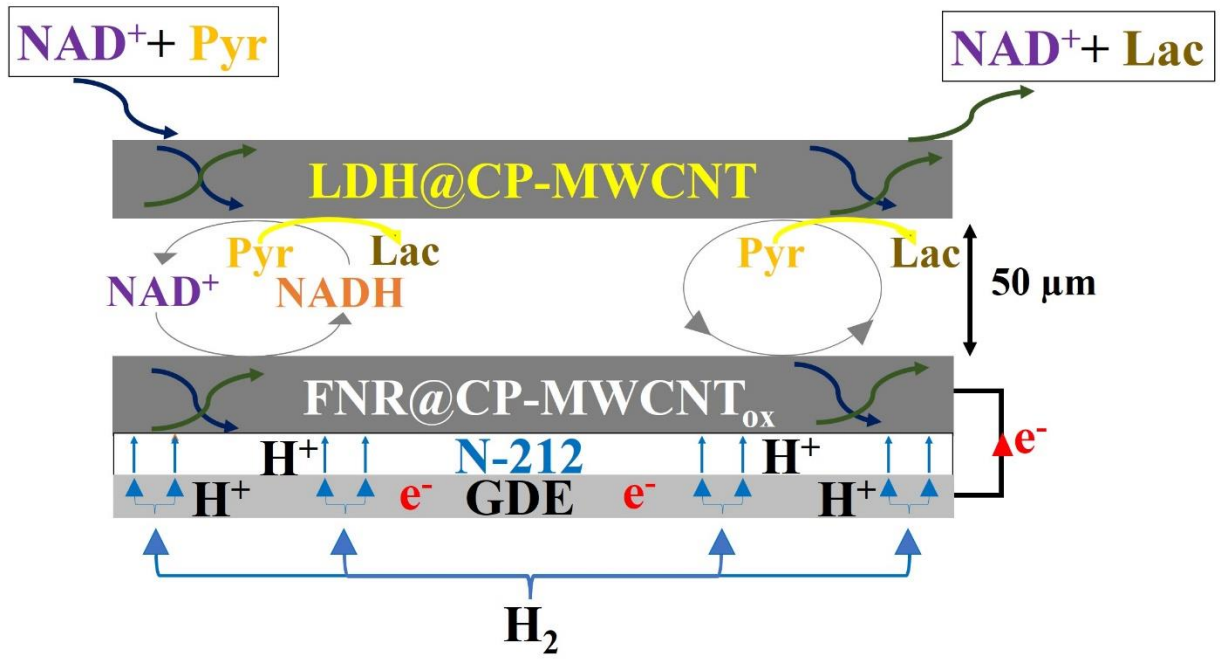

Scheme V.1. Schematic view of the flow electroenzymatic reactor

V.2 Materials and methods

V.2.1 Chemical and reagents

β-nicotinamide adenine dinucleotide (NAD^+, >98%) and β-nicotinamide adenine dinucleotide reduced dipotassium salt (NADH, >97%), L-lactate dehydrogenase (LDH) from rabbit muscle (≥ 600 units/mg protein), pyruvate (98 %) and lactate (98 %), H_2O_2 (98 %) were from Sigma-Aldrich. TAPS buffer (50 mM) was used to investigate the electrocatalytic properties of FNR towards $NAD(P)^+$ reduction and was reported to be one of the most appropriate for such experiments. Multi-walled carbon nanotubes (MWCNT, NC7000™ series) were from Nanocyl (Belgium). Gas diffusion electrodes (GDE), Nafion solution (5 %), and carbon papers (SpectraCarb 2050L-0550 Carbon Paper) were acquired from Fuel Cell Store (USA). MWCNT were dispersed in a solution of ethanol (96 %). All solutions were prepared with high purity water (18 MΩ cm) from a Purelab Option water purification system.

V.2.2 FNR purification [44]

The sequence coding for the mature form (amino acids 27 to 346) of *Chlamydomonas reinhardtii* ferredoxin $NADP^+$ reductase (FNR, Cre11.g476750) was cloned into the bacterial pET3d expression vector between NcoI and BamHI restriction sites using the following forward and reverse primers: 5' ccccccatgggccaccaaggcttcgacc 3' and 5' ccccggatccttagtagacctccacgtg 3'. The *E. coli* BL21(DE3) strain containing the helper pSBET plasmid was used for protein expression (Schenk et al., 1995). A culture of 2.4 L in lysogenic broth medium was performed at 37 °C supplemented with 50 µg/mL of kanamycin and ampicillin. Protein expression was induced at exponential phase by adding 100 µM of isopropyl β-D-1-thiogalactopyranoside during 4 h. Cells were harvested by centrifugation (Beckman Coulter JLA 8.1000; 20 min; 6,200 x g) and resuspended in 12 mL buffer A containing 30 mM Tris-HCl pH 8.0, 200 mM NaCl and 1 mM EDTA. Cell lysis was performed by sonication (20 % amplitude; 2 times 1 min), then soluble and insoluble fractions were separated by centrifugation (Beckman Coulter JA 25.50; 20 min; 48,000 x g; 4°C). The soluble fraction was precipitated at 40% of the ammonium sulfate saturation and then at 80% in two successive steps separated by a centrifugation step (JA 25.50; 20 min; 30,800 x g; 4°C). The 40-80% precipitated fraction was resuspended in 8 mL buffer A and loaded on size exclusion chromatography (ACA 34, PALL Biosepra) equilibrated with buffer A. Fractions containing the protein of interest were pooled and dialyzed against buffer B containing 30 mM Tris-HCl pH 8.0 and 1 mM EDTA and loaded on Q-sepharose column (Cytiva). The non-retained protein fraction, containing FNR, was pooled and concentrated. Sample purity was assessed via SDS-PAGE and the concentration determined spectrophotometrically using theoretical molar extinction coefficients at 280 nm of 48735 $M^{-1}.cm^{-1}$ and at 455 nm of 8434 $M^{-1}.cm^{-1}$.

V.2.3 MWCNT oxidation with 30% w/v H_2O_2

The oxidation of MWCNT was proceeded following a reported protocol in the literature.[30] 200 mg of MWCNTs were treated with 100 ml of a 30% w/v H_2O_2 solution at 80°C. In a round-bottom flask equipped with a condenser, thermocouple, and thermometer, the reaction was conducted. After stabilizing the temperature of the oil bath at 80°C, the flask was immersed in the oil bath to initiate the oxidation process at a stirring rate of 200 rpm (the slurry temperature was approximately 65 °C). After oxidation, MWCNTs were filtered and washed multiple times with distilled water until the pH of the filtered solution was neutral, and then dried overnight at 80 °C.

V.2.4 Preparation of FNR@CP-MWCNT$_{ox}$ electrode

The preparation of the enzyme-modified electrode followed two steps. First, as the system operates in a flow and following the immobilization of the Rh complex on a carbon paper coated with MWCNT presented in a work previously,[24] the immobilization of FNR was proceeded by being drop-casted on a 4 x 4 cm^2 CP-MWCNT$_{ox}$. The electrode was left at a temperature of 2 °C until total adsorption of FNR on MWCNT.

V.2.5 Prepapation of LDH@CP-MWCNT

The Cp-MWCNT was prepared using the same method as in a prior study.[24] LDH enzyme was adsorbed onto the surface of MWCNTs (16 cm^2) by depositing a 50 µL suspension of LDH and leaving it at 3°C for 2 hours.

V.2.6 Electroenzymatic reactor

The electrocatalytic behavior of the formed FNR@CP-MWCNT$_{ox}$ electrode was evaluated by cyclic voltammetry in the flow reactor. The FNR-functionalized CP was stacked on a macroporous graphite felt in the cathodic chamber of the reactor: this felt was shown to allow a uniform distribution of the solution and to maintain a good electrical conduction of the

graphite bipolar plate. [27] A 16 cm^2 gas diffusion electrode acted as the anode for hydrogen oxidation and a Nafion (N-212) membrane was inserted between the anode and the FNR@CP-MWCNT (working) electrode for the separation of the two compartments while allowing migration of protons from the anode to the cathode. In all tests reported here, hydrogen and the electrolytic solution (50 mM TAPS buffer solution at pH 8) were continuously fed at 20 $mL.min^{-1}$. [27] Cyclic voltammetry was performed by scanning the FNR@CP-$MWCNT_{ox}$ electrode at 5 mV s^{-1}. Because of the low polarization of the hydrogen anode (below 10 mV), the potential of the working electrode was referred to the anode potential.

Quantitative analysis of pyruvate bioconversion was performed by HPLC, using the Aminex HPX-87H HPLC column (300 mm×7.8 mm, Phenomenex) thermostated at 55°C, and a refractive index detector. The aqueous phase was flowed at 0.2 $mLmin^{-1}$. 200 µL aliquots were taken at different intervals from the reaction mixture. These aliquots were further analyzed by HPLC to determine the pyruvate and lactate.

V.3 Results and Discussion

As previously mentioned, FNR is the enzyme that catalyzes the production of NADPH in photosynthetic reactions by using two electrons previously accepted (one at a time) from reduced ferredoxin (Fd):

$$2\ Fd_{red} + NADP^+ + H^+ \xrightarrow{FNR} 2\ Fd_{ox} + NADPH \qquad (1)$$

The Fd is negatively charged and contains an abundance of amino acids with acidic side chains. As for FNR, the negatively charged Fd binds to a positively charged patch.[25] Thus, electrostatic forces are generated to ensure interaction between Fd and FNR. The electrostatically driven binding between Fd and FNR facilitates the close alignment of the [2Fe-2S] cluster in Fd with the FAD in FNR. [25]

Methyl viologens (MV) are one of the most widely utilized mediators for FNR. This mediator was chosen because its E° is favorable and comparable to that of Fd. The reduction potential for the $MV^{2+}/MV^{+\cdot}$ couple is -0.446 V (vs. SHE), compared to -0.42 V for spinach FNR Fd.[26] On the other hand, it is possible to study the direct electron transfer between FNR and the electrode by omitting electron mediators. Enzymes adsorbed on an electrode are capable of forming stable protein films in which direct interfacial electron transfer (electrode to enzyme) occurs without the need for an electron mediator. Ideal candidates for electrode materials are those with biocompatible properties, such as carboxylates and oxides. [27]

One of the immobilization techniques of FNR is its direct adsorption on an ITO foil as suggested by Armstrong and co-workers.[28] Besides, based on the fact of the high electroactive surface of MWCNT[29] and on the targeted use of electrode materials suitable with a flow reactor a CP was coated with oxidized MWCNT following a former work [30] in which MWCNTs were oxidized with hydrogen peroxide (30 %) at a temperature of 80 °C. This oxidative treatment is to favor the formation of CO-related oxygen groups such as phenol, carbonyl quinones and ether, which could improve the surface hydrophilicity and affinity of MWCNT toward FNR enzyme.

V.3.1 CV experiments

V.3.1.1 FNR@CP-MWCNT$_{ox}$ electrocatalytic activity towards NADPH regeneration

The electroenzymatic behavior of 20 nmol of FNR immobilized on CP-MWCNT$_{ox}$ was evaluated by cyclic voltammetry at 5 $mV.s^{-1}$ and with hydrogen and solution flow rates of 20 $mL.min^{-1}$.

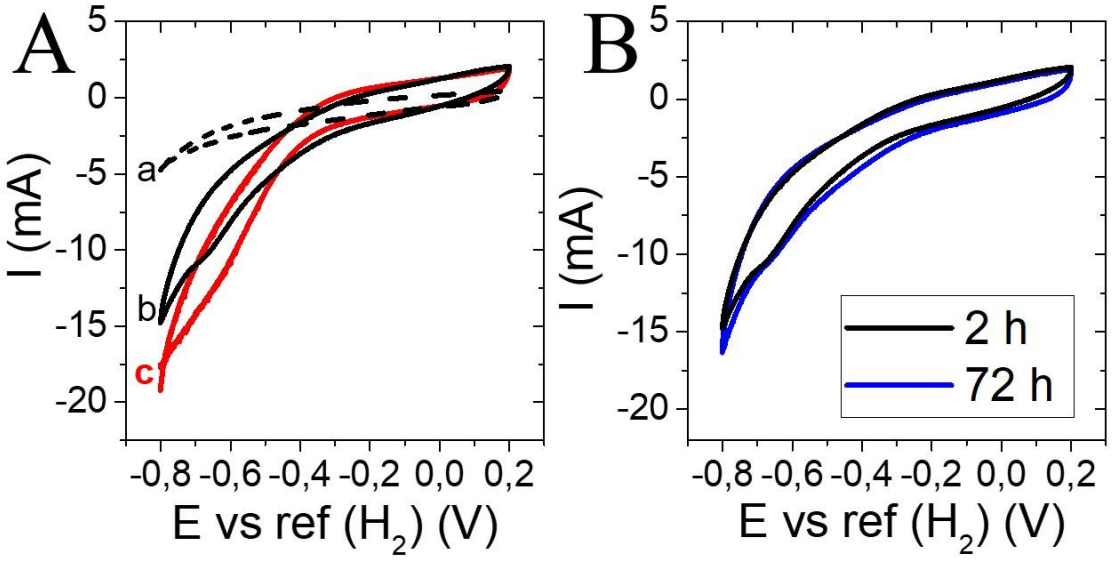

Figure V.1. (A) Cyclic voltammograms recorded at a potential scan rate of 5 $mV.s^{-1}$ in 50 mM TAPS buffer at pH 8 under nitrogen of (a) CP-$MWCNT_{ox}$ and FNR@ CP-$MWCNT_{ox}$ in the presence of (b) 0 mM and (c) 2 mM $NAD(P)^+$. (B) Evaluation of the FNR@CP-$MWCNT_{ox}$ activity through cyclic voltammetry 2 hours (replicate of Figure V. 1A curve b) and 72 hours after its preparation in the absence of $NADP^+$. Conditions: V = 20 mL, H_2 and solution flow rates: 20 $mL.min^{-1}$.

Without FNR or $NADP^+$, the electrode does not exhibit any redox activity (**Figure V.1A curve a**). With 20 nmol drop-casted FNR on the CP-$MWCNT_{ox}$, the electroenzymatic activity of FNR (**Figure V.1A curve b**) was revealed by the onset of reduction current at -0.45 V vs ref (H_2) and with a reduction peak at -0.67 V vs ref (H_2). Besides, the electrochemical activity of FNR supported by the carbon material does not exhibit an oxidation peak in the reverse scan as reported in other works.[13,31] This difference in the electrochemical behavior could be due to the difference in supporting material on which FNR was immobilized or to the presence of FNR in direct contact of the nafion membrane. The addition of 2 mM of the $NADP^+$ cofactor, **Figure V.1A curve c**, showed an appreciable increase in the current at -0.7 V vs ref (H_2) attributed to the electrocatalytic reduction of the cofactor by FNR.

In order to evaluate the robustness of the FNR@CP-MWCNT$_{ox}$ and its activity, the prepared electrode, stored at 2 °C, was further tested 72 hours later. As shown in **Figure V.1B**, the electrode exhibited an electrochemical activity featured by a cathodic current very similar to that recorded two hours after the cathode preparation, showing a maintained activity and stability with time due to the high affinity of FNR towards CP-MWCNT$_{ox}$ surface. This result could be explained based on the negatively charged surface of oxidized MWCNT at pH 8 and the positively charged patch on FNR.[25] Thus, the binding between FNR and MWCNT appears mainly electrostatic where oxidized MWCNTs mimic Fd while binding to FNR.

On the other hand, in order to evaluate the effect of MWCNT oxidation on FNR activity and stability, FNR@CP-MWCNT electrode was tested without the oxidation of MWCNT.

The electroenzymatic activity of 20 nmol of FNR immobilized on the CP-MWCNT showed the onset of a reduction current at -0.28 V vs ref (H_2) and a cathodic shouldering at -0.37 V vs ref (H_2) with a current of 0.6 mA (**Figure V.2A curve a**). This reduction peak is approximately 300 mV more positive than the one with oxidized MWCNT.

On the other hand, the reduction current for FNR immobilized on pristine MWCNT is approximately 9 times lower than the one observed on oxidized MWCNT (5.3 mA vs 0.6 mA). Adding 0.5 mM of $NADP^+$ led to the increase in the cathodic current to 1.1 mA (**Figure V.2A curve b**) which proves the activity of FNR towards the regeneration of the cofactor.

The regeneration of 0.5 mM of NADPH after 2 hours of the electrode preparation, FNR@CP-MWCNT, carried out at an applied electrolysis potential of -0.4 V vs ref (H_2) showed a current starting at approx. -2 mA then decreasing strongly after 25 min (**Figure V.2B**). After this lapse of time, 56 % of NADPH was regenerated. Within 60 min of electrolysis, a total regeneration of NADPH was reached with a faradaic efficiency of 74.8 % and with a TTN for FNR near 1000. This obtained value is higher than the value obtained with the Rh complex system (300) without the application of an enzymatic reaction.[24]

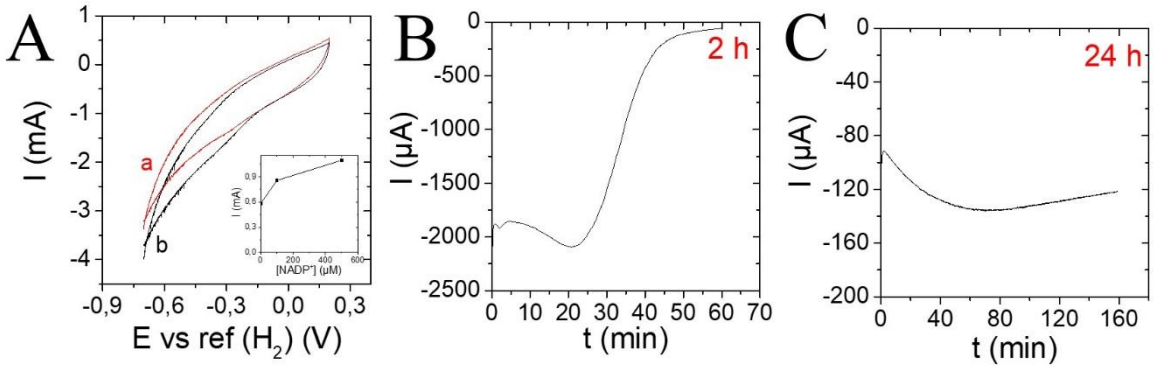

Figure V.2. (A) Cyclic voltammograms of FNR@CP-MWCNT electrode recorded at a potential scan rate of 5 $mV.s^{-1}$ in the presence of (a) 0 mM and (b) 0.5 mM of $NADP^+$ 2 hours after the electrode preparation. (B) Current recorded from the electrolysis of 0.5 mM $NADP^+$ carried out at -0.4 V vs ref (H_2) (B) 2 hours and (C) 24 hours after FNR@CP-MWCNT electrode preparation. The geometric surface area of the electrode was 16 cm^2 and hydrogen and solution flow rates were at 20 $mL.min^{-1}$. Conditions: V = 20 mL, Hydrogen and solution flow rates 20 $mL.min^{-1}$, T = 20 °C, and 50 mM TAPS (pH = 8).

In order to evaluate the activity and the stability FNR@CP-MWCNT electrode, the electrode was left 24 hours at 2°C after the electrolysis test. The electrolysis test, was repeated at the same electrolysis potential and following the same protocol *e.g.,* 0.5 mM $NADP^+$, 20 mL solution, hydrogen and solution flow rates of 20 $mL.min^{-1}$ **(Figure V.2C)**. The electrolysis current monitored was more than 10 times lower than the one obtained after the preparation of the electrode. This strong reduction in the current indicates that FNR drop-casted on the CP-MWCNT has almost lost its activity with time. The average current of the electrolysis was equal to 110 µA during the 160 min-long electrolysis allowing regeneration of 125 µM NADPH only out of the 500 µM $NADP^+$ initially introduced. This clearly shows that immobilization of FNR on a CP coated with MWCNT cannot lead to a fully active, stable electrode.

Thus, it is obviously clear that the usage of oxidized MWCNT maintains and enhances the activity of FNR towards the NADPH cofactor regeneration.

For further tests, a carbon paper modified with a layer of oxidized MWCNT on which FNR was drop-casted was thus selected here as the best one for regeneration of the cofactor.

V.3.1.2 Can FNR regenerate NADH?

Ferredoxin $NADP^+$ reductase (FNR) is known as an electroenzymatic biocatalyst for the regeneration of the NADPH cofactor. All reported works in the literature demonstrate the activity of FNR towards the regeneration of the NADPH cofactor.[13,32,33] Other works focused on the regeneration of NADH by NAD^+ reductase.[34,35] It was reported in the literature that if NAD^+ instead of $NADP^+$ is added (i.e., the structure does not contain a phosphate at the 2′-position of the ribose), catalysis may be impaired: the selectivity of FNR for NAD^+ is significantly lower than for $NADP^+$ (K_M for $NADP^+$ is typically 8–39 µM,[15] while for NAD^+ it is 4–11 mM[36]).

For assessment of the route investigated in this work, comparison of the rhodium complex as an electrochemical catalyst and of FNR as an electroenzymatic biocatalyst for the cofactor regeneration has been conducted. A series of experiments was thus carried out for the electrochemical regeneration of NADH instead of NADPH by FNR.

The electroenzymatic of FNR towards NADH regeneration was evaluated through cyclic voltammetry and a scan rate of 5 $mV.s^{-1}$ (**Figure V. 3A**). Without NAD^+, a cathodic current was observed at -0.67 V vs ref (H_2) referred to the activity of FNR@CP-$MWCNT_{ox}$ electrode as previously observed (**Figure V. 3A curve a**). The cathodic current peak of 20 nmol of FNR@CP-$MWCNT_{ox}$ electrode without NAD^+ ,**Figure V. 3B curve b** (260 µA.$nmol^{-1}$ FNR), is largely higher than the one observed with the Rh@CP-MWCNT , **Figure V.3B curve b,** where the calculated surface coverage with Rh complex was equal to 66 nmol (2.4 µA.$nmol^{-1}$ Rh complex).[24]

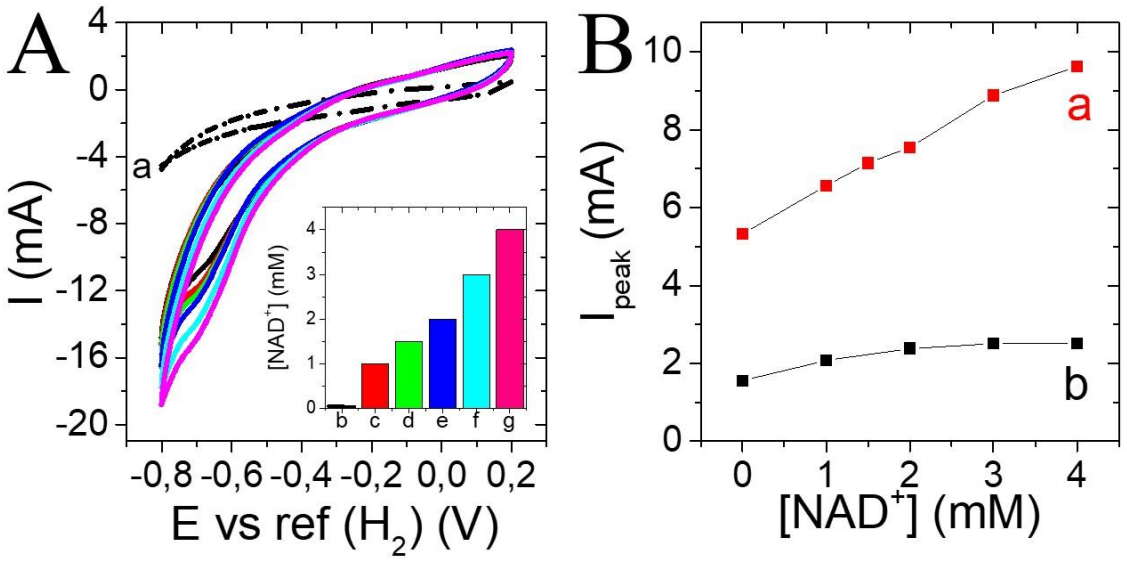

Figure V.3. (A) Cyclic voltammograms recorded at a potential scan rate of 5 $mV.s^{-1}$ using 20 nmol FNR immobilized by adsorption on CP-$MWCNT_{ox}$ electrode in 50 mM TAPS buffer at pH 8 under nitrogen and in the presence of increasing concentrations of NAD^+ (b) 0 mM, (c) 1 mM, (d) 1.5 mM, (e) 2 mM, (f) 3mM, and (g) 4 mM. (B) Influence of NAD^+ concentration on the cathodic current peak measured by CV for (a) FNR@CP-$MWCNT_{ox}$ electrode at -0.7 V vs ref (H_2) and (b) Rh@CP-MWCNT electrode at -0.36 V vs ref (H_2). Conditions: V = 20 mL, Hydrogen and solution flow rates 20 $mL.min^{-1}$, and T = 20 °C.

The addition of 1 mM of NAD^+ (**Figure V.3A curve b**) led to an increase in the cathodic current at -0.67 V vs ref (H_2) to 6.6 mA. This result evidences the electrocatalytic activity of FNR@CP-$MWCNT_{ox}$ electrode towards NADH regeneration. Adding increased amounts of NAD^+ led to the increase of the cathodic current. For example, the cathodic current, **Figure V.3B curve a**, increased from 6.6 mA with 1 mM of NAD^+ to 9.8 mA with 4 mM NAD^+. On the other hand, the cathodic current does not level off with high amounts of NAD^+ (higher than 3 mM) as observed with the Rh complex (**Figure V.3B curve b)** [24] which reveals that the kinetic of regeneration of the cofactor with FNR system is faster than that with the Rh complex where both are immobilized at CP-MWCNT support.

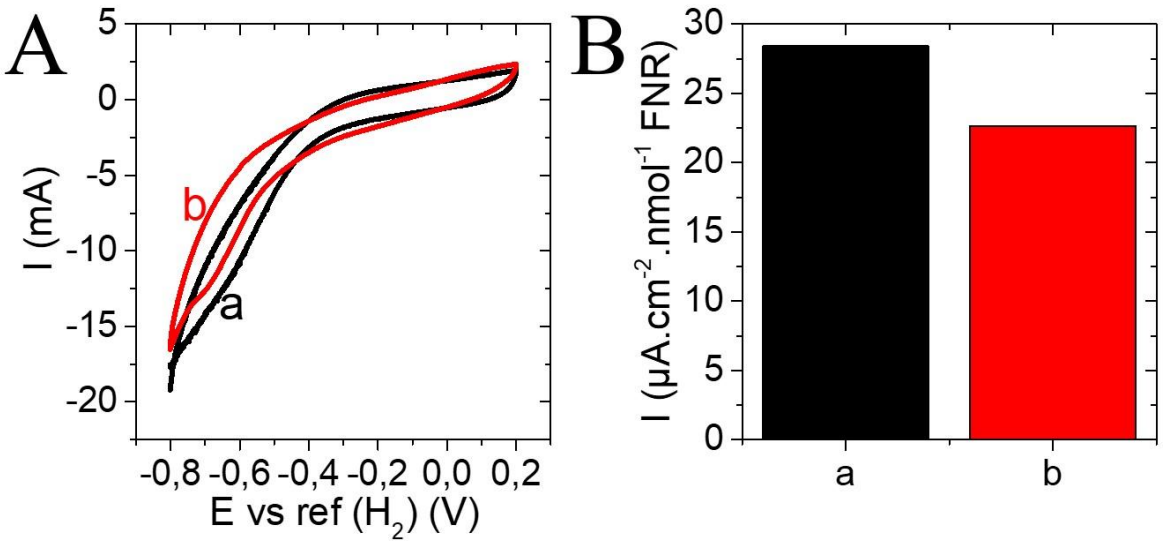

Figure V.4. (A) Cyclic voltammograms recorded and (B) cathodic current peak measured by CV at a potential scan rate of 5 $mV.s^{-1}$ using 20 nmol FNR immobilized by adsorption on CP-$MWCNT_{ox}$ electrode in 50 mM TAPS buffer at pH 8 under nitrogen and in the presence of 2 mM of (a) $NADP^+$ (CV curve: replicate of Figure V. 1A curve c) and (b) NAD^+ (CV curve: replicate of Figure V. 2A curve e). Conditions: V = 20 mL, Hydrogen and solution flow rates 20 $mL.min^{-1}$, and T = 20 °C.

In addition, the electrochemical behavior of the FNR@CP-$MWCNT_{ox}$ electrode at -0.7 V vs ref (H_2) after the addition of 2 mM $NADP^+$ shows a cathodic current of 9.1 mA (**Figure V.4A curve a**). On the other hand, FNR@CP-$MWCNT_{ox}$ behavior after the addition of 2 mM NAD^+ shows a lower reduction current of 7.25 mA (**Figure V.4A curve b**). This low difference (approx. 5.7 $\mu A.cm^{-2}.nmol^{-1}$FNR) as shown in **Figure V.4B** can be due to the lower affinity of FNR towards NAD^+ than $NADP^+$ as reported in the literature. [36]

As a consequence, the activity of FNR@CP-$MWCNT_{ox}$ electrode was demonstrated towards NADH regeneration. After confirming the electrode activity towards NADH regeneration mediated by FNR, its application in electroenzymatic biosynthesis was further explored.

V.3.2 Use of FNR@CP-MWCNT$_{ox}$-regenerated NADH by in an enzymatic reaction

V.3.2.1 Parameters optimization for the efficient bioconversion of pyruvate

Coupling an enzymatic reaction to the regeneration of NADH by FNR@CP-MWCNT$_{ox}$ can demonstrate the existence of the active form of NADH (1,4-NADH)[37] . This would be heartly desired for its application in the synthesis of pure chemicals. As carried out previously with NADH regenerated by mediation of immobilized rhodium catalyst, the FNR-regeneration of the cofactor was coupled to the bioconversion of pyruvate to lactate by lactate dehydrogenase (LDH) to demonstrate the in-situ regenerated NADH.

In this part, two factors of importance can be addressed: (i) the molar ratio of the two enzymes employed; (ii) the immobilization procedure of the two biocatalysts i.e. either on the same carbon layer as reported in the literature[31,34] or separately, as done previously with Rh complex.[24]

The selected pH for the bioconversion of pyruvate was equal to 7.6 as a compromise between FNR optimal pH (pH = 8) and LDH one (pH = 7.2). The electroenzymatic behavior of 20 nmol FNR immobilized on CP-MWCNT$_{ox}$ in the absence of NAD^+ is expressed by a cathodic current of 3.3 mA after subtraction of the residual current (**Figure V.5 curve b**) at -0.67 V vs ref (H2). This obtained cathodic current is lower (in absolute value) than the current recorded at pH 8 (**Figure V.5 curve a**) which can lower the activity of the system towards the regeneration of the cofactor as well as the bioconversion.

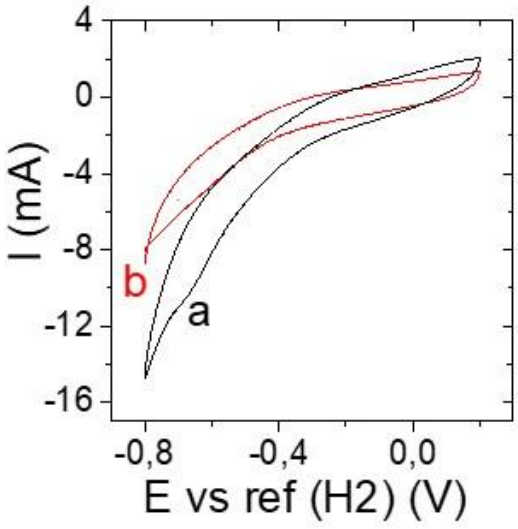

Figure V.5. Cyclic voltammograms recorded at a potential scan rate of 5 $mV.s^{-1}$ using 20 nmol FNR immobilized by adsorption on CP-$MWCNT_{ox}$ at a pH of (a) 8 and (b) 7.6. Conditions: 0 mM NAD^+, V = 20 mL, Hydrogen and solution flow rates 20 $mL.min^{-1}$, and T = 20 °C.

In the first study, two simple experiments were carried out to determine how the catalytic performance depends on the ratio of the two enzymes (FNR and LDH) added on the same electrode (CP-$MWCNT_{ox}$). **Figure V.6** shows the time variations of the current for the reduction of pyruvate to lactate, performed with a 16 cm^2 (FNR+LDH) @CP-$MWCNT_{ox}$ pre-loaded by drop-casting with 20 nmol of FNR and (20 nmol or 4 nmol) LDH in two different ratios. The study was performed in the presence of 5 mM of pyr and 1 mM of NAD^+.

At -0.7 V vs ref (H_2) and for an FNR: LDH ratio of 1 (**Figure V.6 curve a**), the bioconversion current rapidly attained a maximum current of -22 mA after 2 hours and decreased gradually in intensity over time until reaching -15 mA after 9 hours. The bioconversion was total after 9 hours and the faradaic efficiency was equal to 6 %. The high amount of LDH added corresponding to a ratio at unity, on the FNR@CP-$MWCNT_{ox}$ might be a possible cause in the decreased activity of FNR or the partial blockage of the electrode surface.

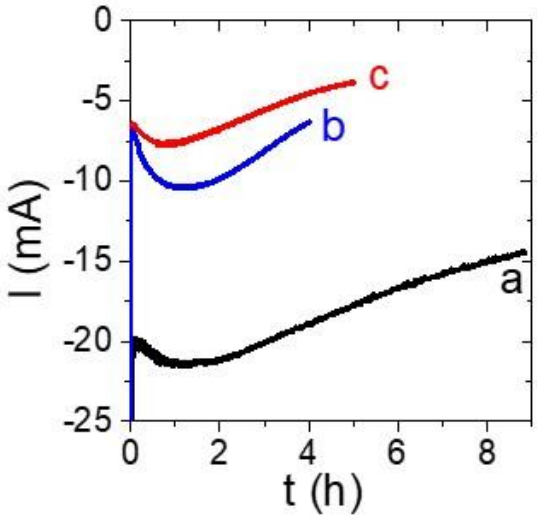

Figure V.6. Study of the effect of the ratio between FNR and LDH and the immobilization of FNR and LDH on the same 16 cm^2 CP-MWCNT layer or on separate ones in batch tests with recirculation, at -0.7 V vs ref. (H_2). (a) 20 nmol FNR:20 nmol LDH@CP-MWCNTox, (b) 20 nmol FNR:4 nmol LDH@CP-MWCNTox, and (c) 20 nmol FNR@CP-MWCNTox and 4 nmol LDH@CP-MWCNT-LDH. Conditions: 1 mM NAD^+, 5 mM Pyr, hydrogen and solution flow rates: 20 $mL.min^{-1}$, V = 30 mL.

The test with the lower amount of adsorbed LDH on the FNR@CP-$MWCNT_{ox}$ electrode (4 nmol, corresponding to FNR: LDH ratio at 5) showed an electrolysis current starting at -12 mA (**Figure V.6 curve b**) and decreasing (in absolute value) to – 3.7 mA after 4 hours. At this time, the bioconversion was found complete.

The current monitored here (Ratio FNR: LDH = 5) was approx. 3 times lower than that with identical amounts of FNR and LDH. The faradaic efficiency of pyruvate conversion was accordingly equal to 22 %. In both bioconversion tests, the faradaic efficiency is low compared with that obtained with Rh complex (78 %).[24] This low value can be due to the negative potential applied for which hydrogen evolution can be observed or to the presence of impurities on the electrode, or to the low density of both catalysts on the 16 cm^2 electrode. Nevertheless,

these two experiments led us to a primary optimization that the ratio between FNR and LDH for an efficient bioconversion of pyruvate has to be in the order of 5.

In order to evaluate the effect of the separation of the two biocatalysts on the pyruvate conversion and its faradaic efficiency, the same experiment with an FNR:LDH ratio at 5 was repeated, where each catalyst was drop-casted on a separate CP-MWCNT as illustrated in scheme 1.

The obtained current of the bioconversion was found to be lower in comparison with those in the last two experiments (**Figure V.6 curve c**). After a "maximum" value near -7.5 mA, the current decreased gradually with time to reach -3.5 mA after 5 hours. The bioconversion was shown total after 5 hours and the faradaic efficiency was equal to 27 %. Pyruvate bioconversion was faster when the two enzymes were placed on the same carbon layer, presumably thanks to facilitated transfer between catalysts mediated by the regenerated cofactor. However, the lower faradaic efficiency (22%) observed might affect the reactants activity over time owing to the likely degradation of the cofactor or the carboxylates.

To conclude, the best strategy for the immobilization of these two enzymes with an accepted faradaic efficiency and a high amplification rates [38,39] and applying a ratio of 5 between them.

V.3.2.2 Towards higher production rate of lactate

An important criterion to address is the production rate of the designed system. For this purpose, it was important to increase the concentration of pyruvate in the initial solution in addition to increased number of enzymes separately immobilized on the CP-MWCNT with the previously optimized ratio (FNR: LDH = 5). Another important point to be investigated is the effect of the enzymes amount on the faradaic efficiency of the overall system. Furthermore, the application of low NAD^+ amounts (10 µM) was targeted for the sake of high TTN levels that can compete with values reported in the literature ($TTN_{NAD(P)} > 2000$)[28,34] and for the possible economic

viability of the process.[28] In addition, the success in the application of such amount of NAD^+ validates the fact that FNR can regenerate NADPH as well as NADH.

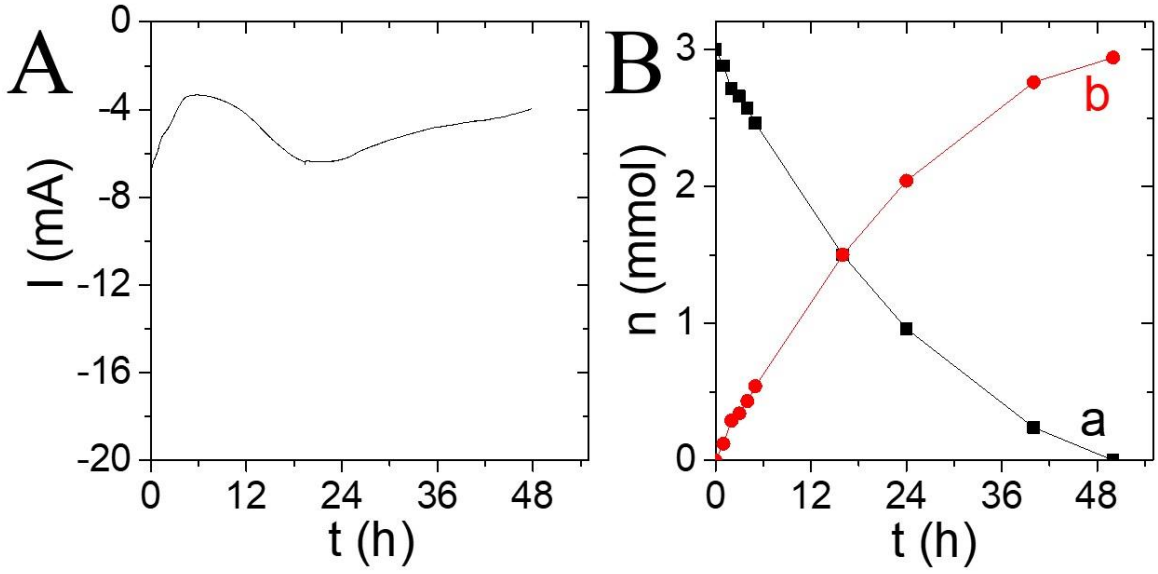

Figure V.7. (A) Variation of the current with time during the electroenzymatic synthesis of lactate at room temperature from 50 mM of pyruvate in 60 mL solution containing 10 µM NAD^+ (and 50 mM TAPS, pH 7.6) in the flow reactor provided with one 50 nmol FNR@CP-MWCNT$_{ox}$ electrode and one 10 nmol LDH@CP-MWCNT (1080 units) layer. (B) Variation of amounts with time of (a) Pyruvate and (b) Lactate, as determined by HPLC.

The bioconversion of 50 mM pyruvate in 60 mL solution containing 10 µM NAD^+ – i.e., 3 mmol pyruvate introduced – in the process described in **Scheme V.1** was carried out potentiostatically at -0.7 V vs ref. (H_2) for 48 hours, with the two enzyme carbon-based layers: 50 nmol FNR@CP-MWCNTox and 10 nmol LDH@CP-MWCNT, i.e., 1080 units LDH.

The bioconversion current was in the order of – 7 mA in the first instants of the run, then gradually decreased (in abs. value) to reach -3 mA after 5 hours (**Figure V.7A**) whereas 20 % of the pyruvate introduced was converted to lactate within this period (**Figure V.7B**). Then, the (absolute) current increased and reached back (- 7 mA) after 24 hours with 2.1 mmol of lactate

produced, i.e., with a 70% conversion extent. Afterward, the current slowly decreased in the second day to reach - 4 mA after 48 hours: 47.5 mM lactate (2.85 mmol) had been produced.

The current of this bioconversion was in the same order of magnitude that the one with the system with far lower amounts of pyruvate and enzymes (**Figure V.6, curves b and c)**. However, the faradaic efficiency obtained for the bioconversion in the presence of 50 nmol of FNR and 10 nmol of LDH, at 68.1 %, was more than 2 times higher than the one observed with 20 nmol FNR and 4 nmol LDH casted separately on CP-MWCNT layers. The low faradaic efficiency obtained previously (**Figure V.6**) may be attributed to non-optimal amounts of enzymes casted on CP-MWCNT layers with too high currents in comparison to the reactant concentrations, thus making the occurrence of side electrode reactions possible.

TTNs of FNR, NAD^+, and LDH were respectively larger than 5.7×10^4, 4750, and 2.8×10^5. A product rate formation of 74 $nmol.cm^{-2}.h^{-1}.nmol^{-1}$ FNR and a turnover frequency (TOF) of 0.32 s^{-1} were calculated at the end of the 48 h-bioconversion. These values are far higher than the values obtained previously with Rh complex system with 9.5 $nmol.cm^{-2}.h^{-1}.nmol^{-1}$ Rh and a TOF near 0.083 s^{-1} . [24]

As a further work in this project regarding the regeneration of the cofactor catalyzed whether by Rh complex (**explored in Chapter VII**) or by FNR (**not explored yet**), platinum will be exchanged by hydrogenase known as an active enzyme for the electrocatalytic oxidation of hydrogen. The activity of hydrogenase is known to be enhanced by temperature.[40,41]

Despite that the temperature chosen in **Chapter VII** is 40 °C, a bioconversion reaction was run at 35 °C because FNR becomes inactive at a temperature higher than 37 °C due to unfolding of the protein and dissociation of the $FADH_2$ cofactor.[42] Not only the activity of FNR increases with temperature (not higher than 37 °C), but also the activity of LDH increases with temperature.[43]

The 48 h-long tests consisted in the treatment of 100 mM pyruvate solution, corresponding to 6 mmol of pyruvate, introduced in two volume fractions at t = 0 (50 mL of 3mmol Pyr) and t = 19 h (10 mL of 3 mmol Pyr) in the flow reactor. The two enzymes casted CP-MWCNT layers were the same as for the run previously described (**Figure V.7**) and the temperature was fixed at 35°C.

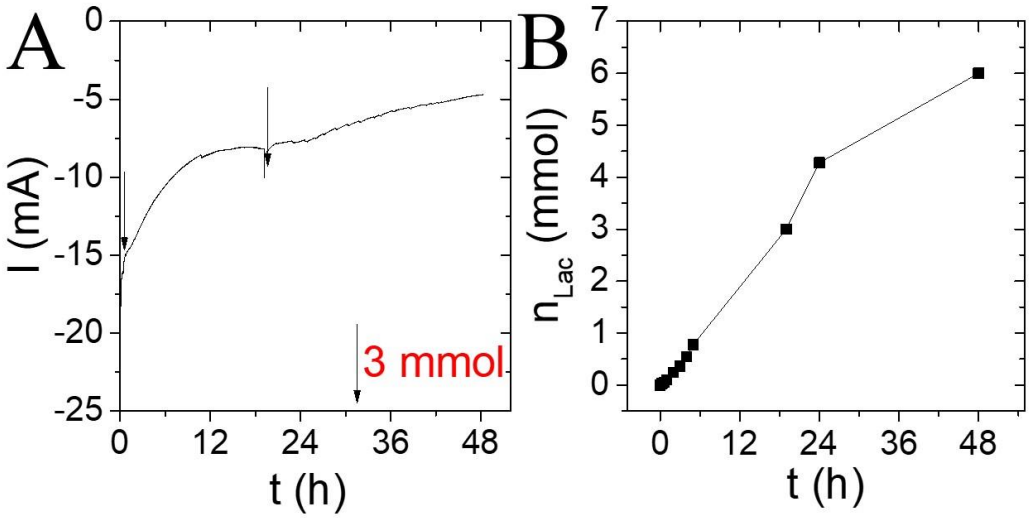

Figure V.8. (A) Variation of sampled currents with time during the electroenzymatic synthesis of lactate at 35 °C from 100 mM of pyruvate in 60 mL solution containing 10 µM NAD^+, 50 mM TAPS, pH 7.6. The solution was introduced in two 50 mL steps at t = 0 h and t = 19 h. The flow reactor was provided with one 50 nmol FNR@CP-$MWCNT_{ox}$ electrode and one 10 nmol LDH@CP-MWCNT (1080 units) layer. (B) Lactate synthetized amount with time as determined by HPLC.

The current recorded starting at approx. -15 mA decreased to – 7.5 mA after 18 hours, whereas the first pyruvate charge introduced could be nearly totally converted to lactate. On average, the current recorded here (**Figure V.8A**) was nearly two times larger than that recorded at ambient temperature (**Figure V.7A**). In the second part of the test, pyruvate conversion was slower (**Figure V.8B**), linked to the lower current in this period. The addition of 3 mmol of pyruvate after 19 hours resulted in a small pulse in the current, which then decreased until the

end of the run (**Figure V. 8B**). The overall faradaic efficiency attained 88 %, to be compared to the 68 % at ambient temperature (**Table V.1**). This result shows that the activity of both FNR and LDH increases with temperature, which enhances the kinetics of the cofactor regeneration as well as the bioconversion of pyruvate. In comparison with the experiment at room temperature, the production rate of lactate at 156 $nmol.h^{-1}.cm^{-2}.nmol^{-1}$ FNR (**table V.1**), was two times larger at 35 °C, in addition to the larger faradaic efficiency.

With the increase in the production rate, TTNs for FNR, NAD^+, and LDH reached a high record with 1.2 x 10^5, 10^4, and 6 x 10^5 respectively. TTN for the cofactor is more than 2 times higher than one obtained at room temperature (**Table V.1**).TTN obtained for FNR and NAD^+ are – to our state of knowledge – the highest value among those reported in the literature.[13,28,34]

Table V.1. Effect of the temperature on pyruvate bioconversion kinetics and on the current efficiency. (*) Current efficiency is for lactate production.

Experiment	T (°C)	Pyruvate at t=0 (mmol)	Lactate (mmol)	t (h)	Production rate ($nmol.h^{-1}.cm^{-2}.nmol^{-1}$FNR)	TTN_{NAD}	(*) Current efficiency (%)
1	20	3	2.85	48	74	4750	68.1
2	35	6	6	48	156	10000	88
3	35	50	45.5	120	113 (*After 24 h*)	9200	81

V.3.2.3 Scale-up and performance

Having a system that confirmed its activity towards the bioconversion of pyruvate with a high faradaic efficiency, it was important to test the possible scaling up of the system by using higher amounts of pyruvate and higher amounts of enzymes loaded on both electrodes surfaces. This has been done in the same reactor, with larger enzymes amounts and larger volumes of solutions to be treated.

Following the optimization applied before *e.g.*, FNR: LDH = 5, immobilization of enzymes on separated supports with a minimized distance between them, at T = 35 °C, and the electrolysis potential (-0.7 V vs ref (H_2), the volume of solution was increased ten times, with an initial volume at 500 mL while 100 mL pyruvate (0.5 M) solution was added in several steps along the 6-day run. (Final volume = 600 mL). The addition steps of pyruvate were planned as follows: (15 mmol – 30 mL at t = 0 h, 15 mmol – 30 mL at t = 24 h, 10 mmol – 20 mL at t = 43 h, 5 mmol – 10 mL at t = 91 h, and 5 mmol – 10 mL at t = 120 h). The amount of drop-casted enzymes was 5-fold increased (250 nmol FNR@CP-MWCNTox and 50 nmol (4200 units) LDH@CP-MWCNT, still in the presence of 10 µM NAD^+.

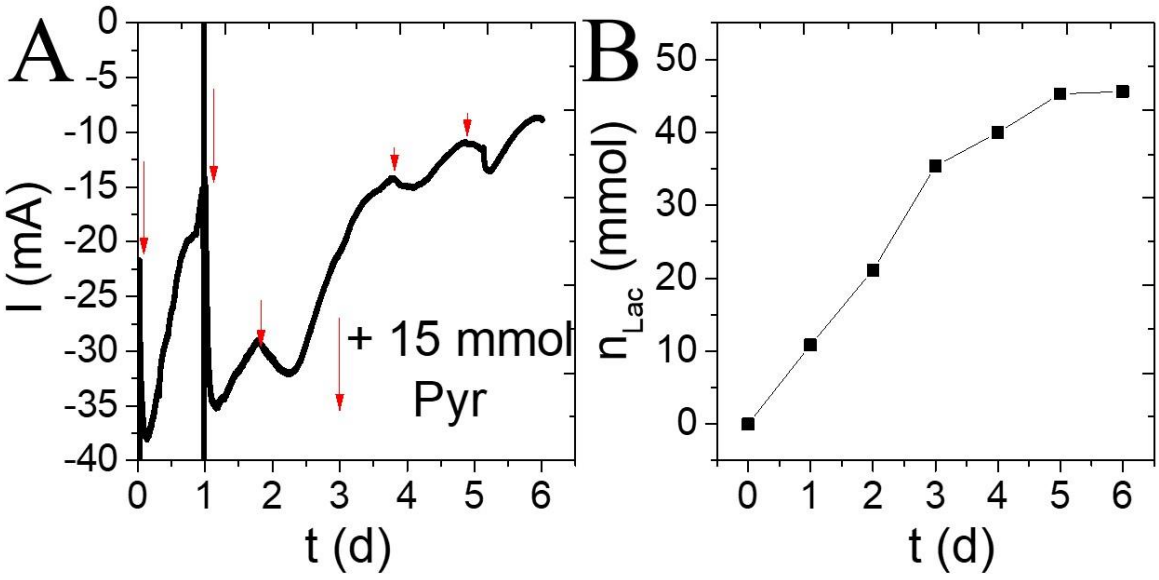

Figure V.9. (A) Variation of sampled currents with time during the electroenzymatic synthesis of lactate at a temperature of 35 °C in 600 mL solution containing 10 µM NAD^+ (and 50 mM TAPS, pH 7.6) in the flow reactor provided with one 250 nmol FNR@CP-$MWCNT_{ox}$ electrode and one 100 nmol LDH@CP-MWCNT layer. (B) Variation of the amount with time of Lactate as determined by HPLC.

The first addition of 15 mmol pyruvate resulted in a rapid increase in the current from -22.5 mA to -37.5 mA (**Figure V. 9A**). Then, the current sharply decreased as the reactant was

depleted: 10.8 mmol of lactate (20.3 mM) were produced within the first 24 hours (**Figure V. 9B**) with a faradaic efficiency of 93 %. The corresponding production rate was found equal to 113 $nmol.h^{-1}.cm^{-2}.nmol^{-1}$ FNR. This value is in the same order of magnitude as the value reported before with the lower volume and catalysts amounts (**Figure V.8; Table V.1 experiment 2**). The continuous addition of pyruvate showed a continuous increase in the bioconversion of pyruvate within the first 5 days. After this time, the bioconversion stabilized at 45.5 mmol of Lac (76 mM) with a faradaic efficiency of 81 % at 120 h (**Figure V.9B; Table V.1 experiment 3**) and TTNs for FNR, NAD^+, and LDH attained 1.82 x 10^5 ,9200, and 9.1 x 10^5 respectively. The TTN for FNR and LDH are higher than those obtained at smaller scale (**Figure V.8**), whereas the TTN for the cofactor (**Experiment 2 and 3 Table V.1**) was in the same order of magnitude.

In order to investigate the cause of the conversion stop after 5 days (120h), the electrocatalytic activity of FNR after 6 days operation was evaluated by cyclic voltammetry under the same conditions (**Figure V.10**).

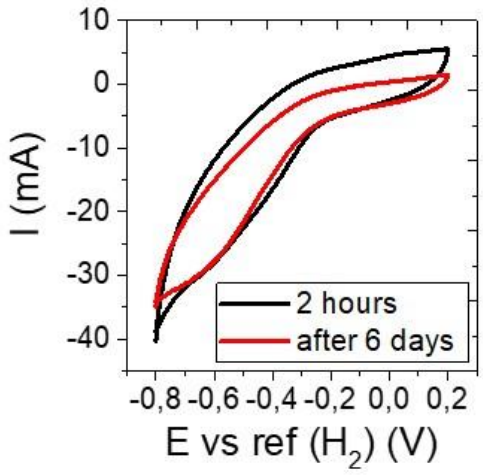

Figure V.10. Evaluation FNR@CP-MWCNTox electrode activity after 2 hours of preparation and 6 days electrolysis in the absence of NAD^+ (0 mM NAD^+). Conditions: 50 mM TAPS (pH =8), Hydrogen and solution flow rates: 20 $mL.min^{-1}$, and scan rate : 5 $mV.s^{-1}$.

Although different, the two voltammograms exhibit comparable profiles and the cathodic current peak at -0.7 V vs ref (H_2), at -31 mA, was almost the same as that measured 2 hours after the electrode preparation. Besides, we noticed that the pH of the solution decreased from 7.6 to 6.9 in the course of the 6-day run. Whereas LDH can remain active for pH near 7.0, FNR is known to require larger pH: therefore, the stop in the conversion could be due to the decay of FNR activity after day 4 with the decrease in pH. In an industrial process, this issue could be avoided with a regular pH control system.

The reported experiments show that FNR immobilized on the oxidized MWCNT keeps its activity over time in the regeneration of 1,4-NADH form required for the bioconversion of pyruvate. Besides, scaling-up the reactor was shown possible with larger amounts of enzymes loaded on the carbon layer surfaces.

V.4 Conclusion

In summary, we have demonstrated in this work a full potential of an electroenzymatic flow reactor that couples efficiently the cofactor regeneration to the oxidation of hydrogen where FNR was immobilized on carbon paper coated with oxidized MWCNT. The prepared electrode of FNR@CP-$MWCNT_{ox}$ has shown its activity with time for more than 6 days under continuous electrolysis and flow.

In addition, in the set of experiments presented, FNR shows its activity not only towards the NADPH cofactor regeneration, but also towards the NADH cofactor which has not been reported in previous works. The electroenzymatic regeneration of NADH by FNR has been coupled to the bioconversion of pyruvate and showed that the active form of NADH has been regenerated (1,4-NADH).

In this work, experimental techniques, namely FNR immobilization on oxidized MWCNT, the immobilization of FNR and LDH on stacked but distinct CP-MWCNT layer, as well as

operating conditions *e.g.*, temperature at 35°C and FNR: LDH ratio near 5, have been largely improved. Under optimal conditions, the bioconversion system of pyruvate to lactate with low amounts of the cofactor (10 µM) has scored high levels of TTNs for FNR, NAD^+, and LDH with 1.2×10^5, 10^4, and 6×10^5 respectively with a faradaic efficiency of 88 % and a productivity of 156 $nmol.h^{-1}.cm^{-2}.nmol^{-1}$ FNR. The scaling up of the system from 60 mL to 600 mL was shown successful with a preserved high productivity level (113 $nmol.h^{-1}.cm^{-2}.nmol^{-1}$ FNR), high levels of TTNs for FNR, NAD^+, and LDH of 1.82×10^5, 9200, and 9.2×10^5 respectively, and the faradaic efficiency of 83 %. This suggests that the linear scaling 5L of solution, for example, might be possible with the application of cascades of electrodes of both FNR@CP-$MWCNT_{ox}$ and LDH@CP-MWCNT supported with high amounts of enzymes.

This idea can be an important milestone for moving from laboratory scale to industrial scale based on several points:

- The ability to control and monitor the process with information gained from the yield and the rate of the reaction.

- The low cost of the material support applied for the immobilization of catalysts in the reactor.

- The low amount of the cofactor applied in the bioconversion (10 µM).

- The easy separation of products after the electroenzymatic process.

- The possibility of application of numerous NAD-dependent dehydrogenase, using one enzymatic reaction or a cascade of enzymatic reactions, for the synthesis of fine chemicals.

Finally, as previously aforementioned, the perspective will be to move to a fully electroenzymatic reactor coupling the oxidation of hydrogen catalyzed by hydrogenase I to the reduction of $NAD(P)^+$ catalyzed by FNR for the biosynthesis of chemicals.

References

[1] S. Broussy, R. W. Cheloha, D. B. Berkowitz, *Org. Lett.* **2009**, *11*, 305–308.

[2] N. J. Turner, *Nat. Chem. Biol.* **2009**, *5*, 567–573.

[3] H. A. Reeve, P. A. Ash, H. Park, A. Huang, M. Posidias, C. Tomlinson, O. Lenz, K. A. Vincent, *Biochem. J.* **2017**, *474*, 215–230.

[4] L. Zhang, M. Etienne, N. Vilà, T. X. H. Le, G.-W. Kohring, A. Walcarius, *ChemCatChem* **2018**, *10*, 4067–4073.

[5] C. F. Megarity, B. Siritanaratkul, B. Cheng, G. Morello, L. Wan, A. J. Sills, R. S. Heath, N. J. Turner, F. A. Armstrong, *ChemCatChem* **2019**, *11*, 5662–5670.

[6] J. B. Jones, D. W. Sneddon, W. Higgins, A. J. Lewis, *J. Chem. Soc. Chem. Commun.* **1972**, 856–857.

[7] G. T. Hçfler, M. Pesic, S. H. Younes, E. Choi, Y. H. Kim, V. B. Urlacher, I. W. C. E. Arends, F. Hollmann, *ChemBioChem* **2018**, *19*, 2344–2347.

[8] C. Virto, I. Svensson, P. Adlercreutz, B. Mattiasson, *Biotechnol. Lett.* **1995**, *17*, 877–882.

[9] B. Siritanaratkul, C. F. Megarity, T. G. Roberts, T. O. M. Samuels, M. Winkler, J. H. Warner, T. Happe, F. A. Armstrong, *Chem. Sci.* **2017**, *8*, 4579–4586.

[10] L. Lauterbach, O. Lenz, K. A. Vincent, **2013**, *280*, 3058–3068.

[11] P. K. Robinson, *Essays Biochem* **2015**, *59*, 1–41.

[12] I. Mazurenko, M. Etienne, G.-W. Kohring, F. Lapicque, A. Walcarius, *Electrochim. Acta* **2016**, *199*, 342–348.

[13] L. Castañeda-Losada, D. Adam, N. Paczia, D. Buesen, F. Steffler, V. Sieber, T. J. Erb,

M. Richter, N. Plumeré, *Angew. Chemie - Int. Ed.* **2021**, *60*, 21056–21061.

[14] H. A. Reeve, L. Lauterbach, O. Lenz, K. A. Vincent, *ChemCatChem* **2015**, *7*, 3480–3487.

[15] B. Siritanaratkul, C. F. Megarity, T. G. Roberts, T. O. M. Samuels, M. Winkler, J. H. Warner, T. Happe, F. A. Armstrong, *Chem. Sci.* **2017**, *8*, 4579–4586.

[16] B. Alkotaini, S. Abdellaoui, K. Hasan, M. Grattieri, T. Quah, R. Cai, M. Yuan, S. D. Minteer, *ACS Sustain. Chem. Eng.* **2018**, *6*, 4909–4915.

[17] A. Heller, *Curr. Opin. Chem. Biol.* **2006**, *10*, 664–672.

[18] R. W. Coughlin, M. Aizawa, B. F. Alexander, M. Charles, *Biotechnol. Bioeng.* **1975**, *17*, 515–526.

[19] S. K. Yoon, E. R. Choban, C. Kane, T. Tzedakis, P. J. A. Kenis, *J. Am. Chem. Soc.* **2005**, *127*, 10466–10467.

[20] W. Liu, P. Wang, *Biotechnol. Adv.* **2007**, *25*, 369–384.

[21] I. Shitanda, S. Kato, Y. Hoshi, M. Itagaki, S. Tsujimura, *Chem. Commun.* **2013**, *49*, 11110–11112.

[22] J. Quinson, R. Hidalgo, P. A. Ash, F. Dillon, N. Grobert, K. A. Vincent, *Faraday Discuss.* **2014**, *172*, 473–496.

[23] D. Holtmann, T. Krieg, L. Getrey, J. Schrader, *Catal. Commun.* **2014**, *51*, 82–85.

[24] W. El Housseini, F. Lapicque, S. Pontvianne, N. Vilà, I. Mazurenko, A. Walcarius, M. Etienne, *ChemElectroChem* **2022**, *9*, e202200463.

[25] G. Kurisu, M. Kusunoki, E. Katoh, T. Yamazaki, K. Teshima, Y. Onda, Y. Kimata-Ariga, T. Hase, *Nat. Struct. Biol.* **2001**, *8*, 117–121.

[26] K. Tagawa, D. I. Arnon, *Nature* **1962**, *195*, 537–543.

[27] T. J. Davies, M. E. Hyde, R. G. Compton, *Angew. Chemie* **2005**, *117*, 5251–5256.

[28] B. Cheng, L. Wan, F. A. Armstrong, *ChemElectroChem* **2020**, *7*, 4672–4678.

[29] R. L. McCreery, *Chem. Rev.* **2008**, *108*, 2646–2687.

[30] I. A. Safo, F. Liu, K. Xie, W. Xia, *Mater. Chem. Phys.* **2018**, *214*, 472–481.

[31] C. F. Megarity, B. Siritanaratkul, R. S. Heath, L. Wan, G. Morello, S. R. FitzPatrick, R. L. Booth, A. J. Sills, A. W. Robertson, J. H. Warner, N. J. Turner, F. A. Armstrong, *Angew. Chemie - Int. Ed.* **2019**, *58*, 4948–4952.

[32] X. Wang, T. Saba, H. H. P. Yiu, R. F. Howe, J. A. Anderson, J. Shi, *Chem* **2017**, *2*, 621–654.

[33] B. Siritanaratkul, C. F. Megarity, T. G. Roberts, T. O. M. Samuels, M. Winkler, J. H. Warner, T. Happe, F. A. Armstrong, *Chem. Sci.* **2017**, *8*, 4579–4586.

[34] X. Zhao, S. E. Cleary, C. Zor, N. Grobert, H. A. Reeve, K. A. Vincent, *Chem. Sci.* **2021**, *12*, 8105–8114.

[35] J. a Cracknell, K. a Vincent, F. a Armstrong, *Chem. Rev.* **2008**, *108*, 2439–61.

[36] M. Shin, in *Methods Enzymol.*, Elsevier, **1971**, pp. 440–447.

[37] T. Saba, J. Li, J. W. H. Burnett, R. F. Howe, P. N. Kechagiopoulos, X. Wang, *ACS Catal.* **2020**, *11*, 283–289.

[38] J. M. Limoges, B., Marchal, D., Mavré, F., & Savéant, *J. Am. Chem. Soc.* **2006**, *128*, 2084–2092.

[39] J. M. Limoges, B., Marchal, D., Mavré, F., & Savéant, *J. Am. Chem. Soc.* **2006**, *128*,

6014–6015.

[40] K. Monsalve, I. Mazurenko, C. Gutierrez-Sanchez, M. Ilbert, P. Infossi, S. Frielingsdorf, M. T. Giudici-Orticoni, O. Lenz, E. Lojou, *ChemElectroChem* **2016**, *3*, 2179–2188.

[41] I. Mazurenko, R. Clément, D. Byrne-Kodjabachian, A. de Poulpiquet, S. Tsujimura, E. Lojou, *J. Electroanal. Chem.* **2018**, *812*, 221–226.

[42] J. T. Jarrett, J. T. Wan, *FEBS Lett.* **2002**, *529*, 237–242.

[43] S. N. Buhl, K. Y. Jackson, R. E. Vanderlinde, *Clin. Chim. Acta* **1977**, *80*, 265–270.

[44] P. Schenk, S. Baumann, R. Mattes, H. Steinbiss, *Biotechniques* **1995**, *200*, 196–200.

Objective of the study in Chapter VI

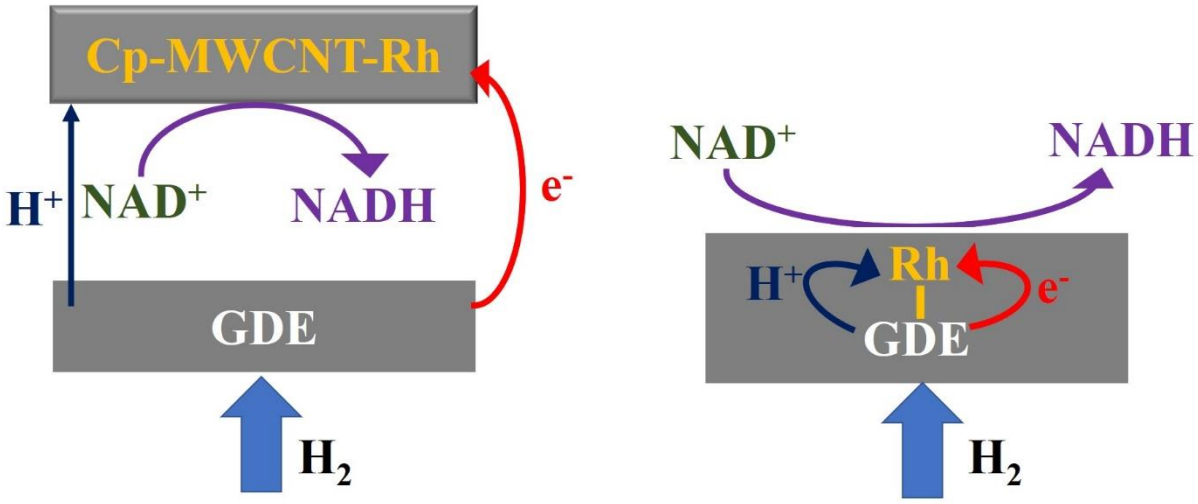

Schematic representation of possible approaches investigated for coupling H_2 oxidation to NAD^+ reduction

After proving the activity and the stability of both Rh complex and FNR towards the regeneration of NADH coupled to the oxidation of hydrogen, the idea was oriented toward coupling of hydrogen oxidation to NADH regeneration in an electroless system, i.e., no power consumption or production. Having that the regeneration of NADH catalyzed by Rh complex and FNR occurs at -0.3 V vs ref (H_2) and -0.7 V vs ref (H_2), Rh complex was selected in this study. Two approaches were investigated to couple the oxidation of hydrogen to the regeneration of NADH: the first approach relied on the presence of both catalysts on the same electrode, while the second one relied on the immobilization of each catalyst on a separate electrode. By coupling the regeneration of NADH to the bioconversion of pyruvate via lactate dehydrogenase catalysis, the activity of regenerated NADH was determined.

Chapter VI. A bioelectrode architecture for coupling H_2 oxidation to 1,4-NADH regeneration in a flow electrochemical bioreactor operated in an overall electroless mode

Abstract

We describe in this work a new modular approach to couple hydrogen oxidation to NADH regeneration using redox Rh complex in an overall electrodeless system. Coupling the two reactions catalyzed by chemical catalysts was carried out either on the same electrode (Pt-Rh) or on separate electrodes using a plastic grid separator acting as a spacer allowing minimized distance between the two catalysts. Both approaches were explored in a flow reactor demonstrated as a strategy for process intensification. Using know-how reported previously such as pH (7.2) and immobilization technique of Rh complex on a carbon paper coated with MWCNT (Rh@CP-MWCNT), regeneration of NADH was achieved on the single electrode and separately, after optimization of Rh complex and Pt amounts with 2.07 nmol active Rh complex per mg Pt, and forcing the pH of the anode compartment to 7.2 as in the cathode chamber. Testing the NADH regenerated under the above conditions towards pyruvate bioconversion by lactate dehydrogenase, showed that NADH regenerated via the separate process is fully active (1,4-NADH) with a total bioconversion. However, NADH regenerated on the single Pt-Rh electrode is not enzymatically active.

VI.1 Introduction

Although the direct electron transfer to oxidoreductase immobilized on a bound electrode for the biosynthesis of pure chemicals was explored for the bioconversion of CO_2 to formate,[1] by formate dehydrogenase immobilized on polyaniline in a NADH-free process, NAD cofactors are still essential redox agents for almost 80 % of oxidoreductases applied for biosynthesis of chemicals.[2,3] The reduced active form of the cofactor (1,4-NADH) involved in the enzymatic reduction is the most crucial ingredient of the redox reaction.[4] Therefore, its efficient regeneration is important for industrial and economic concerns.[5] Different strategies for the regeneration of the cofactor have been explored e.g., chemical, photochemical, enzymatic, and electrochemical techniques. [6–8]

Among all cofactor regeneration techniques cited above, the electrochemical regeneration of NADH is a promising technique due to the control of the reaction via the electrode potential and the low cost of electricity.[2] The direct regeneration of the cofactor on an electrode surface is poorly efficient because the radicals generated are prone to combine and react to form inactive NAD_2 dimers.[9] Therefore, the modification of the electrode surface with a catalyst able to transfer 2 electrons in one step and with a reduction potential lower than that of the cofactor is required to generate 1,4-NADH. Rhodium complex catalysts, particularly those containing Cp* ligand, respond to these criteria.[10,11] In order to simplify the product purification step after the cofactor regeneration, several methods can be used to immobilize Rh complex on electrodes surface.[12–16]

Despite the benefit exploited while proving the indirect electrochemical regeneration of NADH mediated by Rh complex in terms of regeneration of the cofactor active form with remarkable levels of TTNs,[13,15] most electrochemical process only exploit one of the two half-reactions to afford the desired product,1,4-NADH, while the other side undergoes a redox process of electrolyte. Here, we propose to couple the oxidation of hydrogen at the anode with no

production of toxic hazardous to the reduction NAD^+ mediated by the Rh complex at the cathode in an overall electroless mode, i.e. operated without a power supply.

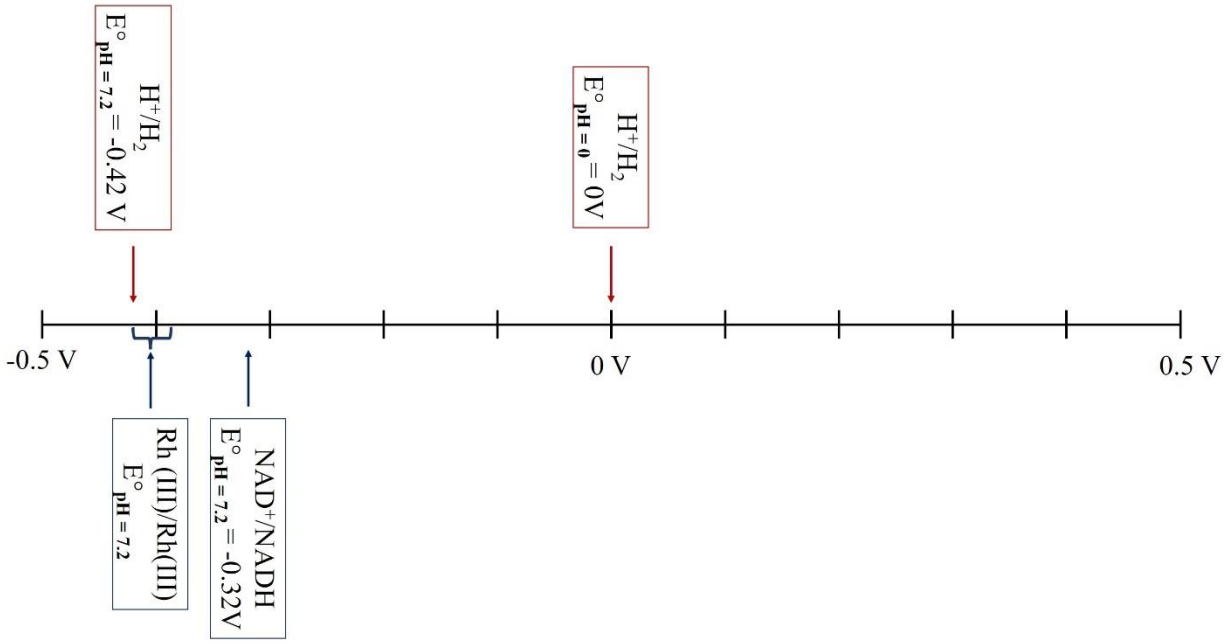

Scheme VI.1. Thermodynamic context for coupling H_2 oxidation to NAD^+ reduction mediated by Rh complex.

While the standard potentials of hydrogen oxidation and the reduction Rh complex at 7.2 differ by less than 80 mV as shown in **Scheme VI.1**, we explored the possible coupling between these two redox reactions. This coupling should be possible with the aid of favorable interaction between the two redox centers allowing the efficient channeling of protons and electrons to Rh complex.

Coupling the oxidation of hydrogen to the reduction of NAD^+ catalyzed respectively by hydrogenase and NAD^+ reductase has been explored by Vincent and co-workers. [17,18] The studied approach is based on the immobilization of hydrogenase and NAD^+ reductase on the same carbon electroactive surface. The same hypothesis has been followed here by replacing electroenzymatic catalysts by chemical ones, namely platinum and rhodium complex. On the other hand, we thought about not to combine the catalysts but to immobilize each catalyst on carbon-based layers. This would be a new modular framework for coupling efficiently

hydrogen oxidation to NAD^+ reduction. The idea is not to produce energy but to couple efficiently the oxidation of hydrogen to the reduction of NAD^+ with a sufficient reaction rate. For enhanced mass transfer phenomena between the reactants and the immobilized catalysts, in addition to channeling of protons and electrons, the two reactions were performed in flow processes instead of batch processes.[19,20]

In previous works, the regeneration of the NADH mediated by a rhodium complex in the cathodic compartment was coupled to the oxidation of hydrogen in a flow electrochemical reactor. Anodic and cathodic compartments were separated with a Nafion membrane. First, hydrogen and solution flow rates were optimized for the case of dissolved Rh complex.[21] Then, the Rh complex was immobilized on a carbon paper (CP) coated with MWCNT following a formerly reported protocol.[13] The immobilized rhodium complex has shown its activity and stability for more than 5 days and the mediated regeneration of NADH at -0.3 V vs ref (H_2) proved effective as demonstrated by in-situ pyruvate reduction tests upon lactate dehydrogenase.[16]

In this work, coupling of hydrogen oxidation to NADH regeneration in an overall electroless system i.e., involving no power consumption or production, was explored based on two different approaches. The first one relied on the presence of the two catalysts on the same electrode whereas the second was based on immobilization of the two catalysts on separate electrodes. The two configurations were tested in a 16 cm^2 flow reactor. The activity of regenerated NADH was assessed by coupling to the bioconversion of pyruvate using lactate dehydrogenase catalysis.

VI.2 Materials and methods

VI.2.1 Chemical and reagents

β-nicotinamide adenine dinucleotide (NAD^+, >98%) and β-nicotinamide adenine dinucleotide reduced dipotassium salt (NADH, >97%), $(RhCp^*Cl_2)_2$ (97 %), dichloromethane DCM (98 %), sodium nitrite (97 %), 2,2-bipyridine (98 %), 4-azidoaniline hydrochloride (98 %), K_2HPO_4 (99%), KH_2PO_4 (99%), HCl (37 %), L-lactic dehydrogenase (LDH) from bovine heart (≥ 250 units/mg protein, 144,000 Da.), pyruvate (98 %) and lactate (98 %), were from Sigma-Aldrich. Phosphate buffer (50 mM) was used to investigate the electrocatalytic properties of the rhodium complex towards NAD^+ reduction and was reported to be the most appropriate for such experiments. Multi-walled carbon nanotubes (MWCNT, NC7000™ series) were from Nanocyl (Belgium). Gas diffusion layers (GDL 28BC), gas diffusion electrodes (GDE), Nafion solution (5 %), and carbon papers (SpectraCarb 2050L-0550 Carbon Paper) were acquired from Fuel Cell Store (USA). MWCNT were dispersed in a solution of ethanol (96 %). All solutions were prepared with high purity water (18 MΩ cm) from a Purelab Option water purification system.

VI.2.2 Carbon paper with MWCNT (CP-MWCNT) preparation

The preparation of a CP-MWCNT was reported in our previous work.[16]

The preparation of CP-$MWCNT_N$ (N: Nafion) was proceeded by adding 500 µL of a Nafion solution (5%) to the suspension of MWCNT in ethanol. The suspension (10 mg MWCNT, 50 mL ethanol, and 500 µL Nafion solution 5 %) was then filtered on a 16 cm^2 carbon paper after being sonicated for 5 hours. The coated CP layer was then allowed to dry overnight.

VI.2.3 CP-MWCNT functionalization with $[Cp * Rh(bpy)Cl]^+$

The carbon support was functionalized following a reported protocol by mixing 4-amino-2,2-bipyridine and 2 mM sodium nitrite in 0.5 M HCl in order to generate 2,2-bipyridyl diazonium cations. Cyclic voltammetry was then conducted between 0.4 V and -0.8 V (vs Ag/AgCl (3M)) at a scan rate of 20 mV/s. The electrode was then rinsed with ultra-pure water and left to dry.

Functionalized electrode with 2,2-bipyridine moieties was then placed into a solution of DCM containing 0.15 mM of $((RhCp^*Cl_2)_2$ for 4 h.

VI.2.4 Enzymatic carbon paper with MWCNT (CP-MWCNT-LDH) preparation

CP-MWCNT was prepared following a work reported previously by drop-casting 50 µL suspension of LDH on a CP-MWCNT and keeping for 2 hours at a temperature of 3°C.

VI.2.5 Zero resistance amperometry (ZRA) technique for testing of coupling hydrogen oxidation to NAD^+ reduction

To simultaneously measure short circuit current and mixed potential, Zero Resistance Amperometry (ZRA) was utilized. ZRA is typically employed in corrosion studies to measure small fluctuations in corrosion current and potential at the metal-solution interface that originate from pitting on the corroding metal at E_{OCP}. It combines electrochemical potential noise and electrochemical current noise measurement. Technically, no noise is measured in the cell containing a solution of phosphate buffer and NAD^+, but this technique allows for the application of zero volts between the anodic and cathodic parts. To be applied in NADH regeneration system, a GDE was used as counter electrode, Rh@CP-MWCNT was used as working electrode, and Ag/AgCl (3M) was used as reference electrode. By measuring the current between these two components and the direction of electron flow with Electrochemical noise (ECN), coupling hydrogen oxidation to NAD^+ reduction is directly confirmed. As the

system is in short circuit, it is also possible to measure the mixed potential against a reference electrode.

Experiments were carried out in a glassy cell containing 5 mL of buffered solution with various amounts of NAD^+. The solution was continuously bubbled with hydrogen at 20 $mL.min^{-1}$.

The solution was sampled at several intervals and the conversion of NAD^+ to NADH was followed by UV adsorption at 340 nm.

VI.2.6 Reactor with separated compartments for NADH regeneration (Scheme VI. 1)

The flow reactor in this section is an update of the reactor used previously.[16,21] The 50 mM phosphate buffer solution (pH = 7.2) in the presence or the absence of NAD^+, was degassed with nitrogen 20 min before and during the tests. Hydrogen is introduced to the anodic compartment through the grooved bipolar plate on which a gas diffusion electrode with Pt at 0.5 or 2 $mg.cm^{-2}$ was installed. On the top of the GDE, a graphite felt electrode is placed for solution circulation, in order to maintain a pH of 7.2 at the anode. The solution fed to the anodic compartment leaves to the cathodic compartment at 20 $mL.min^{-1}$. The cathodic compartment contains the Rh@CP-MWCNT electrode placed on the top of a polymeric grid separator between both compartments used here instead of a Nafion membrane in order to decrease the resistance of the system. A graphite felt electrode is also placed in the cathodic compartment for uniform distribution of the solution. Both compartments and the separator are sandwiched between polymeric plates to prevent the solution leakage. CV tests at 5 $mV.s^{-1}$ and electrolysis test were carried out in a two-electrode configuration where the anode acted as reference. Finally, samples of the electrolytic solution were analyzed with UV-visible at 340 nm.

VI.2.7 Enzymatic cell

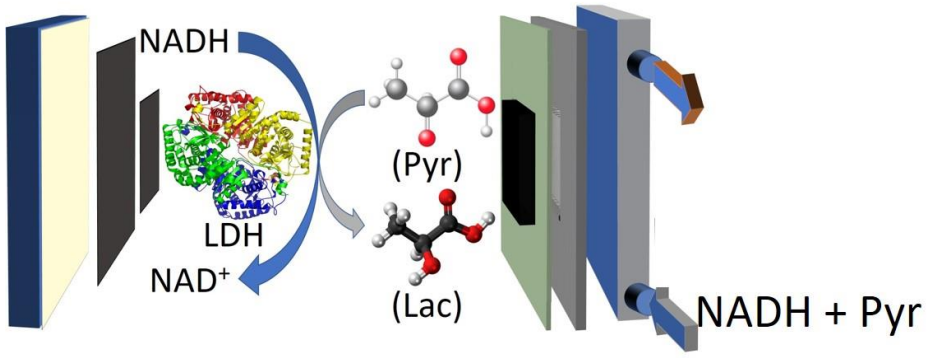

Scheme VI.2. Schematic draw of the enzymatic cell

Testing the activity of regenerated NADH was performed in an enzymatic cell that was previously described.[21] The solution containing regenerated NADH was fed to the enzymatic cell composed of a 16 cm² LDH@CP-MWCNT (6.6 nmol LDH) with a graphite felt electrode on its top for the uniform distribution of solution. The solution leaves the cell to the glass storage provided with nitrogen sparging before being pumped to the cell. The other side of the cell was sealed with parafilm to prevent evaporation, and the cell was stacked between two polymeric plates for mechanical cohesion.

VI.3 Results

VI.3.1 Preliminary investigations

In order to evaluate the possibility to couple hydrogen oxidation to NADH regeneration, it was important to test both catalysts separately. For this purpose, the Rh complex was immobilized on a CP coated with MWCNT, known as conducting material,[22] as successfully made in previous works [13,16] and platinum was tested first with a gas diffusion electrode (0.2 mg $Pt.cm^{-2}$).Both electrodes had a geometric surface area of 0.25 cm² (0.5 cm x 0.5 cm). Each electrode was studied in an electrochemical cell provided with a Pt counter-electrode and a Ag-AgCl (3M) reference electrode. Solutions were deaerated in all tests reported here.

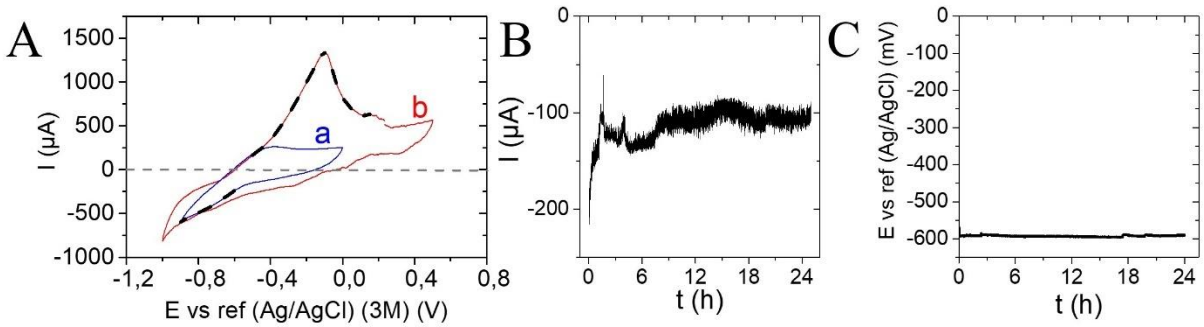

Figure VI.1. (A) Superimposition of the two CV curves of (a) Rh@CP-MWCNT and (b) pt@GDE under H_2 and in the absence of NAD^+. Conditions: Hydrogen flow rates: 20 mL.min-1; 50 mM PBS (pH = 7.2); Scan rate : 5 $mV.s^{-1}$; V = 5 mL. (B) Current and (C) potential recorded from ZRA analysis under H_2 after the addition of 1 mM of NAD^+. WE: Rh@CP-MWCNT, CE: Pt@GDE, ref : Ag/AgCl (3M), 50 mM PBS (pH = 7.2),V = 5 mL.

The electrocatalytic activity of Rh@CP-MWCNT was evaluated through cyclic voltammetry at 5 $mV.s^{-1}$ (**Figure VI.1A**). CV curve shows the onset of the Rh complex reduction at -0.55 V vs ref (Ag/AgCl (3M)) (**Figure VI.1A curve a**) and a reduction peak at -0.7 V vs ref in consistence with what was previously obtained.[13] The current at this peak was near 300 µA (1.2 mA cm^{-2}).

On the other hand, after hydrogen bubbling for 20 minutes, the GDE electrode exhibited an electrocatalytic activity (**Figure VI.1A curve b**) in the reverse scan related to the oxidation of hydrogen, starting at -0.6 V vs ref and attaining its oxidation peak at -0.2 V vs ref (Ag/AgCl (3M)) with a current of 1.1 mA (4.4 $mA.cm^{-2}$).

Superimposition of the two voltammograms, Rh@CP-MWCNT (**Figure VI. 1A curve a**) and GDE (**Figure VI. 1A curve b**), shows that coupling the oxidation of hydrogen to the reduction of the rhodium complex would be possible since H_2 oxidation starts at -0.6 V vs ref (Ag/AgCl (3M)) and the potential window for Rh (III) reduction to Rh (I) lies between -0.55 V and -0.6 V vs ref. as better visualized with the dotted grey line for the zero current axis.

Interestingly, zero-resistance amperometry (ZRA) of the system with the two electrodes short-circuited, was applied in the cell where the Rh@CP-MWCNT acted as working electrode and the GDE as counter electrode, with the reference electrode (Ag/AgCl (3M)). The distance between the two electrodes was kept at 0.2 mm by fixing them on the two faces of a piece of polymeric grid. The current noise of the system is equal to the current between the working and the counter electrode. The reduction current after the addition of 1 mM of NAD^+ fluctuated from -125 µA to -100 µA (**Figure VI. 1B**). As the system is in short circuit, it is also possible to measure the mixed potential against the reference electrode (Ag/AgCl (3M)). The mixed of the system was equal to -580 mV vs ref Ag/AgCl (3M) which correspond to the potential window at which occurs both the oxidation of hydrogen and the reduction of Rh(III) to Rh (I). After 24 hours of ZRA operation, 875 µM of NADH were regenerated under continuous bubbling of hydrogen, as revealed by UV-analysis at 340 nm. Thus, coupling hydrogen oxidation to the regeneration of the NADH mediated by the rhodium complex appears possible.

In order to enhance the kinetics of electrons and protons transport, several techniques can be employed such as fabrication of membranes with composite MWCNT-ionomer membrane for protons and electron conduction,[23] development of a membraneless system in biofuel cells for improving their activity and decreasing the system resistivity,[24] or immobilization of catalysts for both oxidation and reduction on the same electrode coated by carbon nanoparticles.[17,18,25] In addition, working under flow conditions would increase mass transport between species as well as protons and electrons. The study was first initiated in the flow reactor previously used[16] with further optimizations in pH and catalysts amounts.

VI.3.2 NADH regeneration in the flow reactor with separation between GDE and CP-MWCNT

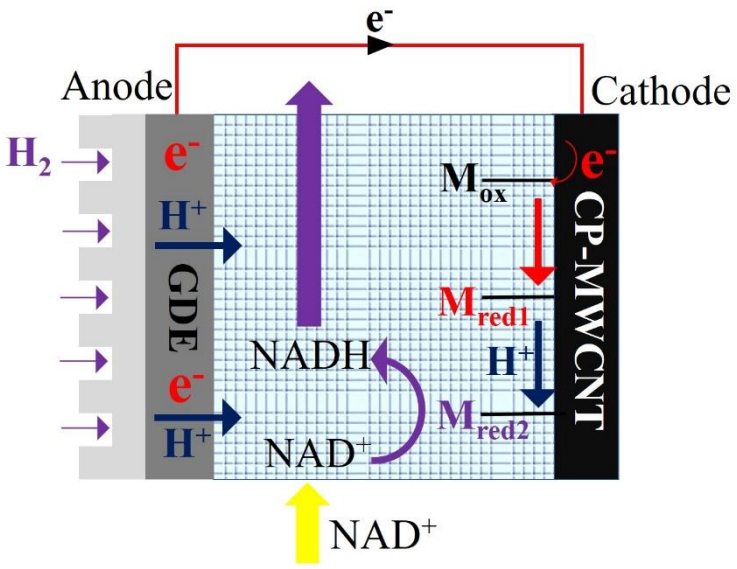

Scheme VI.3. Schematic view of the flow electrochemical reactor. (M): Rh complex.

The separation of the catalyst layers was allowed by a polymeric separator (**Scheme VI.3**). The NAD^+ phosphate buffered solution percolated between the anodic and the cathodic compartment as indicated in **Scheme VI.3**. This flow configuration allowed the pH to be maintained at 7.2 in the two compartments. The regeneration of NADH involves a $2e^-$ resulting from hydrogen oxidation and leading to the reduction of Rh complex (III) ($\mathbf{M_{ox}}$) to Rh complex (I) ($\mathbf{M_{red1}}$) which will be transformed to a Rh hydride complex upon protonation ($\mathbf{M_{red2}}$). $\mathbf{M_{red2}}$ will be then likely able to transfer its hydride to NAD^+ flowing between both compartments to regenerate 1,4-NADH.

The electrocatalytic activity of Rh@CP-MWCNT electrode was evaluated by cyclic voltammetry at 5 $mV.s^{-1}$ and with hydrogen and solution flow rate of 20 $mL.min^{-1}$. With a Rh@CP-MWCNT (16.6 nmol of Rh complex) and a GDE (2 $mg.cm^{-2}$) each of them with an area of 4 cm^2 (**Figure VI. 2A**), the Rh complex shows an electrocatalytic activity featured by an onset of current at 0.03 V vs ref (H_2) and its 600 µA peak at -0.025 V vs ref (H_2) (**Figure**

VI.2A curve a). To confirm that the peak observed was related to the Rh complex reduction, the addition of 2 mM of NAD^+ was accompanied by an increase in the cathodic current related to the activity of Rh complex towards NAD^+ (**Figure VI.2A curve b**). In the presence of NAD^+, the reduction peak was shifted to -0.13 V vs ref (H_2), i.e., nearly 100 mV more cathodic than without NAD^+, whereas the onset of current was not visibly changed.

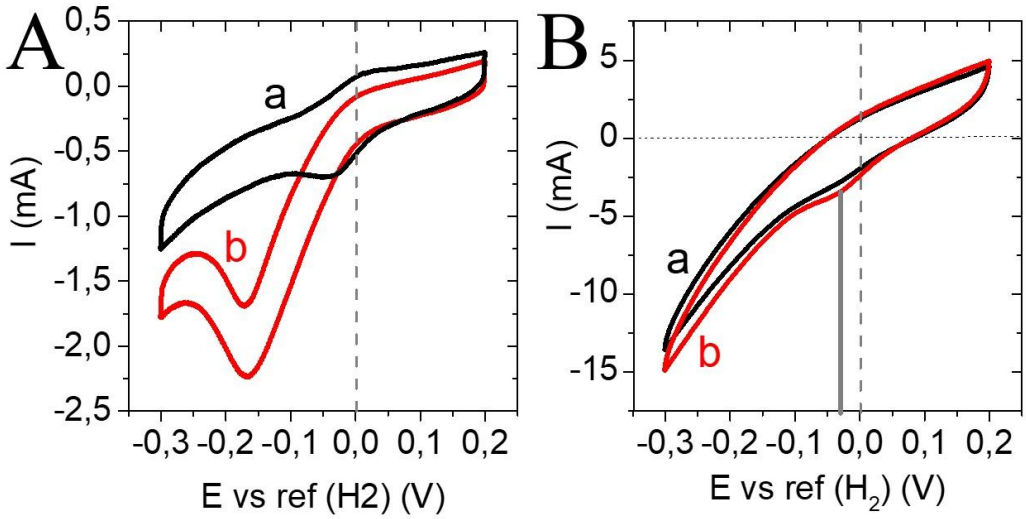

Figure VI.2. (A) Cyclic voltammograms recorded at 5 $mV.s^{-1}$ using a 4 cm^2 Rh@CP-MWCNT electrode and 4 cm^2 GDE (2 $mg.cm^{-2}$), as anode and reference, and in the presence of (a) 0 mM and (b) 2 mM NAD^+. (B) Cyclic voltammograms recorded at 5 $mV.s^{-1}$ using a 16 cm^2 Rh@CP-MWCNT electrode and 16 cm^2 GDE (2 $mg.cm^{-2}$) and in the presence of (a) 0 mM and (b) 0.5 mM NAD^+. pH at the anodic and cathodic compartments is equal to 7.2; hydrogen and solution flow rates are at 20 $mL.min^{-1}$.

To confirm the above observation and investigate possible scale-up of the electrodes, similar tests were carried out with 16 cm^2 electrodes. Comparable observations were made, with 1.1 mA Rh reduction shouldering peak at -0.026 V without NAD^+ (**Figure VI.2B curve a**). Addition of 0.5 mM of NAD^+ induced a 500 µA increase in the reduction current peak (**Figure VI.2B curve b**) but without a shift in the potential as observed before (**Figure VI.2A curve b**).

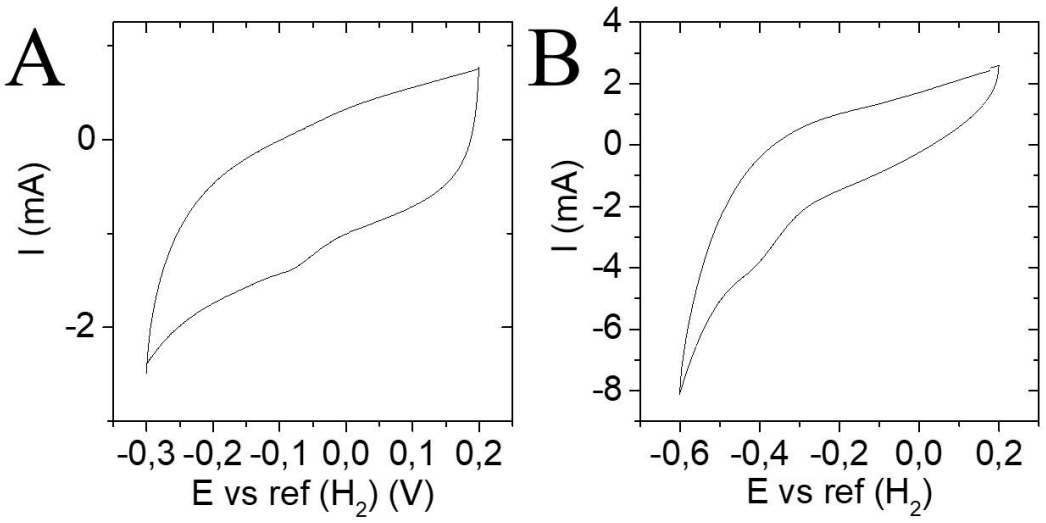

Figure VI.3. (A) Effect of Pt amount on Rh complex reduction potential: Cyclic voltammograms recorded at 5 $mV.s^{-1}$ using a 16 cm^2 Rh@CP-MWCNT electrode and 16 cm^2 GDE (0.5 $mg.cm^{-2}$) in the absence of NAD^+. pH at the anodic and cathodic compartments is equal to 7.2. (B) effect of anode pH (pH= 3.6) on the reduction of Rh complex: Cyclic voltammograms recorded at 5 $mV.s^{-1}$ using a 16 cm^2 Rh@CP-MWCNT electrode and 16 cm^2 GDE (0.5 $mg.cm^{-2}$) and in the absence of NAD^+. In all cases, hydrogen and solution flow rates are equal to 20 $mL.min^{-1}$.

The effect of the Pt charge in the GDE was studied by testing 0.5 mg $Pt.cm^{-2}$ GDE (8.34 nmol Rh complex/mg Pt) instead of 2 mg $Pt.cm^{-2}$ GDE (2.07 nmol Rh complex/mg Pt). All other operation conditions were kept unchanged, in particular the same pH,7.2, in anode and cathode compartments **(Scheme VI.3).** The CV curves recorded exhibited a slight shift in the reduction onset, at -0.03 V and the reduction peak was at -0.09 V (**Figure VI.3A**). Besides, while being in contact with Nafion membrane, the pH in the anodic compartment is in the order of 3.6 if non-humidified H_2 is fed.[26]. Such conditions were tested in **Chapter IV** with an anodic GDE at 0.2 mg $Pt.cm^{-2}$ with a comparable 16 cm^2 Rh@CP-MWCNT cathode. The current of Rh complex reduction started at -0.29 V vs ref (H_2) and the shouldering peak near -0.36 V vs ref (H_2) (**Figure VI.3B**). i.e., approx. 300 mV more negative than obtained with pH 7.2 in the two cell compartments (**Figure VI.3A**). The negative shift can be qualitatively linked to the

decreased pH at the anode according Nernst law. The location of the reduction peak renders here impossible any operation at open circuit voltage.

The above two tests in **Figure VI.3** showed that coupling the oxidation of hydrogen to the reduction of Rh complex in an overall electroless mode is possible at pH of 7.2 at both compartments with a ratio 2.07 nmol of active Rh complex/mg of Pt.

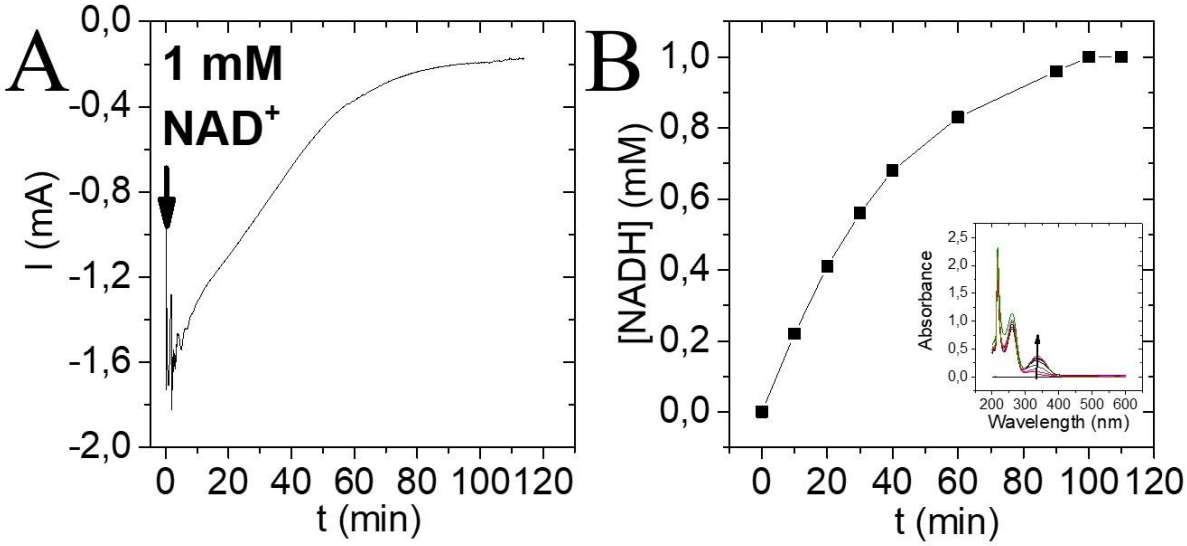

Figure VI.4. (A) Current recorded and (B) NADH regeneration kinetics at open circuit voltage carried out at 0 V vs ref (H_2). Conditions: 16 cm² GDE (2 mg.cm^{-2}) and Rh@CP-MWCNT (0.023 mg active Rh complex) , pH at anodic and cathodic compartments is equal to 7.2 (50 mM phosphate buffer), [NAD_+] = 1 mM , V = 40 mL, and hydrogen and solution flow rates are equal to 20 mL.min^{-1}.

For the studied system in **Scheme VI.3** and following a ratio of 2.07 nmol of active Rh complex /mg of Pt, the open circuit voltage was found slightly positive (95 mV). NADH regeneration was carried out at zero cell voltage versus ref (H_2) (**Figure VI.4A**). After the addition of 1 mM of NAD^+, the current increased rapidly to -1.6 mA expressing the cathodic reduction of Rh complex towards NADH regeneration. Then, the current decreased gradually and depleted to nearly -200 µA after 110 min corresponding to the end of electrolysis with the total regeneration

of NADH assayed by absorption at 340 nm (**Figure VI.4B**). For the first minutes of the NADH regeneration, the production rate attained 0.05 µmol. $min^{-1}.cm^{-2}$, with a current near 80 µA.cm^{-2} which is at an appreciable level for such process conducted at 0 V versus ref (H_2).

Regenerated NADH was coupled to the bioconversion of 1 mM of pyruvate in the presence of 6.6 nmol of LDH immobilized on CP-MWCNT following **the protocol in VI.2.7.** The bioconversion of pyruvate to lactate was carried out in 40 mL buffered solution (50 mM PBS; pH = 7.2) and in the presence of 1 mM of NAD^+ and 1 mM of pyruvate.

Forty minutes later, the whole NADH was oxidized indicating its consumption by the enzymatic desired reaction. Thus, NADH regenerated at 0 V appears to be in its active form (1,4-NADH).

VI.3.3 Coupling hydrogen oxidation to NADH regeneration on the same electrode

Another strategy for coupling hydrogen oxidation to NADH regeneration is their immobilization on the same electrode,[17] we studied the possible regeneration of NADH on an electrode containing platinum for hydrogen oxidation and rhodium complex for NADH regeneration. The motivation behind this study is that the immobilization of the rhodium complex on a surface covered with platinum was reported to boost the regeneration of NADH under nitrogen atmosphere at -0.8 V vs Ag/AgCl (3M).[27] Despite the positive results towards NADH regeneration, regenerated NADH was inactive while being coupled to a NADH-dependent reaction (pyruvate bioconversion by LDH).

Experiments in batch reactor

Rh complex covalent immobilization was carried out on a 0.25 cm^2 (0.5 cm x 0.5 cm) gas diffusion electrode covered with platinum nanoparticles (0.2 mg $Pt.cm^{-2}$). GDE functionalization with 2,2-bipyridine moieties was then proceeded by running 3 cyclic voltammograms between 0.4 V and -0.8 V vs Ag/AgCl (3M) at 20 mV/s (**Figure VI.5A**) in an

acidic aqueous solution containing 1mM of 4-amino-2,2-bipyridine and 2 mM of sodium nitrite.[13]

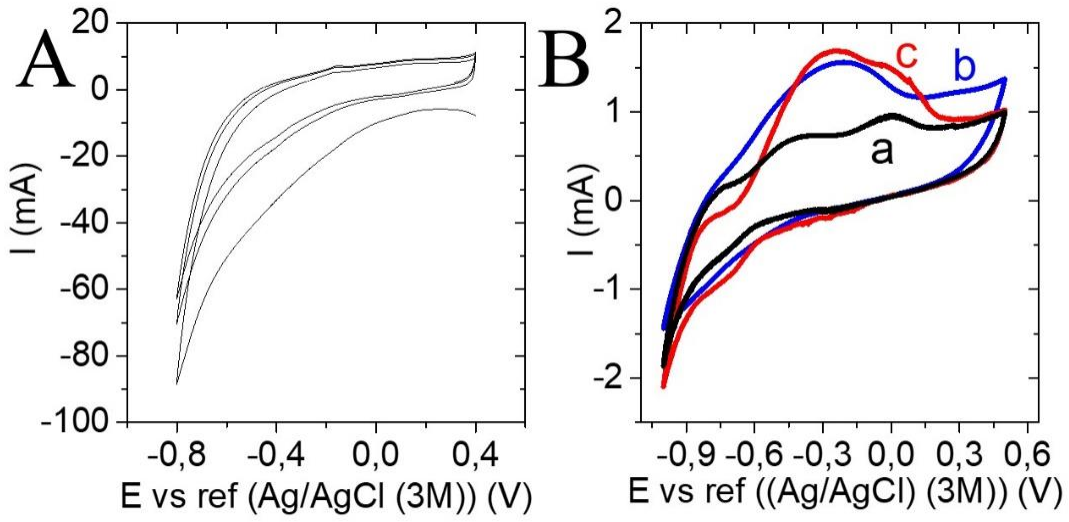

Figure VI.5. (A) Cyclic voltammograms for the reduction of diazonium cations generated 'in situ' from 1 mM 4-amino-2,2'-bipyridine and 2 mM $NaNO_2$ in 0.5 M HCl, as recorded on the GDE electrode at 20 $mV.s^{-1}$. (B)Cyclic voltammograms recorded at 5 $mV.s^{-1}$ using a Rh@ GDE electrode in 50 mM PBS buffer at pH 7.2 under (a) nitrogen and (b-c) hydrogen and in the presence of (b) 0 mM NAD^+ and (c) 0.5 mM NAD^+. The geometric surface area of the electrode is 0.25 cm^2 and hydrogen and nitrogen flow rates are equal to 20 $mL.min^{-1}$.

The electrocatalytic activity of Rh@GDE was evaluated by cyclic voltammetry at 5 $mV.s^{-1}$. In the presence of nitrogen, Rh@GDE shows oxidation and reduction currents starting at -0.59 V and -0.64 V respectively (**Figure VI.5B curve a**). The reduction current observed corresponds to the reduction of Rh (III) to Rh (I) and to the side reduction of H^+ to H_2 (some bubbles referred to H_2 production were observed on the electrode surface). The oxidation current observed in the reverse scan was attributed to the oxidation of hydrogen. The amount of Rh complex immobilized on the surface of the GDE could not be estimated from the voltammogramme because of the above side hydrogen reduction.

In the presence of H_2, the system exhibited higher currents of oxidation and reduction than what observed under nitrogen (**Figure VI.5B curve b**). This shows the activity of platinum towards the oxidation of hydrogen. Oxidation current of hydrogen increased approximately by 750 µA at -0.4 V vs ref in comparison with the oxidation current recorded under nitrogen bubbling.

In order to examine the activity of the Rh@GDE towards the regeneration of NADH, the addition of 0.5 mM of NAD^+ resulted in an increase in the reduction current of 300 µA approx. at -0.7 V vs ref (Ag/AgCl (3M)) (**Figure VI.5B curve c**) due to the electrocatalytic activity of the Rh complex towards the reduction of NAD^+.

CV curves under hydrogen (**Figure VI.5B curves b and c**) are consistent with those observed with separate Pt and Rh complex electrodes (**Figure VI.1A**): hydrogen oxidation starting at -0.7 V in the reverse scan occurs within the potential window of the Rh complex reduction. Therefore, coupling the oxidation of hydrogen to the regeneration of the cofactor mediated by the rhodium complex on the same electrode without applying of an external voltage would be possible.

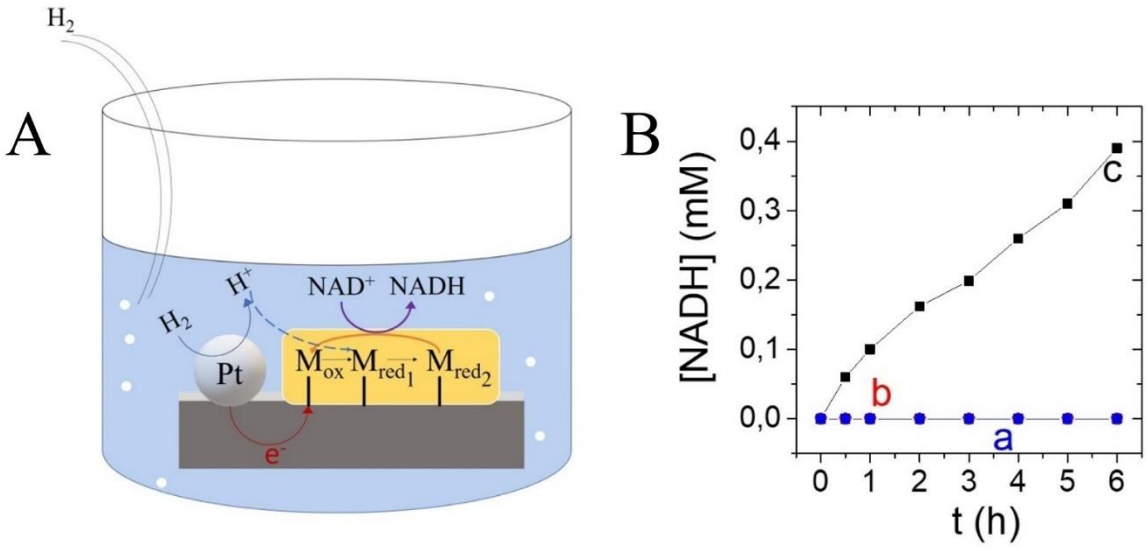

Figure VI.6. Left: A composite chemo-/bio- system for heterogeneous catalysis of H_2-driven NADH generation. This approach involves a gas diffusion electrode acting as anode and cathode with immobilized Rh complex (M)

for NADH regeneration. Right: NADH regeneration under H_2 bubbling on a (a) GDE @ 20 °C, (b) GDE @ 37 °C, and (c) Rh@GDE @ 20 °C. $[NAD^+]_0$ = 0.5 mM, solution volume V = 5 mL, hydrogen flow rate: 20 mL.min^{-1}.

The schematic draw in **Figure VI.6A** shows the possible mechanism involved in the possible simultaneous regeneration of NADH. The Rh complex was immobilized on a 0.25 cm^2 piece of GDE provided with a thin Nafion film. Then, the electrode was placed in 5 mL phosphate buffer solution, 50 mM at pH = 7.2 and in the presence of 0.5 mM NAD^+ under hydrogen bubbling.

It was reported in the literature that NADH can be regenerated under hydrogen and at a temperature of 37 °C on an electrode supported with platinum nanoparticles without the application of a potential and at a pH near 7.[28] Therefore, the regeneration of NADH was first attempted with a GDE (0.2 mg Pt.cm^{-2}, 0.25 cm²) immersed in 5 mL of phosphate buffer containing 0.5 mM of NAD^+ bubbled with hydrogen and at a temperature of 20 °C (**Figure VI.6B curve a**) and 37 °C (**curve b**). However, after 6 hours of hydrogen bubbling, no regeneration of the cofactor was detected by UV-visible.

Besides, the immobilized Rh on the GDE allowed an appreciable activity of the electrode towards the regeneration of the cofactor without the application of external voltage. NADH concentration increased gradually with time and reached 319 µM after 6 hours of continuous hydrogen bubbling at room temperature **(Figure VI.6B right curve c).** This result confirms the mechanism proposed in **Figure VI.6A**. The two electrons generated from the oxidation of hydrogen are transferred to the conductive carbon surface coated with a Nafion film onto which the Rh complex is immobilized. The mechanism of the reduction of Rh(III) (M_{ox}) to Rh(I) (M_{red1}) involves a 2 electron transfer. Electrogenerated Rh(I) is then chemically converted to rhodium hydride complex (M_{red2}) by receiving one proton from solution or from the electrode where H^+ is easily transferred on the carbon support through the coating Nafion film. NADH is afterward regenerated after the transfer of 1 proton and 2 electrons from the rhodium hydride

complex (M_{red2}) to NAD^+, forming back its oxidized form (M_{ox}). This result is similar to that reported by Vincent and co-workers where NADH was electroenzymatically regenerated on conductive particles of carbon for H_2 oxidation coupled to NAD^+ reduction catalyzed by optimized amounts of hydrogenase and NAD^+ reductase.

On the other hand, testing the activity of the regenerated NADH towards the bioconversion of pyruvate catalyzed by lactate dehydrogenase did not show any oxidation of NADH.

NADH regenerated on Rh@GDE electrode thus appears to be in non-active forms *e.g.,* 1,2-NADH, 1,6-NADH, or NAD_2 dimer. The disappointing result might be the fact of interaction between platinum clusters and rhodium complex, or of local changes in pH on the electrode surface modifying the potential of the H_2/H^+ couple, or a deformation in the Rh complex structure, or to a non-optimized amounts of both Rh complex and platinum on the electrode surface.

The activity of reduced NADH cofactor seems to be dependent on the cathode potential of the Rh complex-mediated reduction. In consequence, coupling hydrogen oxidation to the regeneration of the active form of NADH (1,4-NADH) – to form an overall electroless system - was possible in a flow reactor at a pH of 7.2, with separated electrodes by a polymeric grid and with optimized amounts of Pt and Rh complex.

VI.4 Conclusion

To conclude, in this work, we could couple the oxidation of hydrogen to the regeneration of NADH while basing our milestone on the close standard potentials of hydrogen and the Rh complex.

With the combined electrode (Rh@GDE), at a pH of 7.2 (50 mM PBS), a regeneration of the total inactive form of NADH was obtained despite the ability of the Rh complex to regenerate the active form of NADH as previously reported. [13,15]

On the other hand, coupling the oxidation of hydrogen on a GDE to the regeneration of NADH on a Rh@CP-MWCNT electrode in the flow reactor showed a total regeneration of active NADH at 0 V with the following conditions:

- pH = 7.2 and hydrogen and solutions flow rates equal to 20 $mL.min^{-1}$ [21] and the immobilization of Rh complex on CP-MWCNT[16]

- The separation between anodic and cathodic compartments with a plastic grid instead of a Nafion membrane to decrease the resistance of the system.

- A ratio between Rh complex and Pt has to be equal to 2.07 nmol of active Rh complex/mg Pt.

These results in the separated system constitute an important infrastructure to regenerate efficiently active NADH. This paves the way to overall electroless NADH-based biosynthesis.

As a further work, NADH will be coupled to an enzymatic reaction *e.g.,* the bioconversion of pyruvate to lactate catalyzed by LDH or the bioreduction of CO_2 catalyzed by formate dehydrogenase with the application of low amounts of NAD^+ (10 µM) as previously reported[16] in electrochemical cells operated with non-zero cell voltages.

To further expand the study, the separation between both anodic and cathodic compartments can be further explored by replacing the separator with a conductive membrane for protons and electron conduction *e.g.*, MWCNT membrane impregnated by epoxy derivates [23] or the fabrication of copolymeric membrane for proton and anion exchange (Nafion-polyaniline).

References

[1] S. K. Kuk, K. Gopinath, R. K. Singh, T. D. Kim, Y. Lee, W. S. Choi, J. K. Lee, C. B. Park, *ACS Catal.* **2019**, *9*, 5584–5589.

[2] X. Wang, T. Saba, H. H. P. Yiu, R. F. Howe, J. A. Anderson, J. Shi, *Chem* **2017**, *2*, 621–654.

[3] L. Gorton, E. Dominguez, in *Encycl. Electrochem.*, Wiley-VCH Verlag GmbH & Co. KGaA, Weinheim, Germany, **2007**, pp. 67–143.

[4] H. Jaegfeldt, *J. Electroanal. Chem. Interfacial Electrochem.* **1981**, *128*, 355–370.

[5] H. Wu, C. Tian, X. Song, C. Liu, D. Yang, Z. Jiang, *Green Chem.* **2013**, *15*, 1773–1789.

[6] J. B. Jones, D. W. Sneddon, W. Higgins, A. J. Lewis, *J. Chem. Soc. Chem. Commun.* **1972**, *15*, 856.

[7] G. T. Hçfler, M. Pesic, S. H. Younes, E. Choi, Y. H. Kim, V. B. Urlacher, I. W. C. E. Arends, F. Hollmann, *ChemBioChem* **2018**, *19*, 2344–2347.

[8] C. Virto, I. Svensson, P. Adlercreutz, B. Mattiasson, *Biotechnol. Lett.* **1995**, *17*, 877–882.

[9] A. Walcarius, R. Nasraoui, Z. Wang, F. Qu, V. Urbanova, M. Etienne, M. Göllü, A. S. Demir, J. Gajdzik, R. Hempelmann, *Bioelectrochemistry* **2011**, *82*, 46–54.

[10] R. Wienkamp, E. Steckhan, *Angew. Chemie Int. Ed. English* **1982**, *21*, 782–783.

[11] E. Steckhan, S. Herrmann, R. Ruppert, E. Dietz, M. Frede, E. Spika, *Organometallics* **1991**, *10*, 1568–1577.

[12] L. Zhang, M. Etienne, N. Vilà, A. Walcarius, in *Funct. Electrodes Enzym. Microb.*

Electrochem. Syst. (Eds.: N. Brun, V. Flexer), World Scientific, **2017**, pp. 215–271.

[13] L. Zhang, M. Etienne, N. Vilà, T. X. H. Le, G.-W. Kohring, A. Walcarius, *ChemCatChem* **2018**, *10*, 4067–4073.

[14] L. Zhang, N. Vilà, G. W. Kohring, A. Walcarius, M. Etienne, *ACS Catal.* **2017**, *7*, 4386–4394.

[15] B. Tan, D. P. Hickey, R. D. Milton, F. Giroud, S. D. Minteer, *J. Electrochem. Soc.* **2015**, *162*, H102.

[16] W. El Housseini, F. Lapicque, S. Pontvianne, N. Vilà, I. Mazurenko, A. Walcarius, M. Etienne, *ChemElectroChem* **2022**, *9*, e202200463.

[17] H. A. Reeve, L. Lauterbach, O. Lenz, K. A. Vincent, *ChemCatChem* **2015**, *7*, 3480–3487.

[18] X. Zhao, S. E. Cleary, C. Zor, N. Grobert, H. A. Reeve, K. A. Vincent, *Chem. Sci.* **2021**, *12*, 8105–8114.

[19] A. Goršek, P. Glavič, *Chem. Eng. Res. Des.* **1997**, *75*, 709–717.

[20] T. Noë, Y. Cao, G. Laudadio, *Acc. Chem. Res.* **2019**, *52*, 2858–2869.

[21] W. El Housseini, F. Lapicque, A. Walcarius, M. Etienne, *Electrochem. Sci. Adv.* **2021**, 1–11.

[22] J. Quinson, R. Hidalgo, P. A. Ash, F. Dillon, N. Grobert, K. A. Vincent, *Faraday Discuss.* **2014**, *172*, 473–496.

[23] G. A. Pilgrim, J. W. Leadbetter, F. Qiu, A. J. Siitonen, S. M. Pilgrim, T. D. Krauss, *Nano Lett.* **2014**, *14*, 1728–1733.

[24] S. Topcagic, S. D. Minteer, *Electrochim. Acta* **2006**, *51*, 2168–2172.

[25] L. Lauterbach, O. Lenz, K. A. Vincent, **2013**, *280*, 3058–3068.

[26] S. A. Berlinger, B. D. McCloskey, A. Z. Weber, *J. Phys. Chem. B* **2018**, *122*, 7790–7796.

[27] H. K. Song, S. H. Lee, K. Won, J. H. Park, J. K. Kim, H. Lee, S. J. Moon, D. K. Kim, C. B. Park, *Angew. Chemie - Int. Ed.* **2008**, *47*, 1749–1752.

[28] T. Saba, J. Li, J. W. H. Burnett, R. F. Howe, P. N. Kechagiopoulos, X. Wang, *ACS Catal.* **2020**, *11*, 283–289.

Objective of the study in Chapter VII

The indirect electrochemical regeneration of the NAD(P)H cofactor and its derivatives by rhodium-based catalysts e.g. chloro(2,2′-bipyridyl) (pentamethylcyclopentadienyl)-rhodium (III) chloride complex, $[Rh(Cp^*)(bpy)Cl]^+$ was previously studied covalently immobilized on multi walled carbon nanotubes (MWCNT), with H^+ produced by hydrogen oxidation on a Pt-C gas diffusion anode. In this work, the hydrogen oxidation was allowed by enzymatic catalysis with the membrane-bound NiFe hydrogenase from *Aquifex aeolicus* (Hyd-1). Several optimizations were dedicated to improve hydrogenase activity immobilized on a gas diffusion layer (GDL) such as selection of MWCNT functionalization, pH and temperature. Best results in terms of catalytic efficiency were obtained with NH_2-functionalized MWCNTs at pH 7 and 40°C. The regeneration of NADH was shown effective in a conventional glass cell where the Hyd-1 electrode acted as the anode and the reference. For a cell voltage of 0.3 V, the production rate was near 5.7 µmol h^{-1} cm^{-2} with a faradaic yield near 75%.

Chapter VII. Coupling the regeneration of the NAD(P)H cofactor catalyzed by a rhodium complex to the biooxidation of hydrogen catalyzed by a hydrogenase

VII.1 Introduction

Molecular hydrogen produced by solar-driven water splitting in photoelectrochemical cells holds promise as a sustainable and renewable alternative to fossil fuels for future energy technologies.[1–4] Besides, the large amount of energy stored in the chemical bond of the H_2 molecule can be released as electrons in an H_2/O_2 fuel cell by using H_2-oxidation catalysts attached to an anode coupled to an O_2-reducing cathode.[5] However, most commonly used electrocatalysts for H_2 conversion are made of scarce and expensive noble metal-containing materials.[2] Implementing biocatalysts for the fabrication of H_2/O_2 biofuel cells (BFCs) represents an attractive alternative. Hydrogenases with active centers based on earth-abundant metals (Ni and/or Fe)[6] have been shown in these biodevices to be powerful catalysts for the H_2 oxidation process at the bioanode with turnover levels similar to Pt.[7–9]

Apart from power generation, hydrogenase is one of the electroenzymatic catalysts involved in biosynthetic applications, and in particular in the regeneration of the NAD(P)H cofactor. In such systems, H_2 serves as a sacrificial substrate, and the entire process generates no byproducts, making it atom-efficient. Furthermore, excess H_2 in its gaseous form is easily removed from the system. Mertens and co-coworkers proposed a typical H_2-driven cofactor regeneration system based on *Pyrococcus furiosus* hydrogenase I [10] which oxidizes H_2 while catalyzing the reduction of $NADP^+$ into NADPH. [11–13] However, the usage of the same enzymatic catalyst for both oxidation of hydrogen and reduction of the cofactor induces difficulties in optimizing the activity of the enzyme towards both reactions. In addition *P. furiosus* hydrogenase I is a hyperthermophilic enzyme with optimal activity at 80 °C, a temperature incompatible with the activity of the majority of NAD(P)H dependent enzymes.

The fair stability of this hydrogenase especially in the presence of oxygen further restricts the applicability of this method. [14]

Membrane-bound hydrogenase (Hyd-1) from *Aquifex aeolicus* is known as an efficient electroenzymatic catalyst for hydrogen oxidation. It is one of the hydrogenases that is tolerant to oxygen and that can operate at temperatures between 10 °C and 80 °C. Like other [Ni-Fe] hydrogenases from Group I, Hyd-1 from *Aquifex aeolicus* is constituted of a large catalytic subunit hosting the NiFe active site, and a small subunit with three [Fe-S] centers. [15,16]

While the eco-friendly oxidation of hydrogen by Hyd-1 is provided by Ni and Fe on its active site, it is important to take into consideration the drawbacks of using such enzymatic catalysts *e.g.*, their activity and stability with time and their molecular weight e.g. 133 kDa for Hyd-1,[17] that lowers the amount of loaded catalytic units on the electrode. First, the immobilization of hydrogenases on an electroactive surface can sustain their stability and activity. Electron transfer mechanisms between enzymes and the electrode can be of two types: mediated electron transfer (MET) and direct electron transfer (DET). [18,19] In a MET-type system, redox mediators are extrinsic redox-active compounds, such as viologen species, that transfer electrons between hydrogenase and the electrode. [20,21] Small, low-molecular-weight electron mediators that require low overpotentials can be advantageous because they permit rapid electron transfer rates with minimal power losses between the enzyme and the electrode. [20] However, cost, stability, selectivity, affinity, and the capacity of such mediators to exchange electrons in an immobilized state must also be taken into account.[22,23]

DET may be advantageous for biofuel cell applications due to their often lower overpotentials, with less interference, while avoiding prior co-immobilization of a redox mediator.[24]

On the other hand, hydrogenase loading can be increased with large effective surface area of the electrode materials e.g., carbon materials. Electrodes have been modified extensively with

carbon-based substances. [25–27] Carbon nanotubes have unique properties, such as high conductivity and large surface areas. Placing a droplet of an enzyme and carbon nanotube suspension on the surface of an electrode is a straightforward method for modifying electrodes with carbon nanotubes and enzymes. [28]

Lojou et al. used a three-dimensional electrode formed of a carbon felt and multi-walled carbon nanotubes (MWCNT) to support the O_2-tolerant [NiFe]-hydrogenase from *A. aeolicus* and a thermostable bilirubin oxidase in an H_2 fuel cell scheme. The system produced 15.8 mWh of energy after 17 hours of continuous operation, exhibiting at that time the highest power and stability ever reported.[29]

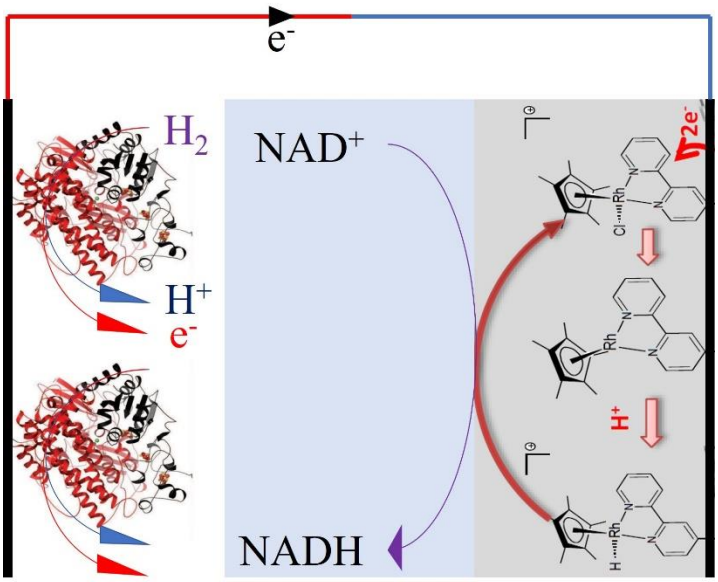

Scheme VII.1. Schematic representation of coupling H_2 oxidation to NADH regeneration catalyzed by Hydrogenase from *Aquifex aeolicus* (on the left) and Rh complex (on the right) respectively, both supported on carbon material.

While the oxidation of hydrogen can be electroenzymatically catalyzed by Hyd-1 supported on an electroactive surface, the electrochemical regeneration of the active form of the NAD(P)H cofactor (1,4-NAD(P)H) requires the usage of a catalyst.[30,31]

After Steckan's luminated the spot-on on Rh complex as a powerful one of the electrochemical catalysts applied in the regeneration of 1,4-NAD(P)H cofactor,[32–35] particularly $[Cp*Rh(bpy)Cl]^+$, several researches focusing on the electrocatalytic activity of Rh complex as well as its immobilization on an electrode surface were conducted in several groups *e.g.*, Minteer and co-workers[36] and Etienne and co-workers.[37,38]

Taking into account that the standard redox potentials for hydrogen oxidation and NAD(P) regeneration biocatalyst are close, previous works have described the electroless regeneration of NADH in systems in which all catalysts *e.g.*, hydrogenase and NAD^+ reduction complex are co-immobilized on the same conductive particles, such as activated carbon particles.[39] Despite the successful results obtained, which demonstrate the simplicity of the two-catalyst-coated particles[40] and the reproducibility of the system when coupled to an enzymatic reaction with high levels of TTNs,[41] combining the two types of catalysts on the same support may be limited in some ways.

The inactivation of one of the two biocatalysts, hydrogenase or NAD^+ reductase, placed on the same electrode may result in the loss of the electrode or the need to separate the two catalysts on their support in order to recover the active catalyst.

Moreover, it has been demonstrated that the interaction between a chemical catalyst, such as the rhodium complex, and a biological catalyst, such as NAD(P)H dependent dehydrogenase, used in the synthesis of chemical compounds on the same electrode, contributes to the deactivation of the biological catalyst. [42] Thus, casting both hydrogenase and Rh complex on the same electrode may lead to hydrogenase deactivation.

Based on the possible drawbacks of using both catalysts for coupling H_2 oxidation to NAD(P)H regeneration on the same electrode, we preferred in this work to separate the two catalysts.

Previously, advantageous results in terms of stability (more than 5 days) and activity (3 mg lactate.h^{-1}) were obtained while coupling hydrogen oxidation to NAD^+ reduction electrochemically catalyzed by platinum and a rhodium complex respectively.[43,44]

In this work, following the advantages of replacing chemical catalysts by biological ones e.g., being environmentally friendly and highly selective,[22] platinum was replaced by the membrane-bound hydrogenase from *Aquifex aeolicus* (Hyd-1)for the oxidation of hydrogen (**scheme VII.1**). Both catalysts for hydrogen oxidation and NADH regeneration were immobilized on separated electrodes. Whereas the immobilization of Rh complexes was previously developed using carbon paper base, a suitable support had to be found for Hyd-1. Starting from fuel cell technology, with Pt loaded gas diffusion electrodes, it was imagined to use a gas diffusion layer (GDL) as the enzyme support base. GDL consists of a porous matrix, which ensures a uniform distribution of gas – while blocking liquid penetration- and acts as a transporter of electrons from or to the external circuit.[45]. Most of them are macroporous carbon-based materials, being 200-300 µm thick, with pore diameters ranging from 4 to 50 µm.[45]. The macroporous layer is often coated by a microporous layer (MPL) formed by finer carbon particles and hydrophobic resins. MPL in its turn can be a suitable support for MWCNT in view to enzyme immobilization. Multiwalled carbon nanotubes (MWCNTs) can allow significant improvements in the efficiency of the electroenzymatic synthesis system by tuning some electrochemical properties e.g. enhancing the electroactive surface area.[46][47]. Parameters of the overall procedure had to be optimized and the efficiency of the method was evaluated by cyclic voltammetry (CV). Moreover, coupling of enzymatic hydrogen oxidation to the regeneration of NADH could be successfully implemented in a glass cell, as reported in the second part of the paper.

VII.2 Experimental section

VII.2.1 Chemical and reagents

Hydrogenase from *Aquifex aeolicus* was obtained as indicated in **section VII.2.3**. β-nicotinamide adenine dinucleotide (NAD^+, >98%) and β-nicotinamide adenine dinucleotide reduced dipotassium salt (NADH, >97%), $(RhCp^*Cl_2)_2$ (97 %), dichloromethane (DCM) (98 %), *N*-methyl-2-pyrrolidone (NMP), sodium nitrite (97 %), 2,2-bipyridine (98 %), 4-azidoaniline hydrochloride (98 %), K_2HPO_4 (99%), KH_2PO_4 (99%), HCl (37 %), were from Sigma-Aldrich. Phosphate buffer (50 mM) was used to investigate the electrocatalytic properties of both the rhodium complex towards NAD^+ reduction and the hydrogenase towards hydrogen oxidation. Multiwall carbon nanotubes (MWCNT, NC7000™ series) were from Nanocyl (Belgium), GDL 39BC, and carbon papers (SpectraCarb 2050L-0550 Carbon Paper) were acquired from Fuel Cell Store (USA). MWCNTs were dispersed in a solution of ethanol (96 %). $MWCNT_{NH2}$ were from Metrohm Dropsens (Spain) and dispersed in NMP. All solutions were prepared with high purity water (18 MΩ cm) from a Purelab Option water purification system.

VII.2.2 CP-MWCNT-Rh electrode preparation

A piece of SpectraCarb carbon paper was used as working electrode or cathode on which the rhodium complex was covalently immobilized. The CP-MWCNT was prepared following the same process used for a bucky paper electrode preparation reported in literature.[48] 10 mg MWCNT were dispersed in 50 mL ethanol by ultrasonication for 5 h. Afterwards, the suspension was decanted and vacuum filtered using the CP as filter. Then, the material was dried at 60 °C overnight.

CP-MWCNT was then functionalized following a reported protocol in the literature. [38]1 mM of 4-amino-2,2-bipyridine (synthetized following a reported work in the literature [38]) was

mixed with 2 mM of sodium nitrite in 0.5 M of HCl under gentle stirring for 5 min in order to generate 2,2-bipyridyl diazonium cations. A negative potential was then applied by running 2 cyclic voltammograms between 0.4 V and -0.8 V (vs Ag/AgCl (3M)) at a scan rate of 20 mV/s. The electrode was then rinsed with ultra-pure water and left to dry.

The functionalized electrode with 2,2-bipyridine moieties was then placed into a solution of DCM containing 0.15 mM of $((RhCp^*Cl_2)_2$ for 4 h with a gentle stirring. The functionalized electrode with the rhodium complex was then rinsed with DCM for 5 min in order to remove the unreacted residues.

VII.2.3 Hyd-1 from *Aquifex aeolicus* purification

Membrane-bound [NiFe]-hydrogenase from *Aquifex aeolicus* (Hyd1) was purified as described in the literature.[17]

VII.2.4 GDL-MWCNT-Hyd-1 preparation

The preparation of the electrode with hydrogenase was performed in a 2-step process. First, a suspension of MWCNT functionalized with amine functions and dispersed in NMP solvent (1 mg $MWCNT_{NH2}$ / mL NMP) was added on the microporous layer of a GDL 39 BC. NMP was evaporated under vacuum. Then, Hyd-1 was adsorbed on functionalized $MWCNT_{NH2}$ and left two hours at 3 °C until its total adsorption.

VII.2.5 Electrochemical tests

Cyclic voltammetry and chronoamperometry were recorded with the Autolab PGSTAT. The working electrode was either CP-MWCNT-Rh, GDL-MWCNT-Hyd-1, or both together. The working electrode, the Ag/AgCl (3M) reference electrode and a stainless-steel wire used as counter electrode, were inserted through the holes of the lid of the glass cell. The cell contained phosphate buffer solution (0.1 M), with other reactants. The anode and cathode were set in the electrochemical cell, with an electrode gap in the order of 2 mm.

The pH of the solution was 7. Twenty minutes before and during cyclic voltammogram recording, the solution was bubbled with nitrogen or hydrogen in order to eliminate residual oxygen.

VII.3 Results

VII.3.1 CV experiments

Relatively small electrodes and supports, with an area of 0.25 cm^2 have been used in this sub-section. Two parameters had to be optimized: the type and the functionalization of the MWCNT and the type of carbon support.

VII.3.1.1 Optimization of the MWCNT supporting layer

On the basis of the hierarchization of the study for the optimal bioelectrocatalytic oxidation of hydrogen catalyzed by Hyd-1, selection of MWCNT type was revealed a critical parameter. The effect of the functionalization of MWCNT casted on a glassy carbon electrode was studied with 2.5 pmol of Hyd-1 casted on a 0.25 cm^2 glassy carbon electrode (GC) beforehand coated with 10 µL suspension of functionalized MWCNT (1 mg MWCNT/mL solvent) and subsequent drying.

Under nitrogen and with all types of MWCNT (**Figure VII.1 black curves**), no ox-red activity was detected in the chosen potential window. In addition to the hindered activity of Hyd-1 under nitrogen, this experiment indicates that no secondary reactions take place in the potential window of the CV tests with various types of MWCNT. Besides, under hydrogen, an activity of Hyd-1 was observed related to the oxidation of H_2 to H^+. A poor activity of H_2 oxidation was observed with non-functionalized MWCNT (**Figure VII.1A, red curve**) with a low current (1 µA) at -0.3 V vs ref. On the other hand, functionalized MWCNTs were found to exhibit far larger electrocatalytic activity of Hyd-1 under hydrogen (**Figures VII.1B and VII.1C; red curves**) in comparison to non-functionalized MWCNT.

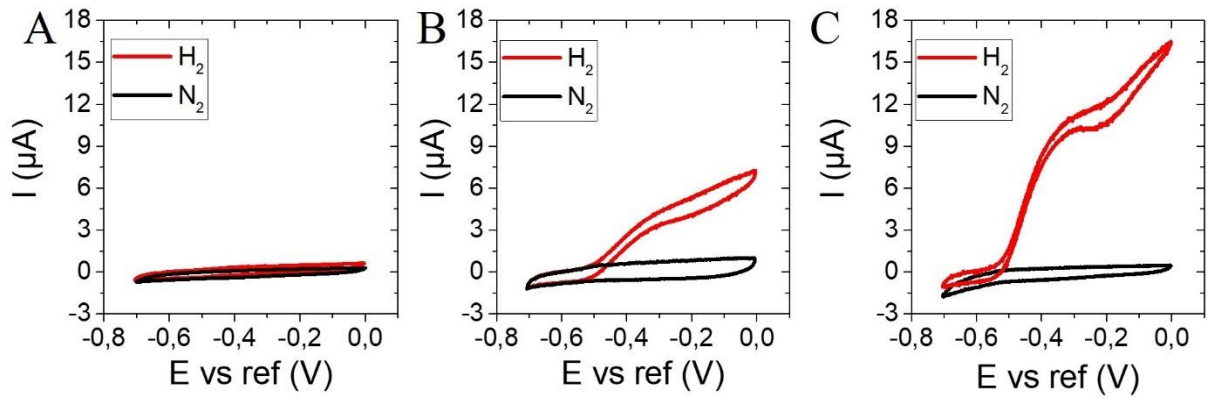

Figure VII.1. CV experiments showing the effect of MWCNT functionalization on hydrogenase activity in a saturated solution with nitrogen (black curve) and hydrogen (red curve) (A) MWCNT, (B) MWCNT-COOH, and (C) MWCNT-NH_2. Conditions: 2.5 pmol Hyd-1, 10 µL MWCNT (1 mg MWCNT/mL solvent) casted on GC electrode (area =0.25 cm^2), scan rate 10.0 $mV.s^{-1}$, pH 7.0, room temperature, and 0.1 M phosphate buffer. Reference: Ag/AgCl (3M).

A higher activity of hydrogenase was obtained with MWCNT functionalized with amine functionnalities (**Figure VII.1C, red curve**) featured by an oxidation current of hydrogen near 11 µA at -0.3 V, two times larger than that observed with MWCNT functionalized with COOH (**Figure VII.1B, red curve**). Furthermore, the onset of hydrogen oxidation with aminated MWCNT (-0.54 V) begins earlier than that observed with carboxylated CNT (-0.5 V). Finally, while comparing the profiles of the two voltammograms (**Figure VII.1B and VII.1C; red curves**), it can be seen the kinetics of hydrogen oxidation is higher than that obtained with Hyd-1 on $MWCNT_{COOH}$. Thus, $MWCNT_{NH2}$ appear as a suitable electroactive surface for tuning Hyd-1 electrocatalytic activity towards H_2 oxidation, and such MWCNT were retained for further tests.

VII.3.1.2 Optimization of the porous carbon-based support

Previously, a hierarchical porosity was produced by modifying a carbon felt (CF) electrode with carbon nanotubes functionalized with amine functions. It has mesopores that are close to the size of the enzyme, making it suitable for enzyme entrapment, while maintaining a

macroporosity that is favorable for substrate diffusion. CF-MWCNT was a suitable matrix for hydrogenase immobilization in terms of enzyme loading and DET-connection.[24]

The second parameter to optimize is the support for MWCNT $_{NH2}$ that could have the same behavior than GC electrode *e.g.*, planar surface but could mimic a gas diffusion electrode used in fuel cell technology. For that, we have chosen a gas diffusion layer as support for MWCNT$_{NH2}$ on which will be casted Hyd-1. The selection of the support is presented below.

Figure VII.2A shows cyclic voltammograms expressing the electrocatalytic activity of Hyd-1 casted on MWCNT$_{NH2}$ deposited on different supports. The idea in this set of experiments is to select the electrode support on which Hyd-1 behaves in a similar manner to that observed with the GC electrode as shown in **Figure VII.2A curve b.**

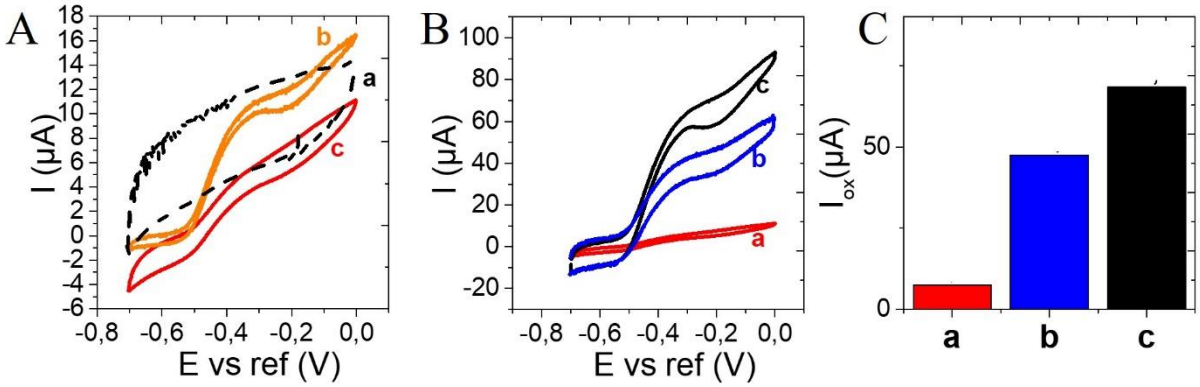

Figure VII.2. (A) Comparison of the electrocatalytic behavior of MWCNT$_{NH2}$ -Hyd1 on (a) a macroporous substrate of a GDL 39 BC, (b) a GC electrode, and (c) a microporous layer of a GDL 39 BC. Conditions: 2.5 pmol Hyd-1, 10 µL MWCNT$_{NH2}$ (1 mg MWCNT$_{NH2}$/mL NMP) casted on GC electrode, 0.25 cm² GDL 39 BC, scan rate 10.0 mV. s^{-1}, pH 7.0, room temperature, and 0.1 M phosphate buffer. Reference: Ag/AgCl (3M). Effect of Hyd-1 and MWCNT$_{NH2}$ on (B) the electrocatalytic activity studied by CV and (C) hydrogen oxidation current at -0.3 V. (a) 10 µL MWCNT$_{NH2}$ (1mg/mL) and 2.5 pmol Hyd-1, (b) 50 µL MWCNT$_{NH2}$ (1mg/mL) and 20 pmol Hyd-1, and (c) 50 µL MWCNT$_{NH2}$ (1mg/mL) and 10 pmol Hyd-1. Conditions: Scan rate 10.0 mV. s^{-1}, pH 7.0, 0.25 cm² GDL 39BC, room temperature, 0.1 M phosphate buffer, and under H_2. Reference: Ag/AgCl (3M).

The activity of Hyd-1 adsorbed on $MWCNT_{NH2}$ coated either on the microporous layer or the macroporous side of the GDL was tested under hydrogen. Low oxidation currents were observed on the macroporous substrate with a high capacitance as shown in **Figure VII.2A curve a**. On the other hand, results showed that adding hydrogenase on $MWCNT_{NH2}$ casting on the microporous side of the GDL (**Figure VII.2A curve c**) as in **scheme VII.2** exhibits an electrochemical response comparable to that observed on a GC electrode (**Figure VII.2A curve b**) with an onset of hydrogen oxidation near -0.52 V vs ref (Ag/AgCl (3M)). This is likely the fact of the sub-micrometric structure of the MPL, onto which the MWCNTs can be more uniformly immobilized.

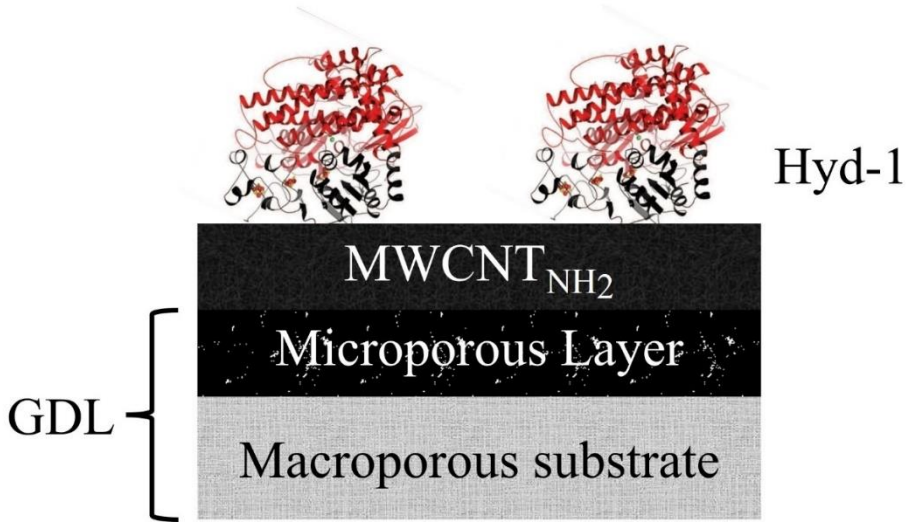

Scheme VII.2. Schematic representation of Hyd-1@GDL-$MWCNT_{NH2}$. (Not scalable)

Besides, the addition of Hyd-1 on MPL side of the GDL in the absence of $MWCNT_{NH2}$ didn't exhibit any activity of hydrogenase (data not shown here). To note that with experiments in **Figures VII.1 and VII.2A** low amounts of $MWCNT_{NH2}$ and Hyd-1 were used. In consequence, higher amounts of both components can be considered to efficiently couple hydrogen oxidation to NADH regeneration.

On the microporous layer of a 0.25 cm² GDL (Sigracet 39 BC), various amounts of Hyd-1 and $MWCNT_{NH2}$ were added. **Figure VII.2B curve a** is the replicate of **Figure VII.2A curve c**

with 2.5 pmol Hyd-1 and 10 µL of $MWCNT_{NH2}$ (suspension) immobilized on the electrode. Increasing the amounts of both MWCNT and Hyd-1 by a factor 4 and 5 respectively, led to an increase in the catalytic response of Hyd-1 featured by an early onset of hydrogen oxidation at -0.52 V vs ref (Ag/AgCl (3M)) (**Figure VII.2B curve c**) and a hydrogen oxidation current more than 6 times higher (**Figure VII.2C data c**) than that obtained with the lower amounts of $MWCNT_{NH2}$ and Hyd-1 (**Figure VII.2C data a**). With the larger amount of MWCNT, 50 µL, increasing the amount of hydrogenase from 10 pmol to 20 pmol resulted in a lower oxidation current at -0.3 V from 68 µA to 47 µA (**Figure VII.2B curve c and Figure VII.2C data c**) contrary to expectations. This result may be due to the presence of surfactant that may create a partial blockage on the electrode surface leading to lower currents of oxidation.

VII.3.1.3 CV experiments with optimized parameters

The electrocatalytic activity of 10 pmol Hyd-1 drop-casted on 50 µg MWCNT functionalized with NH_2 functions (**deposited following the protocol described in section VII.2)** and supported on the microporous side of a gas diffusion layer (GDL), as shown in **Scheme VII.2**, was evaluated through cyclic voltammetry at a scan rate of 10 $mV.s^{-1}$. While the solution was bubbled with nitrogen 20 min prior to the test and during the test at 20 °C, no redox activity was observed (**Figure VII.3A curve a**).

Besides, in the presence of hydrogen, Hyd-1@GDL-$MWCNT_{NH2}$ exhibits an electrocatalytic activity. The oxidation of hydrogen starts at -0.52 V vs ref (Ag/AgCl (3M)) and reaches its peak at -0.3 V with a current at 68 µA. Then, Hyd-1 undergoes a well-known reversible deactivation phenomenon, with slight declining currents, but from -0.2V, the anodic polarization allows further increase in the anodic current for hydrogen oxidation (**Figure VII.3A, curve b**).

Increasing the temperature from 20 °C to 40°C (**Figure VII.3A curve c**) induced an increase in the activity of Hyd-1 towards hydrogen oxidation with higher oxidation current and an onset

of hydrogen oxidation at -0.58 V (**Figure VII.3A curve c**) approx. 60 mV less anodic than at 20°C. The hydrogen oxidation peak at -0.3 V was found nearly two times larger (125 µA) than that obtained at 20 °C.

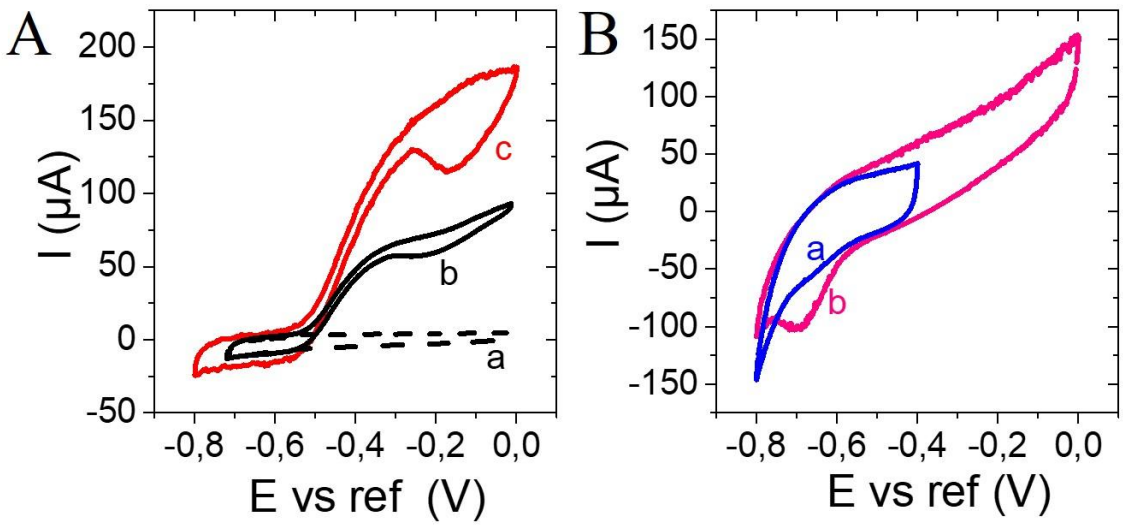

Figure VII.3. CV experiments of Hyd-1@GDL-MWCNT$_{NH2}$ and Rh@CP-MWCNT. (A) Study of the electrocatalytic activity of 10 pmol Hyd1@ GDL-MWCNT$_{NH2}$ (50 µL MWCNT$_{NH2}$). Electrode area =0.25 cm^2. Under nitrogen (a) and under hydrogen at a temperature of (b) 20 °C and (c) 40 °C. (B) Cyclic voltammograms recorded using a Rh@CP-MWCNT electrode at a temperature of (a) 20 °C and (b) 40 °C. Conditions: scan rate 10.0 mV.s^{-1}, pH 7.0, and 0.1 M phosphate buffer. Reference: Ag/AgCl (3M).

The electrode potential is function of temperature, pressure, and pH, as expressed by Nernst law:

$$E_{H^+/H_2} = E_0 - 2.303\frac{RT}{nF}log\left\{\frac{P_{H_2}}{(a_{H^+})^2}\right\} = E_0 - 2.303\frac{RT}{nF}logP_{H_2} - 2.303\frac{RT}{nF}pH \quad (1)$$

with P_{H_2}, partial pressure of H_2, a_{H^+}, activity of H^+ and n the number of electrons involved in the redox reaction, *i.e.*, 2.

$E_{H^+/H_2} = -0.42\ V$ at neutral pH, room temperature, and at standard pressure conditions. As can be calculated from **relation 1**, the potential of hydrogen oxidation decreases with higher

temperature and pH. This phenomenon enhances the probability of coupling simultaneously the oxidation of hydrogen catalyzed by Hyd-1 to the reduction of NAD^+ catalyzed by Rh complex while both placed on separated electrodes as depicted in **scheme VII.1**.

Figure VII.3A curve b corresponds to the result obtained after several optimizations such as the nature and functionalization of MWCNT, development of Hyd-1 deposition on GDL, and amounts of both $MWCNT_{NH2}$ and Hyd-1.

Optimal amounts of MWCNT and hydrogenase have to be used (5 µL $MWCNT_{NH2}$/ 1 pmol hydrogenase) on the GDL microporous layer. In addition, increasing the temperature to 40 °C has a positive effect on the Hyd-1 activity towards hydrogen oxidation.

The next step is to evaluate the ability of the Rh complex to operate with Hyd-1 under fixed parameters. **Figure VII.3B** shows cyclic voltammetry experiments of 0.25 cm^2 Rh@CP-MWCNT at 10 $mV.s^{-1}$. Without NAD^+ and at a temperature near 20°C, the reduction of Rh(III) to Rh (I) was observed to start at -0.58 V vs ref (Ag/AgCl (3M)) and the cathodic peak was reached at -0.7 V with a current near 20 µA (**Figure VII.3B curve a**). As observed with hydrogenase, increasing the temperature to 40 °C led to a two-times larger cathodic current (**Figure VII.3B curve b**). In addition, working with the same CV potential window as that used with Hyd-1 (between 0 V and -0.8 V) does not reveal any secondary reactions on Rh@CP-MWCNT surface. Thus, higher temperatures up to 40°C enhance the activity of the Rh complex towards NADH regeneration.

VII.3.2 NADH regeneration

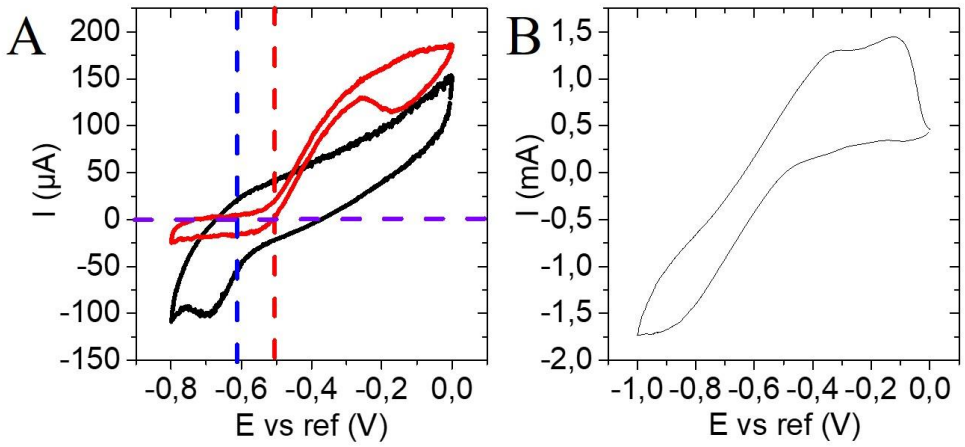

Figure VII.4. (A) Superimposition of CV of Hyd-1@GDL-MWCNT$_{NH2}$ and Rh@CP-MWCNT. (B) CV experiment showing Rh- Hyd-1@GDL-MWCNT$_{NH2}$. Conditions: 10 pmol Hyd-1, 50 µL MWCNT$_{NH2}$, Scan rate 10.0 mV.s^{-1}, pH 7.0, 0.25 cm² GDL 39BC,T = 40 °C , 0.1 M phosphate buffer, and under H_2. Reference: Ag/AgCl (3M).

Coupling NADH regeneration to H_2 biooxidation is the main objective of this work. It is thus required to define the potential of electrolysis allowing the efficient regeneration of NADH with a high faradaic efficiency.

The superimposition of CV curves of Rh@CP-MWCNT and Hyd-1@GDL-MWCNT$_{NH2}$ shows that the potential difference between the starting potential for the hydrogen oxidation (**Figure VII.4A red dashed line**) and the starting potential for the Rh complex reduction (**Figure VII.4A blue dashed line**) is near 120 mV. Therefore, a minimum difference of -120 mV vs ref (H_2) has to be applied, with Hyd-1@GDL-MWCNT$_{NH2}$ acting as anode and reference. On the other hand, the potential difference between the oxidation peak of H_2 and the reduction peak of Rh(III) can be observed to be near 400 mV.

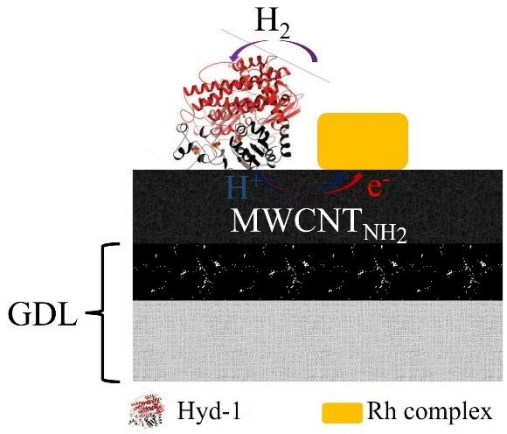

Scheme VII.3. Cartoon representation of Hyd1-Rh@ GDL-MWCNT$_{NH2}$ electrode.

In order to reduce the difference in potential between the Rh complex and Hyd-1 loaded on the catalyst layers and to facilitate the kinetics of electron transfer, the immobilization of two catalysts was first carried out on the same GDL-MWCNT$_{NH2}$ as represented in **scheme VII.3**. High currents of oxidation and reduction in the mA range are observed (**Figure VII.4B**). However, letting the GDL-Rh-Hyd-1 in the solution under hydrogen bubbling at a temperature of 40 °C and in the presence of 100 µM of NAD^+ did not allow any regeneration of the cofactor. Different factors could be at the origin of these high but inefficient currents such as the presence of diazonium film and the combination of both catalysts on the same electrode leading to Hyd-1 deactivation. Based on the aforementioned results related to placing both catalysts on the same electrode, both catalysts were immobilized on separated supports as shown in **scheme VII.1**.

Although the minimal potential required for coupling the NADH regeneration to H_2 oxidation was estimated at 120 mV (**Figure VII.4A)**, no regeneration of the cofactor could be measured by UV-visible after 30 min of electrolysis at -0.1 and -0.2 V vs ref (H_2) (**curves a and b figure VII.5**).

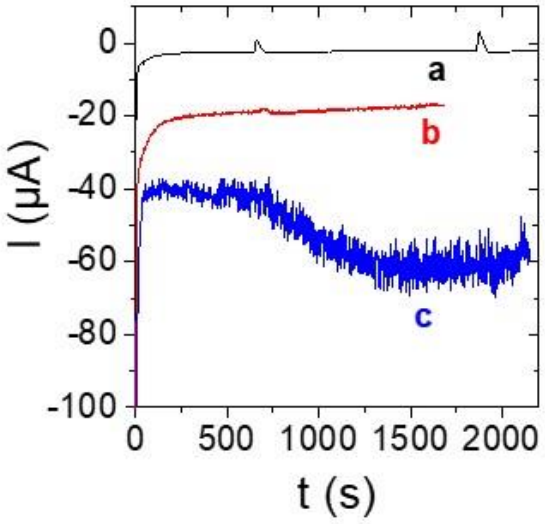

Figure VII.5. Electrolysis tests carried out at various applied potential (a) -0.1 V vs ref (H_2), (b) -0.2 V vs ref (H_2), and (c) -0.3 V vs ref (H_2). Conditions: 0.25 cm² Rh@CP-MWCNT; 0.25 cm² GDL (10 pmol Hyd-1 ; 50 µL MWCNT), Ref : H_2, 0.5 mM NAD^+ in 20 mL solution, under hydrogen, 0.1 M PBS (pH=7), and at T = 40 °C.

On the other hand, electrolysis carried out at -0.3 V vs ref (H_2) (**curve c figure VII.5**) showed an effective regeneration of the cofactor. 90 µM NADH in the 20 mL solution could be regenerated after 30 min electrolysis with a faradaic efficiency of 83 %.

In order to increase the regeneration of the NADH cofactor, higher electrodes surface with higher amounts of catalysts for both the bioxidation of hydrogen and the reduction of NAD^+ were employed.

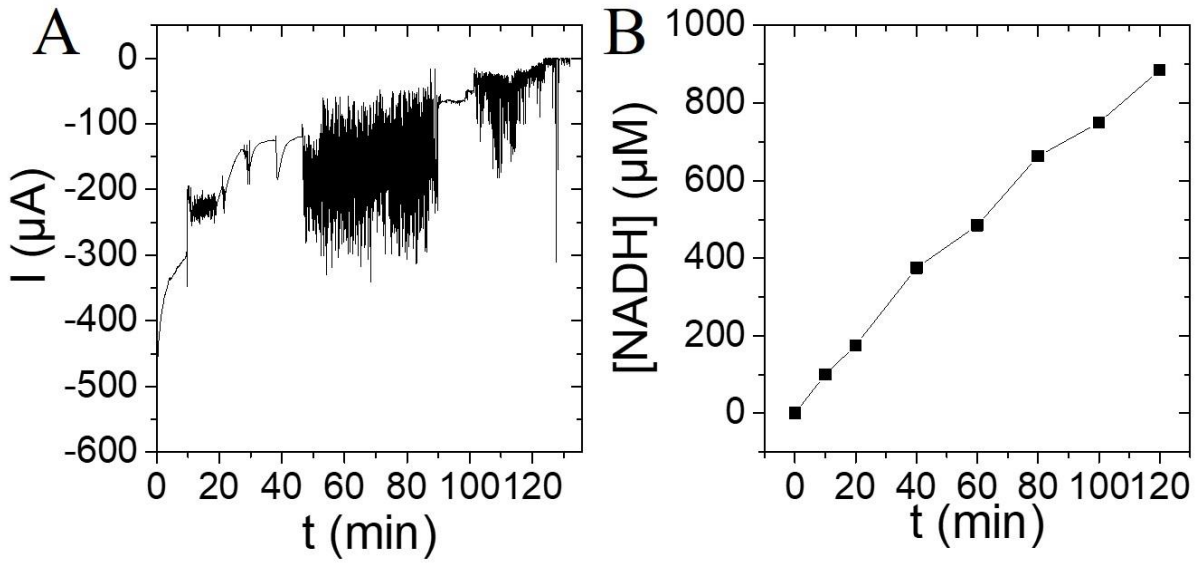

Figure VII.6. (A) Recorded electrolysis current and (B) NADH regeneration kinetics at -0.3 V vs ref (H_2). Conditions: 2.25 cm² Hyd-1@GDL-$MWCNT_{NH2}$ (50 pmol Hyd-1 ; 250 µL MWCNT), 2.25 cm² Rh@CP-MWCNT, 1 mM NAD^+, 30 mL, under hydrogen, 0.1 M PBS (pH=7), and at T = 40 °C.

The study of the regeneration of 1 mM of the cofactor carried out at -0.3 V vs (H_2) on a 2.25 cm² electrode area (50 pmol Hyd-1@GDL-250 µL $MWCNT_{NH2}$), showed a current that started at -450 µA and decreased gradually with time down to -50 µA after 2 hours of electrolysis (**Figure VII.6A**). After this time period, 850 µM of the cofactor were regenerated (**Figure VII.6B**) with a faradaic efficiency of 74.5 %. The gradual increase in NADH concentration with a fairly constant rate – near 12.75 µmol h^{-1} - denotes that both catalysts are stable under the chosen operating conditions *e.g.* 0.1 PBS (pH=7), temperature (40 °C), and hydrogen bubbling.

VII.4 Conclusion and perspectives

The present work led to the design of a system for the electrochemical regeneration of NADH cofactor relying upon hydrogen oxidation catalyzed by an O_2-tolerant hydrogenase and the reduction of NAD^+ mediated by a rhodium complex.

In designed experiments, with selecting aminated-MWCNT as electroactive support for the immobilization of the *A. aeolicus* hydrogenase, different system parameters were optimized for efficient oxidation of hydrogen by the hydrogenase on a gas diffusion layer, namely deposition of MWCNT and Hyd-1 on the MPL surface, the amounts of MWCNT and hydrogenase (1 pmol Hyd-1 : 2.5 µL MWCNT), and the temperature (40 °C). Further tests will be conducted in the presence of low amounts of the cofactor to reach high cofactor TTN and the system will be coupled to an enzymatic reaction.

Coupling the oxidation of hydrogen to the reduction of NAD^+ showed a difference in potential between the two catalysts layers larger than 0.12 V. In order to overcome this problem and to allow possible spontaneous regeneration of the cofactor without applied potential, further developments have still to be made, in particular by:

- Decreasing as much as possible the electrode gap – currently near 2 mm -

- Increasing the size of electrodes and /or the amounts of $MWCNT_{NH2}$-Hyd-1 on GDL and Rh complex covalently immobilized CP-MWCNT. We recently observed that the increase in the amount of Rh complex by using two stacked Rh@CP-MWCNT electrodes instead of one, shifts positively the reduction potential. [43]

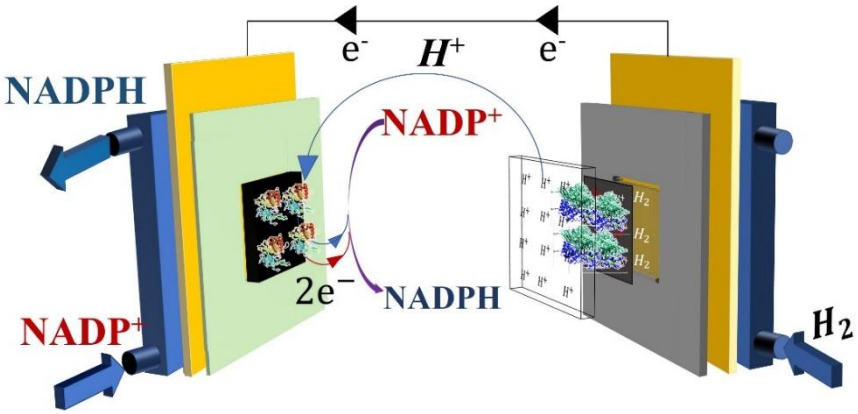

Scheme VII.4. Schematic representation of coupling hydrogen oxidation by Hyd-1 to $NAD(P)^+$ reduction by FNR.

Finally, as the objective in this work is to couple between fuel cell technology and redox flow device for the efficient regeneration of NADH, the biooxidation of H_2 gas by Hyd-1@GDL-$MWCNT_{NH2}$ will be explored in further experiments as shown in **Scheme VII.4**.

In addition, aside from coupling the biooxidation of hydrogen to the reduction of NAD^+ in an electroless process, the passage to a fully electroenzymatic reactor coupling the biooxidation of hydrogen by Hyd-1@CP-$MWCNT_{NH2}$ to $NAD(P)^+$ bioreduction by FNR@CP-$MWCNT_{ox}$ will be explored (**Scheme VII.4**).

References

[1] J. J. Concepcion, R. L. House, J. M. Papanikolas, T. J. Meyer, *Proc. Natl. Acad. Sci.* **2012**, *109*, 15560–15564.

[2] T. A. Faunce, W. Lubitz, A. W. B. Rutherford, D. MacFarlane, G. F. Moore, P. Yang, D. G. Nocera, T. A. Moore, D. H. Gregory, S. Fukuzumi, others, *Energy Environ. Sci.* **2013**, *6*, 695–698.

[3] J. R. McKone, S. C. Marinescu, B. S. Brunschwig, J. R. Winkler, H. B. Gray, *Chem. Sci.* **2014**, *5*, 865–878.

[4] K. P. Sokol, W. E. Robinson, J. Warnan, N. Kornienko, M. M. Nowaczyk, A. Ruff, J. Z. Zhang, E. Reisner, *Nat. Energy* **2018**, *3*, 944–951.

[5] M. S. Dresselhaus, I. L. Thomas, *Nature* **2001**, *414*, 332–337.

[6] W. Lubitz, H. Ogata, O. Rudiger, E. Reijerse, *Chem. Rev.* **2014**, *114*, 4081–4148.

[7] S. D. Varfolomeev, A. I. Yaropolov, I. V Berezin, M. R. Tarasevich, V. A. Bogdanovskaya, *Bioelectrochemistry Bioenerg.* **1977**, *4*, 314–326.

[8] A. A. Karyakin, S. V Morozov, O. G. Voronin, N. A. Zorin, E. E. Karyakina, V. N. Fateyev, S. Cosnier, *Angew. Chemie* **2007**, *119*, 7382–7384.

[9] A. K. Jones, E. Sillery, S. P. J. Albracht, F. A. Armstrong, *Chem. Commun.* **2002**, 866–867.

[10] R. Mertens, L. Greiner, E. C. D. van den Ban, H. B. C. M. Haaker, A. Liese, *J. Mol. Catal. B Enzym.* **2003**, *24*, 39–52.

[11] K. Ma, R. N. Schicho, R. M. Kelly, M. W. Adams, *Proc. Natl. Acad. Sci.* **1993**, *90*, 5341–5344.

[12] F. O. Bryant, M. W. Adams, *J. Biol. Chem.* **1989**, *264*, 5070–5079.

[13] Y. Wang, Z. Kang, L. Zhang, Z. Zhu, *ACS Catal.* **2022**, *12*, 1415–1427.

[14] K. Ma, M. W. W. Adams, *J. Bacteriol* **1999**, *181*, 1163–1170.

[15] K. Monsalve, I. Mazurenko, C. Gutierrez-Sanchez, M. Ilbert, P. Infossi, S. Frielingsdorf, M. T. Giudici-Orticoni, O. Lenz, E. Lojou, *ChemElectroChem* **2016**, *3*, 2179–2188.

[16] I. Mazurenko, R. Clément, D. Byrne-Kodjabachian, A. de Poulpiquet, S. Tsujimura, E. Lojou, *J. Electroanal. Chem.* **2018**, *812*, 221–226.

[17] M. Brugna-Guiral, P. Tron, W. Nitschke, K.-O. Stetter, B. Burlat, B. Guigliarelli, M. Bruschi, M. T. Giudici-Orticoni, *Extremophiles* **2003**, *7*, 145–157.

[18] A. L. Ghindilis, P. Atanasov, E. Wilkins, *Electroanalysis* **1997**, *9*, 661–674.

[19] S. Cosnier, A. J. Gross, A. Le Goff, M. Holzinger, *J. Power Sources* **2016**, *325*, 252–263.

[20] K. Kano, T. Ikeda, *Anal. Sci.* **2000**, *16*, 1013–1021.

[21] A. A. Oughli, M. Vélez, J. A. Birrell, W. Schuhmann, W. Lubitz, N. Plumeré, O. Rüdiger, *Dalt. Trans.* **2018**, *47*, 10685–10691.

[22] E. Lojou, *Electrochim. Acta* **2011**, *56*, 10385–10397.

[23] J. a Cracknell, K. a Vincent, F. a Armstrong, *Chem. Rev.* **2008**, *108*, 2439–61.

[24] I. Mazurenko, X. Wang, A. De Poulpiquet, E. Lojou, *Sustain. Energy Fuels* **2017**, *1*, 1475–1501.

[25] S. A. Kumar, S.-M. Chen, *Sensors* **2008**, *8*, 739–766.

[26] J. J. Gooding, *Electrochim. Acta* **2005**, *50*, 3049–3060.

[27] Z. Zhu, L. Garcia-Gancedo, A. J. Flewitt, H. Xie, F. Moussy, W. I. Milne, *Sensors* **2012**, *12*, 5996–6022.

[28] N. D. J. Yates, M. A. Fascione, A. Parkin, *Chem. Eur. J.* **2018**, *24*, 12164–12182.

[29] I. Mazurenko, K. Monsalve, P. Infossi, M. T. Giudici-Orticoni, F. Topin, N. Mano, E. Lojou, *Energy Environ. Sci.* **2017**, *10*, 1966–1982.

[30] L. Gorton, E. Dominguez, in *Encycl. Electrochem.*, Wiley-VCH Verlag GmbH & Co. KGaA, Weinheim, Germany, **2007**, pp. 67–143.

[31] X. Wang, T. Saba, H. H. P. Yiu, R. F. Howe, J. A. Anderson, J. Shi, *Chem* **2017**, *2*, 621–654.

[32] R. Wienkamp, E. Steckhan, *Angew. Chemie Int. Ed. English* **1982**, *21*, 782–783.

[33] R. Ruppert, S. Herrmann, E. Steckhan, *J. Chem. Soc. Chem. Commun.* **1988**, 1150–1151.

[34] R. Ruppert, S. Herrmann, E. Steckhan, *Tetrahedron Lett.* **1987**, *28*, 6583–6586.

[35] E. Steckhan, S. Herrmann, R. Ruppert, E. Dietz, M. Frede, E. Spika, *Organometallics* **1991**, *10*, 1568–1577.

[36] B. Tan, D. P. Hickey, R. D. Milton, F. Giroud, S. D. Minteer, *J. Electrochem. Soc.* **2015**, *162*, H102.

[37] L. Zhang, M. Etienne, N. Vilà, A. Walcarius, in *Funct. Electrodes Enzym. Microb. Electrochem. Syst.* (Eds.: N. Brun, V. Flexer), World Scientific, **2017**, pp. 215–271.

[38] L. Zhang, M. Etienne, N. Vilà, T. X. H. Le, G.-W. Kohring, A. Walcarius, *ChemCatChem* **2018**, *10*, 4067–4073.

[39] H. A. Reeve, P. A. Ash, H. Park, A. Huang, M. Posidias, C. Tomlinson, O. Lenz, K. A. Vincent, *Biochem. J.* **2017**, *474*, 215–230.

[40] J. A. Cracknell, K. A. Vincent, F. A. Armstrong, *Chem. Rev.* **2008**, *108*, 2439–2461.

[41] X. Zhao, S. E. Cleary, C. Zor, N. Grobert, H. A. Reeve, K. A. Vincent, *Chem. Sci.* **2021**, *12*, 8105–8114.

[42] F. Hildebrand, S. Lütz, *Chem. - A Eur. J.* **2009**, *15*, 4998–5001.

[43] W. El Housseini, F. Lapicque, S. Pontvianne, N. Vilà, I. Mazurenko, A. Walcarius, M. Etienne, *ChemElectroChem* **2022**, *9*, e202200463.

[44] W. El Housseini, F. Lapicque, A. Walcarius, M. Etienne, *Electrochem. Sci. Adv.* **2021**, 1–11.

[45] I. V. Zenyuk, D. Y. Parkinson, L. G. Connolly, A. Z. Weber, *J. Power Sources* **2016**, *328*, 364–376.

[46] I. Mazurenko, M. Etienne, G.-W. Kohring, F. Lapicque, A. Walcarius, *Electrochim. Acta* **2016**, *199*, 342–348.

[47] S. Gentil, S. M. Che Mansor, H. Jamet, S. Cosnier, C. Cavazza, A. Le Goff, *ACS Catal.* **2018**, *8*, 3957–3964.

[48] L. Hussein, G. Urban, M. Krüger, *Phys. Chem. Chem. Phys.* **2011**, *13*, 5831–5839.

General conclusion and outlooks

General Conclusion

In conclusion, we have demonstrated the full potential of a bioelectrochemical reactor for the regeneration of NADH that couples efficiently hydrogen oxidation to NAD^+ reduction, in view to enzyme-catalyzed synthesis.

Different chemical and biological catalysts for both the oxidation of hydrogen and the reduction of NAD^+ have been used in this PhD work such as platinum and hydrogenase I for hydrogen oxidation and Rh complex and FNR for $NAD(P)^+$ reduction.

First, while being electrochemically catalyzed by a Rh complex dissolved in solution, the efficient regeneration of NADH with a complete conversion and a high faradaic yield can be achieved by optimizing the flow reactor parameters: hydrogen and solution flow rates of 20 $mL.min^{-1}$, at a pH close to neutral to prevent NADH and NAD^+ degradation. Then, a model was developed to prove the efficiency of mediated electrochemical reactions conducted at a fixed potential in terms of current density and conversion rates, employing the methodology developed in gas–liquid absorption accompanied by chemical reaction of the dissolved gas. Using a diffusion-controlled electrochemical process and applying it to NADH regeneration mediated by a Rh complex, it was possible to estimate the rate constants of the chemical reaction between Rh(I) and NAD^+ relative to the mass transfer coefficient at the electrode surface ($k = 47 \pm 20\ m^3.mol^{-1}.s^{-1}$) .

Second, the immobilization of the Rh complex on carbon paper with MWCNT and the subsequent pressing at 40 bars of this catalytic layer (Rh@CP-MWCNT) with a GDE coated with a Nafion membrane for protons conductions, resulted in an active system for the efficient electrochemical regeneration of the NADH cofactor system with a stability of over 5 days under continuous flow. In addition, the reduction of the distance between the Rh complex and LDH

by immobilizing them on separate, stacked layers produced an active loop for the continuous regeneration of the cofactor used in low amounts (10 µM). Levels of cofactor TTN as high as 2500 were reached.

Besides, the replacement of chemical catalyst, Rh complex, for the regeneration of NAD(P)H by a biological one, FNR, with the usage of the same conformation applied with Rh complex *e.g.*, GDE - Nafion membrane – FNR@CP-MWCNT, showed a robust system for the regeneration of NAD(P)H with sustained activity for more than 6 days under flow and electrolysis conditions. However, FNR drop-casted on MWCNTs was found much more active on oxidized multiwalled carbon nanotubes (MWCNT) compared with normal MWCNTs. With the application of low amounts of the cofactor (10 µM) in the bioconversion of pyruvate to lactate, FNR was not only able to regenerate NADPH but NADH with very high levels of cofactor TTN (10000).

The reduction of NAD^+ by Rh complex and FNR takes place at -0.3 V vs ref (H_2) and -0.7 V vs ref (H_2) respectively, Rh complex system was selected to study the electroless coupling of hydrogen oxidation to NADH regeneration. The presence of the Nafion membrane stacked to the GDE imposes a pH in the anodic compartment in the order of 3 to 4. The increase in pH in the anodic compartment to 7.2 led to a decrease in the potential window between hydrogen oxidation and Rh complex reduction (Rh (III) to Rh(I). In order to decrease the resistivity of the system, the Nafion membrane has been replaced by a polymeric grid separator. Finally, an optimization of the amount of both platinum and Rh complex (2.07 nmol active Rh complex/mg Pt) immobilized both separately on a gas diffusion electrode and a carbon paper coated with MWCNT respectively led to a total regeneration of 1,4-NADH at 0 V vs ref (H_2). Besides, the direct immobilization of both catalysts on the same electrode support led to the formation of the inactive form of the cofactor. As a further work, the system is to be coupled to an enzymatic

reaction (NAD(P) dependent reaction) for the biosynthesis of pure chemicals or the reduction of CO_2.

Replacement of platinum by hydrogenase was first tested in a batch reactor. Several experiments were designed to boost the oxidation of hydrogen by hydrogenase on a gas diffusion layer mimicking a gas diffusion electrode coated with platinum. The deposition of MWCNT and Hyd-1 on the MPL surface of the GDL, the amounts of MWCNT and hydrogenase (1 pmol Hase:2.5 µL MWCNT), and the temperature (40 °C) were optimized with aminated-MWCNT as the electroactive support for hydrogenase immobilization. Combining the oxidation of hydrogen to the reduction of NAD^+ resulted in a potential difference between the two catalyst layers that exceeded 0.25 V and the regeneration of NADH was possible after the application of an electrolysis potential of -0.3 V vs ref (H_2). Passing from the batch system to a membraneless flow bioreactor would decrease the resistivity of the system due to a higher interconnection between the hydrogen oxidation and the Rh complex reduction favored by a closer distance between both electrodes: higher performance of the system can be expected.

Outlooks

The presented system shows the coupling of the regenerated NAD(P)H to a mono NAD(P) dependent reaction. In further works, the cofactor regeneration system could be coupled to a cascade of enzymatic reactions as shown in **Scheme 1**. Biocatalytic cascades circumvent the isolation of reaction intermediates, thereby saving time and reagents. In addition, it is possible to synthesize chemicals with unstable intermediates because isolating the intermediates is unnecessary.[1]

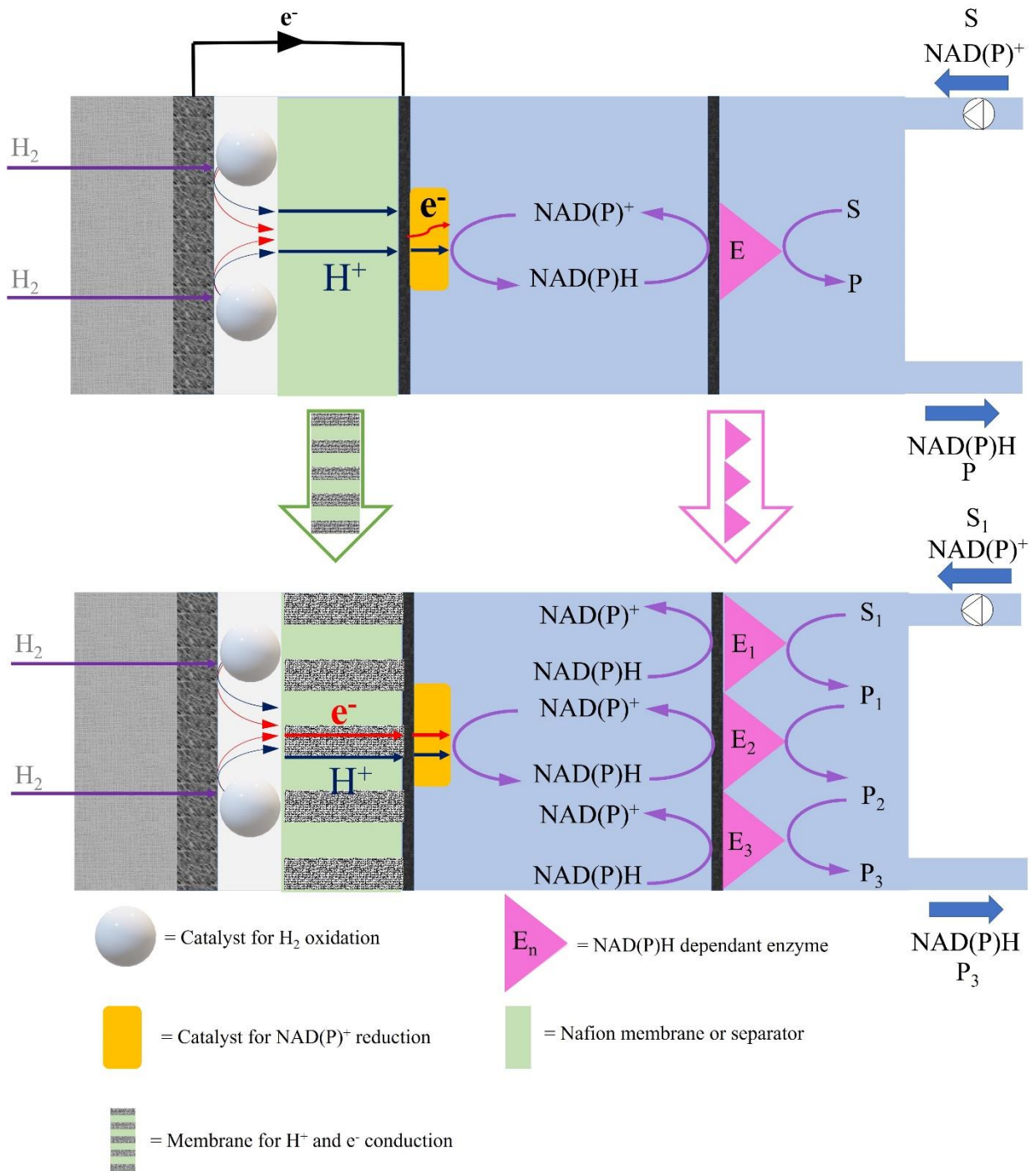

Scheme 1. Cartoon representation of the developed bioelectrochemical reactor for coupling H_2 oxidation to NADH regeneration with future perspectives.

One of the examples of cascade enzymatic reactions is the bioconversion of CO_2. Kuk et al. developed a photoelectrochemical system for the production of methanol from CO_2 by a

multienzyme cascade ,a three-dehydrogenase cascade system, and the efficient regeneration of NADH with the aid of visible light.[2]

To further expand the study, the separation the anodic and cathodic compartments can be further explored by replacing the separator by a membrane exhibiting protonic and electronic conductivity *e.g.*, MWCNT membrane impregnated by epoxy derivates [3] or the fabrication of copolymeric membrane for proton and anion exchange (Nafion-polyaniline). This membrane would improve the connection and the charge transport from the anodic compartment to the cathodic chamber, as shown in lower part of **Scheme 1**.

References

[1] J. H. Schrittwieser, S. Velikogne, M. Hall, W. Kroutil, *Chem. Rev.* **2018**, *118*, 270–348.

[2] S. K. Kuk, R. K. Singh, D. H. Nam, R. Singh, J. K. Lee, C. B. Park, *Angew. Chemie - Int. Ed.* **2017**, *56*, 3827–3832.

[3] G. A. Pilgrim, J. W. Leadbetter, F. Qiu, A. J. Siitonen, S. M. Pilgrim, T. D. Krauss, *Nano Lett.* **2014**, *14*, 1728–1733.